

**Obstacles to DNA replication in
Escherichia coli and the role of UvrD
helicase in their resolution**

Dominika Weronika Warecka

Doctor of Philosophy

University of York

Biology

January 2024

Abstract

UvrD is a multi-functional *Escherichia coli* helicase. It is widely involved in DNA repair, including its DNA unwinding role during mismatch repair and RNAP removal role during transcription coupled repair. UvrD has also been shown to colocalise with the replisome during DNA replication and has an important role in nucleoprotein block removal to clear the path for the replication fork.

The main aims of this project were to test UvrD ability to unwind DNA and displace nucleoprotein blocks and to test whether addition of the mismatch protein MutL could improve UvrD function. Our *in vitro* results showed that UvrD alone was capable of unwinding past a physiologically relevant block, Tus-*terB*, in 'easy' and 'challenging' conditions. The addition of MutL increased the ability of UvrD to unwind long double-stranded DNA substrates in multiple challenging conditions as well as against a physiologically unfamiliar nucleoprotein block (EcoRI E111G). Our results showed that UvrD activity appeared to be enhanced when tasked with unwinding past the Tus-*terB* block and presented better DNA unwinding alone rather than with MutL. To understand more about the UvrD:MutL physical and functional interaction, we designed two UvrD mutants with large N-terminal deletions for UvrD:MutL interaction tests. Additionally, since UvrD:MutL complex formation causes the rotation of the UvrD 2B subdomain, we designed a UvrD Δ 2B mutant, to test for MutL interaction and determine how the 2B subdomain deletion affects UvrD function.

We also developed a new *in vitro* biochemical assay designed to test for the displacement of Tus by the replisome during DNA replication termination. Our preliminary findings suggest that replication forks colliding with the non-permissive orientation of the Tus-*ter* block can displace Tus. Establishment of the Tus jumping assay will allow us to investigate the interaction of DNA replication forks with Tus-*ter* and to test whether other proteins, such as UvrD, are involved in replication termination.

Table of Contents

Contents

| | |
|--|----|
| Abstract..... | 2 |
| Table of Contents..... | 3 |
| Acknowledgements..... | 5 |
| Declaration..... | 6 |
| Chapter 1. Introduction..... | 8 |
| 1.1. Helicases..... | 8 |
| 1.1.1. Superfamily 1 helicases..... | 11 |
| 1.1.2 UvrD-like family..... | 13 |
| 1.2. UvrD structure and function..... | 14 |
| 1.2.1 UvrD subdomain functions..... | 14 |
| 1.2.2. UvrD as a monomer, dimer, and tetramer..... | 17 |
| 1.3. DNA repair and UvrD..... | 19 |
| 1.3.1 Mismatch Repair..... | 19 |
| 1.3.2 Nucleotide Excision Repair..... | 27 |
| 1.3.3 Double-stranded break repair and recombination in E. coli..... | 32 |
| 1.4. DNA Replication and UvrD..... | 35 |
| 1.4.1. DNA replication initiation..... | 35 |
| 1.4.2. DNA replication elongation..... | 41 |
| 1.4.3. DNA replication termination..... | 46 |
| 1.5. Aims and objectives..... | 56 |
| Chapter 2. Materials and Methods..... | 58 |
| 2.1 Materials..... | 58 |
| 2.1.1 Chemicals..... | 58 |
| 2.1.1 Plasmid sequencing..... | 58 |
| 2.1.2 Software and systems..... | 59 |
| 2.1.3 Oligos and Plasmids..... | 61 |
| 2.1.4 Buffers..... | 64 |
| 2.2 Methods..... | 68 |
| 2.2.1 Gels..... | 68 |
| 2.2.2 Molecular Biology..... | 71 |
| 2.2.3 Microbiology..... | 75 |
| 2.2.4 Protein Purification..... | 76 |
| 2.2.5 Biochemical Techniques..... | 81 |
| 2.2.6 Analytical Chromatography..... | 91 |

| | |
|---|-----|
| Chapter 3. Protein Purification of MutL and Its Role in Assisting UvrD Helicase in DNA Unwinding and Nucleoprotein Block Displacement | 93 |
| 3.1 Introduction..... | 93 |
| 3.2 Results | 95 |
| 3.2.1 Protein Purification of MutL..... | 95 |
| 3.2.2 UvrD Helicase was able to unwind DNA past both orientations of the <i>E. coli</i> Tus- ter block..... | 107 |
| 3.2.3 The effect of adding MutL to UvrD helicase assays | 112 |
| 3.3 Discussion | 125 |
| 3.3.1 What can UvrD tell us about how helicases displace DNA-bound proteins? .. | 127 |
| Chapter 4. Protein Purification of UvrD Helicase with N-Terminal Deletions and 2B Subdomain Deletion..... | 132 |
| 4.1 Introduction..... | 132 |
| 4.2 Results | 135 |
| 4.2.1 Cloning <i>uvrD</i> into pET28 α -HisSUMO..... | 135 |
| 4.2.2 Cloning and protein purification of UvrD Δ 108N | 136 |
| 4.2.3 Cloning and protein purification of UvrD Δ 53N | 148 |
| 4.2.4 Cloning and protein purification of UvrD Δ 52N | 150 |
| 4.2.5 Cloning and protein purification of UvrD Δ 2B | 153 |
| 4.3 Discussion | 158 |
| 4.3.1 Solubility Problems | 159 |
| 4.3.2 Chromatography Strategy..... | 160 |
| 4.3.3 Expression plasmid design | 161 |
| 4.3.4 Future work..... | 162 |
| Chapter 5. Tus Jumping Assay Development and Preliminary Results..... | 165 |
| 5.1 Introduction..... | 165 |
| 5.2 Results | 168 |
| 5.2.1 Assay Development..... | 168 |
| 5.2.2 Tus Jumping Assay | 171 |
| 5.2.3 Tus jumping Assay | 173 |
| 5.2.4 One Fork Tus jumping Assay..... | 176 |
| 5.2.5 Creating Tus-bound template..... | 183 |
| 5.3 Discussion | 186 |
| 5.3.1 Method Development..... | 186 |
| 5.3.2 Future Work..... | 189 |
| Chapter 6. Concluding Remarks..... | 193 |
| References | 198 |
| List of Abbreviations..... | 234 |

Acknowledgements

First and foremost, I want to thank my supervisor Michelle Hawkins for her support and advice during this project. Doing a PhD during Covid was challenging, so thank you for supporting me and helping this thesis come to life despite all the obstacles in its way. I wouldn't be where I am today without you. Thank you also to Prof Daniela Barilla for being an excellent secondary supervisor and always a great help.

A special thank you to Dr. Katie Jameson who was an amazing help during her time in the Hawkins group. Many aspects of this thesis would not be here if not for Katie's patience, kindness, and willingness to share her knowledge.

A warm thank you to all friends and colleagues. A special mention to Aisha Syeda for her help with cloning, but also for being a kind presence and a great friend. I would also like to thank Chris Hill, Maria Chechlik and Tim Passchier for their tremendous help with protein purification, for answering my endless questions and for teaching me how to use, and not break, the AKTA.

Thank you to my dear friends: Rebecca Roberts, Lewis Byrom, Joseph McGrory, Miguel Velazquez, Sophie James and Charlotte Head. Thank you for being there for me over the past 2-3 years, for being a shoulder to cry on and a person to vent to. Thank you for putting a smile on my face during those rainy and hard days in the lab and during the covid pandemic.

I would also like to thank my parents, grandparents and in-laws, especially my mum Aleksandra McCabe, for love and support. Thank you for believing in me.

Finally, a very sincere and loving thank you to my wonderful fiancé, Bashir Muttawa. I would not be here without you. Thank you for your love, care, and endless support during this chapter of my life.

Declaration

I declare that the work presented in this thesis is an original report of my research, it has been written by me and has not been submitted for any previous degree at this or any other university.

The experimental work presented here was performed by myself, unless otherwise indicated. Any collaborative contributions have been indicated clearly and acknowledged. References have been provided for supporting literature and resources.

Dominika Warecka

January 2024

CHAPTER 1

INTRODUCTION

Chapter 1. Introduction

1.1. Helicases

Helicases are evolutionarily conserved enzymes able to translocate along single-stranded and double-stranded nucleic acid, displace nucleoprotein blocks and hydrolyse ATP in order to process DNA unwinding (reviewed in Raney et al., 2013).

Helicases are divided based on their nucleic acid processivity into DNA and RNA helicases. DNA helicases unwind DNA and have been identified across all life, including examples in bacteria, bacteriophages and viruses, both budding and fission yeast, in plants and in eukaryotes, including humans (reviewed in Tuteja and Tuteja, 2004; Frick and Lam, 2006; Dorn and Puchta, 2019; Dhar et al., 2020; fission yeast example Pizzul et al., 2022; bacteriophage example Chmielewska-Jeznach et al., 2022). DNA helicases are a potential medical target for cancer therapy, such as the RecQ and Iron-Sulfur DNA repair helicases (Datta and Brosh, 2018). RNA helicases process ribonucleic acid and coordinate gene expression. Some examples of RNA helicases, from multiple domains, include DDX1, DDX5, DDX17, DDX20 and RHA (Bourgeois et al., 2016). RNA helicases eIF4A, DDX3 and DDX5 are considered to be promising therapeutic targets (Sergeeva and Zatsepin, 2021). Rare helicases also exist that can process both DNA and RNA (Zhang and Grosse, 1994) or that process RNA-DNA hybrids, such as helicase Pif1 (Boué and Zakian, 2007; reviewed in Abdelhaleem, 2019) and *E. coli* Rho (Steinmetz et al., 1990).

TABLE 1.1 *E. COLI* DNA HELICASES

| DNA HELICASE | Function/Role | Reference |
|-------------------|---|--|
| DnaB | DNA replication, an essential part of the replisome | (LeBowitz and McMacken, 1986) |
| PriA | Replisome reloading | (Lee and Marians, 1990) |
| Rep | Nucleoprotein removal and DNA replication-transcription conflict resolution | (Yarranton and Gefter, 1979; reviewed in Matson and Kaiser-Rogers, 1990) |
| UvrAB | Nucleotide Excision Repair | (Oh and Grossman, 1989) |
| UvrD | Nucleotide Excision Repair, Mismatch Repair, RNA polymerase removal, nucleoprotein block removal, Tus removal | (Runyon et al., 1990) |
| Helicase IV | Unknown, but stimulated by SSB | (Wood and Matson, 1987; Dubaele, Lourdel and Chène, 2006) |
| RecQ | Recombination | (Umezu et al., 1990) |
| RecBCD | Homologous recombination and double-stranded break repair | (Roman and Kowalczykowski, 1992) |
| RuvAB | Recombination, Holliday junction migration | (Tsaneva et al., 1993) |
| Helicase I / TraI | Bacterial conjugative DNA transfer | (Abdel-Monem et al., 1976; Klinkert et al., 1980; Byrd et al., 2002) |
| RecG | Recombination, branch migration | (Whitby and Lloyd, 1995) |
| Helicase III | Unknown, ATPase function inhibited by SSB | (Yarranton et al., 1979; Matson and Wood, 1985) |
| DinG | SOS response protein, role unknown | (Voloshin et al., 2003) |

DNA helicases across all domains have been classified into six superfamilies (SF1-6) that vary in function and structure.

The first two superfamilies, SF1 and SF2, share roles in DNA repair, recombination, DNA replication and transcription regulation (O'Donnell and Li, 2018). They also share structural similarities, including a conserved helicase core (Singleton, Dillingham and Wigley, 2007). Both families also contain their own features, such as the Pif1-like region in SF1, and the

DEAD-box and Swi/Snf region in SF2 (reviewed in Fairman-Williams et al., 2010). Examples of SF1 helicases include UvrD and Rep helicases in *E. coli*, Srs2p and Sen1p in *S. cerevisiae*, and Pif1, Upf1 and SetX in humans (*Homo sapiens*) (Fairman-Williams et al., 2010). Examples of SF2 helicases include DinG, RecG and PriA in *E. coli*, Mph1p, Rad54p and Dhh1p in *S. cerevisiae*, and Rad54, DDX11, HELC1, and FANCM in *H. sapiens* (Fairman-Williams et al., 2010).

SF3-6 helicases are hexameric and either classified as AAA+ or RecA-like helicases (Trakselis, 2016). SF3 are AAA+ helicases that translocate in the 3' to 5' orientation and are found in DNA and RNA viruses (Trakselis, 2016). SF3 helicases function at the origin-binding domain and bypass the host regulation pathway to initiate replication. Examples include the LTag helicase of simian virus 40 (Li et al., 2003), Rep40 from the adeno-associated virus type 2 (James et al., 2003) and E1 viral initiator from the human papilloma virus serotype 18 (Abbate et al., 2004). SF4 5' to 3' helicases have a characteristic RecA-like domain and are involved in the initiation and elongation stages of DNA replication (Thomsen and Berger, 2009; Trakselis, 2016). Examples of SF4 helicases include DnaB helicase, the main replicative helicase of *E. coli*, mitochondrial helicase Twinkle, and the T7 bacteriophage helicase Gp4 (Trakselis, 2016). SF5 are a relatively understudied group of helicases and are similar to SF4 in that they also contain a RecA-like domain and translocate in the 5' to 3' orientation. An example of an SF5 helicase is the bacterial Rho RNA translocase (O'Donnell and Li, 2018). Lastly, SF6 AAA+ helicases translocate in the 3' to 5' orientation (Thomsen and Berger, 2009) and are involved in DNA replication. The replicative CMG helicase complex in eukaryotes and the MCM complex in archaea are the most common examples (O'Donnell and Li, 2018).

1.1.1. Superfamily 1 helicases

SF1 are one of the largest groups of helicases. Classification into this subfamily is dependent on the presence of certain motifs, such as motif III sequence GDxxQ (reviewed in Gilhooly et al., 2013) and motif IVa (Korolev et al., 1998) which are unique to SF1. Other motifs are found in both SF1 and SF2 and include I, Ia, II, V, VI and Q (figure 1.1 A) (Gilhooly et al., 2013; Tanner et al., 2003; Singleton et al., 2007; Abdelhaleem, 2019).

Motifs I and II, also called Walker A and Walker B, are strictly conserved sites for NTP binding and hydrolysis. They allow the helicase to act as a nucleic acid motor and as a translocase (Abdelhaleem, 2019; reviewed in Gilhooly et al., 2013). Motifs Ia, III and V meanwhile have been identified to be involved in ssDNA binding (Lee and Yang, 2006). SF1 helicases also share a similarity in their tertiary structure by forming four subdomains: 1A, 2A, 1B, and 2B (figure 1.1 B) (Bird et al., 1998; Meir and Greene, 2021).

SF1 is further divided into SF1A and SF1B sub-families based on the orientation of their DNA processing (3' to 5' or 5' to 3' orientation, respectively) (Singleton et al., 2007; Meir and Greene, 2021). Studies carried out on UvrD (SF1A), PcrA (SF1A) and RecD2 (SF1B) (figure 1.1 A) increased our understanding of the mechanism of translocation in the different orientations (figure 1.1 C). All three helicases bind to ssDNA with the 2A subdomain orientated towards the 5' end of the DNA and the 1A subdomain facing the 3' end (Velankar et al., 1999; Lee and Yang, 2006; Saikrishnan et al., 2009; Meir and Greene, 2021). The cleft between the 1A and 2A subdomains opens and closes when ATP is present or missing respectively (Meir and Greene, 2021). In the SF1A helicases (PcrA and UvrD), subdomain 1A binds to ssDNA when the cleft opens before the 2A subdomain grips the DNA, leading to a slide in the 3' to 5' orientation (Velankar et al., 1999; Soutanas and Wigley, 2000; Meir and Greene, 2021). For SF1B helicases (RecD2) the cleft closes when ATP is bound, causing the 2A subdomain, which has been tightly bound to the ssDNA, to weaken its binding and allow the helicase to 'slide' in the 5' to 3' orientation (Saikrishnan et al., 2009; Meir and Greene, 2021).

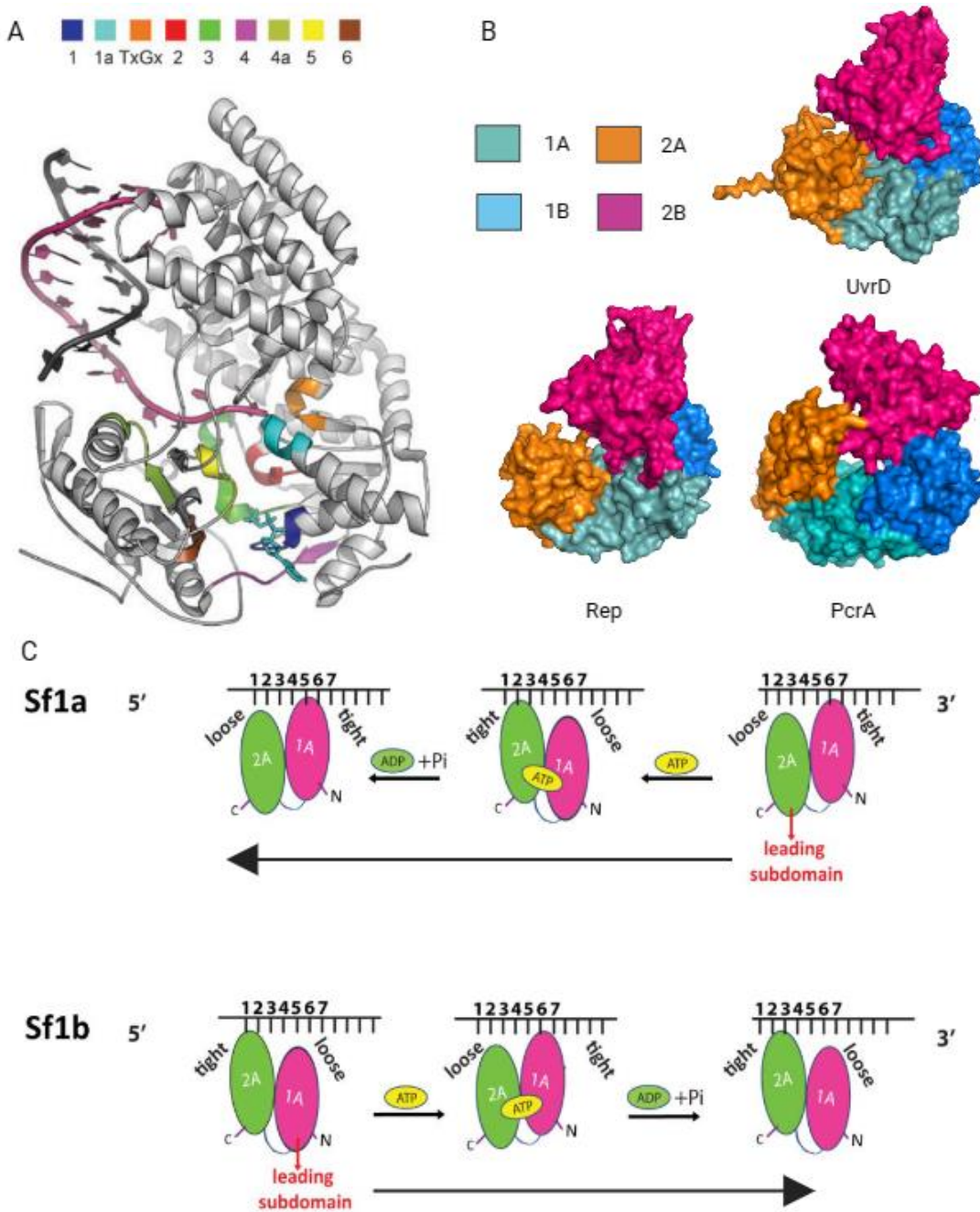


Figure 1.1 Superfamily 1 helicase translocation mechanism and examples. A. SF1 protein structure and common motifs. Adapted from Singleton et al., 2007. B. Protein structures of SF1 helicases UvrD (PDB 2IS1), Rep (PDB 1UAA) and PcrA (PDB 1QHH) showing tertiary structure similarities. The four subdomains of each helicase have been colour-coded: 1A teal, 1B, blue, 2A orange, 2B pink. C. ATP hydrolysis conducted when unwinding DNA by SF1A and SF1B helicases, which determines the orientation of translocation from 3' to 5' and from 5' to 3' respectively. Figure adapted from Meir and Greene, 2021. Figure created on Biorender.com.

SF1 helicases have also been divided into three different subgroups based on their homology to well-studied SF1 helicases: UvrD-like, Pif1-like and Upf1-like (Fairman-Williams et al., 2010; Gilhooly et al., 2013).

1.1.2 UvrD-like family

The most well-known helicases from the UvrD-like family are its namesake the *E. coli* UvrD (also known as Helicase II) and Rep, and *Bacillus subtilis* homologue, PcrA. These three helicases have similar known cellular functions, biochemical properties and primary structures, suggesting they are evolutionary related (Gilhooly et al., 2013; Syeda et al., 2019). In fact, PcrA is suggested to share the roles of both Rep and UvrD in *B. subtilis* (Petit et al., 1998).

UvrD helicase, described in detail in subsection 1.2, is involved in a number of mechanisms in *E. coli*, including mismatch repair (MMR) (Dao and Modrich, 1998; Yamaguchi et al., 1998; Mechanic et al., 1999; Mechanic et al., 2000), nucleotide excision repair (NER) (Epshtein et al., 2014), recombination (Veaute et al., 2005), Holliday junction resolution (Carter et al., 2012), and the removal of DNA-bound Tus (Bidnenko et al., 2006) and RNA polymerase (RNAP) (Hawkins et al., 2019). The helicase Rep has been shown to colocalise with the DNA replication fork (Guy et al., 2009; Atkinson et al., 2011; Syeda et al., 2019) and to remove DNA-bound proteins, such as RNAP, during DNA replication-transcription conflicts; a role that can be conducted by UvrD when Rep is absent (Guy et al., 2009; Hawkins et al., 2019). Rep has also been identified to have roles in DNA replication initiation (Brüning et al., 2016) and in replication restart (Heller and Marians, 2005). PcrA has been shown to bind tightly to transcription elongation complexes and to RNAP, as well as to limit the amount of DNA replication-transcription conflicts by suppressing the formation of R-loops (Merrikh et al., 2015; Urrutia-Irazabal et al., 2021). Genetic analysis has also linked PcrA to UV repair and rolling-circle replication, though the exact mechanism has not been identified (Petit et al., 1998).

1.2. UvrD structure and function

UvrD is an *E. coli* DNA helicase belonging to the SF1A subfamily and the UvrD-like family of helicases. UvrD translocates on ssDNA and unwinds dsDNA in the 3' to 5' orientation and is able to displace nucleoprotein blocks (Matson, 1986; Lee et al., 1989; Bidnenko et al., 2006). As with all SF1 helicases, UvrD contains four subdomains. The Rec-A like subdomains 1A and 1B share a hydrophobic core, while 2A and 2B are joined by salt bridges formed by amino acids K389 to D115 and R396 to D118 (Lee and Yang, 2006). UvrD also contains a mostly uncharacterised C-terminal tail (Lee and Yang, 2006; Manelyte et al., 2009; reviewed in Yokota, 2022). Recent biomolecular nuclear magnetic resonance (NMR) spectroscopy investigated the carboxy-terminal of UvrD and showed a Tudor-domain-like fold, made of five β -strands in a strongly bent antiparallel orientation (Kawale and Burmann, 2020). In addition to the nine motifs identified in SF1 helicases, UvrD also has seven unique sequence motifs Ib, Ic, Id, IVb, IVc, Va and VIa, found to participate in DNA binding, or in 1B and 2B domain interactions (Lee and Yang, 2006)

1.2.1 UvrD subdomain functions

Lee and Yang crystallised UvrD helicase alongside a non-hydrolysable ATP analog, adenylyl-imidodiphosphate, to characterise the ATP binding of UvrD (figure 1.2 A). They demonstrated that ATP binds between the 1A and 2A subdomains of UvrD, with the adenine base found between motif IV (Y283) and motif I (R37) (Lee and Yang, 2006). The 2'-OH of ATP is weakly bound to R37, while 3'-OH has a stronger bond to E566 (motif V) (Matson, 1991; reviewed in Lee and Yang, 2006). For successful ATP hydrolysis, the β and γ phosphates of ATP coordinate with T36 (motif I), D220 and E221 (motif II/Walker B) to acquire a Mg^{2+} ion (Lee and Yang, 2006). Binding of the ATP analogue induces a 20° rotation of the 2A subdomain (Lee and Yang, 2006).

While the 1A and 2A subdomains of UvrD are important for ATP binding, the 2B subdomain has been found to have a significant role in DNA unwinding (Jia et al., 2011). When the UvrD structure was first visualised bound to nucleic acid (Lee and Yang, 2006), the 2B subdomain appeared to be 'closed' (figure 1.2 A). When generating the apo structure of UvrD in high salt conditions (600 mM NaCl) Jia and coworkers described a 160° rotation of the 2B subdomain into an 'open' position using the hinge between the 2B and 2A subdomains (figure 1.2 B) (Jia et al., 2011). Fluorescence resonance energy transfer (FRET) analysis showed that binding of a MutL dimer (protein involved in mismatch repair, section 1.3) to a UvrD monomer caused a rotation of the UvrD 2B subdomain from 'closed' towards the 'open' conformation, generating an 'intermediate' state when the complex is formed (Ordabayev et al., 2018, 2019).

The function of the C-terminal domain of UvrD has not been fully identified and the region has not been crystallised to visualise its structure. The C-terminal 'tail' has however been identified to be involved in UvrD protein interaction, including interactions with nucleotide excision repair (NER) protein UvrB (Manelyte et al., 2009) and the transcription machinery RNA Polymerase (RNAP) (Gwynn et al., 2013; Kawale and Burmann, 2020). The structure of the C-terminal domain of a UvrD homologue PcrA has however been crystallised, showing a Tudor-like fold (Sanders et al., 2017), which agrees with the NMR estimations for UvrD helicase C-tail (Kawale and Burmann, 2020).

Mechanic and coworkers conducted a yeast two-hybrid test on UvrD with deletion of the last 40 amino acids from its C-terminal, UvrD Δ 40C (Mechanic et al., 1999a; 1999b). They showed that UvrD Δ 40C was still able to unwind DNA and take part in both NER and MMR (Mechanic et al., 1999a). Genetic analysis of UvrD with the deletion of the last 102 and 107 amino acids (UvrD Δ 102C and UvrD Δ 107C, respectively), showed that the mutants were no longer able to participate in both NER and MMR repair mechanisms (Mechanic et al., 1999b). UvrD Δ 102C was also not able to bind ssDNA, *in vitro*, and exhibited a reduced ATPase activity (Mechanic et al., 1999b).

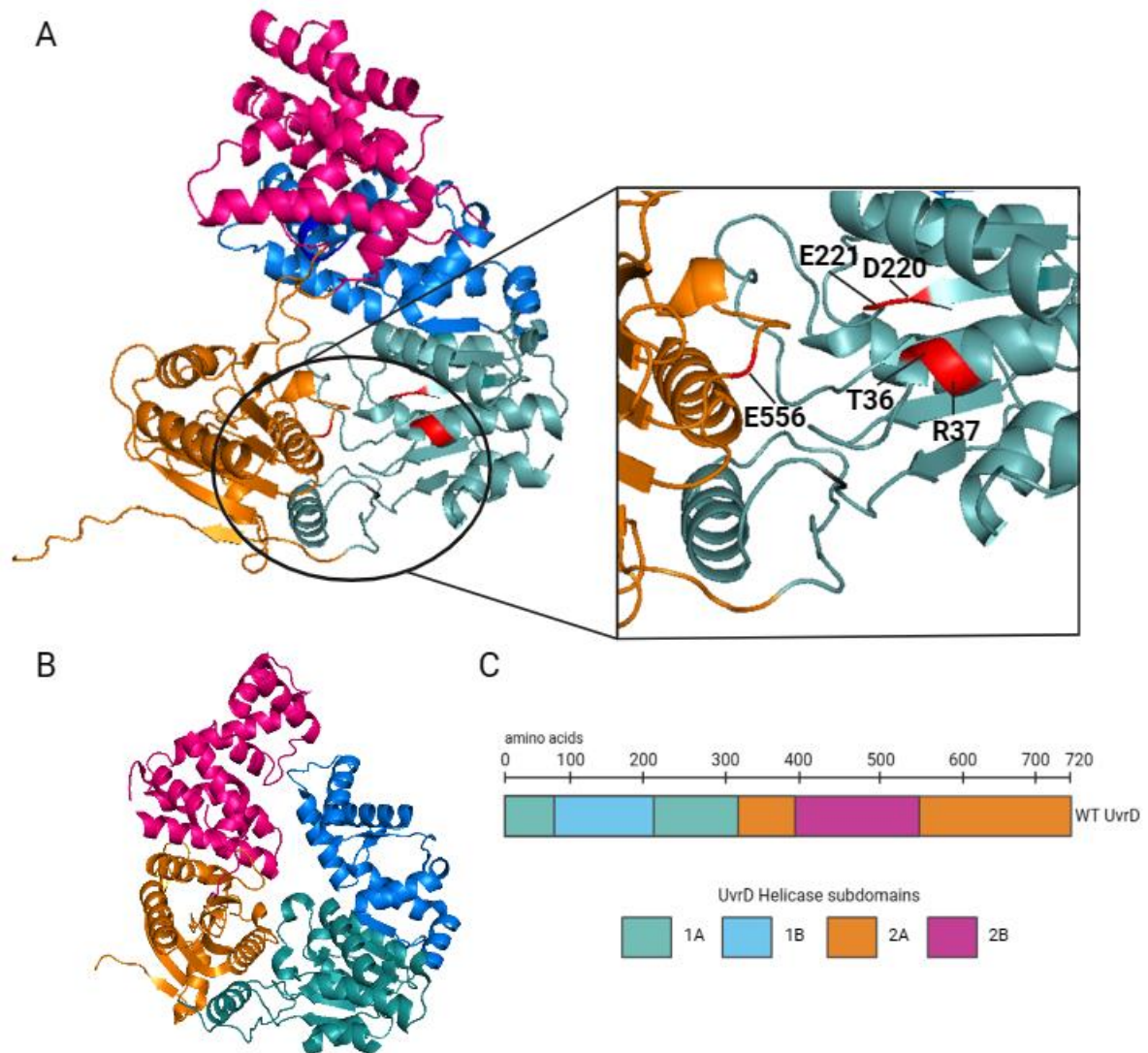


Figure 1.2 UvrD helicase structure. A. The four subdomains of UvrD have been colour coded as per figure 1.1. ATP binding residues have been labelled in the magnification panel and colour-coded in red and can be mostly found in the 1A subdomain, with E556 found in the 1B subdomain. UvrD structure from Lee and Yang, 2006 (PDB ID 2IS1). B. Apo UvrD structure without DNA with an open 2B subdomain (pink). UvrD structure from Jia et al., 2011 (PDB ID 3LFU). C. Distribution of the four subdomains across the amino acid chain of UvrD helicase. Figure created on biorender.com.

Manelyte and coworkers conducted further studies on C-terminal truncation and found that UvrD Δ 73C retained its ATPase ability but had a slightly reduced ssDNA binding affinity; and that UvrD Δ 102C had a significantly reduced ssDNA binding affinity, had no ATPase ability, and was unable to assist in DNA repair mechanisms (Manelyte et al., 2009). The loss of ssDNA binding ability hints to a role of the C-terminal in ssDNA binding and potentially translocation, though it is also likely that the condition was affected function was caused by region deleted from the 2A domain.

1.2.2. UvrD as a monomer, dimer, and tetramer

UvrD has been found to function as a monomer (Mechanic et al., 1999; Lee and Yang, 2006), a dimer (Maluf et al., 2003a; Maluf et al., 2003b; Sun et al., 2008; Yokota et al., 2013; Lee et al., 2013; Comstock et al., 2015; Nguyen et al., 2017; Yokota, 2020), and even a tetramer (Wollman et al., 2023).

The first monomeric model was presented by Mechanic and coworkers, showing that while UvrD Δ 40C could not dimerise, it could still unwind dsDNA (Mechanic et al., 1999a). However further sedimentation studies contradicted this by showing UvrD Δ 40C dimerisation (Maluf et al., 2003a; 2003b). Single molecule analysis also showed that two or even three UvrD Δ 40C molecules were required for DNA unwinding. UvrD Δ 40C was however found to dimerise less frequently than WT UvrD (Yokota, 2020). UvrD monomers form a complex with a MutL dimer during the mismatch repair mechanism (MMR) (section 1.3.1) (Ordabayev et al., 2018), to RNAP (Epshtein, 2015). UvrD dimer was however found to be necessary to conduct UvrD-mediated transcription coupled repair (TCR) (section 1.3.2.2) (Epshtein et al., 2014; Epshtein, 2015).

Support towards the dimer model was however presented by Maluf and coworkers who found that UvrD unwound DNA more efficiently when the UvrD/DNA ratio was greater than or equal

to two (Maluf et al., 2003a; 2003b) and by Sun and coworkers who used magnetic tweezers to show dimerisation (Sun et al., 2008; reviewed in Yokota, 2022). Other evidence for the dimer model includes single-molecule direct visualisation studies which found that 2-3 WT UvrD molecules participated in DNA unwinding (Yokota et al., 2013), while a monomer was blocked at a ssDNA/dsDNA junction and had to be unblocked through addition of another monomer (Lee et al., 2013). Comstock and coworkers also showed limited unwinding of a WT monomer UvrD, while two UvrD molecules allowed for long-distance unwinding (Comstock et al., 2015). Lastly, Nguyen and coworkers showed that when UvrD was prebound to DNA, the binding of a second UvrD closed the 2B subdomain and allowed for DNA unwinding to begin (Nguyen et al., 2017).

Lastly, UvrD has also been found to form tetramers through *in vivo* photobleaching analysis (Wollman et al., 2023) and through analytical ultracentrifugation (Maluf and Lohman, 2003). Maluf and Lohman found that UvrD tetramers, and even octamers, become favoured at temperatures higher than 35 °C. When investigating the effect of salt on UvrD, they found that concentrations above 150 mM NaCl favoured monomers and dimers, but <150 mM showed populations of monomers, dimers and tetramers. Similarly, an increase in glycerol concentration also decreased the amount of UvrD tetramers in the population (Maluf and Lohman, 2003). Wollman and coworkers detected tetramers *in vivo* through slimfield microscopy using mGFP-UvrD. They found that tetrameric mGFP-UvrD was often colocalised with mCherry-DnaQ, a protein involved in DNA replication, suggesting that tetrameric UvrD helicase was colocalised to the replication fork (Wollman et al., 2023).

Based on the literature highlighted, UvrD likely acts as a monomer, dimer, and tetramer *in vivo*, switching states depending on its varying roles in the cell.

1.3. DNA repair and UvrD

1.3.1 Mismatch Repair

1.3.1.1 Mismatch repair in *E. coli*

During DNA replication, the DNA replication machinery, the replisome, creates a copy of the genetic material of the cell. *E. coli* DNA polymerase has a high fidelity, with an approximate error rate of 5×10^{-10} per base pair (Drake et al., 1998). Errors which can occur include an insertion of a base (10^{-5}), a proofreading (10^{-2}), and a mismatch of a base (10^{-3}) (Schaaper, 1993; Fijalkowska et al., 2012).

The mismatch repair mechanism (MMR) is a DNA repair mechanism responsible for repairing DNA mismatches, first discovered in 1986 when the binding of MutS to mismatched nucleotides was detected (Su and Modrich, 1986). While correcting DNA mismatches is not always crucial to cell survival, but it is important in ensuring that all genomic information of the cell is correct for protein production. A mismatched base can cause a change in the amino acid sequence of proteins or can even alter the reading frame of genes through insertion of an early stop codon.

The first step to successful MMR in *E. coli* (figure 1.3) is the correct function of Dam methyltransferase – an enzyme responsible for methylating the N⁶ of adenine within palindromic GATC sites on DNA (Hattman et al., 1978; Løbner-Olesen et al., 2005). After DNA replication, DNA is found in a hemi-methylated state, with the template strand being methylated and the nascent strand unmethylated. This allows for a recognition of freshly replicated DNA regions by their hemi-methylation. During MMR these hemi-methylated GATC sites are used as signals for freshly replicated DNA and to aid recognition of which strand was not the template and was therefore incorrectly replicated (Campbell and Kleckner, 1990; Marinus, Poteete and Arraj, 1984; Marinus, 1976; Herman and Modrich, 1981).

The mismatch recognition protein MutS scans newly replicated DNA for mismatches and binds to them (Su and Modrich, 1986). MutS forms a homodimer around the mismatch by specifically interacting with the incorrect base and non-specifically interacting with surrounding nucleotides (Sixma, 2001). A MutL dimer binds to the MutS:DNA complex and stabilises it, preventing MutS dissociation which would otherwise occur after 15 secs in ATP-rich conditions (Schofield et al., 2001). MutS:MutL complex activates MutH to cleave the hemimethylated d(GATC) sites nearby to the mismatch on the unmethylated strand (Au et al., 1992). Binding of the N-terminal of MutL and C-terminal of MutH partly enhances the endonuclease activity of MutH and promotes cleavage of the unmethylated DNA strand (Hall and Matson, 1999). The process requires interaction of MutH with the MutS:DNA:MutL complex and ATP hydrolysis by MutL (Au et al., 1992).

After the mismatched strand is cleaved, MutL recruits UvrD and loads the helicase onto the nicked DNA. Importantly, MutL ensures that UvrD is loaded in the correct orientation, so that DNA is unwound towards the mismatch, rather than away from it (Dao and Modrich, 1998; Yamaguchi et al., 1998; Mechanic et al., 2000). The binding of UvrD and MutL into a stable MutL:UvrD:ssDNA complex (Hall et al., 1998) leads to a 130-160° rotation of the 2B subdomain of UvrD (Ordabayev et al., 2019, 2018). Rotation of the 2B subdomain into an open conformation increases UvrD helicase's affinity for DNA and its DNA processivity (Jia et al., 2011; Ordabayev et al., 2019).

During the last stage of MMR, once dsDNA is unwound, the unmethylated ssDNA is excised by 3' to 5' exonucleases ExoI and ExoX and the 5' to 3' exonucleases RecJ and ExoVIII (Burdett et al., 2001). The single-stranded binding protein (SSB) stabilises the ssDNA template until DNA polymerase III closes the gap, guided by MutL and MutS (López De Saro et al., 2006). Finally, DNA ligase seals the nascent strand (Lahue et al., 1989).

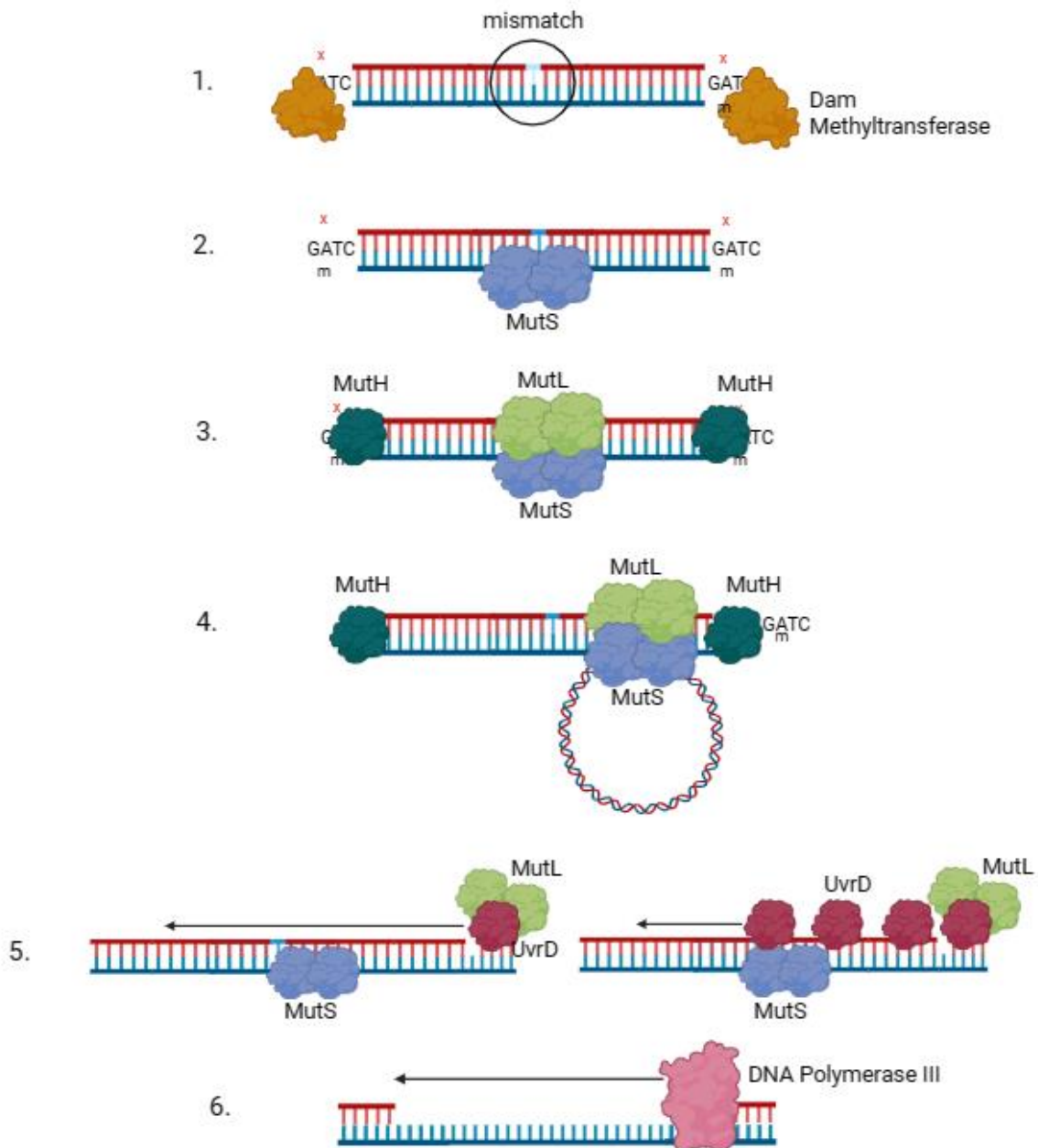


Figure 1.3 Mismatch repair mechanism in *E. coli*. 1. Dam methyltransferase methylates GATC sites before DNA replication. Only the template strand is methylated in newly replicated DNA 2. After DNA replication, MutS detects and binds to mismatches. 3. MutL dimer binds to MutS and MutH binds to hemimethylated GATC sites. 4. MutL:MutS pumps the DNA until it encounters a MutH site bound to a hemimethylated GATC site. MutH cleaves the site 5. MutL loads UvrD helicase on to DNA. Two models exist for loading either a single UvrD molecule or multiple UvrD's by MutL to unwind the region. 6. DNA polymerase III replicates the created ssDNA gap. Created using biorender.com.

1.3.1.2 MutL and UvrD – the power couple

How do MutL and UvrD interact during MMR? Over the past few decades two contradicting models emerged describing MutL loading of UvrD onto DNA during MMR (Mechanic et al., 2000; Ordabayev et al., 2019).

In the first model, presented by Mechanic and coworkers, MutL loads UvrD onto nicked DNA at a nearby hemi-methylated d(GATC) site in the correct orientation towards the mismatch. In this model, MutL does not remain in the complex (Mechanic et al., 2000), but instead loads several UvrD molecules. The first UvrD loaded receives a 'boost' from MutL to allow for a short increase in dsDNA processivity. This is followed by MutL reloading UvrD molecules to the same site, allowing them to translocate along the ssDNA until they reach the dsDNA region which they unwind at their modest processivity of 40-50 bp (Ali et al., 1997; Mechanic et al., 2000; Matson and Robertson, 2006). This model is supported by the oligomeric binding of UvrD suggested by Ali, Maluf and Lohman (Ali et al., 1999).

In the second model, put forward by Ordabayev and coworkers, MutL not only loads UvrD onto the nicked DNA, but also remains in the UvrD:MutL complex. This increases the processivity of UvrD and allows UvrD to unwind the whole region past the mismatched base (Ordabayev et al., 2018). Their evidence was based on single-molecule fluorescence studies which showed that MutL dimer binding to an inactive UvrD monomer activates it and increases its DNA processivity (Ordabayev et al., 2018). The increase in processivity was linked to the rotation of the 2B subdomain of UvrD caused by the binding of the MutL dimer (Ordabayev et al., 2019). The logic of the hypothesis was that if MutL causes the rotation of the 2B subdomain (Jia et al., 2011), which has been shown to increase the processivity of UvrD helicases then it must remain bound to continue stimulating UvrD's helicase ability. The Mechanic paper that published the first model also showed that the MutL:UvrD:ssDNA complex was more stable than the UvrD:ssDNA complex (Mechanic et al., 2000), evidence which supports the Ordabayev model.

While the models disagree about the persistence of the UvrD:MutL complex, both models require UvrD:MutL binding. In 1998, Hall and coworkers conducted a yeast two-hybrid test to determine which regions of UvrD and MutL might be responsible for UvrD:MutL complex formation (figure 1.4 A). When amino acids 1-397 of MutL were removed the protein was able to interact with UvrD, however deletion of 1-438 amino acids prevented the interaction. This suggested that UvrD interacts with amino acids 398-439 of MutL (Hall et al., 1998). Deletion analysis by Matson and Robertson, found that removal of amino acids 197-438 and 559-615 prevented MutL from forming a complex with UvrD (Matson and Robertson, 2006). Crystal structure of the C-terminal of MutL showed a conserved hydrophobic patch on the surface of MutL in residues 439-459 and 597-615 predicted to have a role in protein interaction (Kosinski et al., 2005). The C-terminal of MutL is however associated with dimer formation, so an alternative reason for the lack of UvrD interaction with MutL Δ 559-615 is that the deletion of the C-terminal prevented MutL dimerisation and limited its function (Kosinski et al., 2005; Matson and Robertson, 2006).

The yeast two-hybrid analysis for MutL binding to UvrD found that deletion of amino acids 1-101 and 680-720 (separately) from UvrD prevented its interaction with MutL (figure 1.4 B) (Hall et al., 1998). The C-terminal result was contradicted by Ordabayev and coworkers, who found that the truncated UvrD Δ 73, 647-720 deletion, could still be activated by MutL (Ordabayev et al., 2018). The unstructured C-terminal of UvrD has however been shown to interact with other proteins, such as UvrB during NER (Manelyte et al., 2009) and RNAP (Gwynn et al., 2013; Kawale and Burmann, 2020), and might be an interesting future target for UvrD:MutL analysis.

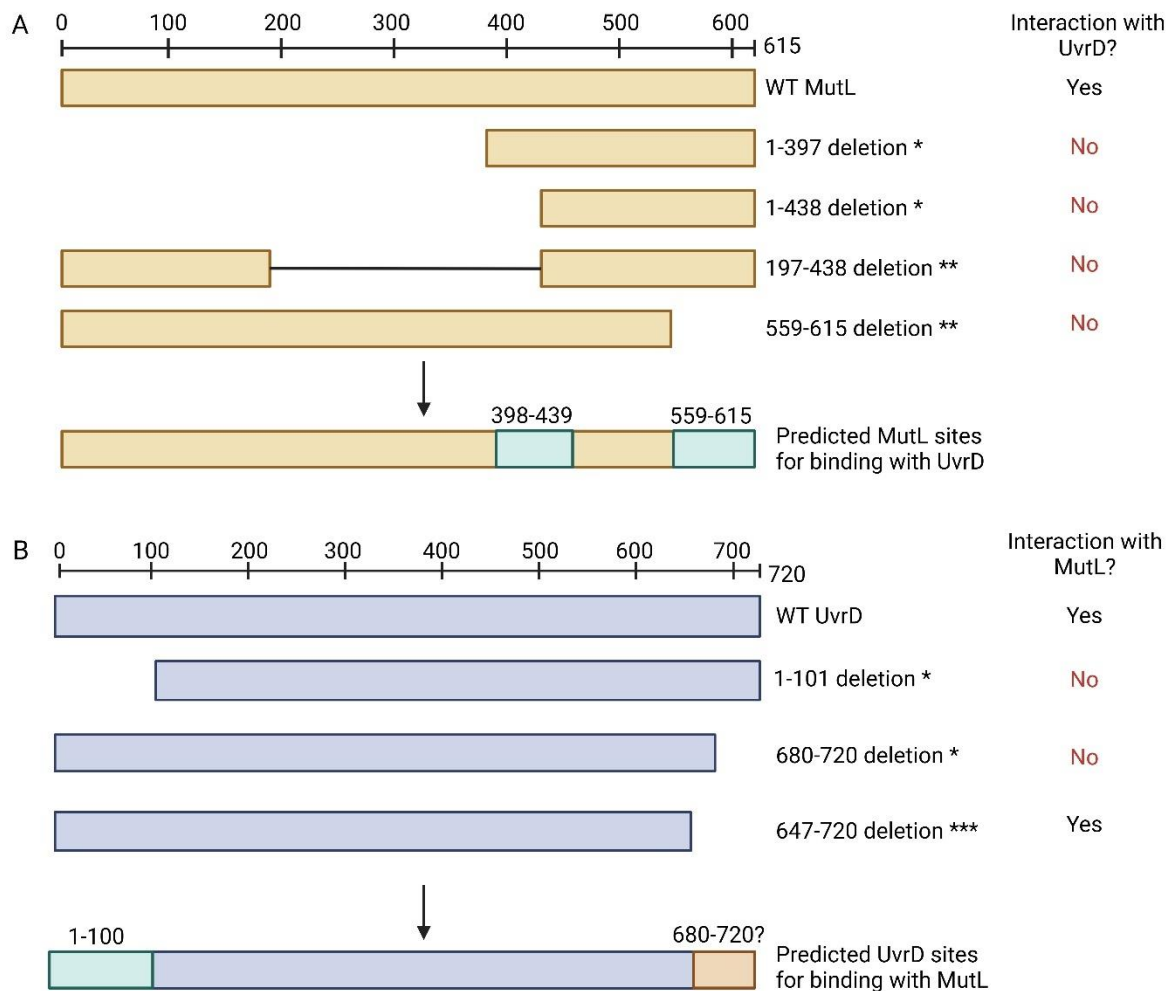


Figure 1.4 Summary of predicted binding sites for the UvrD:MutL complex from the literature. A. MutL deletions tested in literature for interaction with UvrD helicase and their outcomes. Amino acids 398-439 and the C-terminal of 559-615 were suggested to be responsible for MutL interaction with UvrD. **B.** UvrD deletions tested in literature for interaction with MutL and their outcomes. Amino acids 1-100 and the C-terminal of 680-720 were suggested to be responsible for UvrD interaction with MutL, though the C-terminal deletion presented varying results. * Hall et al., 1989, ** Matson and Robertson 2006, *** Ordabayev et al., 2018. Created on biorender.com

1.3.1.3 Mismatch repair in Eukaryotes and Archaea

In eukaryotic cells, strand discrimination is not dependent on hemi-methylation of d(GATC) sites. No MutH homologs have been identified (Marti et al., 2002) and the mechanism for strand discrimination has not yet been determined. Five MutS homologs (MSH), three of which can recognise a mismatch (Reenan and Kolodner, 1992; Fishel et al., 1993; Palombo et al., 1995; Drummond et al., 1995), and four MutL homologs (MLH) (Liskay et al., 1999; Flores-Rozas and Kolodner, 1998), with MutL α (MLH1-PMS2) being essential (Torres et al., 2022), have been identified in eukaryotes. Other *E. coli* MMR protein homologues include ExoI (Tishkoff et al., 1997, 1998), RPA, a single-strand binding protein (Ramilo et al., 2002), DNA polymerase δ , and DNA ligase (Longley et al., 1997; Zhang et al., 2005)

MutS eukaryote homologue complexes MSH2:MSH6 and MSH2:MSH3 are responsible for recognising the mismatched base (Acharya et al., 1996; Downen et al., 2010) and for recruitment of the MutL homologue (complex MLH1-PMS2) (Prolla et al., 1994; Mendillo et al., 2005; 2009). When bound to a mismatched base, MSH2:MSH6 undergoes ATP hydrolysis and forms a sliding clamp that remains associated with the mismatch while conducting hydrolysis-independent diffusion towards a downstream signalling region (Gradia et al., 1999). Single molecule FRET analysis showed that the MSH sliding clamp, which is more stable than the bacterial MutS clamp, scans the DNA by translocating at a speed of approximately 700 bp per second before pausing for 3 seconds at a mismatch (Jeong et al., 2011). MSH2:MSH6 then forms a high affinity bond, dependant on ATP and magnesium, with MLH1:PMS2 (Mendillo et al., 2005). Interestingly, MLH1:PMS2 in eukaryotes and budding yeast, *S. cerevisiae*, is an endonuclease, while the homologous *E. coli* protein does not have this function (Kadyrov et al., 2006, 2007). Formation of the 5' excision requires an interaction between the MutS α complex and the ExoI restriction enzyme and is regulated by RPA (reviewed in Fishel, 2015). The 3' excision requires a complex formed of MSH, MLH and PMS that interacts with PCNA and is loaded onto the strand before activating the MLH:PMS endonuclease (reviewed in Fishel, 2015).

MMR has also been found to take place in some archaea, though the process lacks the homologues for the MutL, MutS, and MutH enzymes (reviewed in Marshall and Santangelo, 2020). NucS/EndoMS nuclease, a prominent complex in archaeal MMR, can recognise a mismatch and cleave the backbone (a role accomplished by the MutS, MutL, and MutH proteins in *E. coli*) through dimer formation and 'base-flipping' while forming a complex with the PCNA clamp (Creze et al., 2012). The NucS/EndoMS pathway produces a dual DNA cut, which leads to a double-stranded break (DSB) and requires further repair. This suggests that the NucS/EndoMS MMR pathway is likely closely linked to the archaeal homologous recombination double-stranded break repair pathway (Marshall and Santangelo, 2020)

Some archaea, such as *Methanosaeta thermophila*, do however encode MutS and MutL analogues and perform MMR that occurs with similar initial steps to eukaryotic MMR (Minobe et al., 2019). These homologues are however non-essential for *M. thermophila* (Busch and DiRuggiero, 2010), and together with the lack of a MutH homolog, suggest an alternative pathway must be present (reviewed in Marshall and Santangelo, 2020). Recent evolutionary studies on Asgard archaea discovered an archaeal origin for MMR in eukaryotes (Hofstatter and Lahr, 2021).

1.3.2 Nucleotide Excision Repair

Nucleotide excision repair (NER) was first identified in 1964 when Setlow and Carrier noticed the disappearance of thymine dimers caused by UV radiation in *E. coli* (Setlow and Carrier, 1964). UV radiation has been found to promote formation of a range of DNA lesions; including thymine dimers, cyclobutane pyrimidine dimers and photoproducts (Reardon and Sancar, 2005). DNA damage can also be caused by chemical agents, such as carcinogens acetylaminofluorene and benzo(a)pyrene, and drugs tamoxifen and nitrogen mustard (Reardon and Sancar, 2005). DNA damage has to be repaired to maintain genomic integrity.

During NER the UvrA₂B₂ (UvrAB) complex detects DNA damage. UvrB is made of five subdomains: 1a, 1b, 2, 3, and 4 (Manelyte et al., 2009) and contains a flexible, hydrophobic beta-hairpin. UvrB inserts the hairpin between DNA and uses residues Y95 and Y96 to detect DNA damage (Moolenaar et al., 2001). UvrAB flips the 3' end of the lesion and its base-pairing partner in the non-damaged strand out of the helix (Malta et al., 2008) with the help of four stable tyrosine residues (Moolenaar et al., 2001). The UvrAB complex breaks apart and UvrB binds to the DNA and recruits UvrC to form a UvrC:UvrB:DNA complex. This complex can translocate on DNA, allowing UvrC to nick the DNA twice: at the fourth and fifth nucleotide of the 3' end of the lesion, and at the 8th nucleotide of the 5' end of the lesion (van Sluis et al., 1983; Zou et al., 1997; reviewed in Manelyte et al., 2009). UvrD is then recruited to displace UvrC and to unwind the DNA to remove the DNA lesion. DNA polymerase I and ligase are then able to fill the gap and ligate it to the rest of the strand (reviewed in Manelyte et al., 2009; Brosh, Jr., 2014; Epshtein, 2015).

Two types of NER have been identified in prokaryotes: global genomic repair (GGR) and transcription coupled repair (TCR). GGR can occur anywhere on the genome and follows the NER mechanism as described above. TCR is triggered by signals from transcribing RNAP and is responsible for processing lesions on the transcribed strand of expressed genes (Selby and Sancar, 1990; reviewed in Epshtein, 2015; Kamarthapu and Nudler, 2015).

1.3.2.1. Transcription coupled repair

TCR was first described by Evelyn Witkin in 1956 as a phenomenon where protein synthesis was briefly inhibited after irradiation with UV light. Witkin called it mutation frequency decline (Witkin, 1956). This was later confirmed by Mellon and Hanawalt who noticed that transcribed DNA was repaired faster than non-transcribed DNA (Mellon and Hanawalt, 1989). In 1991, Witkin linked the mutation frequency decline to the *mfd* gene and called the protein produced the transcription repair coupling factor (TRCF) or simply Mfd (Selby et al., 1991). Mfd was found to be recruited to the site of DNA damage to help move stalled RNAP and nascent RNA to expose the DNA lesion in need of repair (Selby et al., 1991; Selby and Sancar, 1993). This allowed the NER pathway to repair the damaged DNA (Selby and Sancar, 1995).

Mfd is a large 130 kDa translocase with eight subdomains (D1a, D1b, and D2-D7 connected by flexible linkers) that contains an ATPase domain and multiple RecA motifs. Mfd acts as a monomer and belongs to the DExH/D family of SF2 translocases (Selby and Sancar, 1993b; Deaconescu et al., 2006). Mfd and RNAP directly interact via the RNAP-interaction domain (RID) of Mfd and the beta-subunit of RNAP (figure 1.5 A). The Mfd and RNAP interaction changes the conformation of Mfd and stimulates its motor activity (Smith et al., 2012). Active Mfd is able to displace RNAP by pushing it downstream in an ATP dependant manner (Park et al., 2002; Smith and Savery, 2005; Howan et al., 2012) to make space for Mfd interaction with UvrA; triggering the start of NER (Selby and Sancar, 1993, 1995).

During the last active stage of transcription RNAP is engaged in transcribing DNA into RNA by adding nucleotides to the 3' end of the growing RNA and therefore forming the elongation complex (EC) (Summarised in Nudler, 2009). To remove RNAP, Mfd binds to dsDNA upstream from stalled RNAP and pushes RNAP forward until it either resumes mRNA elongation or is dislodged (reviewed in Epshtein, 2015). An Mfd limitation to RNAP removal is the required long dwell time of EC after RNAP stalling (Howan et al., 2014) which Mfd detects by binding to the 5' region of the EC (Park et al., 2002; Smith and Savery, 2005). Allowing for

RNAP to remain stalled for an extended period of time for Mfd-mediated TCR is not ideal and can lead to an increase in DNA replication-transcription conflicts. To explain the long dwell time required, Epshtein suggested that Mfd-mediated TCR might be necessary for irreversibly stalled RNAP and ECs, but might not be the only method used by cells to recover stalled RNAP blocks (Epshtein, 2015).

1.3.2.2. UvrD-mediated TCR

In 2014, Epshtein and coworkers published an alternative TCR route for *E. coli*; utilising UvrD helicase instead of Mfd (figure 1.5 B) (Epshtein et al., 2014). This route was not identified earlier as the deletion of UvrD makes cells UV sensitive (Manelyte et al., 2009) and prevents the completion of NER, therefore sheltering this pathway from discovery.

An estimated 2400-3000 molecules of UvrD, with some estimations as high as 5000 molecules, can be found in the cell (Arthur and Eastlake, 1983; Klinkert et al., 1980). This places the UvrD concentration at approximately between 1.4-4 μ M (Veaute et al., 2005). While these estimates are very high, it is important to consider that UvrD is an SOS protein and would therefore be overexpressed when cell is under stress. Additionally, when considering the role of UvrD in TCR, it is interesting to notice the similarities between the estimated concentrations of UvrD and RNAP, where RNAP is found at 1600-8000 molecules per cell, with 400-2000 being active at one time (Shepherd et al., 1980).

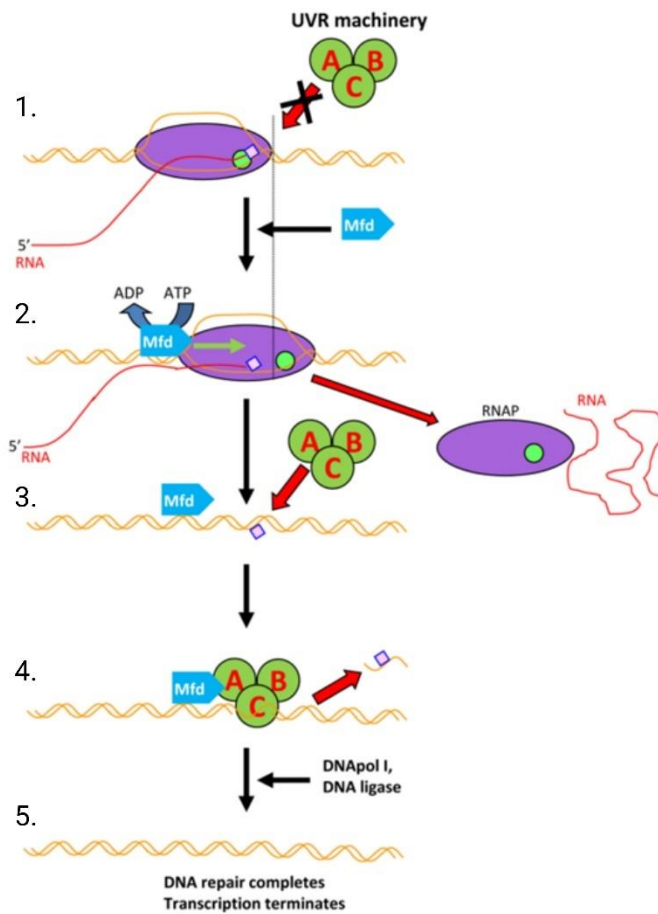
UvrD has been found to be bound to the upstream portion of the transcription bubble at the elongation complex (EC) of RNAP (Epshtein et al., 2014). UvrD unwinds the replication bubble in the 3' to 5' orientation, which causes for RNAP to be pulled backwards. (Epshtein et al., 2014). The EC acts as a perfect UvrD substrate, as the single-stranded non-transcribed DNA strand in the bubble is not only fully exposed, but also at least 10 bp long for UvrD binding (Korzheva et al., 2000). The abundance of UvrD in the cell and preloading at the ECs makes

it readily available to displace stalled RNAP faster than Mfd, giving UvrD-mediated TCR an advantage over Mfd-mediated TCR.

However, while UvrD-mediated TCR can be seen as the faster and preferable route, it does have disadvantages. RNAP backtracking has been linked to an increase in DSBs (Dutta et al., 2011), which can lead to a decrease in genomic stability. Epshtein suggests that the high abundance of UvrD in cells could potentially allow it to conduct all TCR, but that this could also prevent transcription from ever being completed and could generate too many DSBs for the cell to repair (Epshtein, 2015). GreA and GreB proteins have been found to regulate UvrD-mediated TCR activity by stimulating the cleavage activity of RNAP. This removes the 3'-end of nascent RNA in back-tracked complexes (Laptenko et al., 2003) and restores the UvrD back-tracked RNAP complexes to complete transcription (Epshtein et al., 2014). Without GreA/B regulation, UvrD could be too efficient and prevent any transcription from being complete (reviewed in Epshtein, 2015).

The Nudler group suggested a model of distinguishing when Mfd- and UvrD-mediated TCR will take place (Epshtein, 2015). Mfd-mediated TCR is mostly active in non-stressed cells, allowing for a steady, but not-rushed, stalled RNAP removal without the risk of inducing further breaks (Epshtein, 2015). In non-stressed cells, UvrD monomer is bound to RNAP, ready for upcoming DNA damage and for SOS response (Arthur and Eastlake, 1983). When cells are stressed, the SOS response overexpresses UvrD three-fold through Lex-dependent upregulation (Easton and Kushner, 1983). Since UvrD has been shown to act as a dimer when pushing RNAP backwards (Maluf et al., 2003; Epshtein et al., 2014), the three-fold increase in UvrD concentration would encourage dimer formation, allowing UvrD to take charge of TCR. This model links the ability of UvrD to mediate TCR and its role in the SOS response and proposes that UvrD-mediated TCR is an SOS response pathway.

A) Mfd-mediated TCR



B) UvrD-mediated TCR

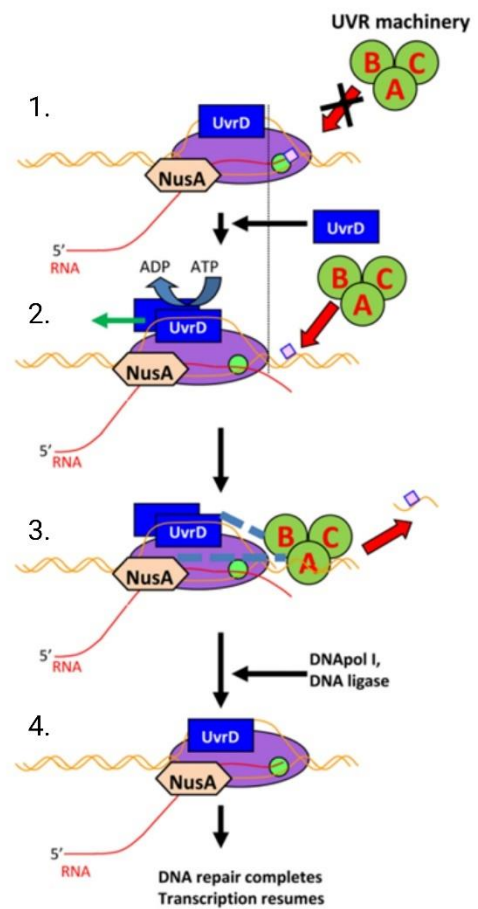


Figure 1.5 Mfd and UvrD-mediated TCR. A) Mfd-mediated TCR steps. 1. DNA lesion is blocked by stalled RNAP and the UvrABC machinery is unable to reach it. 2. Mfd binds upstream of RNAP and uses ATP hydrolysis to push RNAP forward until it is dislodged. 3. UvrABC recognises the DNA lesion. 4. Mfd assists UvrABC in DNA lesion removal and repair. 5. DNA Polymerase I and DNA ligase are employed to synthesise the region. B) UvrD-mediated TCR steps. 1. UvrD and NusA are already bound to RNAP when it stalls. 2. UvrD uses ATP hydrolysis to pull RNAP backwards, exposing the DNA lesion. 3. RNAP remains bound to DNA while UvrABC removes the DNA lesion and repairs the DNA. 4. DNA Polymerase I and DNA ligase synthesise the region before RNAP resumes transcription. Figure adapted from Epshtein 2015.

1.3.3 Double-stranded break repair and recombination in *E. coli*

DSBs are defined as the breakage of both DNA strands in the duplex. They cause a separation of the dsDNA into two dsDNA fragments and can lead to cell lethality (reviewed in Amarh and Arthur, 2019). In fact, the formation and repair of DSBs have both been identified as targets for antibiotic resistance. Examples include quinolones as antibiotic agents, which target type II topoisomerases to prevent re-ligation of the cleaved DNA (Levine et al., 1998; Wohlkonig et al., 2010; Dalhoff, 2012). DSBs have also been proposed as a chemotherapy target and as a way to boost chemotherapy by combining ribosome inhibitors and DSB inducing agents (Amarh and Arthur, 2019).

Double stranded break repair (DSBR) in *E. coli* uses homologous recombination (HR) to connect broken dsDNA strands (Kowalczykowski et al., 1994). Eukaryotic DSBR also utilises HR, but can additionally follow a pathway called non-homologous end joining (NHEJ) where unrelated broken strands can be joined together. It is conducted by important eukaryotic proteins Ku70-80 and Ligase D (Amarh and Arthur, 2019). A version of NHEJ has also been shown in *E. coli*, called alternative end-joining (A-EJ), but it does not however rely on Ku70-80 and Ligase-D, but instead on extensive end-resection by RecBCD and Ligase A (Chayot et al., 2010). Some bacteria, such as *Bacillus Sp.*, *Mycobacterium tuberculosis*, *Mycobacterium smegmatis*, *Streptomyces coelicolor*, *Pseudomonas sp.*, and *Xanthomonas sp.*, do encode for *ku* and *ligase D* genes, and might therefore be able to conduct NHEJ (Wilson et al., 2003; Pitcher et al., 2007; reviewed in Amarh and Arthur, 2019).

1.3.3.1. Homologous DSBR in *E. coli*

The major DSBR pathway in *E. coli* is conducted using HR and utilising the RecBCD complex, *chi* sites and RecA filament binding. DSBR is an important process for DNA replication elongation and fork convergence.

RecBCD complex is formed from a 5' to 3' helicase and an exonuclease with an affinity for blunt DSBs (Taylor and Smith, 1985). During DSBR, RecBCD loads onto the 5' end of a blunt DSB and unwinds dsDNA while degrading the unwound 5' to 3' strand. Exonuclease activity of RecBCD is much reduced when the helicase reaches an asymmetric 5'-GCTGGTGG-3' DNA site called *Chi* (crossover hot spot investigator), at which point the helicase can continue unwinding the strand or can dissociate from DNA (Lam et al., 1974; Smith, 2012; Smith et al., 1981; Triman et al., 1982; Dixon and Kowalczykowski, 1993).

Once RecBCD has degraded the 5' to 3' strand, RecA, an ATPase with an affinity for ssDNA, binds to the 3' overhang by forming RecA filaments; with each filament made of six RecA molecules bound to three nucleotides each (van Loenhout et al., 2009). The RecA bound ssDNA forms a D-loop (DNA:DNA hybrid) with a complementary dsDNA end by displacing one of the dsDNA strands and binding instead (reviewed in Bell, 2005; Chen et al., 2008). DNA synthesis is initiated at the free 3' end of the D-loop, which extends the D-loop and converts it into a Holliday junction (reviewed in McGlynn et al., 1997).

Holliday junctions undergo branch migration to DNA ends with the help of RuvA and RuvB proteins (Iwasaki et al., 1992). Once migrated to DNA ends (Iwasaki et al., 1992), RuvC can catalyse the Holliday junctions (Iwasaki et al., 1991). It does so by folding the junction and introducing two nicks into the DNA, allowing for the junction to be converted into linear dsDNA and ligated by DNA ligase (Dunderdale et al., 1991; Iwasaki et al., 1991; Connolly et al., 1991)

PriA, a primosome responsible for reloading the replisome on DNA outside of *oriC*, is recruited to a side of DSBR if the replication fork has to be reassembled (Marians, 2000). This has been

shown to be regulated by PriB, PriC (Sandler, 2000) and RecG (Azeroglu et al., 2016; Azeroglu and Leach, 2017) and likely by RecA and RecB (McCool and Sandler, 2001; McCool et al., 2004; reviewed in Michel et al., 2018).

RecG helicase is involved in HR by stabilising joint molecules, unwinding Holliday junctions, and limiting DNA amplification at break sites through reverse restart, caused by incorrect replisome loading at D-loops (Azeroglu et al., 2016; Azeroglu and Leach, 2017). RecG and PriA have been suggested to act in concert to stabilise arrested replication forks, with RecG helping PriA load forks in the correct orientation (Gabbai and Marians, 2010). PriA and RecG have also been shown to bind to SSB *in vivo* when DNA is not present (Yu et al., 2016), likely as a storage mechanism to ensure that PriA and RecG are available if needed at ssDNA when SSB binds.

Lastly, UvrD helicase is also able to resolve Holliday junctions *in vitro* by binding to the middle of the junction (Carter et al., 2012). UvrD has been colocalised to replication intermediates *in vivo* and is able to remove RecA filaments from DNA *in vitro* (Veaute et al., 2005). While UvrD does not appear to be essential for DSBR, these results suggest that UvrD might act as a 'back up' protein to ensure DSBR is performed correctly.

1.4. DNA Replication and UvrD

DNA replication is a fundamental process that occurs in all living cells with the purpose of creating an identical copy of the genetic material of the cell. The complexity of replication varies between different organisms. Eukaryotes undergo hundreds to thousands of replication initiation events spread around the genome during the synthesis stage of the cell cycle (Cvetič and Walter, 2005), while most bacteria have a single, circular chromosome within which replication initiates at a single origin of replication (reviewed in Kaguni, 2011).

DNA replication has three distinct stages: initiation, elongation, and termination (reviewed in Dewar and Walter, 2017). During initiation, the proteins assemble at the origin of replication and form the replication machinery, known as the replisome (Postow et al., 2004). During elongation, two replication forks proceed away from the origin using a helicase to 'unzip' the DNA double helix and DNA polymerase to add complementary bases to each strand (Wickner, 1976). Lastly, during termination two replication forks meet and the new DNA strands fuse (reviewed in Dewar and Walter, 2017).

UvrD has been shown to colocalise with the replisome (Wollman et al., 2023). Due to the multitude of roles of UvrD on the chromosome, including DNA repair, removal of nucleoprotein blocks, and assisting in DNA replication-transcription conflicts, UvrD is considered an important protein for successful DNA replication and genomic integrity.

1.4.1. DNA replication initiation

DNA replication in *E. coli* begins at the origin of replication, known as *oriC* (figure 1.6 A) (Bird et al., 1972; Nagata and Meselson, 1968; Wolanski et al., 2015), which includes specific motifs called DnaA boxes, the DUE (duplex-unwinding element) region and the integration host factor (IHF).

DnaA, an essential initiation protein, binds to the DnaA boxes on *oriC* throughout the cell cycle (figure 1.6 A) (Fuller and Kornberg, 1983; Fuller et al., 1984; Weigel et al., 1997). The accumulation of DnaA causes the hydrogen bonds between the dsDNA at *oriC* to break (Bramhill and Kornberg, 1988; Hansen and Atlung, 1995). IHF also binds at *oriC* to the IHF binding site, which causes the DNA to bend and for the DUE region to open (Hwang and Kornberg, 1992). Splitting of the DUE into two ssDNA strands allows for DnaC to load the replicative helicase DnaB (Wickner and Hurwitz, 1975; Kobori and Kornberg, 1982); action which is stimulated by DnaA (Marszalek and Kaguni, 1994; Sutton et al., 1998). DnaC then dissociates from the DNA and DnaB (Wahle et al., 1989) and the replisome proteins begin binding to DnaB.

The replisome includes primase (DnaG), β sliding clamp, two units of DNA polymerase III, and the ATPase clamp loader (figure 1.6 B) (McGlynn and Lloyd, 2002; Felczak et al., 2017). SSB can also be found at the replication fork where it prevents hairpin formation of ssDNA and has been found to be associated with fork reversal and regression through SSB interaction with RecG (Bianco and Lyubchenko, 2017) and PriA (Tan and Bianco, 2021). The accessory helicase Rep also associates with DnaB (Guy et al., 2009; Atkinson et al., 2011; Syeda et al., 2019) and assists with DNA replication block removal, such as during DNA replication-transcription conflicts (Hawkins et al., 2019).

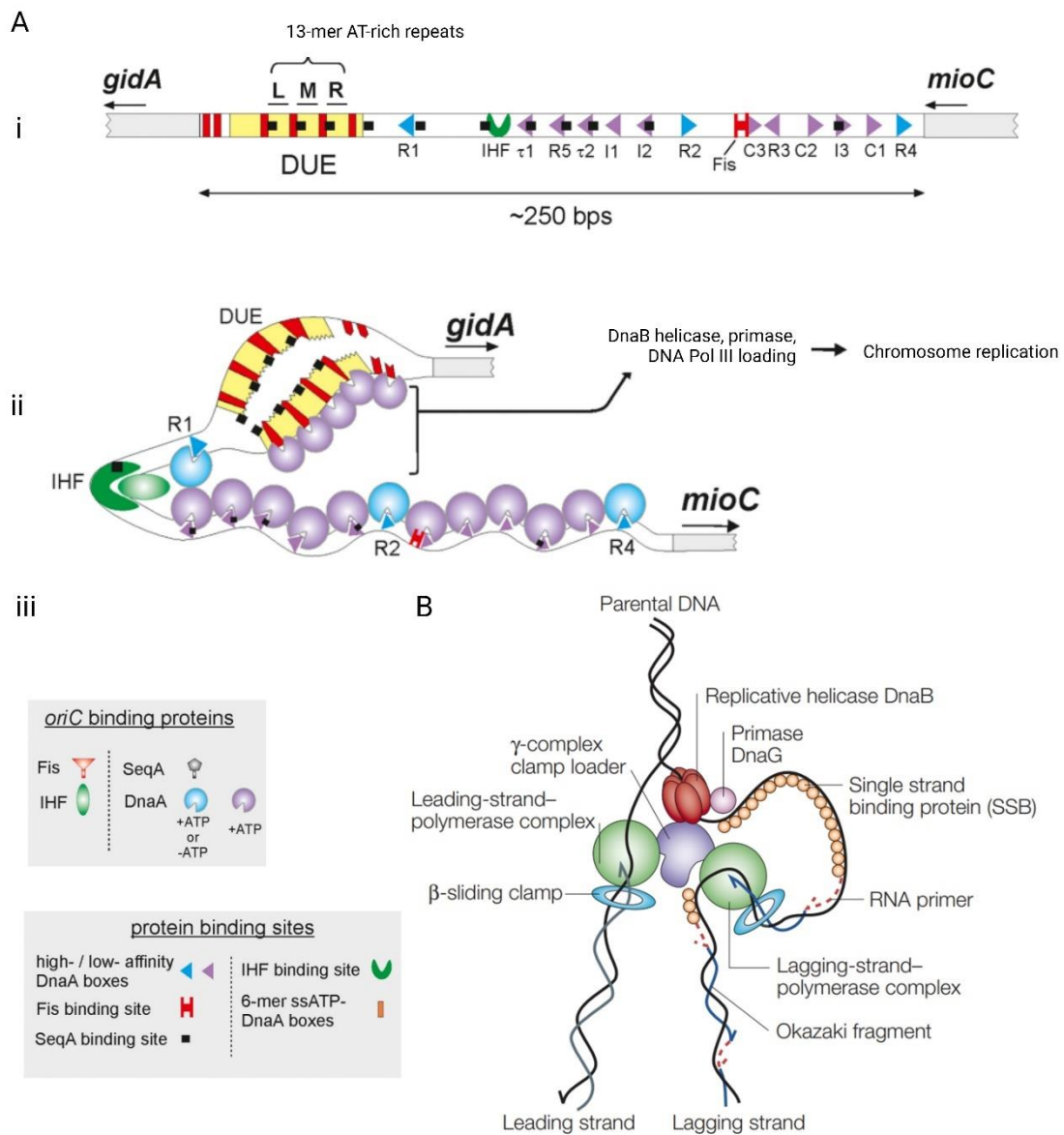


Figure 1.6 *E. coli* DNA replication initiation. A. Model of DNA replication initiation in *E. coli*. i) *oriC* region. ii) *oriC* after initiation, with DnaA and IHF bound to the origin before the replication fork is assembled. iii) legend to i) and ii). Figure adapted from Wolański et al., 2015. B. *E. coli* replication fork, including the DnaB helicase, DNA Polymerase III (two units), β sliding clamps and the ATPase clamp loader, DnaG primase and SSB. Figure adapted from McGlynn and Lloyd, 2002.

Regulation of initiation through DnaA binding and activation

DNA replication initiation is regulated by DnaA activation and DnaA-binding region availability. Regulation is essential to ensure that a fresh round of DNA replication does not start too early – which is especially important due to concurrent replication occurring in *E. coli*. New initiation occurs approximately half-way through elongation of the preceding DNA replication, meaning that DNA replication takes approximately 40 min, but cell duplication only 20 min (Cooper and Helmstetter, 1968). There are various mechanisms in *E. coli* of regulating initiation. The first requires DNA sequestration, second phosphorylation of inactive DnaA-ADP into active DnaA-ATP, the last requires dephosphorylation of active DnaA-ATP either through regulatory inactivation of DnaA (RIDA) or *datA* dependent DnaA-ATP hydrolysis (DDAH).

First, DNA sequestration is the process of recognising recently replicated DNA regions through hemi-methylation of d(GATC) sequences by Dam methyltransferase. *E. coli* DNA sequestration protein, SeqA, binds to the hemi-methylated d(GATC) sites, which can be found within *oriC* (Slater et al., 1995; Nievera et al., 2006) and the *dnaA* gene (Campbell and Kleckner, 1990). The *dnaA* gene cannot be read and transcribed by RNAP until SeqA dissociates from the gene, which *in vitro* occurs once every 10 minutes (Kang et al., 1999). The binding of SeqA to *oriC* does not however completely block the binding of DnaA already present in the cell. *oriC* contains high (R1, R2 and R4) and low (R3 and R5, I2, I3) affinity DnaA boxes and SeqA only prevents the binding of DnaA to the low affinity boxes (Nievera et al., 2006). DnaA only binds to R3 and R5 right before initiation occurs (Nievera et al., 2006).

Second, DnaA-ATP is the active state of the DnaA protein. DnaA-reactivating sequence (DARS) can be used to activate DnaA-ADP through phosphorylation (figure 1.7) (Fujimitsu et al., 2009). There are two chromosomal DARS sites, *DARS1* and *DARS2*, which allow for DnaA binding and regeneration into DnaA-ATP through nucleotide exchange. DARS promotes initiation of DNA replication (Fujimitsu et al., 2009; reviewed in Kohiyama et al., 2023).

Lastly, there are two regulatory systems based on dephosphorylation of active DnaA-ATP into inactive DnaA-ADP: RIDA and DDAH (figure 1.7).

RIDA regulation of DnaA is believed to be the predominant mechanism for regulation of excessive initiation (Camara et al., 2005). RIDA occurs through interaction of the Hda protein, a DnaA homologue, and DnaA at *oriC*. During RIDA, the AAA+ domain of Hda interacts with DnaA and stimulates hydrolysis of DnaA-ATP, into DnaA-ADP (Kato and Katayama, 2001; Su'etsugu et al., 2005). Importantly, Hda forms a complex with the replication fork β clamp, which ensures that DnaA hydrolysis is linked to replication initiation (Su'etsugu et al., 2005).

DDAH uses a chromosomal DnaA-binding site, *datA*, to promote DnaA inactivation. Regulation using *datA* requires for the *datA* site to be replicated. Once the site undergoes replication it leads to two *datA* sites being available for DnaA binding instead of one, and therefore an increase in DnaA inactivation. More DnaA bound to *datA* also leads to a smaller amount of DnaA available to bind to *oriC* (Kitagawa et al., 1998; reviewed in Kohiyama et al., 2023).

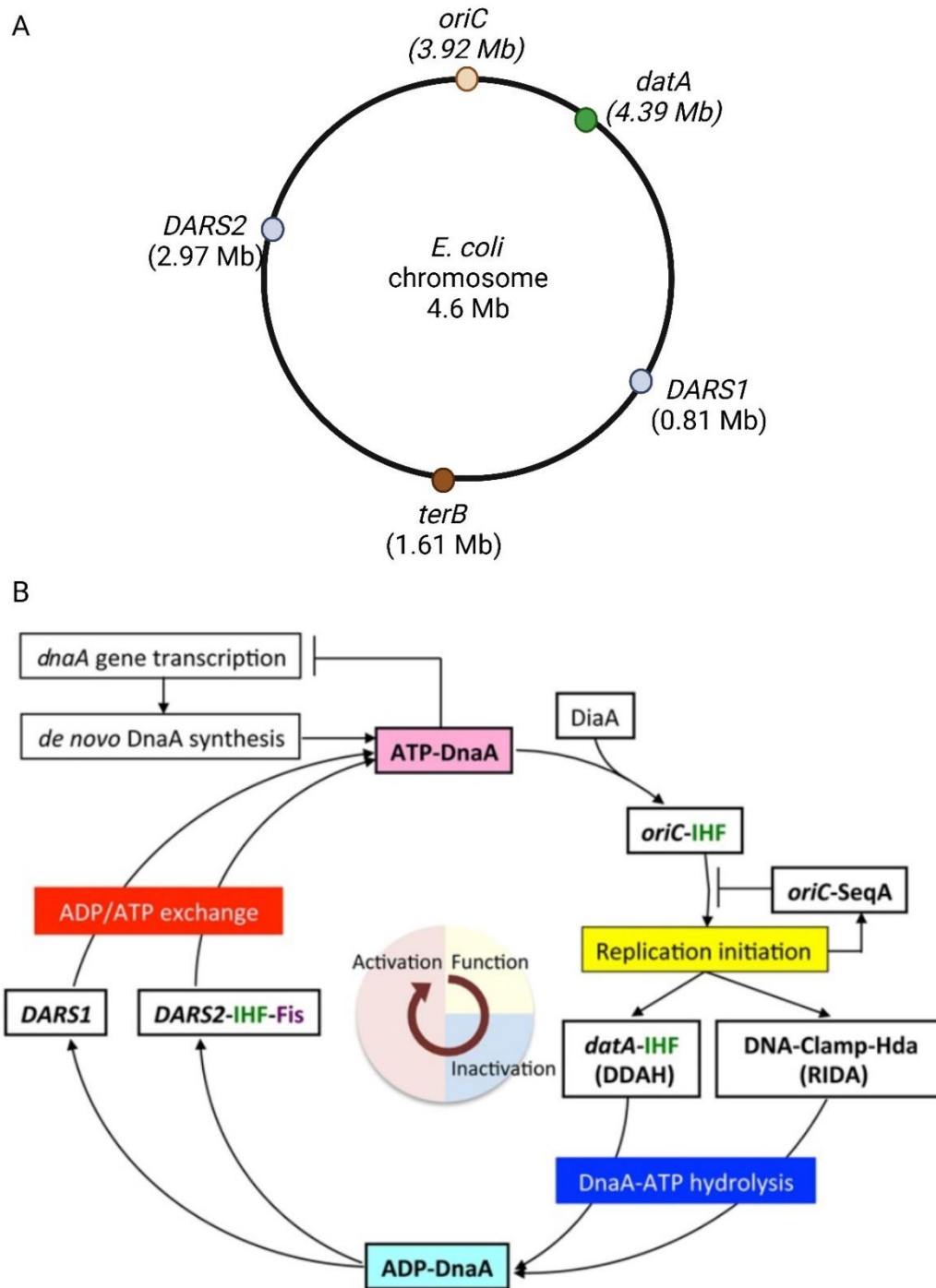


Figure 1.7 DnaA regulation. A. *E. coli* chromosome map showing the origin of replication, *oriC*, and one termination site, *terB*, as well as the DnaA regulation sites: *dataA*, *DARS1*, and *DARS2*. B. DnaA regulation map for DnaA activation and deactivation and function. Adapted from Katayama et al., 2017.

1.4.2. DNA replication elongation

Two replication forks are generated at *oriC* and travel bi-directionally away from the origin and around the circular chromosome of *E. coli* (Tabata et al., 1983). In organisms with a linear chromosome and multiple origins of replication, the replication forks also travel away from the origin (Li and O'Donnell, 2018), but towards either chromosome end or a replication fork released from a different origin of replication.

DNA synthesis is catalysed by DNA polymerase III, DnaZ, and DNA elongation factors I and III (Wickner, 1976) found at the replication fork. Each replication fork processes both the 5' to 3' (leading) and the 3' to 5' (lagging) strands to generate two duplexes. Since DnaB helicase unwinds and DNA polymerase III reads the DNA template in the 5' to 3' direction, the leading strand can be copied continuously. The 3' to 5' lagging strand however is copied through the discontinuous synthesis. Okazaki primers are synthesised by DnaG primase on the lagging strand approximately every 1200 nucleotides and enable DNA polymerase III to copy the lagging template in 5' to 3' direction in short fragments, known as Okazaki fragments (Okazaki et al., 1968; Ogawa and Okazaki, 1980).

1.4.2.1 DNA Replication – Transcription Conflicts

DNA replication and transcription are conducted on the same template and in prokaryotes, and some eukaryotes (Bhowmick et al., 2023), during the same stage of the cell cycle. This can lead to collisions between the two molecular machines.

RNAP is slower than the replication fork, reading the template at approximately 20-90 nt per sec (Wang et al., 1998; Abbondanzieri et al., 2005), compared to the replisome at 550-750 nt per sec (Pham et al., 2013). Because both can be found on the DNA template at the same time, collisions between the two machineries are not uncommon, though can still have severe consequences. DNA replication-transcription collisions can happen either codirectionally,

when the machineries travel in the same direction and the slower RNAP is hit by the faster replisome; or head-on, when the replisome collides with RNAP travelling towards it.

When the replisome and RNAP collide co-directionally, RNAP is forced to stall and is displaced either by Rep or UvrD (Hawkins et al., 2019) or Mfd (Park et al., 2002; Smith and Savery, 2005; Howan et al., 2012). Recently, Brüning and coworkers showed that during a co-directional collision, the replisome 'skipped' over the RNAP obstacle by resynthesising a downstream replication primer and leaving behind a short ssDNA gap (Brüning and Marians, 2021). This is supported by 1996 findings of chromosome deletions after DNA replication-transcription conflicts (Vilette et al., 1996). Displaced RNAP has also been shown to leave behind R-loops (DNA:RNA hybrids) (Thomas et al., 1976; Belotserkovskii et al., 2018; Hamperl et al., 2017), which, if present, increase the severity of co-directional replication-transcription collisions (Brüning and Marians, 2021). To aid replication, the 3' terminus of mRNA has been found to act as a primer for the replisome to continue synthesis. This is hypothesised to occur alongside the primosome (PriA) which is responsible for origin-independent DNA replication initiation (Pomerantz and O'Donnell, 2008; reviewed in Merrikh et al., 2012).

UvrD has been shown to remove stalled RNAP blocks by Epshtein by pulling RNAP backwards (section 1.3.2.2) (Epshtein et al., 2014). Hawkins and coworkers have also showed that UvrD was able to remove RNAP (Hawkins et al., 2019). They found that both UvrD and its homologue Rep were able to remove an RNAP block, and showed that Rep is the main helicase responsible for RNAP removal during replication-transcription conflicts, while UvrD is able to fill the role when Rep is absent (Hawkins et al., 2019). UvrD and Rep were also unable to remove RNAP when the replisome was not present (Hawkins et al., 2019). Deletion of either *rep* or *uvrD* still produces viable cells (as shown in Bidnenko et al., 2006), but a double *rep uvrD* mutant is not viable (Taucher-Scholzt and Hoffmann-Berling, 1983). This is noteworthy considering their shared role of RNAP removal and suggest their importance in replication-transcription conflict resolution. Rep acts as a secondary motor at the replisome (Guy et al.,

2009; Atkinson et al., 2011; Syeda et al., 2019) while UvrD has been found bound to RNAP (Epshtein et al., 2014) and recently colocalised with the replisome (Wollman et al., 2023). This places both helicases at the site of replication-transcription conflicts and means that if a replication-transcription conflict occurs both UvrD and Rep are already present at the site to coordinate RNAP removal.

Head-on collisions occurs when the replisome and RNAP travel towards each other and collide. They have been suggested to have more severe consequences than co-directional collisions (Mirkin and Mirkin, 2005), likely due to an increased chance of replisome stalling (Pomerantz and O'Donnell, 2010) and higher likelihood for R-loop formation (Lang et al., 2017). *E. coli* and *B. subtilis* genomes encode most of their essential genes for transcription co-directionally to the direction of the replication fork. *B. subtilis* has approximately 75% coordinated genes, while *E. coli* has about 55% (Kunst et al., 1997; Blattner et al., 1997), with 70% and 90% of essential genes (respectively) being transcribed co-directionally (reviewed in Merrih et al., 2012). This has likely evolved to limit unnecessary head-on collisions, especially on essential genes.

What can cause head-on collisions to be more threatening to genome stability? During DNA replication, as the replication fork progresses forward on the naturally negatively supercoiled *E. coli* chromosome (Wang, 1984), it generates positive supercoiling of the DNA ahead of it as the parental strands are unwound (Peter et al., 1998; Schwartzman et al., 2019). During head-on collisions between the DNA replication and transcription machineries, both machineries generate positive supercoils as they progress towards one another, which could lead to both machineries being restrained before their encounter, including a noted increase in 'DNA knots' on plasmids on which head-on collisions occurred (Mirkin and Mirkin, 2005; Olavarrieta et al., 2002). These 'DNA knots' however appear to be formed behind the machineries and are often linked to DNA gyrase (Viguera et al., 1996). Another obstacle to DNA replication which may occur during head-on collisions is the formation of R-loops (Stoy et al., 2023; Lang et al., 2017). R-loops form naturally during transcription as RNA binds to

DNA within the transcription machinery. During head-on collisions, over 50% of RNAP and nascent RNA has been shown to remain bound to the DNA after the collision (Wang et al., 2023) – meaning that both the transcription complex and the R-loop would need to be removed. Unresolved R-loops can act as obstacles to replication restart, but can also lead to the formation of DSB, which can severely impact genomic stability (Hamperl et al., 2017). DinG and DnaC aid the replisome by removing R-loops to allow for fork progression (De Septenville et al., 2012; Lang et al., 2017).

1.4.2.2 Nucleoprotein block removal by UvrD

UvrD can promote DNA replication by displacing DNA-bound proteins (Veaute et al., 2005; Bidnenko, Lestini and Michel, 2006; Guy et al., 2009; Epshtein et al., 2014; Petrova et al., 2015; Hawkins et al., 2019; Wollman et al., 2023).

Besides RNAP removal (Epshtein et al., 2014; Hawkins et al., 2019), Guy and coworkers showed that UvrD was also capable, *in vitro*, of promoting replication fork movement past two and eight EcoRI E111G blocks, a small block that is not physiologically relevant to UvrD as it does not encounter it normally *in vivo* (Guy et al., 2009). EcoRI E111G is an EcoRI restriction enzyme mutant which has a very limited cleavage ability (King, Benkovic and Modrich, 1989). UvrD can also remove RecA nucleoprotein filaments and Holliday junctions (DNA:DNA hybrids) both which are generated during homologous recombination (Veaute et al., 2005; Carter et al., 2012).

While UvrD does not have a binding partner on the replisome (Guy et al., 2009), a recent *in vivo* fluorescent study showed that it does colocalise with the replisome where it is available to aid the replication fork through nucleoprotein blocks (Wollman et al., 2023). Other UvrD processes were impaired by Wollman and coworkers by deletion of *mutS* and *uvrA* (separately) to test whether disabling MMR and NER, respectively, affects UvrD colocalisation

with the replisome (Wollman et al., 2023). Results showed that no colocalisation change was seen when MMR was disabled through *mutS* deletion, while the removal of the *uvrA* gene to disable NER did cause a 25% decrease in UvrD colocalised with the replisome (Wollman et al., 2023). These results suggest that UvrD colocalisation to the replisome might be relevant to UvrD helicase's role in NER.

An *in vitro* replication assay was also conducted to assess whether the timing of UvrD addition altered its ability to assist replication (Wollman et al., 2023). When testing if replication forks can proceed past stalled RNAP blocks, addition of UvrD at the start of the reaction (early) produced better results than addition after the replisome was blocked at RNAP (late), which produced very variable, and not statistically significant, results. Wollman and coworkers also tested for the ability of UvrD to release a replisome blocked by EcoRI E111G block. While UvrD was able to remove EcoRI E111G when added at the start of the reaction and after the blockage occurred, addition of UvrD after the fork was blocked increased the ability to remove EcoRI E111G from 41% to 84% (Wollman et al., 2023).

The difference in the RNAP and EcoRI results may be explained by the UvrD:RNAP interaction and the role of UvrD in the SOS response. UvrD has been found colocalised to RNAP, meaning that whether it was added early nor late, it would already be found at the RNAP block before the replisome arrives (Epshtein et al., 2014). When removing a block unfamiliar to UvrD, or one the helicase haven't evolved to remove, it would likely only remove it when the SOS response is triggered and UvrD overexpressed (Finch and Emmerson, 1983). Therefore, the late addition of UvrD when the replication fork is already blocked by EcoRI E111G can simulate the SOS response and therefore direct UvrD to the blocked fork more efficiently.

1.4.3. DNA replication termination

The final stage of DNA replication occurs when two replication forks meet and fuse, eventually leading to formation of two separate chromosomes. In *E. coli*, termination can occur either through free fusion, the random meeting of the two replication forks, usually around the *dif* (deletion-induced filamentation) site (location shown in figure 1.8 A), or at a replication fork barrier created by the Tus-*ter* complex (Dimude et al., 2018). Incorrect termination can have severe consequences for genetic integrity so research in this area is ongoing in most model organisms (reviewed in Dewar and Walter, 2017; Dewar et al., 2015).

1.4.3.1 DNA replication termination through fork convergence

DNA replication termination in *E. coli* can occur through free fusion of the replication forks, otherwise known as fork convergence.

The current model for termination via fork convergence utilises the RecBCD mechanism of DSBR (section 1.3.3), and the nucleases SbcCD and ExoI (Courcelle et al., 2015; Wendel et al., 2018; Hamilton et al., 2019, 2023). When completing DNA synthesis, the two replication forks bypass one another, creating a small region of over-replication. Nucleases SbcCD and ExoI, bacterial orthologs of human and yeast Mre11-Rad50 (Sharples and Leach, 1995), resect the over-replicated region, which allows for RecBCD to begin processing the region and catalysing the joining of the strands (Courcelle et al., 2015; Wendel et al., 2018; Hamilton et al., 2019, 2023).

Recently, Hamilton and coworkers explored the role of *chi* and *ter* sites in fork convergence (figure 1.8) (Hamilton et al., 2023). Their results suggested that when RecBCD encounters a *chi* site it ceases to digest the DNA, and instead induces replication of the region. This function severely disrupted genomic integrity and caused severe problems for the cells when occurring during fork convergence (Hamilton et al., 2023). Interestingly, when the group placed a *ter* site

on the plasmid as well as *chi* site, the presence of *ter* seemed to limit the *chi*-induced replication (Hamilton et al., 2023). This finding creates a link between DSBR and the *ter* sites.

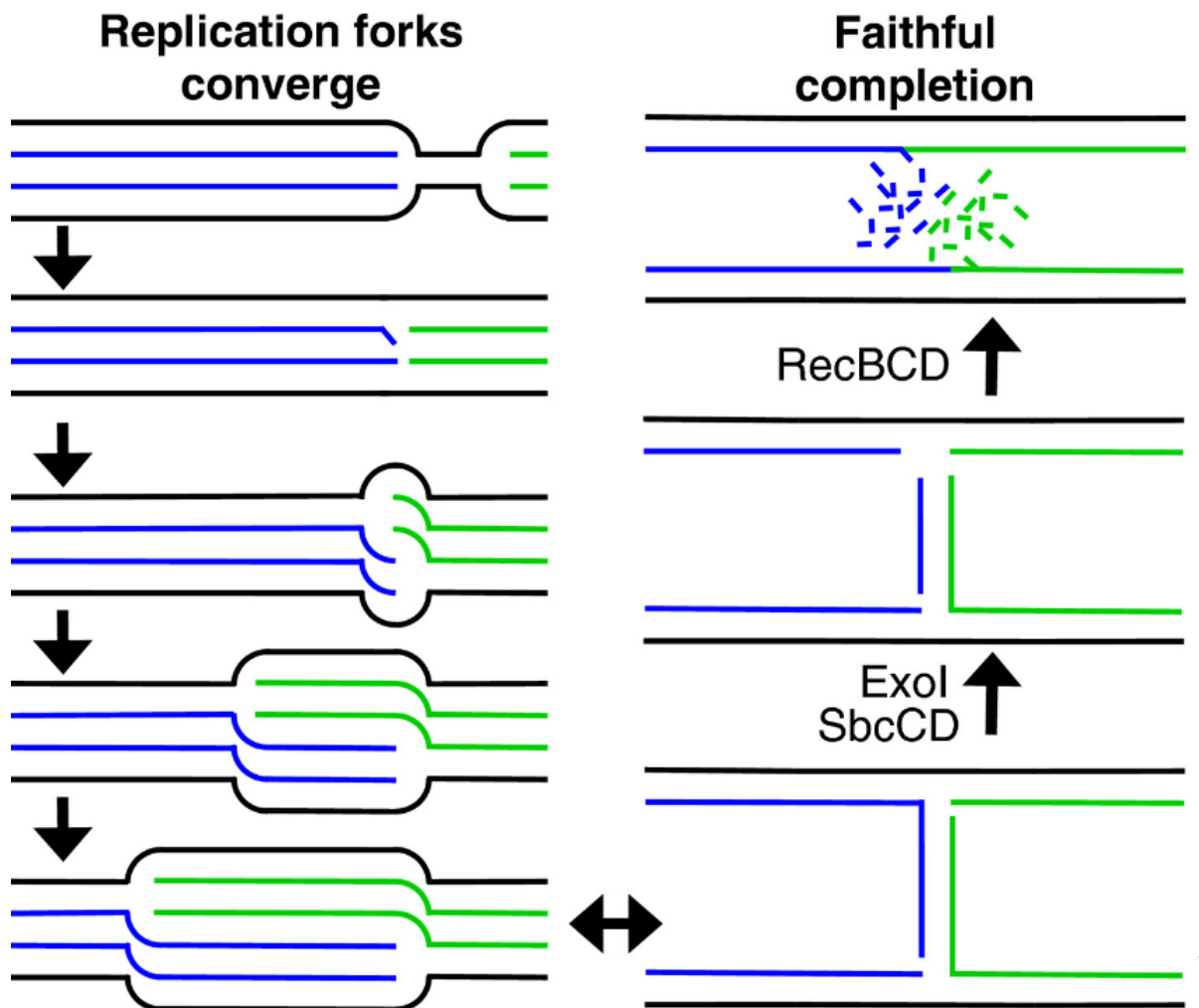


Figure 1.8 Current model for DNA replication termination through free fusion. Replication fork convergence can cause over-replication, which can be relieved by cleavage with ExoI and SbcCD, followed by strand repair with RecBCD. The model has been adapted from Hamilton et al., 2019.

1.4.3.2 DNA replication termination at Tus-ter

The *E. coli* chromosome contains ten 23-bp termination sequences called *ter*, found on the opposite half of the chromosome from the origin of replication, *oriC* (figure 1.9) (Kuempel, Duerr and Seeley, 1977; Louarn, Patte and Louarn, 1977; Coskun-Ari and Hill, 1997; Neylon et al., 2005). This region, known as the termination region, is the site of all termination events in *E. coli*. The protein Tus (terminus utilization substance) binds to *ter* in an asymmetric manner and forms a unidirectional barrier for the replication fork, creating a replication fork trap (Mulcair et al., 2006; Elshenawy et al., 2015). This means that during replication, the replication fork can pass through the first five Tus-*ter* blocks via their permissive orientation but is blocked by the sixth (and any consecutive) non-permissive Tus-*ter* blocks (Mulcair et al., 2006; Elshenawy et al., 2015). The region containing the *ter* sites is called the replication fork trap.

The DNA sequence of each *ter* sites varies slightly (figure 1.9 B), but they all have a highly conserved C6 base within a conserved 13 bp region (Neylon et al., 2005). The C6 base is essential for binding of Tus to *ter* through the “mousetrap mechanism” (Mulcair et al., 2006). During the mousetrap mechanism, Tus binds to *ter* and the conserved C6 base flips into a cytosine pocket found within Tus (figure 1.9 C) (Mulcair et al., 2006; Elshenawy et al., 2015). The timing of this process is essential as interaction between the R198 amino acid, opposite of the cytosine pocket (figure 1.9 C), and the A(5) and G(6) bases of *ter* must occur before DnaB starts unwinding the site. The mousetrap mechanism prolongs the stability of the Tus-*ter* complex by 40-fold and forms a strong non-permissive barrier (Elshenawy et al., 2015).

While ten *ter* sites are present on the *E. coli* chromosome, they have been shown to vary in their affinity to Tus (figure 1.9). Most termination events at Tus-*ter* occur at the innermost Tus-*ter* blocks (Duggin and Bell, 2009), while the outermost *ter* sites, F, H, I and J have not shown any significant Tus binding (Toft et al., 2021). The affinity of each *ter* site to Tus ranges from high, to moderate, to low (Toft et al., 2021; Moreau and Schaeffer, 2012). Some *ter* sites might

act as a 'fail-safe' in case the innermost sites fail to block the replisome; which can occur if Tus does not bind to *ter* quickly enough before DnaB begins to unwind the region (Elshenawy et al., 2015). However, the outermost *ter* sites, with very low affinity to Tus, are likely conserved on the genome due to their sequence being a part of an open reading frame (ORF), rather than for Tus binding (Toft et al., 2021).

A termination block like Tus-*ter* in *E. coli* (Kuempel et al., 1977; Louarn et al., 1977) is not found in all bacterial cells. Another well studied termination block can be found in *B. subtilis*, called RTP-*ter* (Weiss et al., 1981). Other blocks that have not been studied in great detail, can be found in most *Enterobacteriales*, *Pseudoalteromonas*, and *Aeromonadales* (Galli et al., 2019; reviewed in Goodall et al., 2023). For specific examples, *Edwardsiella tarda* and *Cedecea neteri* have a single *ter* site, while *Dickeya paradisiaca* has two (Toft et al., 2021; Toft et al., 2022; reviewed in Goodall et al., 2023).

Since a termination fork trap is not a conserved bacterial feature, why does the replication fork trap exist in the first place? One suggestion is the prevention of unnecessary head-on replication-transcription collisions. 90% and 70% of *E. coli* and *B. subtilis* essential genes show co-directionality to the replication fork (Kunst et al., 1997; Blattner et al., 1997). It can therefore be presumed that progression of the replication fork past the non-permissive face of the Tus-*ter* block can lead to an increase in head-on replication-transcription collisions. Since head-on collisions are commonly stated to have more dire consequences than co-directional collisions (Mirkin and Mirkin, 2005), their prevention by blocking the replication fork is a logical conclusion. It is however surprising that Δ tus cells do not display any major phenotype problems compared to WT cells (Rudolph et al., 2013; Ivanova et al., 2015). This would suggest that head-on collision prevention is not the main reason for the existence of termination blocks, especially since they have been shown to be highly conserved (once they evolved into the species genome) and therefore should hold an important physiological role with an evolutionary advantage (Goodall et al., 2021).

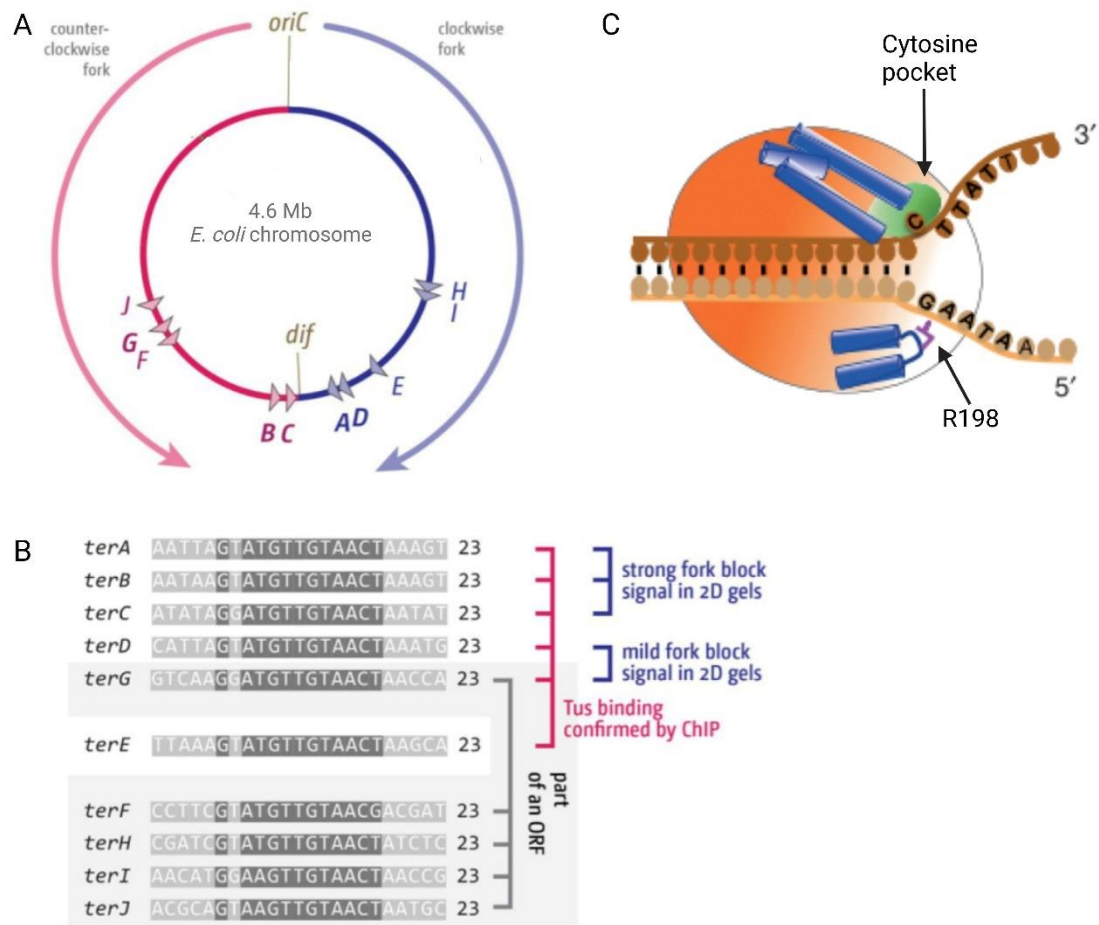


Figure 1.9 Elements of DNA replication termination at Tus-*ter*. A. *E. coli* chromosome diagram with the origin of replication, *oriC*, ten *ter* sites, *terA-J*, and *dif*. B. 23 bp sequences of the ten *ter* sites, including conserved sites in dark gray. Strong and mild *ter* sites, sites with confirmed Tus binding, and sites that are part of an ORF have been annotated. C. The mousetrap mechanism model of Tus-*ter* binding, including the cytosine pocket and the flipped base pair. A and B have been adapted from Goodall et al., 2023, C has been adapted from Elshenawy et al., 2015.

1.4.3.3 What happens to Tus during replication termination at Tus-ter?

A recent study published by our group explored termination at Tus-*ter* *in vitro* (Jameson et al., 2021). Jameson and coworkers conducted a biochemical replication assay to study replication termination at Tus-*ter* by reconstituting replication forks on a plasmid. The plasmid used was designed to contain a single origin of replication, *oriC*, and two replication blocks: a *lacO*₂₂ array for binding of LacI in a reversible block, and a single *terB* site for binding of Tus. The clockwise replication work from *oriC* would be blocked by the non-permissive face of the Tus-*terB* block. Replication fork fusion at Tus-*ter* can be achieved in this system by blocking both forks, clockwise at Tus-*terB* and counterclockwise at LacI-*lacO*. Addition of IPTG removes LacI and releases the counterclockwise fork to reach the Tus-*terB* site at which the clockwise fork should be stalled. The assay incorporates radioactive ³²P dCTP into the nascent DNA for visualisation (Jameson et al., 2021).

Replication assay products were treated with single side cutters, Nb.BsmI, Nt.BspQI, Nb.Bpu101, and Nt.Bpu101, to isolate the leading strands around *terB* and determine individual replisome progression in the termination region (figure 1.10 A and B). Termination mapping assay results showed that when controlled fork fusion occurred at Tus-*terB*, a 15-23 bp unreplicated gap was found with a similar footprint to the binding of Tus (Jameson et al., 2021).

Two hypotheses were discussed as to the reason for these results. The first hypothesis (figure 1.10 C i) suggests that Tus was not present at *ter* during termination at Tus-*terB* in the termination mapping assay. This could occur if Tus was dislodged by impact with either the first fork, travelling towards the non-permissive orientation of Tus-*ter*, or by the second fork which would alone pass by the permissive orientation of Tus-*ter*. Current literature model suggests that when the replisome is stalled by the non-permissive orientation of Tus-*ter* that the replication machinery dissociates from the DNA and needs to be reloaded for replication

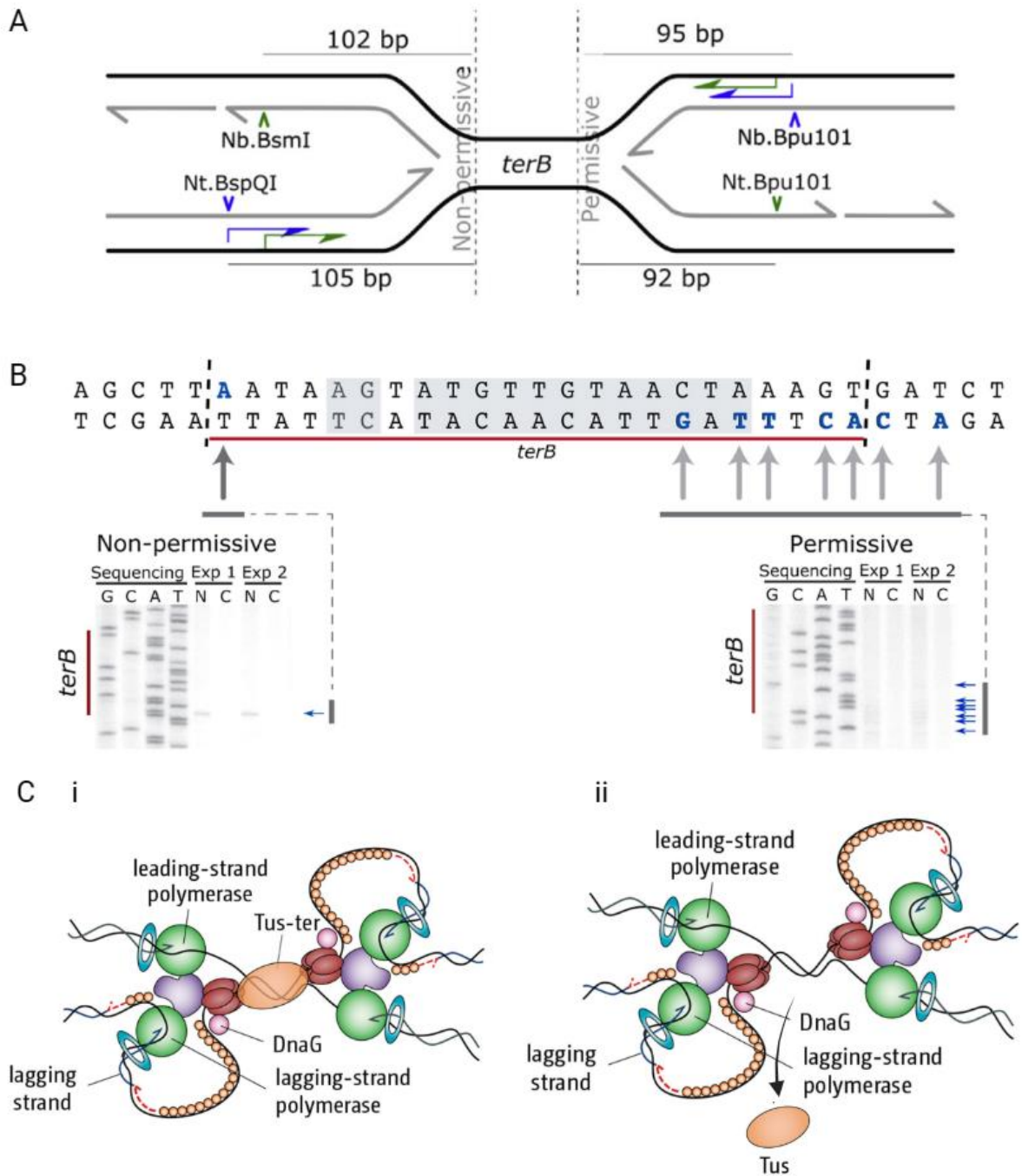


Figure 1.10 Termination mapping assay shows unreplicated gap at Tus-*ter*. A. *terB* region during the termination assay, including the location of the single side cutters Nb.BsmI, Nt.BspQI, Nb.Bpu101, and Nt.Bpu101. B. *terB* sequence on the replication assay plasmid and the gel results from the termination assay. Arrows indicate which nucleotide is shown by the bands on the gel. C. Schematics of two theories of what happens to Tus during termination at Tus-*ter*. i) Tus is dislodged by one of the replication forks. ii) Tus is sandwiched between the two replication forks.

to continue, while Tus remains bound to *ter* (Gabbai and Marians, 2010; Bidnenko et al., 2006). If the first replisome is however still bound to the DNA when the second one approaches, and Tus is potentially not, the collision between replisomes might cause an arrest of the second fork and incomplete DNA synthesis even without Tus between them. Replication forks are very large machineries, and their collision might not permit either of them to reach the final DNA region between them until one or both replisome dissociate, and replication restarts to complete the region. A full structure of the replication fork has not yet been generated, therefore we are unable to know whether two replication forks meeting 'head-to-head' would prevent the DNA between them from being 'reached'.

In our second hypothesis (figure 1.10 C ii), when termination occurs at Tus-*terB*, the *terB* site is unable to be replicated because Tus is still bound and likely 'stuck' between the two replisomes. If this occurs, another protein would likely need to be employed to remove Tus. Jameson and coworkers tested UvrD, Rep and RecG as candidates, but neither helicase was able to increase the amount of full replication product generated (Jameson et al., 2021). This was especially surprising for UvrD, which is commonly cited as the helicase able to remove Tus (Bidnenko et al., 2006).

The Michel group conducted *in vivo* investigations where addition of two ectopic *ter* sites blocked replication forks half-way around the chromosome. They found that overexpression of UvrD helicase caused a reduction of replication forks stuck at Tus (Bidnenko et al., 2006) and generated a model based on their results (figure 1.11). They suggested that in their assay the replication fork which reached the Tus-*ter* block would either be stalled and dissociate from the DNA, or would 'ran off' the template due to the formation of a DSB. When a second fork arrived, either through DNA replication or recombination-mediated initiation (figure 1.11 ii, dark and light gray), it also ran off, leaving four sets of incomplete dsDNA regions. RecBCD-dependent recombination rearranged the nucleic acid into homologous sequences, while PriA loaded DnaB onto both strands. The model suggests that UvrD was also loaded onto the DNA and was able to remove Tus. While one new replication fork was free to proceed past the

empty *ter* site, the second fork ran off the other discontinuous strand. The presence of a blunt-ended strand caused another RecBCD-mediated double-stranded break repair (DSBR) to occur through recombination. While the first replication fork was able to continue past Tus, new sets of replication forks were assembled through recombination and were blocked again at the quickly re-bound Tus - therefore restarting the process (Bidnenko et al., 2006).

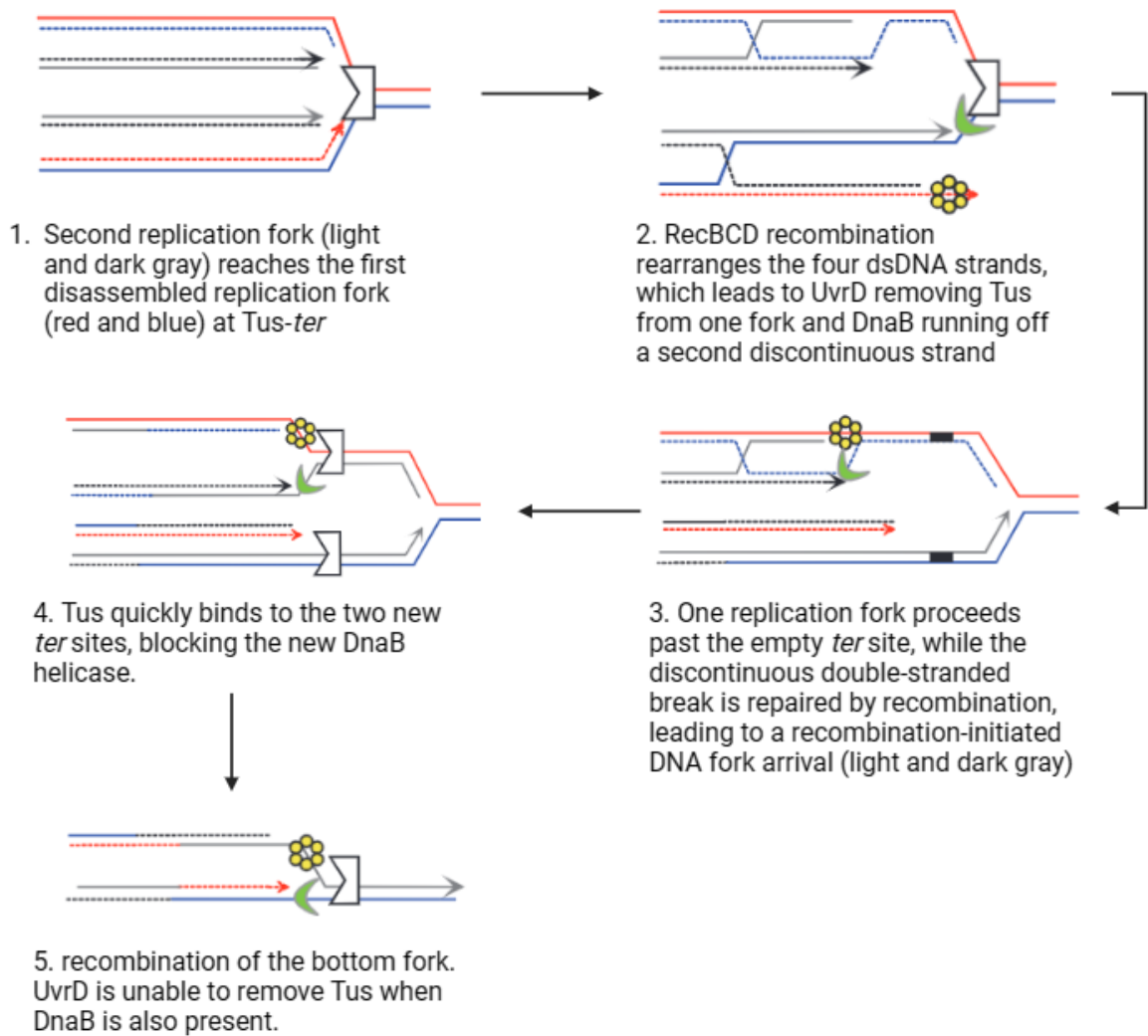


Figure 1.11 Model of Tus removal by UvrD helicase after the arrest of a replication fork. The red and blue lines represent the original replication fork, with the solid and broken lines representing the leading and lagging strands respectively. The 3' end of each strand is shown as an arrow. The second replication fork is represented by light and dark gray lines. UvrD is shown as a green crescent. DnaB is represented by a yellow hexamer. Tus is shown as an indented white rectangle, while *ter* is represented by black blocks. Figure adapted from Bidnenko et al., 2006.

1.5. Aims and objectives

The overall aim of this work is to further our knowledge of UvrD helicase and its role in MMR, nucleoprotein block removal, and DNA replication termination.

Our objectives are:

1. To conduct a series of *in vitro* assays to test whether the ability of UvrD to unwind DNA, especially past DNA-bound protein blocks, can be enhanced by MutL. We will do this by conducting *in vitro* helicase and replication assays of UvrD \pm MutL.
2. To investigate the binding location of MutL on UvrD. Hall and coworkers suggest the region is found within the first 100 amino acids of UvrD helicase (Hall, Jordan and Matson, 1998). We also plan to narrow down whether the site can be found in the first or second 50 amino acids of the N-terminal of UvrD.
3. To investigate the role of the 2B subdomain of UvrD in unwinding past DNA-bound protein blocks or removing DNA-bound proteins by the helicase. We will do this by removing the 2B subdomain of UvrD, as previously done for Rep (Brüning et al., 2018), and testing the mutant helicase against a variety of blocks in helicase assays and replication assays. We are also interested in determining whether MutL can still bind to UvrD Δ 2B and will test this through cross-linking experiments and surface plasmon resonance microscopy (SPR).
4. To develop a new *in vitro* assay in order to determine if Tus remains bound to *ter* when two replication forks fuse at a the Tus-*ter* block.

CHAPTER 2
MATERIALS AND
METHODS

Chapter 2. Materials and Methods

2.1 Materials

2.1.1 Chemicals

All chemicals were purchased from Thermo Fisher, Thermo Fisher Scientific, Sigma-Aldrich, or VWR International unless stated otherwise. All restriction enzymes, the CutSmart buffer, DNA loading dye, and Phusion DNA Polymerase were purchased from New England Biolabs (NEB), while *Taq* polymerase was purchased from Thermo Scientific. All oligos were purchased from IDT, with the exception of oDW070 and oDW071 which were purchased from Life Technologies. All radioactive material was purchased from PerkinElmer (rebranded Revvity).

2.1.1 Plasmid sequencing

Source Bioscience was used for all short fragment plasmid sequencing using the T7 forward and reverse primers unless stated otherwise. Plasmidosaurus nanopore sequencing was used to generate full plasmid maps.

All plasmid maps were visualised using SnapGene software (table 2.1).

2.1.2 Software and systems

TABLE 2.1 Software used for DNA and protein analysis

| Software Name | Purpose | Source |
|----------------------------------|---|---|
| Tm Calculator | Calculating the melting temperature (Tm) of oligos. | (ThermoFisher, 2023) |
| Clustal Omega | Comparing DNA-DNA and amino acid-amino acid sequences. | (EMBL-EBI, 2022; Madeira et al., 2022) |
| Reverse Complement Calculator | Generating the reverse complement of nucleic acid. | (Stothard, 2000) |
| SnapGene Viewer | Visualising plasmid maps and Sanger sequencing data. | SnapGene Viewer Software (version 6.2.1.) |
| Expasy Translator Tool | Translating DNA sequences into amino acid sequences. | Developed by the Swiss Institute of Bioinformatics (SIB) (Expasy, 2020) |
| UniProt Database | Finding protein information, including amino acid sequences for UvrD (P03018) and MutL (P23367). | (Bateman et al., 2023) |
| Protein Data Bank (PDB) database | Finding published protein structures from X-ray crystallography and Cryo-EM experiments. | (Berman et al., 2000) |
| AlphaFold2 ColabFold | Generating protein structure models for MutL, MutL dimer, UvrD Δ 52N, UvrD Δ 108N, and UvrD Δ 2B | (Jumper et al., 2021; AlphaFold, 2021) |

2.1.2.1 Gel Analysis

Quantity One software (version 4.6.2 basic) was used to capture and visualise agarose gels and SDS-PAGE gels via the Biorad ChemiDoc XRS Gel Imaging System.

Radioactive gels were exposed to an phosphor imaging screen (BioRad, 170-7843) for 24 hrs - 5 days before visualising using the Biorad Personal Molecular Imager (BioRad, 170-9400).

The results were viewed using Quantity One software (version 4.6.2 basic) and the generated Tiff file was analysed using ImageJ software (NIH, 2018) or PaintShopPro 2019 (CorelCorp, 2019).

2.1.2.2 Protein Purification

AKTA Start and AKTA Go protein purification systems from GE were used to conduct large scale protein separation chromatography using HisTrap and size exclusion columns. Both systems were operated using Unicorn software (versions 1.3 start and 7.6 respectively) and were used to generate and analyse chromatographs.

AKTA Pure purification system with the capability to detect 260 and 280 UV readings was used for Analytical SEC. It was operated by Unicorn 7.6 software.

2.1.2.3 Writing, data analysis and presentations

Microsoft Office 365 products Microsoft Word and Microsoft Excel were used for writing and data analysis respectively.

Microsoft Office PowerPoint and BioRender were used to create figures used in this work. Publishing licence for the use of BioRender was acquired.

2.1.3 Oligos and Plasmids

TABLE 2.2 OLIGOS USED FOR CLONING

| Oligo Name | Oligo Sequence (5' to 3') | Oligo Purpose |
|------------|--|---|
| oKJ011 | TGG AGC ACC ACC ACC ACC ACT G | pET28 α - <i>HisSUMO</i> linearisation primer for InFusion cloning. |
| oKJ012 | ACC ACC ATT CTG TTC TCT GTG A | pET28 α - <i>HisSUMO</i> linearisation primer for InFusion cloning. |
| oDW004 | GAA CAG ATT GGT GGT CCA ATT CAG GTC TTA CCG | mutL linearisation for infusion cloning into pET28 α - <i>HisSUMO</i> to generate pDW003. |
| oDW005 | GTG GTG GTG CTC GAG TTA TCA CTC ATC TTT | mutL linearisation for infusion cloning into pET28 α - <i>HisSUMO</i> to generate pDW003. |
| oDW019 | CTG AAT TGG GGA AGA ACC ACC AAT CTG TTC TCT G | For pDW005 - Site directed mutagenesis primer to insert 2x serine into pDW003. |
| oDW020 | ATT GGT GGT TCT TCC CCA ATT CAG GTC TTA CC | For pDW005 - Site directed mutagenesis primer to insert 2x serine into pDW003. |
| oDW021 | GAA CAG ATT GGT GGT GAA CAG ATT GGT GGT GAC GTT TC | <i>uvrD</i> linearisation for infusion cloning into pET28 α - <i>HisSUMO</i> to generate pDW006. |
| oDW022 | GTG GTG GTG CTC GAG TTA TTA CAC CGA CTC CAG CCG | <i>uvrD</i> linearisation for infusion cloning into pET28 α - <i>HisSUMO</i> to generate pDW006. |
| oDW056 | TTG GTG GTT GCT CGC CAT ACT CGA TTA T | For pDW010 - Site directed mutagenesis primer to generate <i>uvrD</i> Δ 52N mutation in pDW006. |
| oDW057 | GGC GAG CAA CCA CCA ATC TGT TCT C | For pDW010 - Site directed mutagenesis primer to generate <i>uvrD</i> Δ 52N mutation in pDW006. |
| oDW058 | TTG GTG GTC AGG ATT TCC AGA TCC TCG | For pDW08 - Site directed mutagenesis primer to generate <i>uvrD</i> Δ 108N mutation in pDW006. |
| oDW059 | AAA TCC TGA CCA CCA ATC TGT TCT CTG TGA | For pDW08 - Site directed mutagenesis primer to generate <i>uvrD</i> Δ 108N mutation in pDW006. |
| oDW062 | ACG GCG GGC AGG CGG ATA CCT G | For pDW009 - Site directed mutagenesis primer to generate <i>uvrD</i> Δ 2B mutation in pDW006. |
| oDW063 | TCC GCC TGC CCG CCG TAA ATA CGG TAC | For pDW009 - Site directed mutagenesis primer to generate <i>uvrD</i> Δ 2B mutation in pDW006. |
| oDW068 | TTG GTG GTT CGC CAT ACT CGA TTA TG | For pDW007 - Site directed mutagenesis primer to generate <i>uvrD</i> Δ 53N mutation in pDW006. |
| oDW069 | TAT GGC GAA CCA CCA ATC TGT TCT C | For pDW007 - Site directed mutagenesis primer to generate <i>uvrD</i> Δ 53N mutation in pDW006. |

TABLE 2.3 OLIGOS USED FOR HELICASE ASSAYS AND THE TUS JUMPING ASSAY

| Oligo Name | Oligo Sequence (5' to 3') | Oligo Purpose |
|------------|---|---|
| oJH117 | GAA TAA GTA TGT TGT AAC TAA AGT GAT CAC TGG CAC TGG TAG AAT TCG GC | DNA oligo with a <i>ter</i> site in the permissive orientation for UvrD helicase assays. Contains a complementary region to oJH118 for DNA substrate hybridisation. Used with oDW035 to generate the Tus capture substrate. |
| oJH118 | AAC GTC ATA GAC GAT TAC ATT GCT ACA CTT TAG TTA CAA CAT ACT TAT TC | DNA oligo with a <i>ter</i> site in the permissive orientation for UvrD helicase assays. Contains a complementary region to oJH117 for DNA substrate hybridisation. |
| oJH123 | GAC TTT AGT TAC AAC ATA CTT ATT GAT CAC TGG CAC TGG TAG AAT TCG GC | DNA oligo with a <i>ter</i> site in the non-permissive orientation for UvrD helicase assays. Contains a complementary region to oJH124 for DNA substrate hybridisation. |
| oJH124 | AAC GTC ATA GAC GAT TAC ATT GCT ACA ATA AGT ATG TTG TAA CTA AAG TC | DNA oligo with a <i>ter</i> site in the non-permissive orientation for UvrD helicase assays. Contains a complementary region to oJH123 for DNA substrate hybridisation. |
| oDW035 | GCC GAA TTC TAC CAG TGC CAG TGA TCA CTT TAG TTA CAA CAT ACT TAT TC | Tus jumping substrate component together with oJH117 |
| oDW070 | GCA AGA ATA AGT ATG TTG TAA CTA AAG TCA GGT CGA ATT CCT CGA GAC CGC AAT AGA CCG TCC ACG GAT ACC TTC TAA GGA TCA CTG GCA CTG GTA CAT A | DNA oligo with a <i>ter</i> site in the permissive orientation and an EcoRI cleavage site for EcoRI E111G binding. Contains a complementary region to oDW071 for DNA substrate hybridisation. |
| oDW071 | CAT AGA CGA TTA CAT TGC TAC CTT AGA AGG TAT CCG TGG ACG GTC TAT TGC GGT CTC GAG GAA TTC GAC CTG ACT TTA GTT ACA ACA TAC TTA TTC TTG C | DNA oligo with a <i>ter</i> site in the permissive orientation and an EcoRI cleavage site for EcoRI E111G binding. Contains a complementary region to oDW070 for DNA substrate hybridisation. |

TABLE 2.4 PLASMIDS

| Plasmid Name | Backbone | Features | Antibiotic Resistance | Purpose |
|------------------------|---------------------------|--|-----------------------|---|
| pKJ001 | Jameson et al., 2021 | <i>oriC</i> replication origin, <i>terB</i> , <i>LacO₂₂</i> | <i>Amp</i> | Replication assay DNA template, |
| pET28α- <i>hisSUMO</i> | pET28α | <i>HisSUMO</i> gene | <i>Kan</i> | Cloning backbone |
| oDW003 | pET28α- <i>hisSUMO</i> | <i>mutL</i> gene | <i>Kan</i> | HisSUMO-MutL protein expression plasmid |
| oDW005 | pET28α- <i>hisSUMO</i> | <i>mutL</i> gene | <i>Kan</i> | Variation of pDW003, 2x serine added between <i>SUMO</i> and <i>mutL</i> genes. |
| oDW006 | pET28α- <i>hisSUMO</i> | <i>uvrD</i> gene | <i>Kan</i> | HisSUMO-UvrD protein expression plasmid |
| oDW007 | pET28α- <i>hisSUMO</i> | <i>uvrD</i> Δ53N gene | <i>Kan</i> | HisSUMO-UvrDΔ53N protein expression plasmid |
| oDW008 | pET28α- <i>hisSUMO</i> | <i>uvrD</i> Δ108N gene | <i>Kan</i> | HisSUMO-UvrDΔ108N protein expression plasmid |
| oDW009 | pET28α- <i>hisSUMO</i> | <i>uvrD</i> Δ2B gene | <i>Kan</i> | HisSUMO-UvrDΔ2B protein expression plasmid |
| oDW010 | pET28α- <i>hisSUMO</i> | <i>uvrD</i> Δ52N gene | <i>Kan</i> | HisSUMO-UvrDΔ52N protein expression plasmid |

2.1.4 Buffers

TABLE 2.5 PROTEIN PURIFICATION BUFFERS

| Protein | Thesis section | Purification Step | Buffer Type | Recipe |
|--------------|----------------|-------------------------------|-------------------------|---|
| MutL | 2.2.4.2 | Cell Lysis | Lysis Buffer | 50 mM Tris pH 7.5, 300 mM NaCl, 1 mM DTT, 20 mM Imidazole, 5 mM MgCl ₂ , Pierce™ Protease Inhibitor Tablets (ThermoFisher, A32965) |
| | | Affinity Chromatography | Affinity Binding Buffer | 50 mM Tris pH 7.5, 300 mM NaCl, 1 mM DTT, 20 mM Imidazole, 5 mM MgCl ₂ |
| | | Affinity Chromatography | Affinity Elution Buffer | 50 mM Tris pH 7.5, 300 mM NaCl, 1 mM DTT, 300 mM Imidazole, 5 mM MgCl ₂ |
| | | Dialysis | Dialysis Buffer | 50 mM Tris pH 7.5, 300 mM NaCl, 1 mM DTT, 5 mM MgCl ₂ |
| | | Size Exclusion Chromatography | SEC Buffer | 50 mM Tris pH 7.5, 300 mM NaCl, 1 mM DTT, 5 mM MgCl ₂ |
| | | Storage | Freezing Buffer | 50 mM Tris pH 7.5, 300 mM NaCl, 1 mM DTT, 5 mM MgCl ₂ , 30% Glycerol |
| UvrΔ 52N | 2.2.4.3 | Cell Lysis | Lysis Buffer | 50 mM Tris pH 8, 50 mM NaCl, 20 mM Imidazole, 2% Glycerol, 2 mM DTT, Pierce™ Protease Inhibitor Tablets (ThermoFisher, A32965), DNase |
| | | Affinity Chromatography | Binding Buffer | 50 mM Tris pH 8, 50 mM NaCl, 20 mM Imidazole, 2% Glycerol, 2 mM DTT |
| | | Affinity Chromatography | Elution Buffer | 50 mM Tris pH 8, 50 mM NaCl, 500 mM Imidazole, 2% Glycerol, 2 mM DTT |
| | | Affinity Chromatography | DNA Wash Buffer | 50 mM Tris pH 8, 3 M NaCl |
| | | Ion Exchange Chromatography | Binding Buffer | 50 mM Tris pH 8, 50 mM NaCl, 2 mM DTT |
| | | Ion Exchange Chromatography | Elution Buffer | 50 mM Tris pH 8, 500 mM NaCl, 2 mM DTT |
| | | Storage | Freezing Buffer | 50 mM Tris pH 8, 100 mM NaCl, 2 mM DTT, 30% Glycerol |
| UvrΔ 108N | 2.2.4.2 | Cell Lysis | Lysis Buffer | 50 mM Hepes pH 7, 1 M NaCl, 2mM DTT, 20 mM imidazole, 5 mM MgCl ₂ , 10% Glycerol, Pierce™ Protease Inhibitor Tablets (ThermoFisher, A32965), DNase |
| | | Affinity Chromatography | Binding Buffer | 50 mM Hepes pH 7, 1 M NaCl, 2mM DTT, 20 mM imidazole, 5 mM MgCl ₂ , 10% Glycerol |

| | | | | | | |
|---------------|---------|-------------------------------|-----------------|---|--------------|--|
| | | Affinity Chromatography | Elution Buffer | 50 mM Hepes pH 7, 1 M NaCl, 2 mM DTT, 500 mM imidazole, 5 mM MgCl ₂ | | |
| | | Affinity Chromatography | DNA Wash Buffer | 50 mM Hepes pH 7, 3 M NaCl, 2 mM DTT, 500 mM imidazole, 5 mM MgCl ₂ | | |
| | | Dialysis | Dialysis Buffer | 50 mM Hepes pH 7, 1 M NaCl, 2 mM DTT, 5 mM MgCl ₂ | | |
| | | Size Exclusion Chromatography | SEC Buffer | 50 mM Hepes pH 7, 1 M NaCl, 5 mM MgCl ₂ | | |
| | | Storage | Freezing Buffer | 50 mM Hepes pH 7, 1 M NaCl, 5 mM MgCl ₂ , 30% Glycerol | | |
| | | Cell Lysis | Lysis Buffer | 50 mM Tris pH 8, 50 mM NaCl, 20 mM Imidazole, 2% Glycerol, 2 mM DTT, Pierce™ Protease Inhibitor Tablets (ThermoFisher, A32965), DNase | | |
| UvrDΔ 108N | 2.2.4.3 | Affinity Chromatography | Binding Buffer | 50 mM Tris pH 8, 50 mM NaCl, 20 mM Imidazole, 2% Glycerol, 2 mM DTT | | |
| | | Affinity Chromatography | Elution Buffer | 50 mM Tris pH 8, 50 mM NaCl, 500 mM Imidazole, 2% Glycerol, 2 mM DTT | | |
| | | Affinity Chromatography | DNA Wash Buffer | 50 mM Tris pH 8, 3 M NaCl | | |
| | | Ion Exchange Chromatography | Binding Buffer | 50 mM Tris pH 8, 50 mM NaCl, 2 mM DTT | | |
| | | Ion Exchange Chromatography | Elution Buffer | 50 mM Tris pH 8, 500 mM NaCl, 2 mM DTT | | |
| | | Storage | Freezing Buffer | 50 mM Tris pH 8, 100 mM NaCl, 2 mM DTT, 30% Glycerol | | |
| | | UvrDΔ 2B | n/a | Cell Lysis | Lysis Buffer | 50 mM Hepes pH 7, 1 M NaCl, 5 mM MgCl ₂ , 20 mM Imidazole, 2 mM DTT |

TABLE 2.6 DNA AND PROTEIN ELECTROPHORESIS RECIPES

| Buffer Name | Recipe | Purpose |
|-----------------------------|---|--|
| TBE Buffer | 90 mM Tris Base, 2 mM EDTA, 89 mM Boric Acid | Running buffer and component of agarose gels and 10% native TBE-PAGE gels. |
| SDS Running Buffer | 25 mM Tris, 192 mM Glycine, 3.5 mM SDS | Running buffer for SDS-PAGE protein gels. |
| 6X SDS Loading Dye | 1 M Tris (pH 7.5), 80 mg/ml SDS, 1 mg/ml Bromophenol Blue, 40% Glycerol, 100 mM DTT | Loading dye for SDS-PAGE protein gels. |
| Alkaline Running Buffer | 10 mM NaOH, 2 mM EDTA | Running Buffer for 0.7% denaturing alkaline gels for replication assays |
| 10X Alkaline Loading Buffer | 50 mM NaOH, 30 mM EDTA | Loading Buffer to resuspend samples after ethanol precipitation during replication assays |
| 6X Alkaline Loading Dye | 300 mM NaOH, 6 mM EDTA, 18% (w/v) Ficoll (Type 400), 0.15% (w/v) Bromocresol green, 0.25% (w/v) Xylene cyanol | Loading dye added to replication assay samples before loading onto the 0.7% denaturing alkaline gel. |
| STOP Buffer | 50 mM Tris (pH 7.5), 100 mM NaCl, 1 mM EDTA, 20% Glycerol, 10 mM β Mercaptoethanol | Protein denaturing STOP buffer used in helicase assays and replication assays. |

2.1.4.1 LB

For 1 L LB broth in water: 10 g Tryptone, 5 g Yeast Extract, 5 g NaCl

pH to 7 using NaOH

For LB agar, add 1.8 g of agar powder per 100 ml of LB broth. Dissolve by autoclaving and leave to solidify.

2.1.4.2 Antibiotics

TABLE 2.7 ANTIBIOTICS, STOCK AND WORKING CONCENTRATION

| Antibiotic | Working Concentration ($\mu\text{g/ml}$) | Stock solution (mg/ml) |
|---------------|--|------------------------|
| Kanamycin | 30 | 100 in Water |
| Carbenicillin | 100 | 100 in Water |

2.2 Methods

2.2.1 Gels

2.2.1.1 Agarose gel electrophoresis

Agarose gels were prepared at 0.8% and 1% agarose concentrations in 1x TBE buffer with 1x SYBR Safe DNA gel stain (Invitrogen, S33102) added to the molten agarose. Gel electrophoresis was carried out at 100-150V in 1x TBE buffer. Visualisation of DNA fragments was conducted using Biorad Gel Doc XR+ Imaging system using UV and Quantity One (Basic 4.6.2) software for image manipulation.

DNA samples were mixed with 6x Purple Gel Loading Dye (NEB, B7024S) to a final concentration of 1x. As standard 1 kb DNA Ladder (figure 2.1 A) (NEB, N3232) was run alongside the samples as a DNA fragment size marker.

2.2.1.2 Sodium Dodecyl Sulphate Polyacrylamide gel electrophoresis (SDS-PAGE)

10% SDS PAGE gels for protein separation imaging were prepared in SDS PAGE Gel Cassettes (Novex, NC2015) using a 10% resolving gel (375 mM Tris-HCl pH 8.8, 10% Bis-Acrylamide, 0.1% SDS, 0.1% APS, 0.08% TEMED) and 1.5% stacking gel (133 mM Tris-HCl pH 6.8, 1.5% Bis-Acrylamide, 0.1% SDS, 0.1% APS, 0.08% TEMED).

Protein samples were prepared through the addition of 6x SDS PAGE loading dye to a final concentration of 1x and denaturation for 3 min at 70 °C. Protein ladders used as size markers included Precision Plus Protein All Blue™ Prestained Protein Standards Ladder (Bio-Rad, 1610373) and PageRuler™ Prestained Protein Ladder (figure 2.1 B and C) (ThermoFisher Scientific, 26616).

Loaded samples were run at 200 V for 45 min - 1 hr and the gels were stained in QuickBlue Protein Stain (LubioScience, LU001000) at room temperature until clear, then washed with dH₂O for 30 min. Images were captured using the Bio-Rad Gel Doc XR+ Imaging system.

2.2.1.3 Native 10% TBE-PAGE gel electrophoresis

Native 10% TBE-PAGE gel (1x TBE, 10 % Bis-Acrylamide, 0.1% APS, 0.1% TEMED) was set in a Bio-Rad Protean®II xi tank (Bio-Rad, 165-2029) with an appropriate gel comb and submerged in 1x TBE buffer. Samples were prepared through the addition of 1x Purple Gel Loading Dye (NEB, B7024S) and run at 220 V for 90 min.

Gels were dried on a gel dryer (Bio-Rad, 583) for 70 min at 80 °C. To visualise DNA bands, dried gels were placed in a gel cassette with a storage phosphor screen (Merck, GE28-9564-75) for 12 – 36 hours. Gels were imaged by a Personal Molecular Imager (PMI) System (NEB, 170-9400) and quantified using ImageJ.

2.2.1.4 0.7% Agarose Alkaline gel electrophoresis

Agarose gels were prepared at 0.7% agarose concentration in 2 mM EDTA. When the molten agarose cooled down to 50 °C, 30 mM NaOH was added directly before pouring the gel. Set gels were submerged in Alkaline Running Buffer. Electrophoresis was carried out at 100 V for an initial 20 min to move samples into the gel quickly, followed by 23 V for 17 hrs.

Samples were resuspended in 1x Alkaline Loading Buffer (30 mM EDTA, 50 mM NaOH). λ DNA-HindIII Digest Ladder (figure 2.1 D) (NEB, N3012) labelled (section 2.5.2.) with ATP [γ -³²P] (Perkin Elmer, NEG502X250UC) was used as a DNA size marker.

Gels were dried using a gel dryer (Bio-Rad, 538) for 70 min at 80 °C before being placed in a gel cassette with a storage phosphor screen (Merck, GE28-9564-75) for 12 – 36 hours

exposure. The gels were imaged by a Personal Molecular Imager (PMI) System (NEB, 170-9400) and quantified using ImageJ (FIJI).

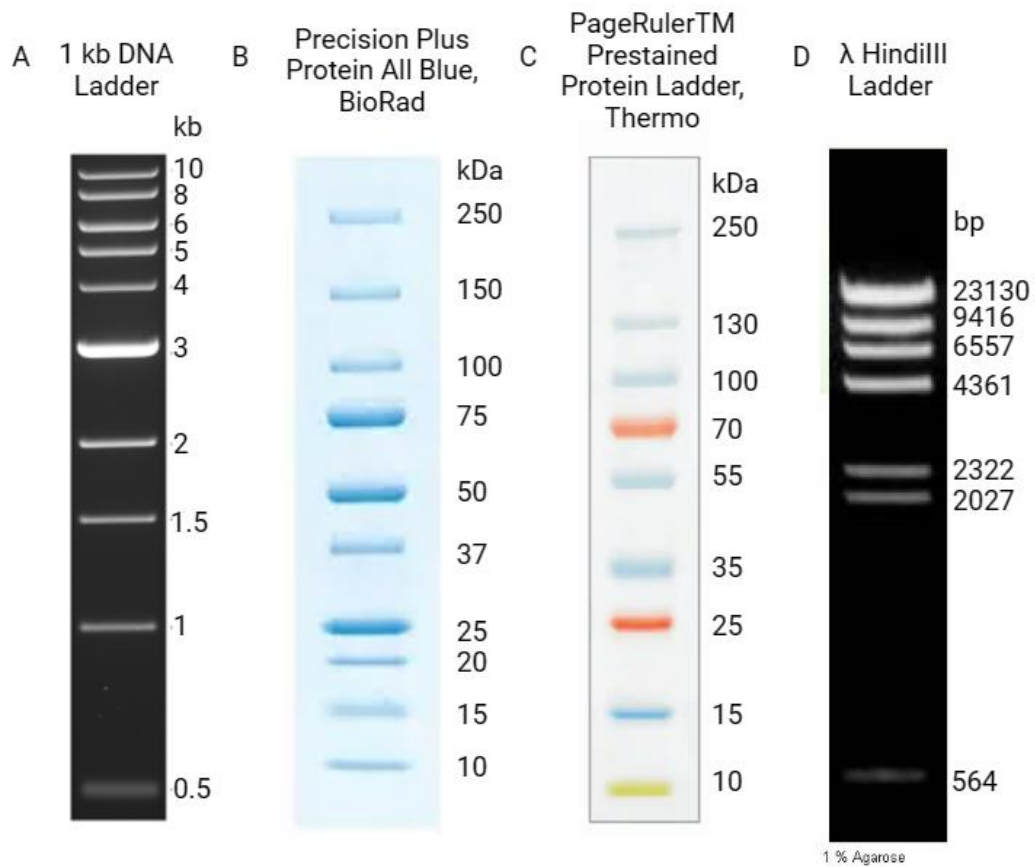


Figure 2.1 DNA and protein ladders. A. 1 kb DNA ladder (NEB, N3232) used in 1% agarose gels. B. Precision Plus Protein All Blue ladder (BioRad, 1610373) used for some protein gels. C. PageRuler™ Prestained Protein ladder (ThermoFisher Scientific, 26616) used in most protein gels. D. λ HindIII ladder used for replication assay gels.

2.2.2 Molecular Biology

2.2.2.1 PCR

The PCR protocols were followed as per the Phusion® DNA Polymerase (NEB, M0530) or *Taq* DNA Polymerase (NEB, M0273) protocols.

For Phusion® DNA Polymerase the reaction (1x Phusion™ HF Buffer, 200 µM dNTPs each, 0.5 µM forward primer, 0.5 µM reverse primer, 0.02 U/µl Phusion™ High-Fidelity DNA Polymerase, <1,000 ng DNA template in 20 µl or 50 µl total volume) underwent initial denaturation at 98 °C for 30 s, followed by 30 rounds of denaturation at 98 °C for 10 s, annealing at varying temperature (<72 °C) depending on the melting temperature (T_m) of oligos for 30 s, and extension at 72 °C for 30 s (per 1kb of template). Lastly, the reaction went through a final extension step at 72 °C for 10 min.

For *Taq* DNA Polymerase the reaction (1x Standard *Taq* Reaction Buffer, 200 µM dNTPs each, 0.2 µM forward primer, 0.2 µM reverse primer, 0.025 U/µl *Taq* DNA Polymerase, <1,000 ng DNA template in 20 µl or 50 µl total volume) underwent initial denaturation at 95°C for 30 s, followed by 30 rounds of denaturation at 95 °C for 30 s, annealing at varying temperature 45-68 °C) depending on the melting temperature (T_m) of oligos for 15-60 s, and extension at 68 °C for 60 s/kb. Lastly, reaction went through a final extension step at 68 °C for 5 min.

2.2.2.2 Site-directed mutagenesis PCR

Site-directed mutagenesis PCR (figure 2.2) was conducted to insert or delete regions of DNA sequence, such as removing regions of the *uvrD* gene or adding two serine amino acids to the MutL expression plasmid. PCR was conducted as in 2.2.2.1 using the Phusion DNA Polymerase protocol.

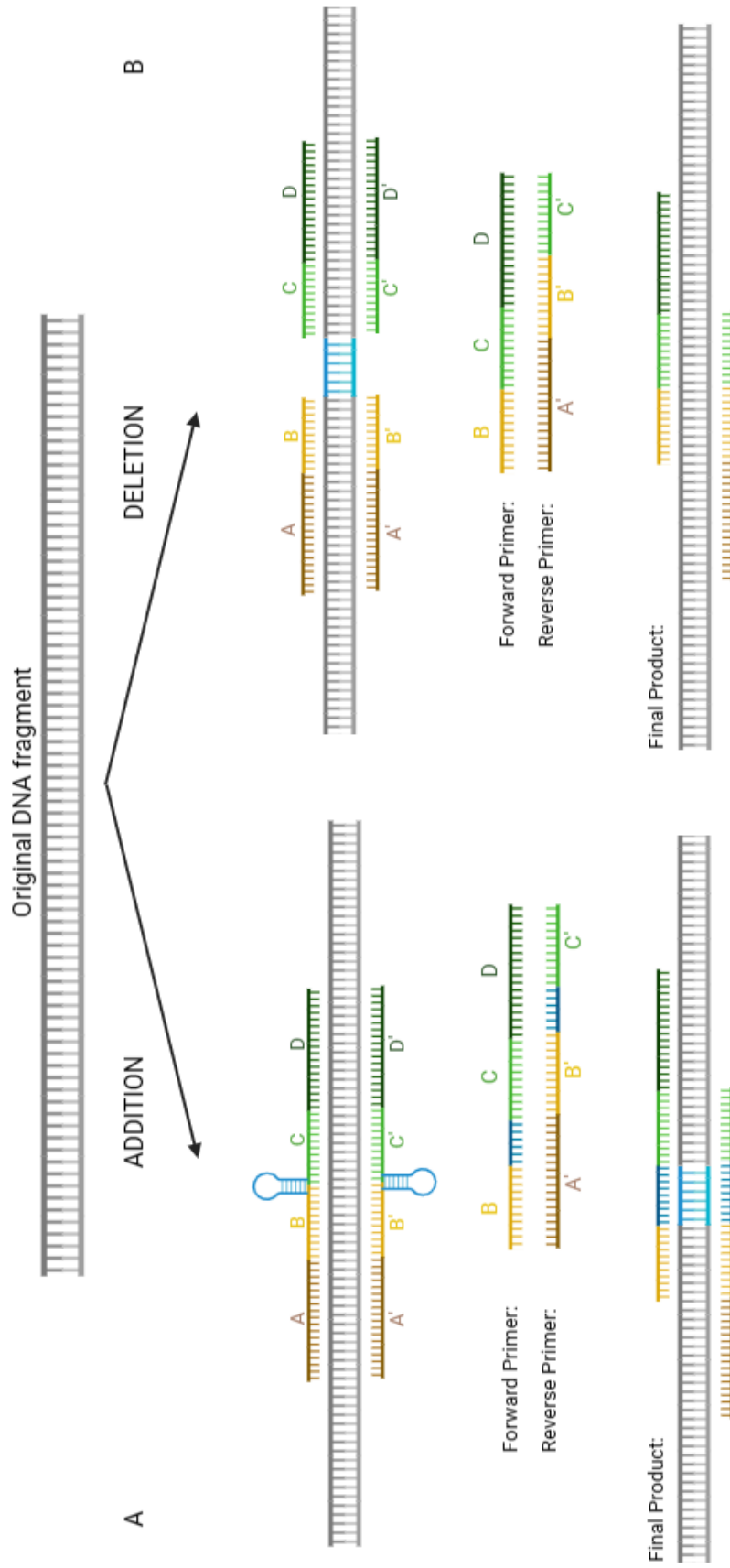


Figure 2.2 Site Directed Mutagenesis PCR Schematic. A. PCR to add a region or individual base pairs to the original DNA fragment. Primers were designed to add DNA (blue), with the forward and reverse primer having large complementary sequences to ensure correct and strong binding. B. PCR to remove a region or base pairs from the original DNA fragment. The primers were designed to exclude unwanted DNA (blue).

2.2.2.3 Diagnostic Restriction Digests

Restriction digests were conducted using 400-600 ng of DNA with 20-50 units of enzyme and 1x CutSmart Buffer (NEB) to confirm the presence of a gene on a plasmid post-cloning. Restriction digest enzymes require specific buffers, and the use of CutSmart buffer was appropriate for all enzymes unless stated otherwise. Restriction digestion reactions were incubated for 1 hr at 37 °C before gel electrophoresis using a 1% agarose gel.

2.2.2.4 DpnI Digest

The DpnI digest was conducted as a cloning step to remove methylated template DNA from samples. It was conducted by adding 20 units of DpnI (NEB, R0176) per 50 µl of PCR product. The samples were incubated for 2 hrs at 37 °C.

2.2.2.5 InFusion Cloning

The linearised DNA products needed were generated using Phusion® PCR followed by a DpnI digest, gel extraction (Qiagen, 28704) and PCR purification (Qiagen, 28104). The InFusion protocol was conducted as per the TakaraBio protocol (figure 2.3) (TakaraBio, 638909). Stellar cells (TakaraBio, 636763) were transformed (section 2.2.3.2) with infusion cloning product and grown on LB agar plates supplemented with appropriate antibiotic.

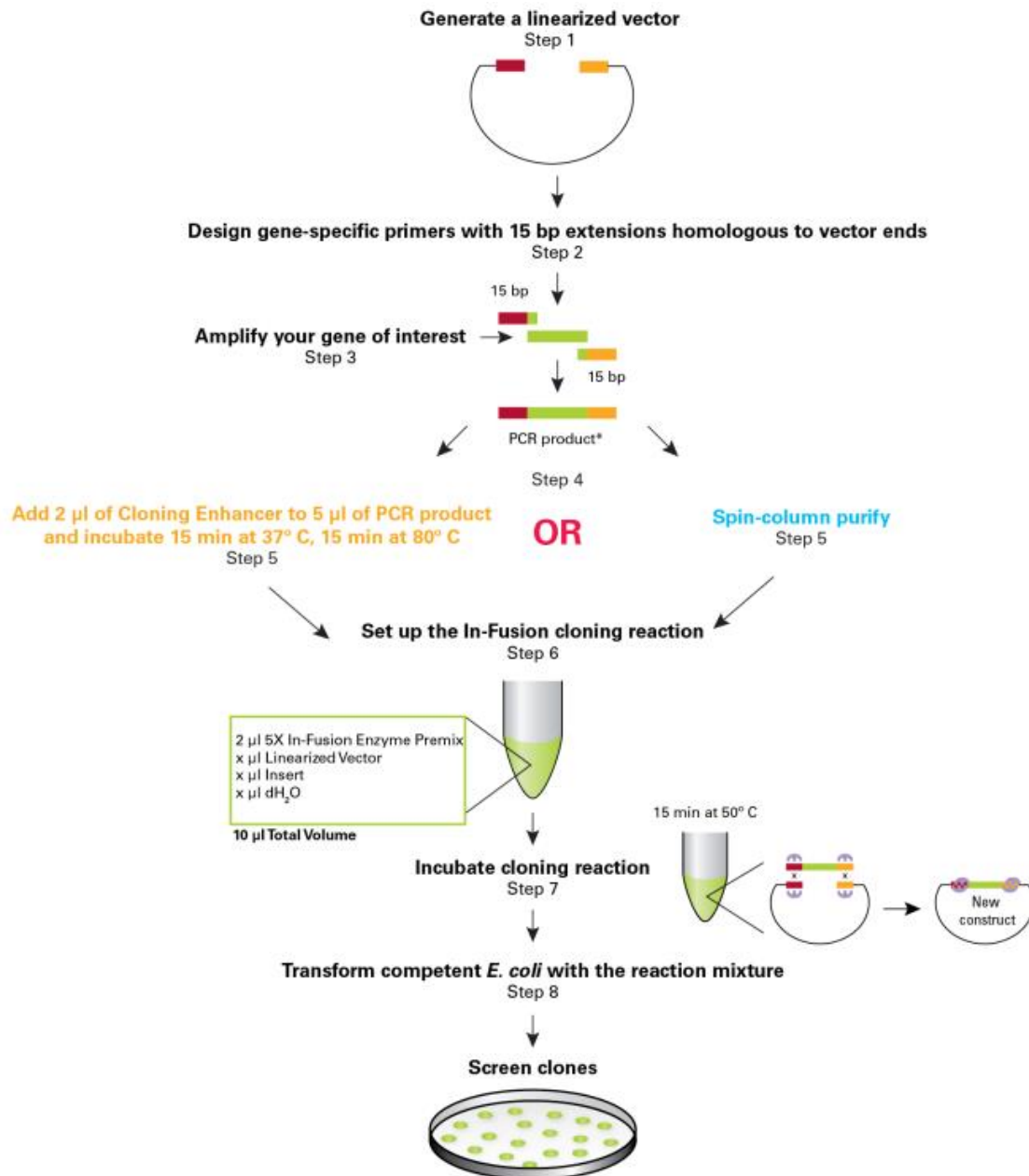


Figure 2.3 InFusion Cloning schematic. PCR was used to linearise the vector and add 15 bp on each end which match the 15 bp from the isolated gene-of-interest. TakaraBio recommends using the cloning enhancer (DpnI digest) on the isolated gene PCR product, though we conducted a DpnI digest and gel extraction for both the gene-of-interest and the linearised vector. The gene and vector were incubated with the In-Fusion Enzyme Premix for 15 min at 50°C and the sample was transformed into competent TakaraBio Stellar cells. Schematic taken from the InFusion TakaraBio Manual (TakaraBio, 2018).

2.2.2.6 Gel Extraction and PCR clean up

Gel extraction of DNA from a 0.8 - 1% agarose gel was conducted using the Qiagen gel extraction kit (Qiagen, 28704). Nanodrop 2000 spectrophotometer (ThermoScientific, ND-2000) was used to determine sample concentration and the 260/230 ratio. The 260/230 ratio was used to determine if the sample was clean of contaminants from the agarose gel. If the generated 260/230 ratio of the final sample was below 1.8, the Qiagen PCR clean up kit (Qiagen, 28104) was used (as per manufacturers instructions) to achieve a 260/230 ratio at or above 1.8.

2.2.2.7 Plasmid Purification

DH5 α competent cells were transformed with plasmids generated through InFusion cloning or bought/received from other sources. Cells were grown overnight for 17-18 hours at 37 °C to replicate the plasmid. To isolate plasmid from cells, plasmid purification was conducted using the Qiagen plasmid mini prep kit protocol (Qiagen, 12123).

2.2.3 Microbiology

2.2.3.1 Making DH5 α and BL21 DE2 transformation competent

Bacterial transformation can only be conducted using competent cells. Overnight cell culture of DH5 α (plasmid purification), Stellar (plasmid purification post cloning) or BL21 DE3 (protein expression) cells was set up by inoculating 5 ml LB broth and growing at 37°C for 17-18 hrs. The overnight culture was used to inoculate a 25 ml diluted culture which was grown until OD₆₅₀ = 0.4 when measured using a spectrophotometer (Beckman, DU 720 model, 18590). Cells were centrifuged at 3300 x g and resuspended in 10 ml ice cold 0.1 M CaCl₂ and

incubated on ice for 1 hr. Cells were centrifuged at 3300 x g for 10 min at 4°C and resuspended in 30 ml of storage buffer (0.1 M CaCl₂, 15% glycerol) before flash freezing in liquid nitrogen.

2.2.3.2 Bacterial Transformations

Bacterial transformations were used to insert a plasmid into cells for plasmid production or protein expression.

50-100 ng of plasmid was incubated on ice with 50 µl competent cells for 30 min. The samples were heat-shocked for 45 s at 42 °C, followed by a 2 min incubation on ice. 450 µl of LB broth was added to the samples and left to incubate for 1 hour at 37 °C in a shaking incubator at 180 RPM. The cells were plated on LB agar supplemented with appropriate antibiotics overnight at 37 °C.

2.2.4 Protein Purification

Protein purification was conducted to produce a stock of recombinant protein. Two strategies were employed using a combination of affinity, size exclusion and ion exchange chromatography (figure 2.4).

A full list of buffers used to purify each protein can be found in table 2.5.

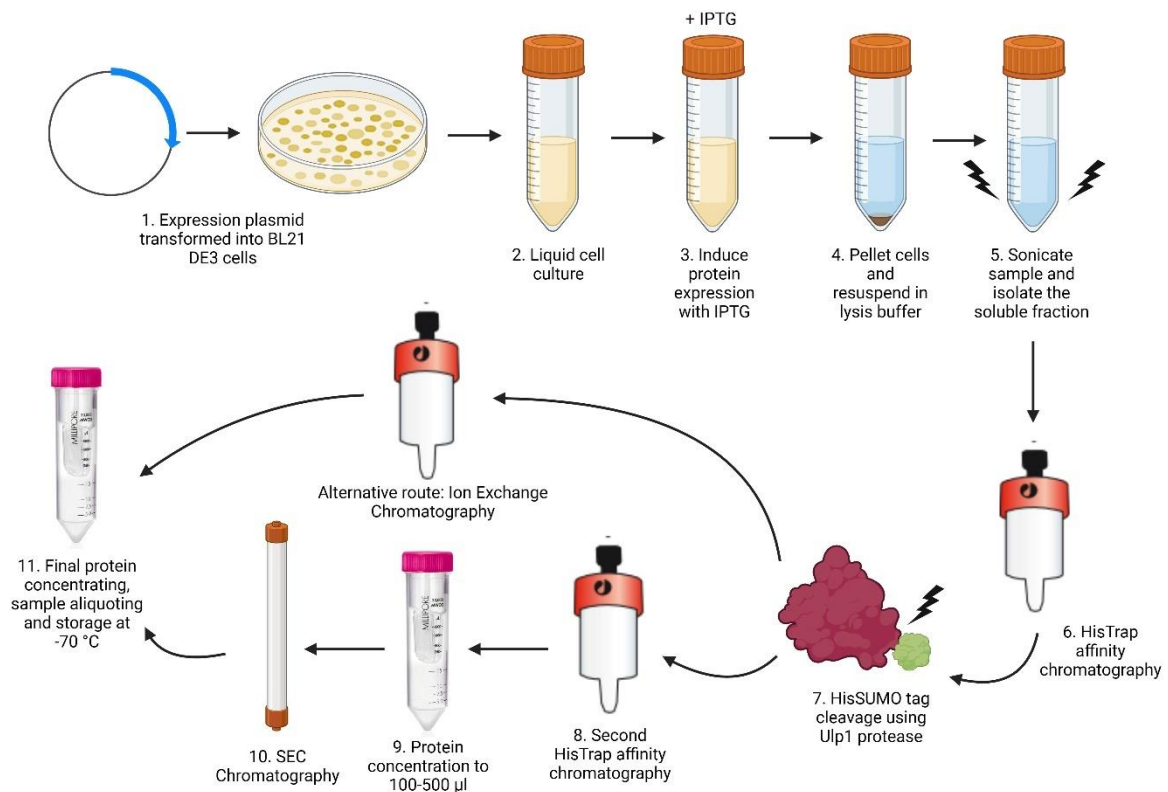


Figure 2.4 Protein purification method summary schematic as per section 2.2.4. BL21 DE3 cells were transformed with an expression plasmid and used to grow a 500 - 1000 ml liquid culture (or 40 ml for expression tests). Overexpression of protein was induced with 1 mM IPTG before pelleting the cells and resuspending in the lysis buffer. The sample was sonicated, and the soluble fraction was isolated after centrifugation. The sample was injected into a HisTrap affinity chromatography column. The purified, HisSUMO tagged, protein underwent tag cleavage using Ulp1 protease, followed by one of two chromatography paths. First path included a second affinity column, followed by a SEC chromatography column after concentrating the protein. The second path included an ion exchange chromatography column. All samples were concentrated down to a storage concentration of minimum 1 mg/ml and stored at -70°C after flash freezing in liquid nitrogen. Figure created on biorender.com.

2.2.4.1 Overexpression of the protein of interest

Competent BL21 DE3 cells were transformed (section 2.2.3.2.) with an expression plasmid containing the gene-of-interest with a His-SUMO tag. Spectrophotometry was used to monitor the cell growth until $OD_{600} = 0.6$. Cell cultures were induced with 1 mM IPTG and grown overnight at 18 °C for 17 hours. Overnight cultures were centrifuged at 4000 x g for 30 min in a high-speed centrifuge. Cell pellets were resuspended in lysis buffer and sonicated 5 times at 60% power using Sonicator SonoPlus HD (Bandelin, GM 2070). The samples were cooled on ice between sonication rounds. Lysed cells were centrifuged at 15000 x g for 20 min to isolate the soluble fraction (supernatant). DNA was precipitated from the soluble fraction using 0.075% Poly(ethyleneimine), also known as PolyminP, solution at 4 °C for 20 min (for MutL protein purification only). The solution was centrifuged at 15000 x g for 20 min and the supernatant was isolated and filtered through a Filtropur S, PES 0.2 µm syringe filter (Sarstedt, 83.1826) in preparation for chromatography.

2.2.4.2 Protein Purification using two affinity chromatography steps and a size exclusion chromatography step

An AKTA Start protein purification system was used for the purification of the MutL protein, and the AKTA Go protein purification system was used for the purification of the UvrD region-deletion mutants. His-tagged protein-of-interest was isolated using a HisTrap HP affinity column (Cytiva, 17524801) through nickel-histamine bonding. The protein was eluted through an elution gradient using a high imidazole elution buffer. The HisSUMO tag was cleaved overnight during dialysis using 100 µg of in-house produced SUMO-specific protease, Ulp1. The HisSUMO and protein-of-interest were isolated in separate peaks using a HisTrap affinity chromatography column. Untagged protein-of-interest was eluted during sample loading, while HisSUMO bound to the nickel column and was eluted using the elution buffer.

The size exclusion step was added to remove protein contaminants from the sample. HiLoad® 16/600 Superdex® 200 pg column (Merck, GE28-9893-35) was used for MutL, while the size exclusion Superose™ 6 10/300 GL column (Cytivia, 17517201) was used for UvrD region-deletion mutants.. The protein-of-interest sample was concentrated using Amicon® Pro Purification System with 30 kDa Amicon® Ultra-0.5 Device (Millipore, ACS505024) and Pierce™ Protein Concentrators (ThermoFisher, 88502) as per manufacturer's instructions. The aliquoted stocks were stored at -70°C after flash-freezing in liquid nitrogen.

2.2.4.3 Protein Purification using one affinity chromatography step and ion exchange chromatography steps

The AKTA Go protein purification system was used for the purification of proteins using one affinity chromatography and one ion exchange chromatography step. His-tagged protein-of-interest was isolated using a HisTrap HP affinity column (Cytivia, 17524801) through nickel-histamine bonding. The protein was eluted through an elution gradient using a high imidazole elution buffer. The HisSUMO tag was cleaved overnight using 100 µg of in-house produced SUMO-specific protease, Ulp1.

The cleaved protein was injected into a 1 ml Mono Q™ 5/50 GL column (Cytivia, 17516601) to separate the proteins based on their negative charge, as the hisSUMO tagged and untagged proteins have different charges. A low salt buffer was used for protein loading and a high salt buffer was used for elution from the column. The ion exchange step, not unlike the size exclusion step, was used to remove protein contaminants, but also to remove a larger proportion of protein heterodimers where some protein remains uncleaved and binds to the column. The protein-of-interest sample was concentrated using Amicon® Pro Purification System with 30 kDa Amicon® Ultra-0.5 Device (Millipore, ACS505024) and Pierce™ Protein Concentrators (ThermoFisher, 88502). The aliquoted stocks were stored at -70°C after flash-freezing in liquid nitrogen.

2.2.4.5 Thermal Shift Assay

Thermal Shift Assays (TSA) were conducted to test for correct folding of purified proteins (figure 2.5). TSA, a type of differential scanning fluorimetry, uses a fluorescent SYPRO dye (ThermoFisher Scientific, S6650) which binds to hydrophobic regions of proteins.

5.56x concentration of the SYPRO dye was added to the protein-of-interest in buffer (binding buffer from protein purification or other appropriate buffer) to a total volume of 27 μ l. Samples were placed in a ThermoFluor Biorad MyIQ5 (BioRad, 170-9780) where they were exposed to temperature increase. The change in fluorescence was detected as the protein unfolded and the dye released.

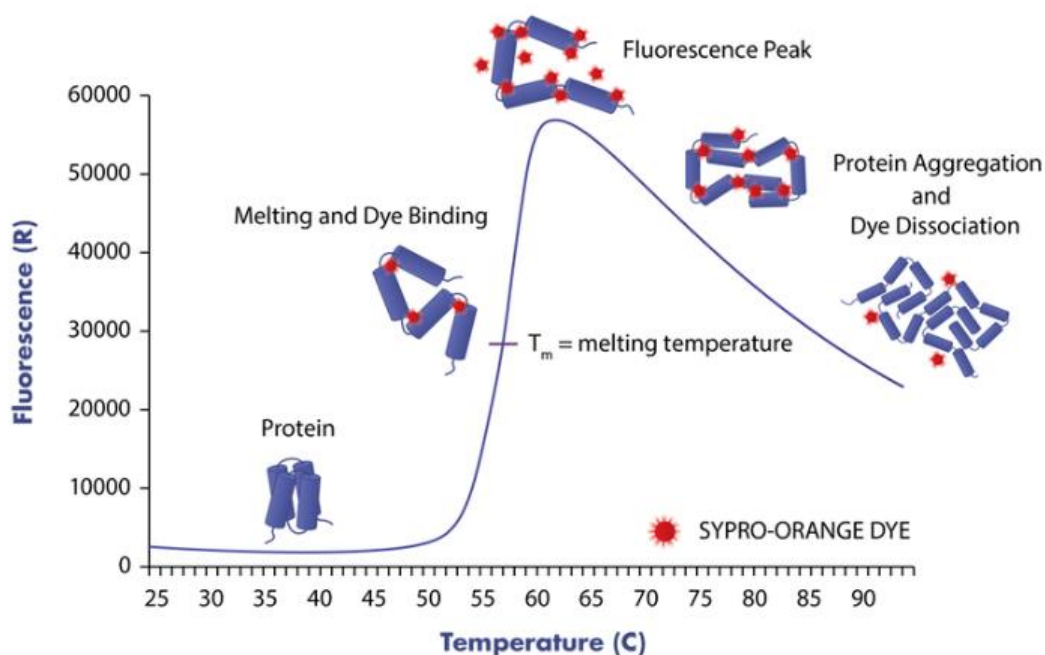


Figure 2.5 Thermal Shift Assay. Diagram illustrating how thermal shift assays (TSA) work. Figure adapted from Reaction Biology Webpage (ReactionBiology).

2.2.5 Biochemical Techniques

2.2.5.1 ³²P labelling of DNA

1 µg of oligo was combined with 10 units of T4 polynucleotide kinase (PNK) (NEB, M0201S), 1X PNK Buffer (NEB, B0201SVIAL), and 10 µCi of γ-³²P ATP and incubated for 30 min at 37 °C followed by a 20 min incubation at 65 °C.

Any unincorporated γ-³²P ATP was removed by size-exclusion purification using the Bio-Spin® P-30 gel columns (BioRad, 7326006) as per the manufacturer's instructions.

If required to be double-stranded, the labelled oligo was incubated for 5 min at 95 °C with 1 µg of complementary oligo and 1x saline-sodium citrate (SSC) buffer, followed by a slow temperature decrease to 25 °C overnight. The overnight sample was run on a 10% TBE-PAGE native gel and visualised using an X-ray film. The film was placed over the sample in the cassette for 30 sec to 5 min (depending on ³²P activity). The X-ray film was then placed in the developer solution for 30 - 90 sec, then washed in water. The X-ray film was then placed in the fixer solution for 30 - 90 sec, then washed in water. The processed X-ray film was used as a template for band location for cutting out the labelled substrate from the gel. The extracted gel was incubated at 4 °C in 1x TE buffer with 50 mM NaCl for a minimum of 2 days. The concentration was checked using a Tri-Carb scintillation counter (PerkinElmer, TriCarb 2900TR) by comparing the counts measured for the hybridised and the non-hybridised sample when calculating the mean of 5 count repeats. Concentration calculated as per:

$$Conc (\mu M) = \left(\frac{\text{hybridised sample}}{\text{non hybridised sample}} \right) \times \text{conc } (\mu M) \text{ of non hybridised oligo in } 30 \mu l$$

2.2.5.2 Helicase Assays

Helicase assays are a biochemical tool to test for helicase activity *in vitro* on a double-stranded DNA (dsDNA) substrate. Additional proteins and blocks were incorporated where indicated.

The reagent mix (for 1 reaction: 100 mM HEPES pH8, 25 mM MgAc, 25 mM DTT, 250 µg/ml BSA) was incubated for 2 min at 37 °C with the proteins (concentrations varied for individual assays) before the addition of 2 nM of a dsDNA substrate labelled with γ -³²P ATP (section 2.5.2.). Following a 2 min at 37 °C incubation, the start buffer (20 mM ATP) was added and the reaction was incubated at 37 °C for 10 min (oDW015-16, oDW017-18 helicase assays) or 3 min (oDW070-71 helicase assays) before the addition of stop buffer (2.5% SDS, 200 mM EDTA, and 10 mg/ml Proteinase K).

Samples were run on 10% TBE-PAGE native gels for 90 min at 220 V before being dried for 70 min at 80 °C and visualised by phosphor imaging.

Bands were quantified using ImageJ and the percentage of unwound substrate was calculated using:

$$\% \text{ unwound} = \frac{ssSample - \left(ssControl \times \left(\frac{dsSample + ssSample}{dsControl + ssControl} \right) \right)}{(dsSample + ssSample) - \left(ssControl \times \frac{dsSample + ssSample}{ssControl + dsControl} \right)} \times 100$$

2.2.5.3 Replication Assays

Replication assays are a biochemical tool which allows for the reconstitution of replication forks on a plasmid *in vitro* (Jameson et al., 2021).

In this work, we used the pKJ001 plasmid template (figure 2.6), which contains a replication origin site, *oriC*, a *lacO*₂₂ array for LacI protein binding (reversible block after an addition of IPTG), and a single *terB* site for binding of Tus in a termination block. The clockwise fork is

designed to travel towards the non-permissive face of the Tus-*terB* block, while the counterclockwise fork is designed to travel towards the permissive face of the Tus-*terB* block.

The reactions were assembled by combining the replication fork proteins (produced in-house) master mix (50 nM DNA Polymerase III core ($\alpha\epsilon\theta$), 25 nM Tau complex, 160 nM DnaB, 160 nM DnaC, 1 μ M SSB, 80 nM β clamp, 30 nM HU, 200 nM DnaG, 133 nM GyraseA₂B₂), protein blocks (400 nM Tus and/or 400 nM LacI), reagents (40 mM HEPES pH 8, 10 mM DTT, 10 mM MgAc, 2 mM ATP, 0.08 mM GCUTP, 0.04 mM dNTPs each, 0.1 mg/ml BSA), and 200 ng of the replication plasmid pKJ001 (approximately 2 nM). Reactions were incubated at 37°C for 2 min, followed by an addition of 300 nM of DnaA. After an additional incubation at 37°C for 2 min, 30 units of Smal (Promega), 46 kBq [α -³²P]-dCTP (111 TBq/mmol), and 1 mM IPTG were added where indicated. Reactions were stopped, after further incubation for 2 min at 37 °C, through the addition of 6x STOP buffer (2.5% SDS, 200 mM EDTA, and 10 mg/ml Proteinase K) to a final concentration of 1x.

Ethanol precipitation was conducted to remove unincorporated [α -³²P]-dCTP from the reaction samples. Ammonium acetate and ethanol were added to the samples to final total concentrations of 800 mM and 67% respectively. The samples were centrifuged for 10 min at 15,500 x g at 4 °C and the pellet was resuspended in 70% ethanol before a repeat centrifugation. The pellet was left to air dry for 10 min before resuspension in the alkaline running buffer (50 mM NaOH, 30 mM EDTA). Gel electrophoresis was conducted using 0.7% submarine denaturing gel.

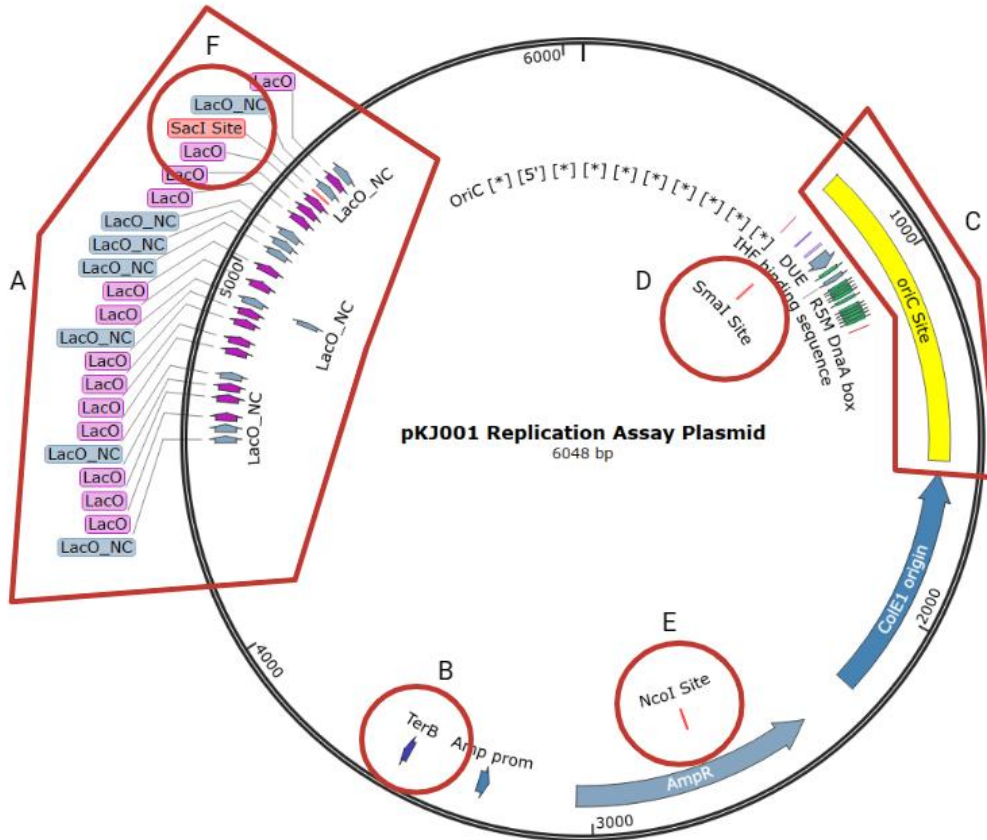


Figure 2.6 Replication Assay template plasmid. pKJ001 was used as DNA template for replication assays conducted as part of this thesis. Plasmid map generated using SnapGene after nanopore sequencing. The plasmid contains a *lacO* region with 22 *lacO* sites (A) for *LacI* binding. The *ter* site (B) allows for *Tus* binding. The non-permissive face of the *Tus-ter* block is approached by the clockwise replication fork. The *oriC* region (C) serves as an origin of replication for replication fork assembly. *SmaI* cleavage site (D) enables plasmid linearisation to release supercoiling. Restriction sites *NcoI* (E) and *SacI* (F) allow for plasmid cleavage to allow for a single fork to reach *Tus-ter*. Figure created on biorender.com

2.2.5.4 Tus Jumping Assay

The Tus jumping assay is a biochemical tool developed in this thesis to test for protein displacement by a replication fork *in vitro*. The aim of using the Tus jumping assay in this work was to determine whether Tus remains bound to *ter* when both replication forks meet at the Tus-*ter* block in replication assay conditions (figure 2.7).

The Tus jumping assay was developed from the replication assay (section 2.2.5.3). The protocol for the Tus Jumping Assay varies from the replication assay in the following ways: 1. Lower Tus concentration (2.5 nM). 2. No addition of [α - 32 P]-dCTP into the assay and instead the addition of 5 nM of a 32 P labelled Tus capture substrate (oDW035-oJH117). 3. No DNA precipitation step (not necessary as no unincorporated 32 P should be present). 4. No STOP buffer was added to the assay in order not to denature. 5. The samples were run on a 10% TBE-PAGE native gel rather than a denaturing gel to prevent the dissociation of Tus from the Tus capture substrate. The Tus capture substrate was labelled with γ - 32 P ATP using T4 PNK end-labelling (section 2.2.5.1) and designed to include a *ter* sequence for Tus binding. When running and loading the assays, six reactions were conducted per one assay and 80% glycerol was added to slow the reaction instead of a STOP buffer and to allow loading of DNA on the native 10% TBE-PAGE gel. Samples were loaded immediately after the addition of 80% glycerol and the current was started before the next round of reactions began. This created a 'step-ladder' look to the gel.

Important concentrations to note that were used in the Tus Jumping Assay: pKJ001 (2 nM), Tus capture substrate (5 nM), Tus (2.5 nM – reduced from the excess of 400 nM in replication assays). All replication proteins were added at the same concentration as in the replication assay.

The percentage of bound Tus capture substrate was calculated using the below equation, where 'sBound' means the bound band of the tested sample, 'sUnbound' means the unbound

band of the tested sample, 'cBound' means the bound band of the control, 'cUnbound' means the unbound band of the control.

$$\% \text{ bound} = \frac{sBound - \left(cBound \times \left(\frac{sUnbound + sBound}{cUnbound + cBound} \right) \right)}{(sUnbound + sBound) - \left(cBound \times \frac{sUnbound + sBound}{cUnbound + cBound} \right)} \times 100$$

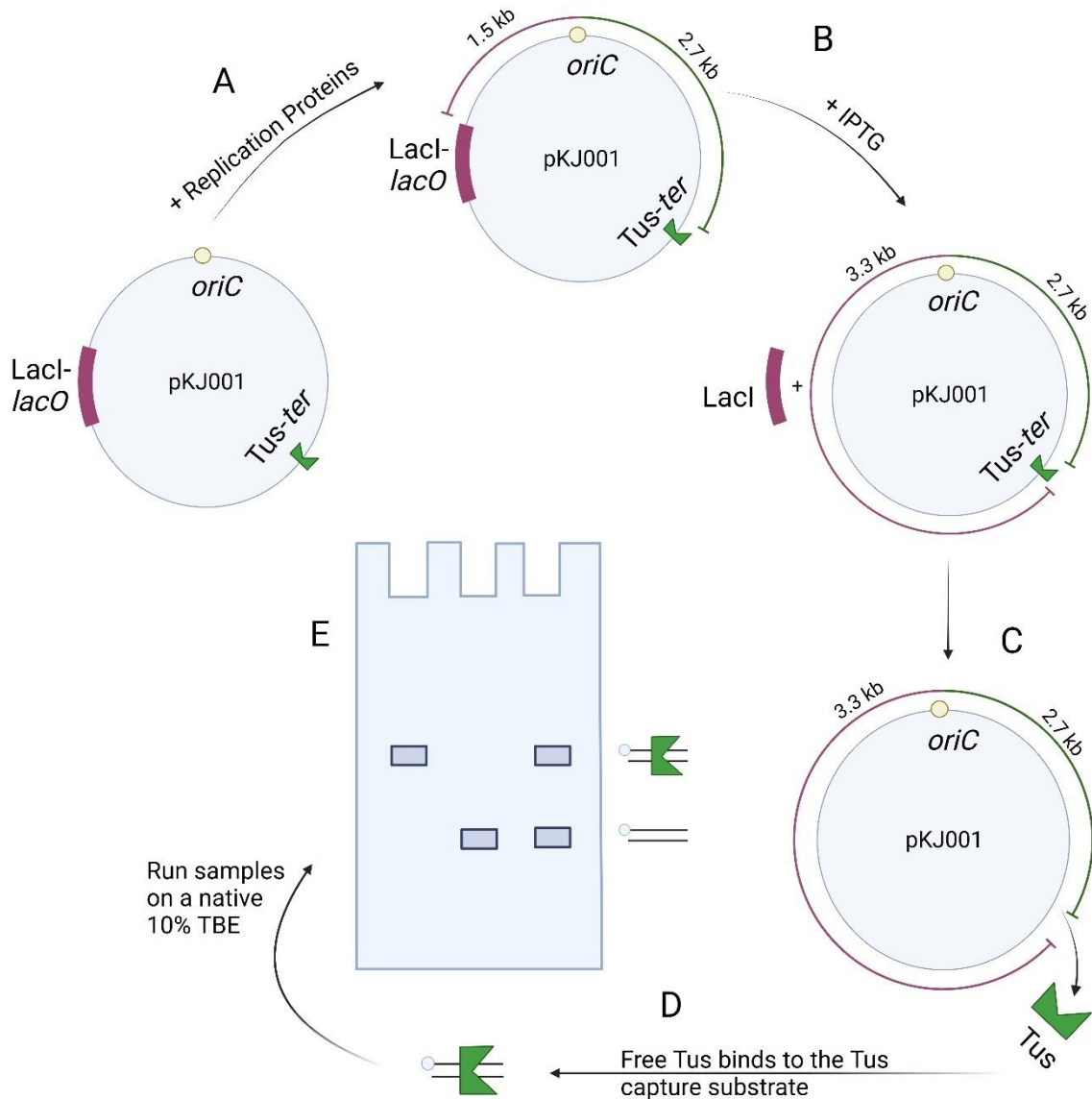


Figure 2.7 Design of the Tus jumping assay. A. Replication forks are reconstituted at *oriC* on pKJ001 and DNA replication is initiated through the addition of DnaA. Both forks get stuck, counterclockwise at *LacI-lacO* and clockwise at *Tus-ter*. B. Addition of IPTG removes *LacI* from *lacO* and releases the paused counterclockwise replication fork. C. Clockwise and counterclockwise replication forks meet at *Tus-ter* and potentially displace *Tus*. D. Free *Tus* binds to the *Tus* capture substrate labelled with radioactive ^{32}P . F. Reactions are run on a 10% TBE-PAGE native gel and the percentage of *Tus*-bound vs unbound *Tus* capture substrate is compared. Figure created on biorender.com

2.2.5.5 Tus Jumping Assay with a single replication fork

The Tus Jumping Assay was adapted to test whether Tus remains bound to *ter* when a single replication fork approaches either the permissive or the non-permissive orientation of the block (figure 2.8).

The assay was conducted as per the Tus jumping assay in section 2.2.5.4, with a difference in the restriction digest enzyme added alongside the Tus capture substrate. For the permissive orientation, 30 units NcoI (NEB, R3193) was added instead of 30 units of SmaI; for the non-permissive orientation, 30 units of SacI (NEB, R3156) was added instead of 30 units of SmaI.

The formula used to calculate the percentage of Tus bound to the Tus capture substrate was:

$$\% \text{ bound} = \frac{sBound - \left(cBound \times \left(\frac{sUnbound + sBound}{cUnbound + cBound} \right) \right)}{(sUnbound + sBound) - \left(cBound \times \frac{sUnbound + sBound}{cUnbound + cBound} \right)} \times 100$$

2.2.5.6 EMSA band shift assay

A band shift assay was conducted to test whether a separation can be seen between a double stranded oligo with Tus bound to it and without Tus bound to it.

2 nM DNA Substrate (labelled with ³²P), reagent mix (for 1 reaction: 100 mM HEPES pH8, 25 mM MgAc, 25 mM DTT, 250 µg/ml BSA), and varied concentrations of Tus (0 nM, 1 nM, 2 nM, 4 nM and 8 nM) were incubated at 37°C for 6 min. No STOP solution was added and the samples were immediately loaded onto a native 10% TBE-PAGE gel. Gel electrophoresis was conducted for 90 min at 220 V before being dried for 70 min at 80 °C and visualised by phosphor imaging..

2.2.5.7 Statistical Analysis

A two-tail and one-tail t-tests were used to calculate the statistical significance of data generated. Two-tail t-test was used when testing for a change in unwinding, while one-tail t-test was used when testing for an increase in unwinding.

The t-test was chosen as it allows for an evaluation of one or two populations, which matches our aim to test for an increase in unwinding/protein binding between two conditions.

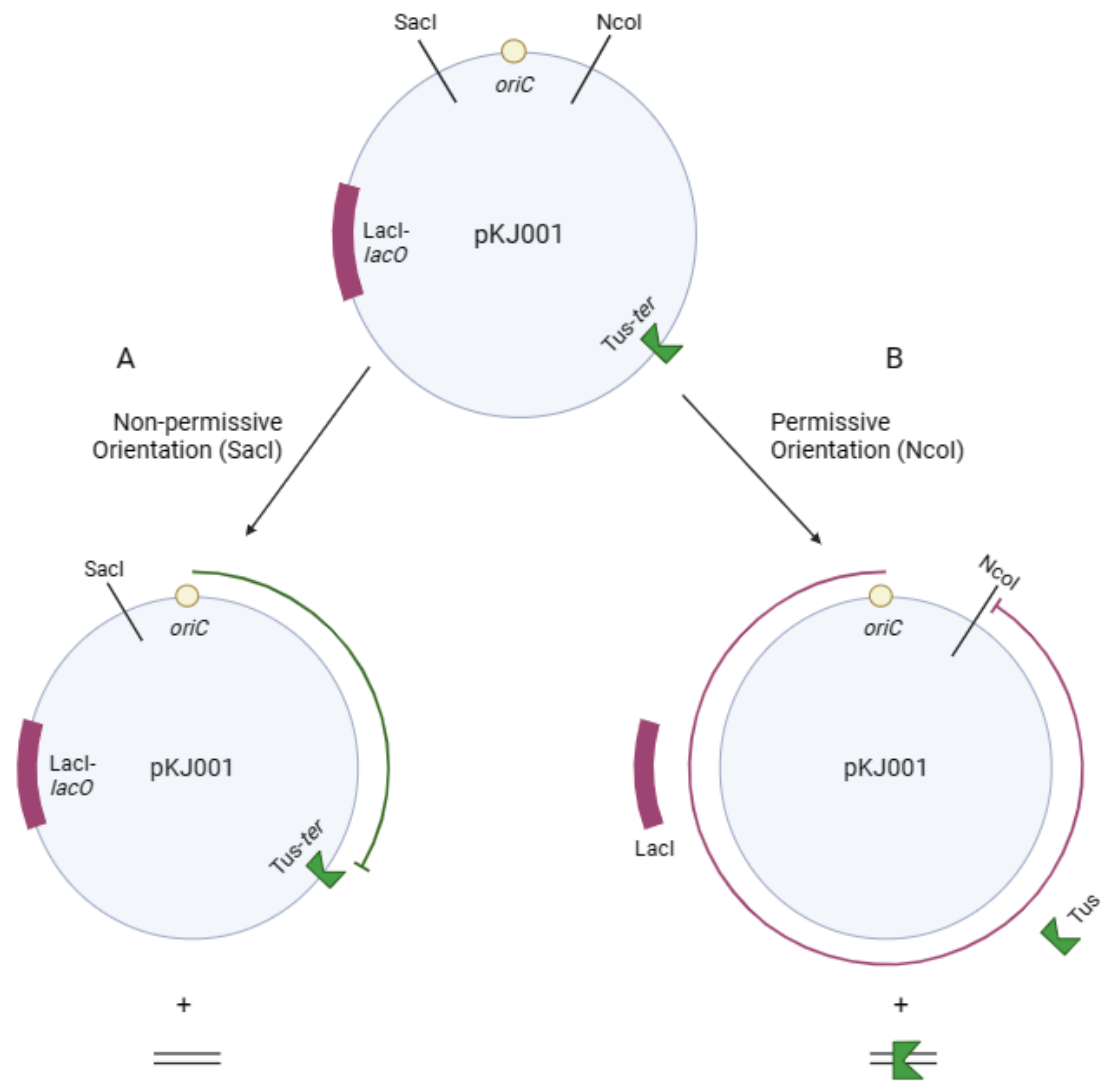


Figure 2.8 Tus jumping assay with a single replication fork. A. Digestion of pKJ001 with *SacI* leads to only the clockwise replication fork reaching the *Tus-ter* block (non-permissive face). B. Digestion of pKJ001 with *NcoI* leads to only the counterclockwise replication fork reaching the *Tus-ter* block (permissive face only). Figure created on biorender.com.

2.2.6 Analytical Chromatography

2.2.6.1 Tus-bound pKJ001 – SEC column

19.05 µg Tus and 40.82 µg pKJ001 plasmid were incubated on ice for 40 min in 50 mM Hepes pH 7.0, 150 mM NaCl buffer. The sample (100 µl) was injected into a size exclusion Superose 10/30 column, using a SEC running buffer (50 mM Hepes pH 7.0, 150 mM NaCl). AKTA Pure protein purification system was used because of its ability to measure the 260 and 280 UV readings. 19.05 µg of Tus only and 40.82 µg of pKJ001 plasmid only sample tests were also conducted using SEC.

2.2.6.2 Tus-bound pKJ001 – MonoQ

84 µg Tus and 75 µg pKJ001 plasmid were incubated on ice for 40 min in a 50 mM Hepes pH 7.0, 50 mM NaCl buffer. The sample was injected into an ion exchange MonoQ column using a low salt running buffer (50 mM Hepes pH 7.0, 50 mM NaCl) and high salt elution buffer (50 mM Hepes, 1 M NaCl). Fractions were collected and analysed by gel electrophoresis, 1% agarose gel for DNA and 10% SDS-PAGE gel.

CHAPTER 3

PROTEIN PURIFICATION OF MUTL AND ITS ROLE IN DNA UNWINDING AND NUCLEOPROTEIN DISPLACEMENT

Chapter 3. Protein Purification of MutL and Its Role in Assisting UvrD Helicase in DNA Unwinding and Nucleoprotein Block Displacement

3.1 Introduction

Since the genetic material of the cell serves as an instruction book for protein production, genetic integrity of the chromosome is essential for cells to thrive. One way of ensuring genetic integrity is high-fidelity DNA replication which ensures that daughter cells are encoded with correct DNA. A threat to accurate DNA replication can be found in DNA-bound protein blocks, which can lead to replication fork stalling (Mulcair et al., 2006; Labib and Hodgson, 2007), DNA breakage (Bidnenko et al., 2002), and incorrect DNA synthesis (Larsen et al., 2014; Larsen et al., 2017).

UvrD helicase is often associated with the removal of DNA-bound proteins, including RNAP blocks (Epshtein et al., 2014; Hawkins et al., 2019), RecA (Petrova et al., 2015), and Tus (Bidnenko et al., 2006). The exact mechanism of UvrD protein displacement has not been identified, though research has showed that removal of RecA and of RNAP by UvrD requires ATP hydrolysis (Epshtein et al., 2014; Petrova et al., 2015), suggesting that an active mechanism might be at play.

In this chapter, we first investigated the ability of UvrD helicase to unwind dsDNA substrates against the Tus-*ter* and EcoRI blocks using *in vitro* helicase and replication assays.

Another aspect of UvrD helicase we also wanted to investigate was the 2B subdomain and whether it plays a role in the ability of UvrD helicase to displace DNA-bound proteins. The 2B subdomain of UvrD has been shown to rotate 160° from a 'closed' to an 'open' conformation either when placed in low salt concentrations (Jia et al., 2011) or when in a MutL:UvrD complex

(Ordabayev et al., 2018, 2019). Both papers showed that rotation of the 2B subdomain into an 'open' conformation increased its DNA processivity, but neither investigated whether the 2B subdomain affected its ability to displace DNA-bound proteins. The 2B subdomain of UvrD can be compared to the 2B subdomain of its homologue, SF1 helicase Rep. Removal of the 2B subdomain of Rep caused an increase in its DNA processivity, but completely eliminated its ability to remove DNA-bound proteins (Brüning et al., 2018). We do not know if the 2B subdomain of UvrD is also involved in DNA-bound protein removal. However, the role of the subdomain in increasing DNA processivity and the structural similarities of UvrD and Rep suggest that it is worth investigating.

In this chapter, we plan to conduct a range of *in vitro* helicase assays to test whether the addition of MutL increases the percentage of unwound DNA substrate by UvrD. We are especially interested in the addition of MutL to assays with DNA-bound blocks on the substrate, to determine if MutL aids UvrD in protein displacement.

3.2 Results

3.2.1 Protein Purification of MutL

3.2.1.1 Generating a MutL expression plasmid

The pET28 α -HisSUMO vector was used as a backbone for the MutL protein expression plasmid. The pET28 α vector is a simple 5369-bp over-expression plasmid with a kanamycin resistance gene, a *lac* operator sequence for inducing expression and a T7 promoter region for protein transcription (Shilling et al., 2020; Dubendorf and Studier, 1991).

SUMO (small ubiquitin-like modifier) is a eukaryotic protein used in aiding the solubility of proteins during protein purification (Malakhov et al., 2004). SUMOylation is a post-translational modification where the SUMO protein binds to specific lysine residues found within the consensus sequence Ψ -K-X-E/D (Ψ : hydrophobic amino acid, X: any amino acid) in substrate proteins (Maejima and Sadoshima, 2014; Feligioni and Nisticò, 2013). SUMO is converted into an active binding form from its precursor by SUMO specific proteases which expose a Gly-Gly motif. The Gly-Gly motif is conjugated with E2, a SUMO-activating enzyme, which binds SUMO to the lysine residues (reviewed in Maejima and Sadoshima, 2014).

SUMO can be used as a protein purification and solubility tag. An expression plasmid for a protein of interest can be designed by inserting an N-tagged SUMO gene at the N-terminal of the gene-of-interest while removing the start codon of the gene-of-interest. When expressed, a covalently bound HisSUMO and protein-of-interest are produced. The addition of SUMO has been found to increase protein solubility (Malakhov et al., 2004; Kimple *et al.*, 2013) and the addition of a His-tag at the N-terminal of SUMO allows for easy affinity chromatography. HisSUMO can be cleaved from the protein-of-interest using a SUMO-specific protease, Ulp1 (Malakhov et al., 2004). Ulp1 cleaves the protein at the 'Gly-Gly bridge', a two amino acid site between SUMO and the protein-of-interest, leaving the protein-of-interest in a native-like state (Kimple *et al.*, 2013).

Infusion cloning using a PCR linearised pET28 α -HisSUMO vector and an isolated *mutL* gene was used to create an expression plasmid for the MutL protein, pET28 α -HisSUMO-*mutL* (pDW003) (figure 3.1). The correct placement of the *mutL* gene and the plasmid map were confirmed using Plasmidsaurus nanopore sequencing.

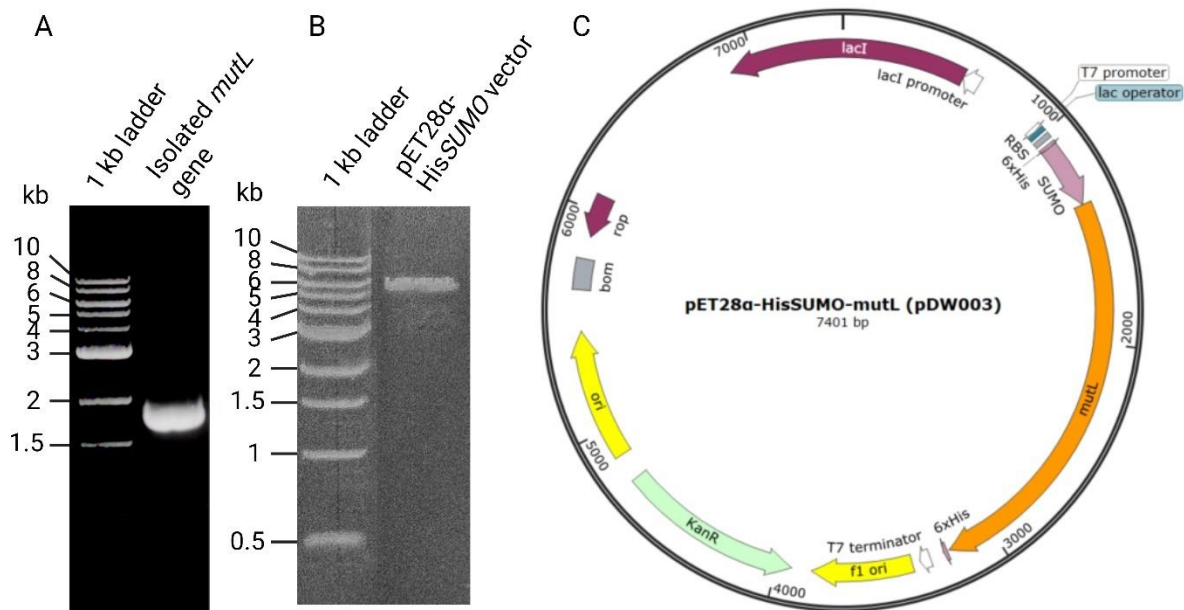


Figure 3.1 MutL expression plasmid construction. A. 1% agarose DNA gel showing PCR amplification of the *mutL* gene using primers oDW004 and oDW005. Expected length 1.85 kb. B. 1% agarose DNA gel of PCR amplification of linearised pET28 α -HisSUMO vector using primers oKJ011 and oKJ012. Expected length 5.55 kb. C. pET28 α -HisSUMO-*mutL* plasmid map (pDW003) verified through Plasmidsaurus nanopore sequencing.

3.2.1.2 Untagged MutL could not be purified from pDW003

BL21 DE3 cells were transformed with pDW003 and induced with IPTG to overexpress HisSUMO-MutL.

The purification process was designed to include two affinity chromatography steps and one size exclusion chromatography step. The first affinity column was used to separate the HisSUMO-MutL protein and the second to separate HisSUMO and MutL after overnight cleavage by Ulp1 protease. Lastly, the size-exclusion chromatography (SEC) step was used to remove protein contaminants. The first affinity chromatography step (figure 3.2 A) successfully isolated HisSUMO-MutL protein from the soluble fraction of the cell lysate, as confirmed by gel electrophoresis using a 10% SDS-PAGE protein gel. The saved fractions were combined and placed for dialysis into a low imidazole buffer with the addition of SUMO-specific protease Ulp1 for HisSUMO cleavage from the MutL protein.

The cleavage of HisSUMO from MutL was not successful. When visualising fractions collected from the second affinity chromatography column (figure 3.2 B), the samples contained both uncleaved HisSUMO-MutL (80 kDa) and cleaved MutL (68 kDa) bands, suggesting incomplete sample cleavage. For an unknown reason we also see the same two bands produced during the first affinity chromatography before the protease was added (figure 3.2 A). While we do not know why we see these two bands, we suggest that the protein might be truncated, potentially due to a change in folding after the covalent binding of HisSUMO or due to a protease contamination in the buffer. This would reduce the HisSUMO-MutL size and correspond with the lower 25 kDa band visible on the gels.

Cleavage conditions were optimised on a small scale (10 ml) through change of buffer conditions from pH 7 to pH 8, and change of incubation conditions during cleavage to either 2 hours on the bench or for 18 hours at 4 °C (personal communication, Jameson 2021). The change in conditions did not improve the cleavage of HisSUMO from MutL (figure 3.2 C).

Further literature searches on the cleavage of the HisSUMO solubility tag during protein purification suggested that SUMO-specific proteases might not be suitable for cleavage when the first amino acid after the Gly-Gly bridge of the protease is a proline, which was the case with the *mutL* gene on pDW003 (Xu and Au, 2005; Owerbach et al., 2005; Kimple, Brill and Pasker, 2013; PeakProteins). Owerbach and coworkers concluded this to be caused by the lack of an NH group in proline, which prevents its participation in the N-bond network (Owerbach et al., 2005).

Two serines were added between the Gly-Gly motif of SUMO and the N-terminal of *mutL* to allow for Ulp1 to cleave the tag and conceal the exposed proline (PeakProteins, 2022).

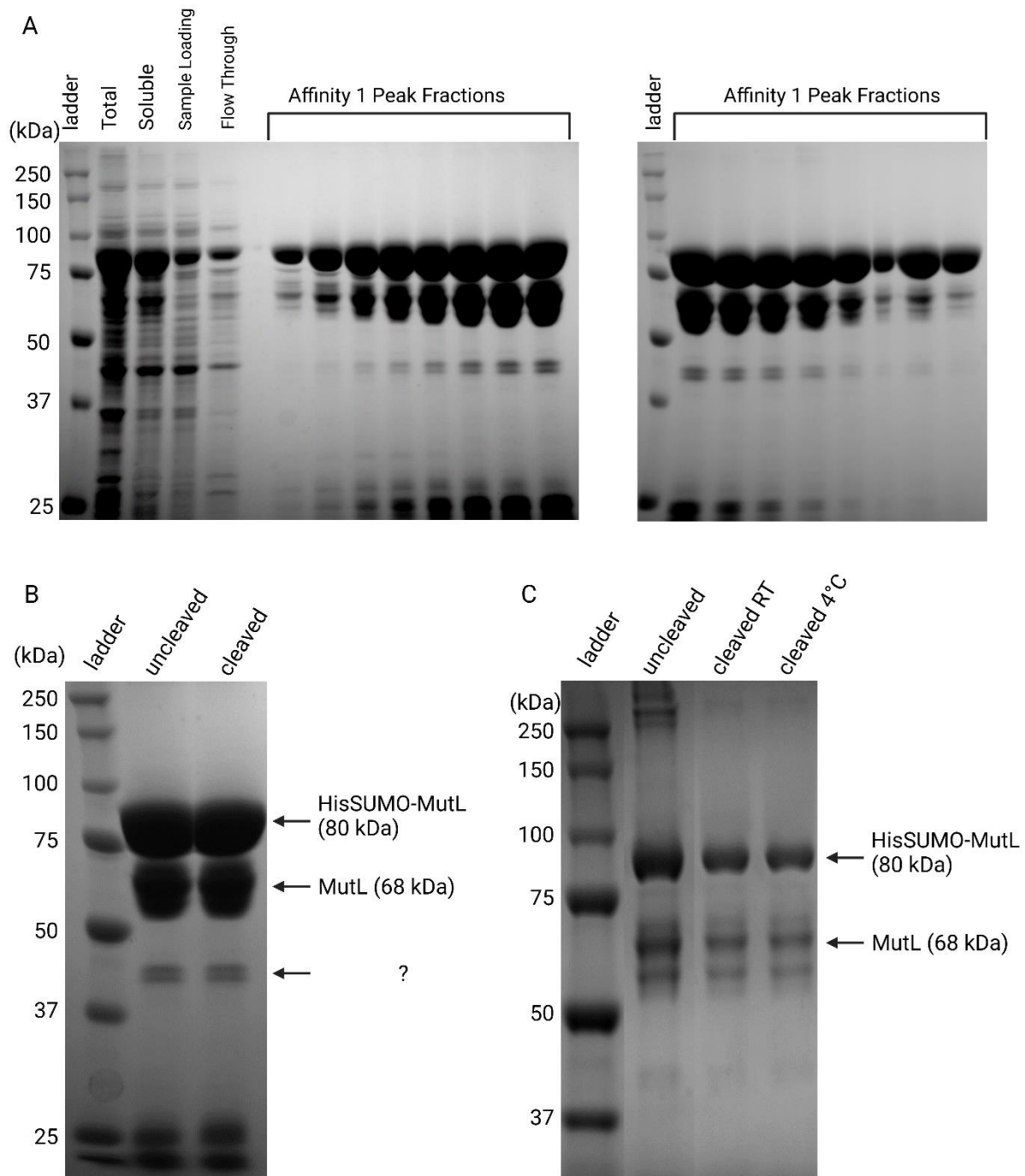


Figure 3.2 Incomplete HisSUMO tag cleavage from MutL. A. 10% SDS-PAGE gel showing the first steps of the HisSUMO-MutL protein purification, including the insoluble and soluble fractions, sample application onto the column ('AF1 wash'), column wash before elution ('flow through'), and elution peak fractions ('affinity 1 peak fractions'). B. 10% SDS-PAGE gel comparing the HisSUMO-MutL sample before and after cleavage with Ulp1 protease. C. 10% SDS-PAGE showing optimisation of HisSUMO cleavage using Ulp1 protease. 'cleaved RT' sample was cleaved for 3 hrs at room temperature. 'cleaved 4°C' sample was cleaved for 18 hrs at 4 °C. Both cleavages were carried at pH 8 instead of pH 7 in compared to 'uncleaved' lane and panels A. and B.

3.2.1.3 Redesign of pDW003 into pDW005 and protein purification of MutL

pDW003 plasmid was redesigned to add two serines after the Gly-Gly bridge cleavage site to generate pDW005. The two serines were added using site-directed mutagenesis PCR (section 2.2.2.2). Primers (oDW019 and oDW020) were designed to complement the two regions around the insertion region and to include the two additional serines. After PCR the nascent DNA synthesised contained the inserted serines (figure 3.3 A)

Presence of the additional serines was confirmed by Sanger sequencing (SourceBioscience) before generating a full plasmid map using Plasmidsaurus nanopore sequencing (figure 3.3 B and C).

BL21 DE3 cells were transformed with pDW005 and induced with IPTG to overexpress HisSUMO-MutL. The HisSUMO tag was successfully cleaved from the MutL protein expressed from the redesigned expression construct, enabling successful protein purification of MutL (figure 3.3 D).

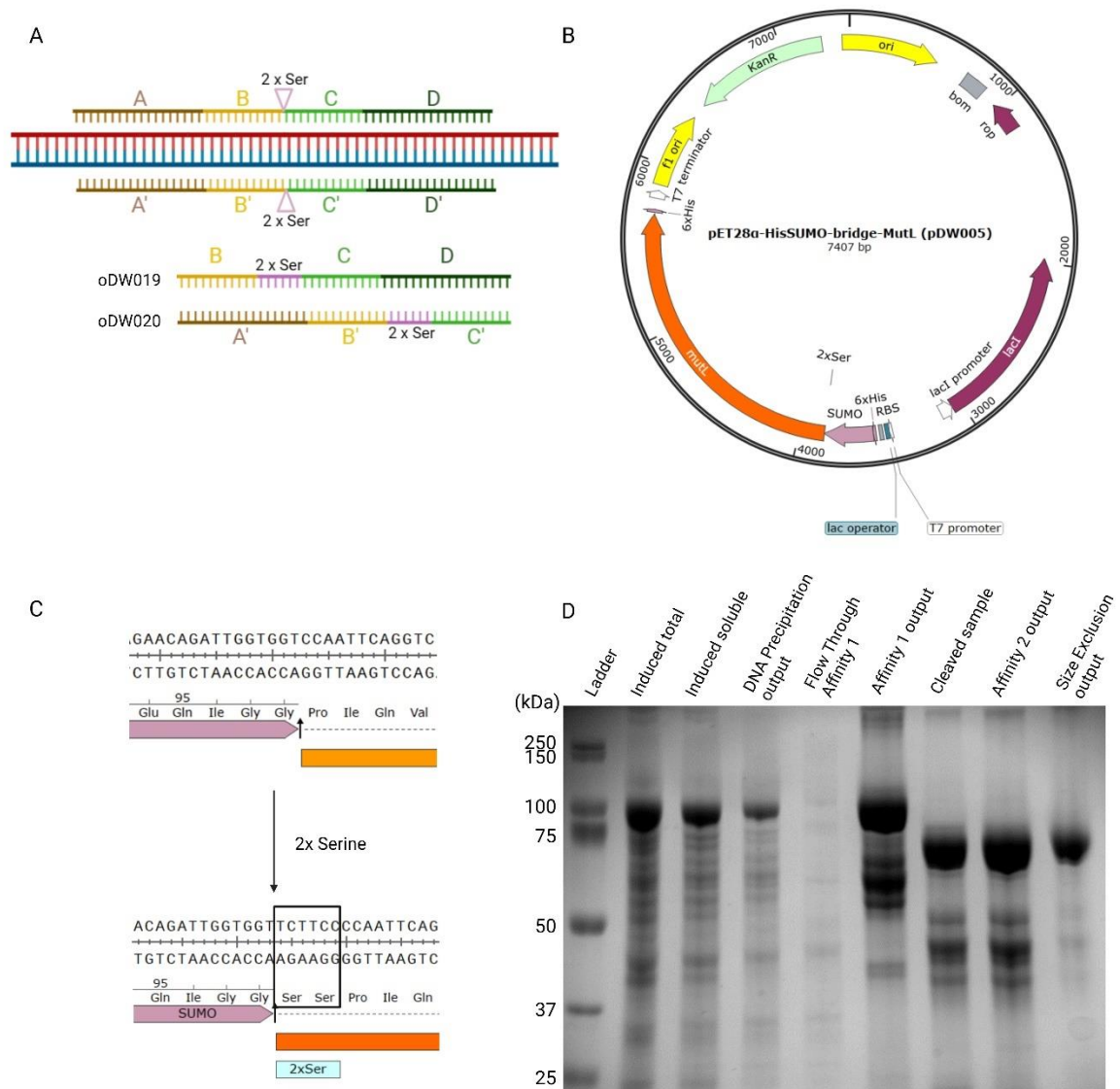


Figure 3.3 MutL protein purification from pDW005. A. Strategy for site-directed mutagenesis insertion PCR. B. pET28α-HisSUMO-Ser-Ser-*mutL* plasmid sequence confirmed using Plasmidsaurus nanopore sequencing. C. Insertion site difference between pDW003 (top) and pDW005 (bottom) with the addition of two serines. D. 10% SDS-PAGE gel showing the protein purification of the MutL protein, confirming successful MutL protein production.

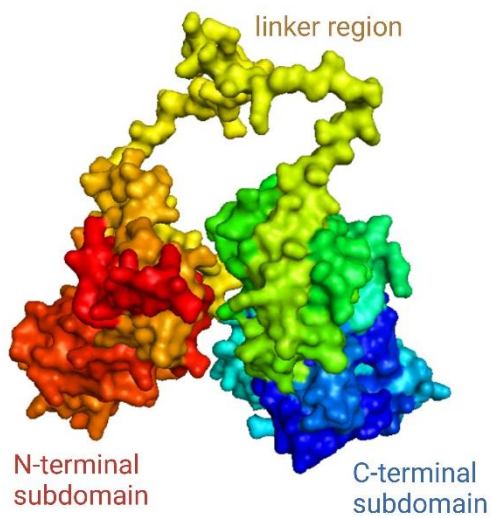
3.2.1.4 MutL protein structure generated through Alpha Fold

A full structure of MutL has not been generated through structural studies. MutL is assumed to have two subdomains, an N-terminal (amino acids 1-335) and a C-terminal domain (amino acids 439-615), joined by a linker region which is predicted to form random coils (amino acids 336 – 438). (Ban and Yang, 1998; Ban et al., 1999; Guarné et al., 2004). While the full protein structure is not available, X-ray diffraction has been used to generate a structure of the N-terminal of MutL from *E. coli* (PDB ID 1NHH, Hu et al., 2003), as well as the C-terminal domain of MutL homologues from *B. subtilis* (PDB ID 3KDG, Pillon et al., 2010), *Aquifex aeolicus* (PDB ID 5X9Y, Fukui et al., 2017), and *S. cerevisiae* (PDB ID 4E4W, Gueneau et al., 2013). No C-terminal domain structure has been generated from *E. coli* MutL protein.

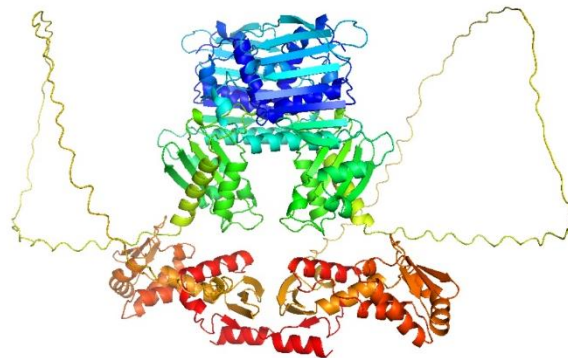
We used AlphaFold (AlphaFold, 2021) to generate models of the MutL monomer (figure 3.4). AlphaFold predicted that the MutL monomer structure was formed of two subdomains joined by a linker region (figure 3.4 A). This interesting ‘tweezers’ structure matches the literature predictions of the full MutL structure.

Since MutL functions as a dimer (Ban and Yang, 1998), we used AlphaFold to predict the dimer form of MutL (figure 3.4 B, C and D). The model predicted that the N- and C- terminals of each monomer interact with one another in a dimer structure. The C-terminal subdomain of MutL has been predicted to mediate MutL dimerisation (Drotschmann, 1998; Guarné et al., 2004). Our AlphaFold model supports this prediction as the C-terminal domains of each monomer are found in the same area and could therefore stimulate dimerisation by binding together and initiating N-terminal subdomain binding or colocalisation. A gap was found between the four bound subdomains when assessing the dimer from the ‘top’ and ‘bottom’ (figure 3.4 D). This gap could potentially be used for DNA to pass through, though we are unable to measure how large the gap is to confirm this. The model also predicts a circular gap found between the two joint domains and going through the complex (figure 3.4 D). Monakhova and coworkers used cross-linking of MutL and DNA to predict that amino acid

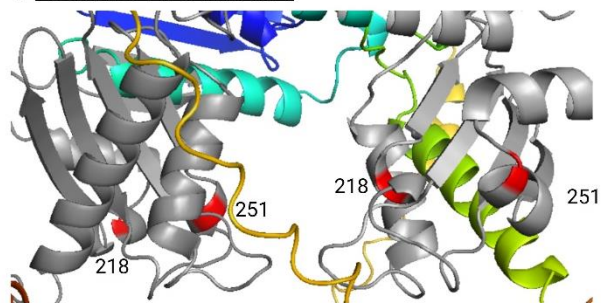
A MutL Monomer



B MutL Dimer



C Residues 218 and 251



D MutL Dimer

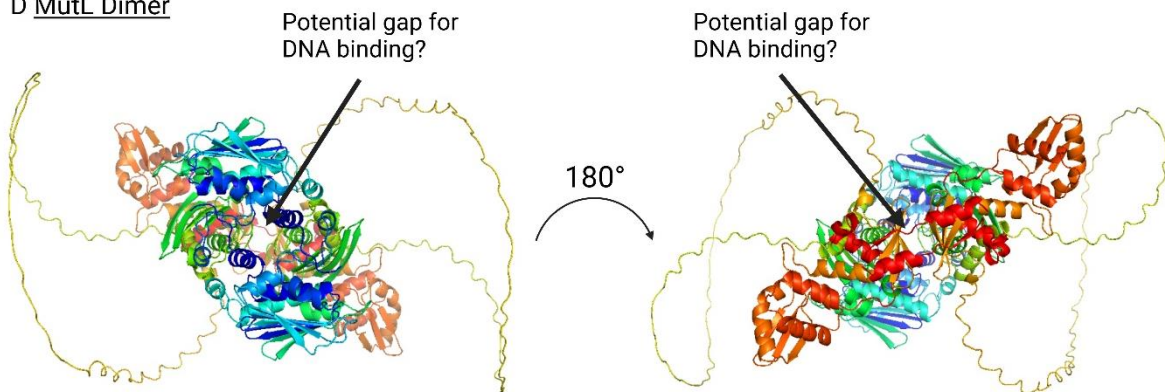


Figure 3.4 AlphaFold prediction for MutL protein monomer and dimer forms. All AlphaFold models shown were top ranked by the AlphaFold software. Warm, red colours indicate regions closer to the N-terminal, while cold, blue colours indicate regions closer to the C-terminal. A. Surface image of the predicted MutL monomer. C. Residues 218 and 251 of MutL predicted to interact with DNA. D. MutL dimer AlphaFold predictions viewed from the 'top' and 'bottom' of the complex in B.

residues 218 and 251 are involved in MutL DNA binding (figure 3.3 C) (Monakhova et al., 2020) and therefore that DNA would pass through the N-terminal subdomain complex.

3.2.1.5 TSA analysis of MutL protein folding and interaction

Thermal shift assay (TSA), a type of differential scanning fluorimetry (DSF), was designed to test for correct protein folding by using a hydrophobic, fluorescent dye (SYPRO Orange). The dye binds to hydrophobic groups of the protein when in an aqueous environment. As the protein is heated, it unfolds and exposes the dye which generates a signal that can be detected spectrophotometrically. Once the dye has been exposed to the laser, its signal fades (Pinz *et al.*, 2022). An ideal TSA result shows a peak that starts low, due to the lack of exposed SYPRO orange, and increases into a peak as the temperature increases and the protein unfolds. The top of the peak should be the highest point of the fluorescence readings.

TSA was used to confirm correct folding of the purified MutL and UvrD proteins (figure 3.5). All assays showed used a double-stranded DNA (dsDNA) substrate (oDW015-16) since MutL is a dsDNA-binding protein. Concentrations of MutL (370 nM, 740 nM, 1.11 μ M) and UvrD (68 nM, 115 nM, 615 nM) tested varied due to protein availability.

MutL TSA analysis showed two peaks (figure 3.5 A), which indicated two stages of unfolding. This result could be interpreted as MutL forming a dimer in the assay and different temperatures (45 °C and 65 °C) being necessary to first break the dimer bonds, followed by individual protein unfolding. Our TSA results confirm that MutL is correctly folded.

The UvrD helicase used was previously purified in our laboratory (Atkinson and McGlynn, 2009) and has been shown to be functional in previous projects (Hawkins et al., 2019; Jameson et al., 2021). During TSA analysis, UvrD produced a single peak showing correct protein folding, with unfolding occurring at around 50 °C (figure 3.5 B).

TSA analysis was also conducted on samples containing MutL + UvrD + DNA. The test was compared against the MutL + DNA only and UvrD + DNA only samples (figure 3.5 C and D). Interestingly, the addition of UvrD helicase to MutL + DNA generated a result with one peak, instead of two peaks, with a similar unfolding temperature to UvrD + DNA (figure 3.5 C). We found that UvrD + MutL + DNA unfolded at a temperature of 45 – 55 °C, while MutL + DNA unfolded at a lower temperature of 35 – 45 °C. UvrD + DNA unfolded at a similar temperature to UvrD + MutL + DNA but over a larger temperature difference of 40 – 60 °C. The temperature shift suggested a change in folding for both UvrD and MutL which could mean that the two proteins were interacting.

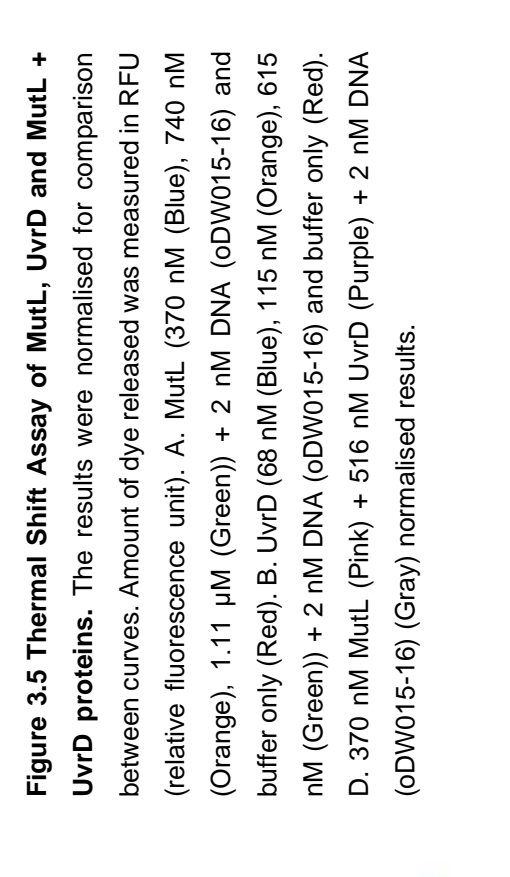
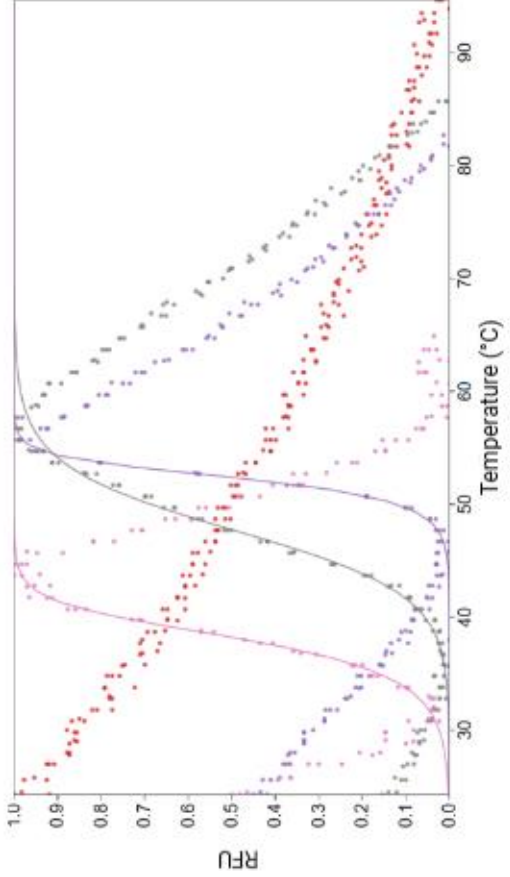
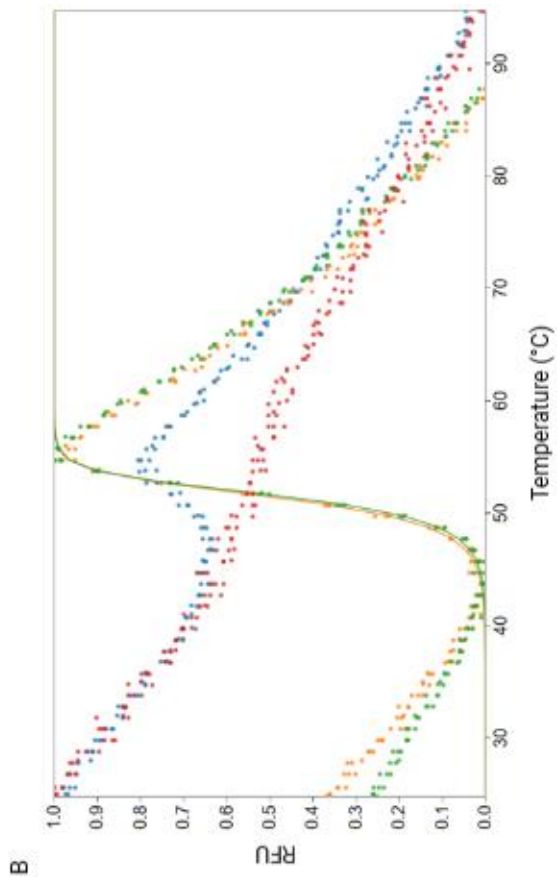
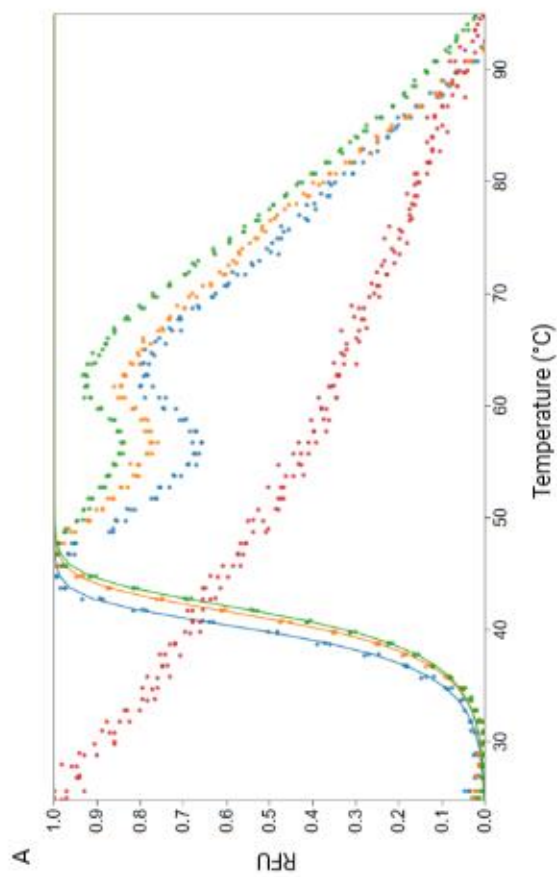


Figure 3.5 Thermal Shift Assay of MutL, UvrD and MutL + UvrD proteins. The results were normalised for comparison between curves. Amount of dye released was measured in RFU (relative fluorescence unit). A. MutL (370 nM (Blue), 740 nM (Orange), 1.11 μ M (Green)) + 2 nM DNA (oDW015-16) and buffer only (Red). B. UvrD (68 nM (Blue), 115 nM (Orange), 615 nM (Green)) + 2 nM DNA (oDW015-16) and buffer only (Red). D. 370 nM MutL (Pink) + 516 nM UvrD (Purple) + 2 nM DNA (oDW015-16) (Gray) normalised results.

3.2.2 UvrD Helicase was able to unwind DNA past both orientations of the *E. coli* Tus-*ter* block

Whether UvrD helicase can remove the Tus protein when approaching the permissive and the non-permissive orientation of the Tus-*ter* block has been subject of debate since the late 80s. Lee and coworkers conducted a series of helicase assays to test various concentrations of UvrD helicase (8.54 nM, 25 nM, 76.22 nM) and Rep helicase for Tus removal against the Tus-*ter* block on the M13mp18 and M13mp19 plasmids with a double-stranded *ter* region (Lee et al., 1989). They concluded that UvrD was unable to unwind past the block in the non-permissive orientation. In the same year, Khatri and coworkers conducted the same test using 0.7 pmol/μl of UvrD (equivalent to 700 nM) and concluded that UvrD was successful in unwinding past the block (Khatri et al., 1989). Next, Hiasa and Marians, tested UvrD (UvrD/DNA molar ratios 10 and 40, DNA 30 fmol) and also found that UvrD helicase was “unaffected by Tus” and able to unwind past both orientations of the block (Hiasa and Marians, 1992).

Bidnenko and coworkers took a different approach and tested for the ability of UvrD to remove Tus *in vivo* when the replication fork is stuck at the non-permissive orientation of the Tus-*ter* block (Bidnenko et al., 2006). Bidnenko and coworkers placed two ectopic *ter* sites on the *E. coli* genome which, when bound by Tus, would block the replication fork half-way around the genome. The Tus protein would have to be removed for cells to finish replication and for the ‘replication intermediates’, forks stuck at Tus-*ter*, to be reduced. When UvrD was overexpressed in cells with ectopic *ter* sites through the use of an expression plasmid, Bidnenko and coworkers saw a reduction in replication intermediates and concluded that UvrD was able, and responsible for, removing Tus from *ter* when the replication forks are stalled by the block (Bidnenko et al., 2006). This conclusion has been widely cited as UvrD being the main *E. coli* helicase responsible for removing Tus during DNA replication.

While our group has been able to show that UvrD is able to remove DNA-bound protein blocks *in vitro* (Hawkins et al., 2019), we were unable to show that UvrD can remove Tus when the two replication forks meet at Tus-*ter*, therefore concluding that UvrD alone is unable to achieve this task (Jameson *et al.*, 2021). Our results do not however fully disagree with Bidnenko, as their model does state that UvrD is unable to remove Tus when DnaB or the replisome is present (Bidnenko et al., 2006).

We tested whether UvrD can remove Tus from Tus-*ter* in both the permissive and the non-permissive orientation using a helicase assay with a replication fork-like substrate (figure 3.6). We designed our helicase assay using short substrates (with *ter* in the permissive and non-permissive orientation to UvrD unwinding) with a 25 bp dsDNA region and a 25 bp ssDNA region; or a long substrate with a 80 bp dsDNA region and a 20 bp ssDNA region. Both substrates resembled a replication fork. Part of the dsDNA region included the *terB* sequence in either the permissive or the non-permissive orientation for a helicase approaching from the 3' to 5' orientation. The long substrate also included an EcoRI restriction enzyme site on the dsDNA region to enable binding of a non-cleaving EcoRI E111G mutant.

For both the short and long DNA substrates, PNK end-labelling was used to place a radioactive ³²P tag at the 5' end of one oligo, with the label found at the dsDNA end of the substrate. This enabled us to detect intact dsDNA as a slow migrating band and an unwound strand as a faster migrating band on a native gel.

A band shift assay (figure 3.6 C) was conducted to show the ability of Tus to bind to the short oligos with Tus in the permissive and the non-permissive orientations. We were able to successfully show band separation when Tus was and was not bound to the substrate. A band shift assay was not conducted to show the binding of Tus, EcoRI and Tus and EcoRI together on the long dsDNA substrate. This may affect the interpretation of some results, which has been further explored in this results chapter.

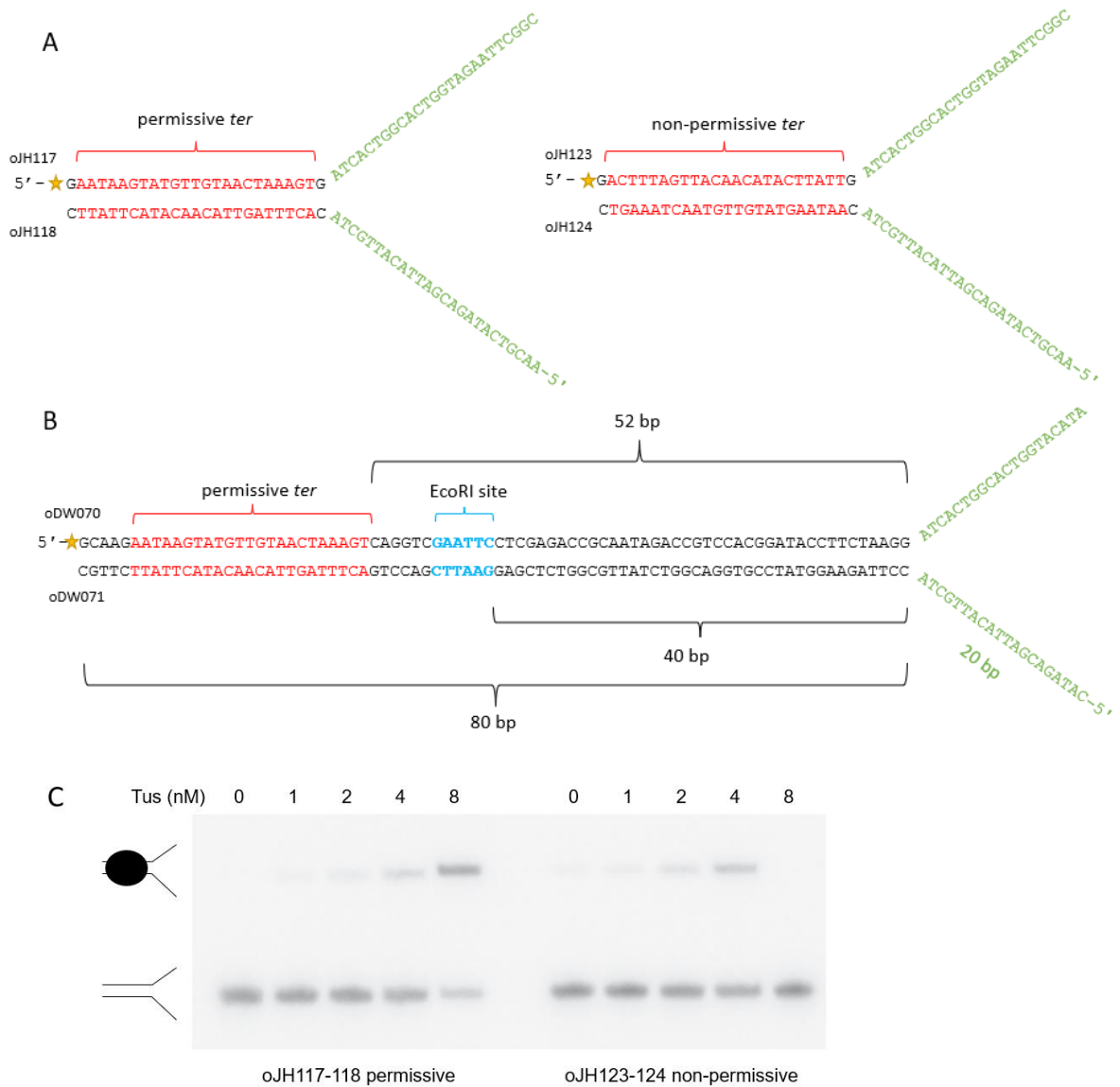


Figure 3.6 Forked DNA substrates used for helicase assays. The green star in A. and B. indicates the radioactive ^{32}P tag. A. Short DNA substrate with a 25 bp dsDNA region and two 25 bp ssDNA regions, 'arms'. *terB* sequence can be found in the dsDNA region in a permissive orientation for a 3' to 5' helicase (oJH117-oJH118) and non-permissive orientation (oJH123-oJH124). B. Long DNA substrate with an 80 bp dsDNA region and two 20 bp ssDNA regions (oDW070-oDW071). *terB* sequence can be found in the dsDNA region in a permissive orientation for a 3' to 5' helicase, and an EcoRI cleavage site for the binding of EcoRI E111G. C. Band shift assay showing Tus binding to the short oligo (as in A.) Concentration of DNA substrate added was 2 nM with a range of Tus concentrations.

We designed a helicase assay using a short dsDNA forked substrate to test for the ability of UvrD to unwind DNA past the permissive and the non-permissive orientation of the Tus-*ter* block *in vitro* (figure 3.7). Due to the variety of UvrD concentrations tested in literature (14-125 ng) (Lee et al., 1989; Khatri et al., 1989; Hiasa and Marians, 1992), we designed our assay to test UvrD at an equivalent concentration range of 20 - 200 nM. All statistical analysis in this chapter was conducted on n=3 (unless stated otherwise) using a one-tail or two-tail t-test assuming unequal variances. One-tail t-test was used when looking for an increase in unwinding, while the two-tail t-test was used when looking for a change between the permissive and non-permissive orientation of Tus-*ter* results. Due to the band shift assay (figure 3.6 C), we feel confident that Tus should have been bound to the dsDNA substrate in the assay, forming an obstacle for UvrD to unwind past.

Our results showed that UvrD was able to unwind dsDNA past both the permissive and the non-permissive orientations of the Tus-*ter* block (figure 3.7). Reactions with +Tus -UvrD and with -Tus +UvrD were added as a controls, where +Tus -UvrD should only produce dsDNA bands, while -Tus +UvrD should only produce ssDNA bands. For quantification, the amount of ssDNA present was normalised against +Tus -UvrD to compensate for any spontaneous unwinding and background noise. There were no significant differences between the unwinding efficiency in either orientation, suggesting that the mousetrap mechanism does not affect UvrD helicase.

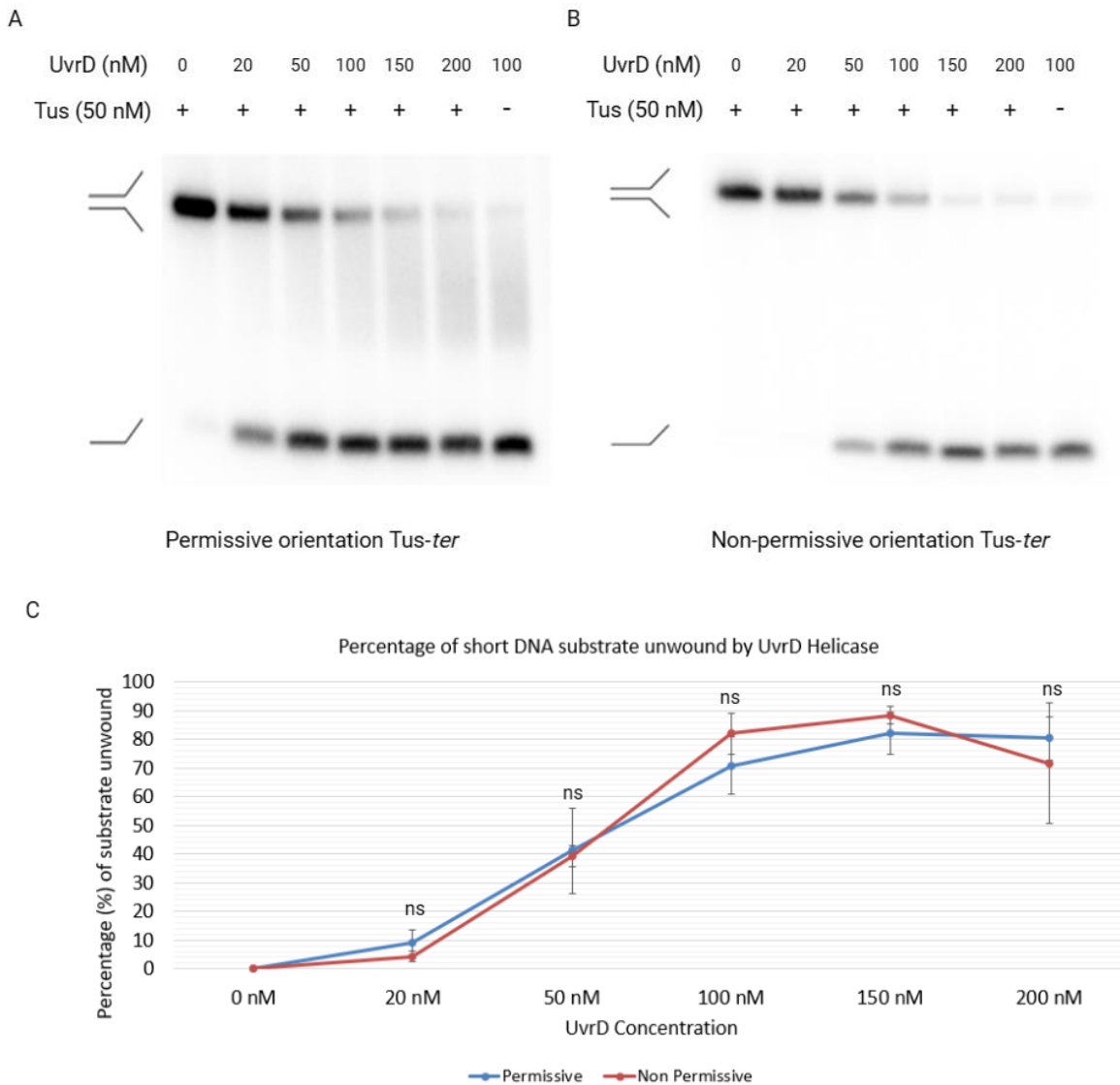


Figure 3.7 UvrD helicase can unwind past the *Tus-ter* block in both the permissive and the non-permissive orientation. A. Representative helicase assay for the permissive orientation of *Tus-ter* using 2 nM of DNA substrate, 2 nM of Tus, and a range of concentrations of UvrD (0 nM, 20 nM, 50 nM, 100 nM, 150 nM, 200 nM). B. Representative helicase assay for the non-permissive orientation of *Tus-ter* using the UvrD and DNA concentrations as in A. C. Quantification of n=3 results of the permissive and non-permissive orientation helicase assays. The error bars represent the standard deviation values. Two-tail T-test was conducted to compare the values for the permissive and non-permissive orientation of the block with $p < 0.05$ considered as significant. (p values calculated 20 nM = 0.3619, 50 nM = 0.908, 100 nM = 0.4169, 150 nM = 0.4794, 200 nM = 0.7363; no values were significant)

3.2.3 The effect of adding MutL to UvrD helicase assays

3.2.3.1 Addition of MutL helps UvrD unwind past a long helicase assay DNA substrate

During MMR, UvrD interacts with the MutL dimer which loads the helicase onto the DNA and increases its DNA processivity (Mechanic et al., 2000; Yamaguchi et al., 1998; Ordabayev et al., 2018, 2019). We wanted to assess whether the addition of MutL to a UvrD helicase assay would assist UvrD in unwinding DNA, but especially in unwinding DNA past a DNA-bound protein block. 50 nM of MutL was used to ensure that the protein was present at excess to assist UvrD.

First we conducted a UvrD ± MutL helicase assay using the short substrate (not shown) and the same conditions as in 3.2.2. We did not see any difference between UvrD and UvrD + MutL. The assay conditions were therefore adapted to make the assay more challenging for UvrD helicase to see if MutL can 'help' the helicase.

First adaptation to the helicase assay was the usage of a longer helicase assay substrate (oDW070-71) when assessing the addition of MutL to the UvrD helicase assay ± protein blocks (figure 3.8). The long DNA substrate was designed to be more challenging for UvrD helicase than the experiments conducted on the short DNA substrate. UvrD alone has been shown to have a limited DNA processivity between 40-50 bp (Matson and Robertson, 2006), therefore 80-bp should challenge the helicase's unwinding ability and allow us to see a potential increase in efficiency upon addition of MutL. The long DNA substrate contained a *ter* site in the permissive orientation to enable testing of the ability of UvrD with and without MutL to unwind past the Tus-*ter* block. Lastly, an EcoRI site within the substrate allows for binding of a mutant version of EcoRI, EcoRI E111G. EcoRI E111G, does not cleave DNA but remains bound to its restriction site (King *et al.*, 1989) and in our assay represents a small and physiologically unfamiliar DNA-bound block that UvrD might encounter when unwinding DNA *in vivo*.

The assay was also adapted by altering the assay temperature. Standard helicase assays are conducted at 37 °C, which is an optimal growth temperature for *E. coli* (Tuttle et al., 2021) though *E. coli* also adapts well to higher temperatures, as high as 52 °C (Fotadar et al., 2005). The temperature in our assays was reduced to 27 °C. The assay time was also reduced to 3 minutes incubation instead of 10 minutes once ATP was added. UvrD alone was not able to unwind the dsDNA region of oDW070-71 under challenging helicase assay conditions (figure 3.8), though we see some limited unwinding. This is likely due to the low processivity of UvrD of 40-50 bp, which would be insufficient to unwind the full 80 bp of dsDNA on the substrate. The addition of MutL resulted in increased unwinding seen by the increased presence of a lower band (unwound) on the gel and through quantification. We conducted a one-tail t-test to determine the significance of our results since we were looking for an increase in substrate unwinding when MutL was added, with p value <0.05 seen as significant. The difference of unwinding with and without MutL at UvrD concentrations of 30 nM and 40 nM was statistically significant, with 20 nM being insignificant with a p value of 0.064. When assessing these results, it is important to remember the small sample number (n=3) and the high standard deviation. The results for 30 nM and 40 nM are also statistically significant if assessed using a two-tail t-test to look for a change instead of an increase, with respective p values of p = 0.008 and p = 0.048).

Our results confirm that the addition of MutL can improve the ability of UvrD helicase to unwind dsDNA.

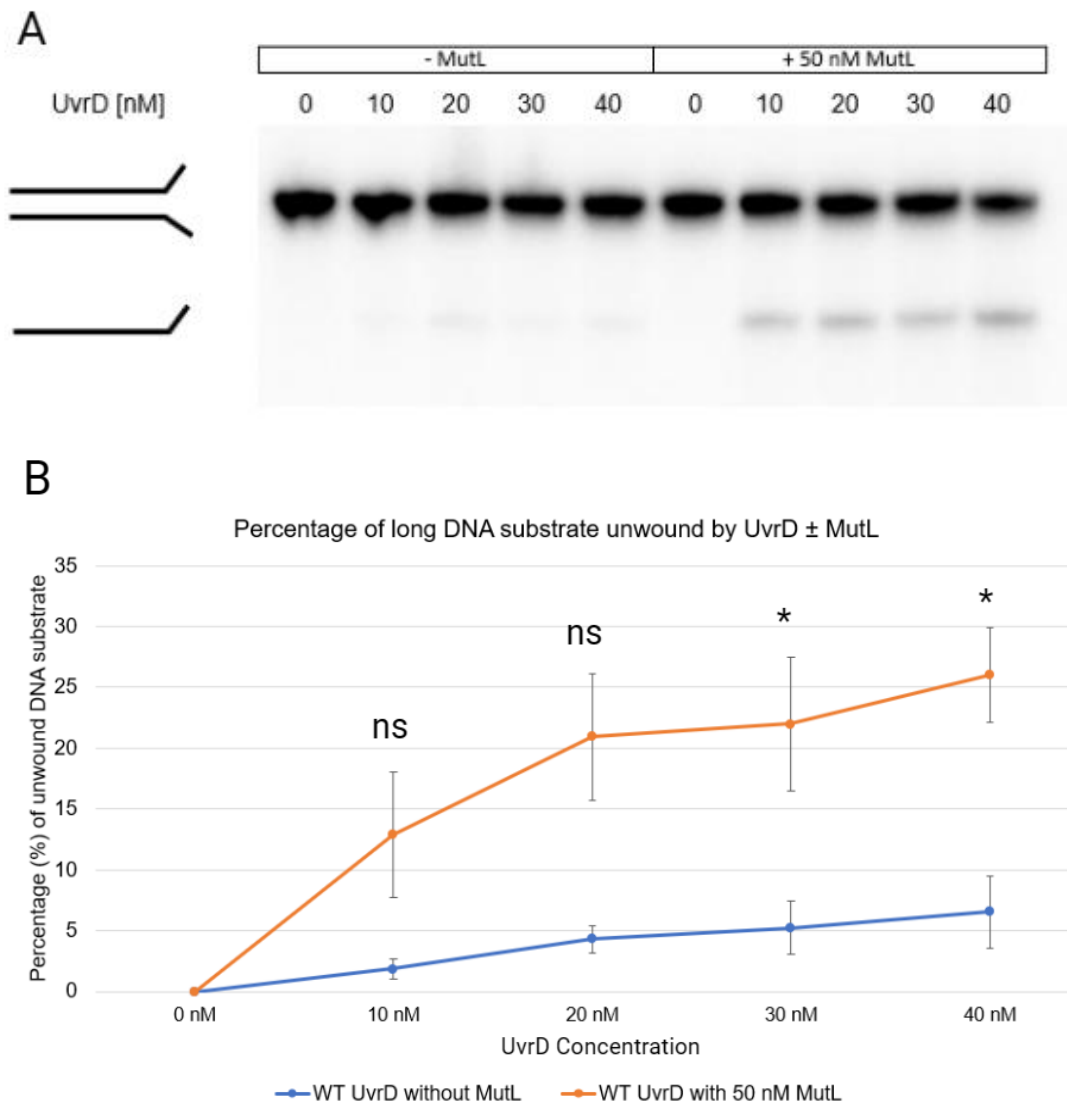


Figure 3.8 The addition of MutL helps UvrD unwind long dsDNA substrate (oDW070-71). A. Representative native 10% TBE-PAGE gel showing UvrD unwinding of oDW070-71 with and without MutL. The concentrations of proteins are as stated above, with 2 nM of oDW070-71 substrate added to the assay with incubation for 3 min at 27 °C. B. Quantification results of n=3 helicase assays. The error bars represent the standard deviation. The p values were generated through a one-tail t-test, with significance decided by a p value of <0.05; significant values were shown for 30 nM and 40 nM (p = 0.004 and p = 0.024 respectively) and non-significant values for 10 nM and 20 nM (p = 0.186 and p = 0.064 respectively).

3.2.3.2 MutL helps UvrD helicase unwind past the EcoRI E111G block, but not the Tus block.

We wanted to determine whether UvrD could unwind the long DNA substrate (oDW070-71) when EcoRI E111G was bound to the EcoRI cleavage site or if Tus was bound to *ter* in the permissive orientation on the double-stranded region of the substrate. While we know that the addition of MutL increases UvrD processivity, we do not know whether it affects the ability of UvrD to unwind dsDNA past DNA-bound proteins. With the long dsDNA region of the substrate, we hypothesised that UvrD alone would not be able to unwind the full substrate (figure 3.8), but were curious to see whether it could unwind past the blocks when MutL was added. UvrD helicase alone was inefficient at unwinding past the long DNA substrate when EcoRI E111G was also added to the assay; however, the addition of 50 nM MutL significantly increased the percentage of unwound DNA at all concentrations (figure 3.9). This result shows that MutL assists UvrD in unwinding the substrate past the EcoRI cleavage site where EcoRI E111G block might be found. Since a band shift assay is not available to show that EcoRI was bound to our substrate we cannot be sure that EcoRI E111G was actually bound to the binding site on the substrate. On oDW070-71, the EcoRI E111G binding site starts after 40 bp of dsDNA (figure 3.6 B), which means that to unwind past the block UvrD would need to unwind a minimum of 46 bp. With a processivity of max 50 bp, 46 bp might be challenging for UvrD alone, with and without a block present. UvrD would also likely not be able to fully unwind the full substrate, as showed in figure 3.8.

Our assay results for UvrD±MutL and UvrD±MutL+EcoRI E111G (figure 3.8 and 3.9 respectively) both show an increase in unwinding when MutL was present and very limited unwinding when MutL was not present. When comparing the results, we do see a lower percentage of unwound substrate by UvrD alone when EcoRI was also added to the assay. We also see a variety in the percentage of unwound substrate by UvrD+MutL, where more substrate was unwound in the assay without EcoRI. These details suggest that EcoRI was

likely bound to the substrate and created an additional obstacle for UvrD that the helicase was able to unwind past.

Next, we tested for the ability of UvrD with and without MutL to unwind the long substrate when Tus was added to the assay and therefore likely past the permissive orientation of the Tus-*ter* block on the long DNA substrate (figure 3.10). The same *terB* sequence was used in oDW070-71 as for the short DNA substrate oJH117-118, which we did show was able to successfully bind with Tus through a band shift assay (Figure 3.6 C). Since Tus has a strong KD of 3.4×10^{-13} (Gottlieb et al., 1992) for *ter* and since it was able to bind a similar substrate, we can assume that Tus has also bound to oDW070-71.

We found that UvrD alone was able to unwind past the substrate designed to include the permissive orientation of the Tus-*ter* block. This was a surprising result when considering the poor processivity of UvrD and that the helicase alone was unable to unwind past the substrate without a block and the substrate when EcoRI E111G was also present in the assay (figures 3.8 and 3.9 respectively). This result suggested that the addition of Tus seemed to somehow stimulate UvrD unwinding to allow it to unwind past the full substrate and likely past the Tus-*ter* block (assuming Tus was able to find the substrate UvrD could unwind >5% substrate when Tus was added to the assay, compared to <2% when EcoRI E111G was added to the assay. Addition of MutL protein to the UvrD+Tus assay presented a not significant increase in the percentage of long DNA substrate unwound, suggesting that UvrD alone was sufficient in the conditions of the test. The efficiency of UvrD + MutL was very similar in the tests that contained Tus and that contained EcoRI E111G. One-tail t-test was conducted to test for a percentage increase of unwound substrate when MutL was added. All values were insignificant.

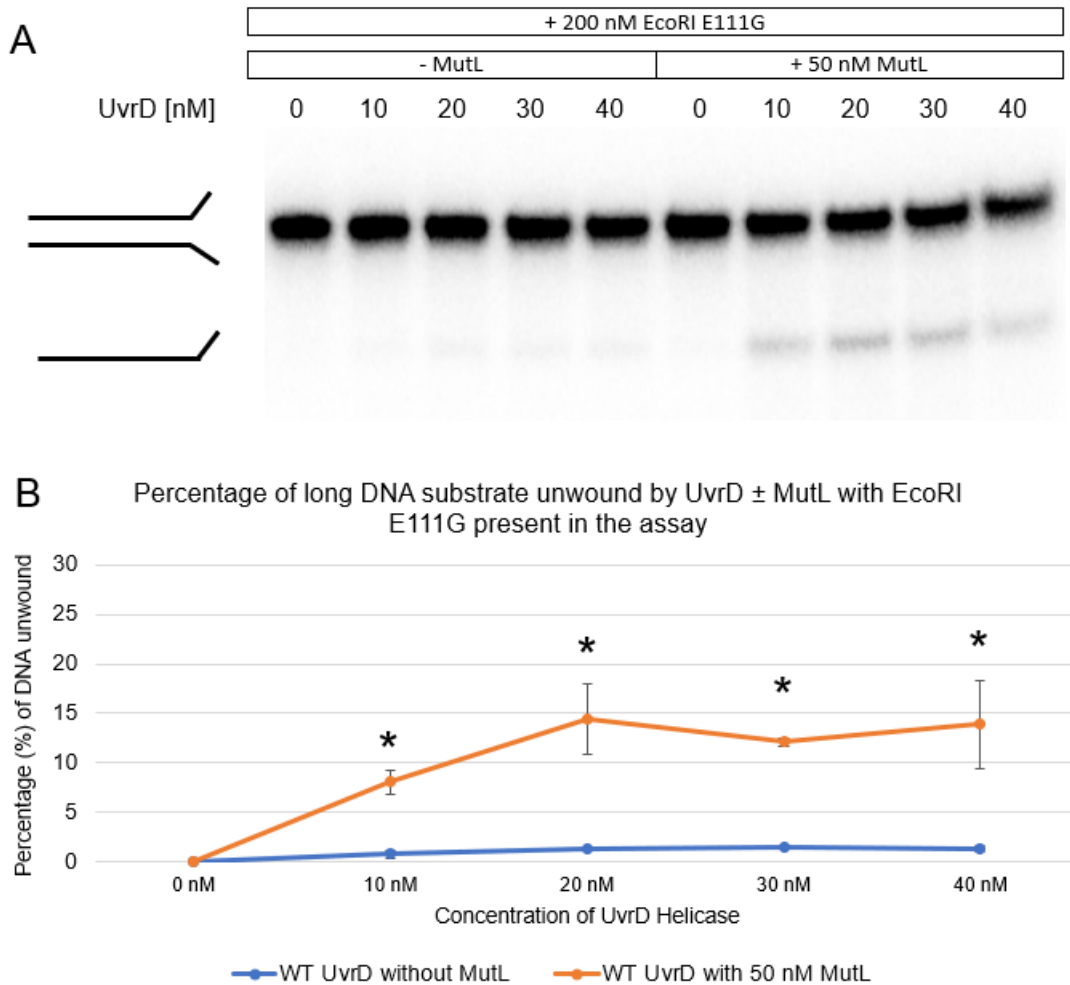


Figure 3.9 The ability of UvrD ± MutL to unwind DNA past an EcoRI E111G block on a long dsDNA substrate. Representative 10% native TBE-PAGE gel of a helicase assay of UvrD ± MutL against the EcoRI E111G block. . 2 nM of oDW070-71 substrate, 50 nM of MutL, and 200 nM of EcoRI E111G added to the assay with incubation for 3 min at 27 °C. B. Helicase assay quantification for UvrD ± MutL against the EcoRI E111G block (n=3). The error bars represent standard deviation. Significance was determined through a one-tail T-test for values <0.05. (10 nM p=0.0087, 20 nM p=0.0069, 30 nM p=0.01413, 40 nM p=0.0502, all differences were significant).

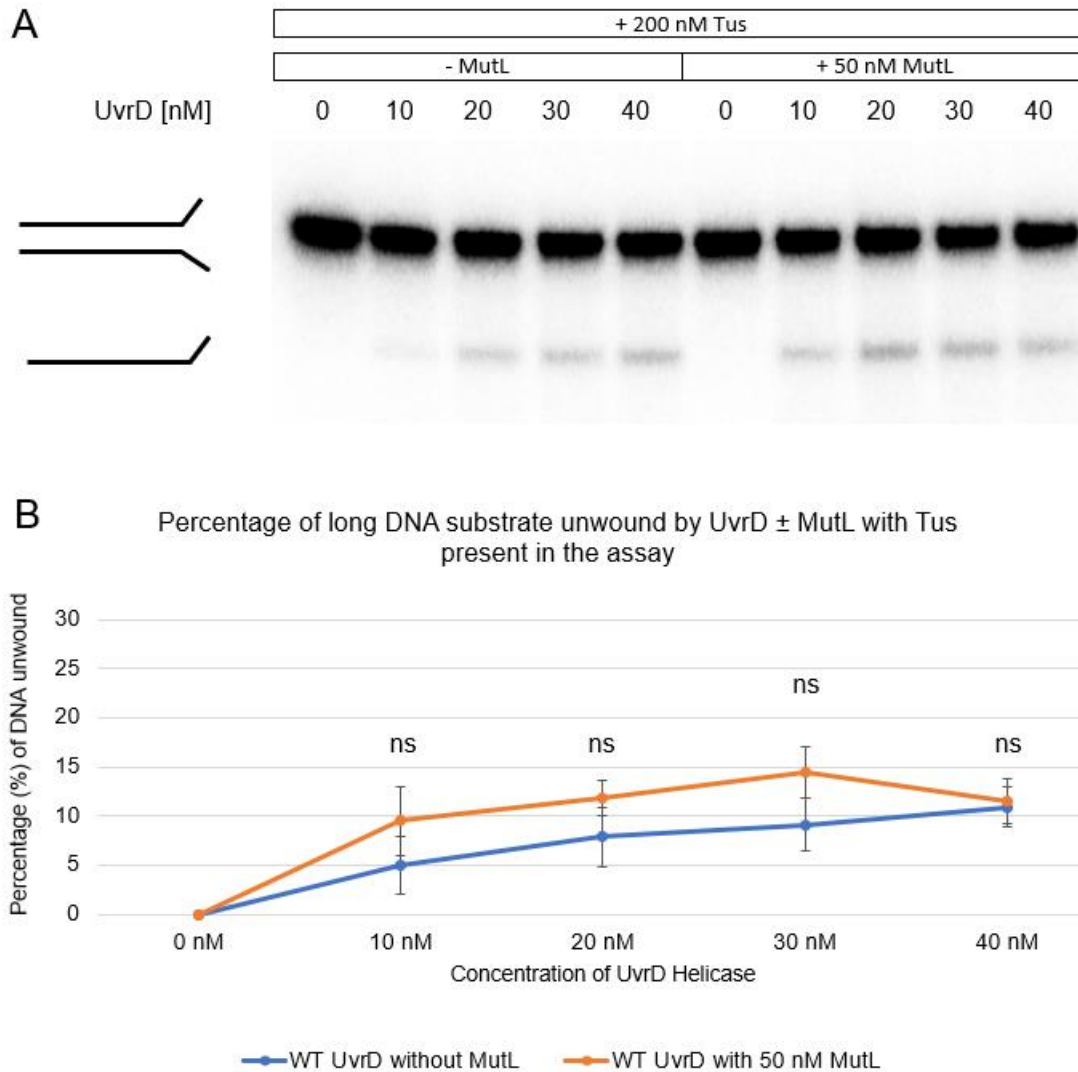


Figure 3.10 The ability of UvrD ± MutL to unwind DNA past the permissive orientation of the Tus-*ter* block on a long dsDNA substrate. Representative 10% native TBE-PAGE gel of a helicase assay of UvrD ± MutL against the permissive orientation of the Tus-*ter* block. . 2 nM of oDW070-71 substrate, 50 nM of MutL, and 200 nM of Tus added to the assay. B. Helicase assay quantification for UvrD ± MutL against the permissive orientation of the Tus-*ter* block (n=3). The error bars represent standard deviation. Significance was determined through a one-tail T-test for values <0.05. (10 nM p=0.2528, 20 nM p=0.2938, 30 nM p=0.1867, 40 nM p=0.3595, all differences were not significant).

Lastly, when testing the long substrate in an assay where both EcoRI and Tus were added (figure 3.11), we found that UvrD alone was able to unwind the substrate with similar effectiveness as unwinding in an assay with Tus only. Due to a lack of a band shift assay, we cannot show whether one or both proteins have bound to the substrate to form the blocks. This means that UvrD might have been unwinding either substrate only, substrate past the Tus-*ter* block, substrate past the EcoRI E111G block, or substrate past both the Tus-*ter* and EcoRI E111G blocks.

The results for 10 nM, 20 nM, and 40 nM of UvrD \pm MutL are similar in the assay with Tus and EcoRI E111G to the assay with Tus only when looking at UvrD only results. The result for UvrD + MutL against both Tus and EcoRI showed a lower percentage of unwound substrate when comparing to the assay against Tus only, while UvrD alone showed an increase. These results suggest that the addition of EcoRI E111G to the assay somehow limited the assist of MutL.

Two-tail t-test was conducted to test for a percentage change of unwound substrate when comparing UvrD and UvrD + MutL.

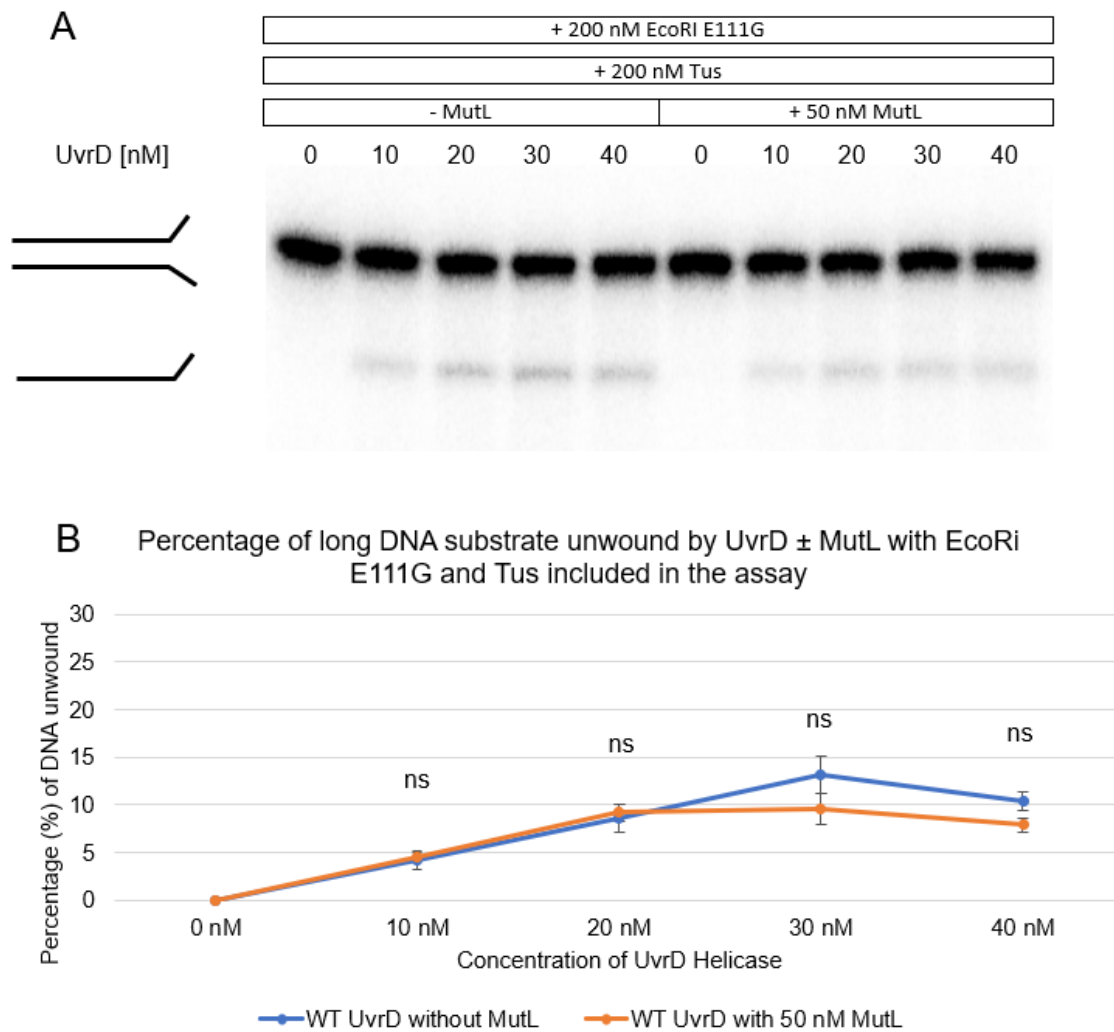


Figure 3.11 The ability of UvrD ± MutL to unwind DNA past the permissive orientation of the Tus-*ter* block and the EcoRI E111G block on the same long DNA substrate. A. Representative 10% native TBE-PAGE gel of a helicase assay of UvrD ± MutL against the permissive orientation of the Tus-*ter* block and the EcoRI E111G block on the same substrate. 2 nM of oDW070-71 substrate, 50 nM of MutL, and 200 nM each of Tus and EcoRI E111G added to the assay. B. Helicase assay quantification for UvrD ± MutL against the permissive orientation of the Tus-*ter* block and the EcoRI E111G block on the same substrate (n=3). The error bars represent standard deviation. Significance was determined through a one-tail T-test for values <0.05. (10 nM p=0.6086, 20 nM p=0.1418, 30 nM p=0.1682, 40 nM p=0.0588, differences for all concentrations were not significant).

3.2.3.3. Addition of UvrD ± MutL to a replication assay to aid DNA replication termination.

Our results support the finding by Bidnenko and coworkers that UvrD is able to remove Tus from *ter* (Bidnenko et al., 2006). This result however does not agree with previous results from our group (Jameson et al., 2021), which showed that UvrD was unable to remove Tus in a replication assay where both replication forks terminated at Tus-*ter*.

Both helicase assays and replication assays are *in vitro* biochemical assays which use ³²P to label DNA. DNA substrates used for helicase assays were end-labelled with a radioactive ³²P phosphate, while a radioactive ³²P d(CTP) base is incorporated into nascent DNA during replication assays. Helicase assays are much simpler than replication assays. While helicase assays test the helicase for unwinding of a short dsDNA substrate (or plasmid region), replication assays are designed to imitate the circular chromosome of bacteria with a circular plasmid. A key comparison between replication assays and helicase assays is the presence of a full replisome, rather than just the helicase.

For our replication assays, we used the pKJ001 plasmid and DNA template. It was designed to contain an *oriC* region for DNA replication initiation, a *lacO₂₂* array for the binding of LacI (forming a reversible block which can be removed through addition of IPTG), and a *terB* site which allows for Tus binding, with the clockwise fork approaching the non-permissive orientation of the Tus-*ter* block (figure 3.12 A).

We wanted to test whether addition of UvrD, as well as the addition of MutL, can aid replication. We conducted a replication assay using the pKJ001 plasmid in which we blocked both replication forks, the clockwise fork at the non-permissive orientation of the Tus-*ter* block and the counterclockwise fork at the LacI-*lacO* block site (figure 3.12 B, C and D). If UvrD helicase, with or without MutL, can remove Tus when the replication fork is present, we would expect to see an increase in forks released from Tus-*ter*, observed through a decrease in the 2.7 kb band and an increase in the 3.8 kb band as replication forks progress though *ter* and are halted at the LacI-*lacO* block. Additionally, UvrD helicase was added into the assay either

early (before the reconstitution of the replication forks) or late (once replication is ongoing and the forks are near/at the block) to test whether this timing has any significance. The addition of UvrD early or late has previously been shown to produce significantly different results, where early addition of UvrD increased RNAP removal and decreased EcoRI E111G removal (Wollman et al., 2023).

We were unable to conduct more than two repeats of this experiment due to time limitations (figure 3.12 B and C). Future work would include repetition of this test to increase the sample size, which would increase our significance strength and make our results more trustworthy. It is also important to note that the strength and clarity of bands often varies from gel to gel and an increased sample size would allow for a better estimation on the average values.

The first lane of each gel (figure 3.12 B and C) represents our control sample with no UvrD, MutL, Tus, or LacI added. In this lane we would expect a full length replication product of 6 kb. Surprisingly we see additional bands at 3.8 kb and 1.5 kb, which indicates a LacI contamination. We confirmed that this contamination existed in our Gyrase sample (personal communication, Hawkins 2023). The LacI contamination did not affect our experimental reactions as we block the counterclockwise fork in the assay through an addition of LacI to form the LacI-*lacO* block.

Quantification showed that early addition of UvrD did not produce a significant increase in the percentage of clockwise replication forks able to proceed past the non-permissive orientation of the Tus-*ter* block compared to the control. The addition of UvrD + MutL did however show an increased percentage of replication forks past the non-permissive orientation of the Tus-*ter* block compared to early UvrD only sample. This value was marginally non-significant (p value of 0.052).

When attempting to compare the two gel results for late addition of UvrD, we saw large variation between values generated from gel one and gel two (figure 3.12 B and C). Difference between late addition UvrD only samples was 10.5%, compared to 1% for early addition UvrD.

Similarly, the difference between late addition of UvrD + MutL was 8.8%, compared to 0.2% for early addition of UvrD + MutL. Due to the low number of repeats, we did not feel that the mean value of $n=2$ would represent these results correctly and therefore decided that statistical analysis was not possible and that the comparison of UvrD added late with and without MutL cannot be analysed with the data available.

The early results generated are however promising, suggesting that the addition of MutL helps UvrD remove Tus when the full replisome is present.

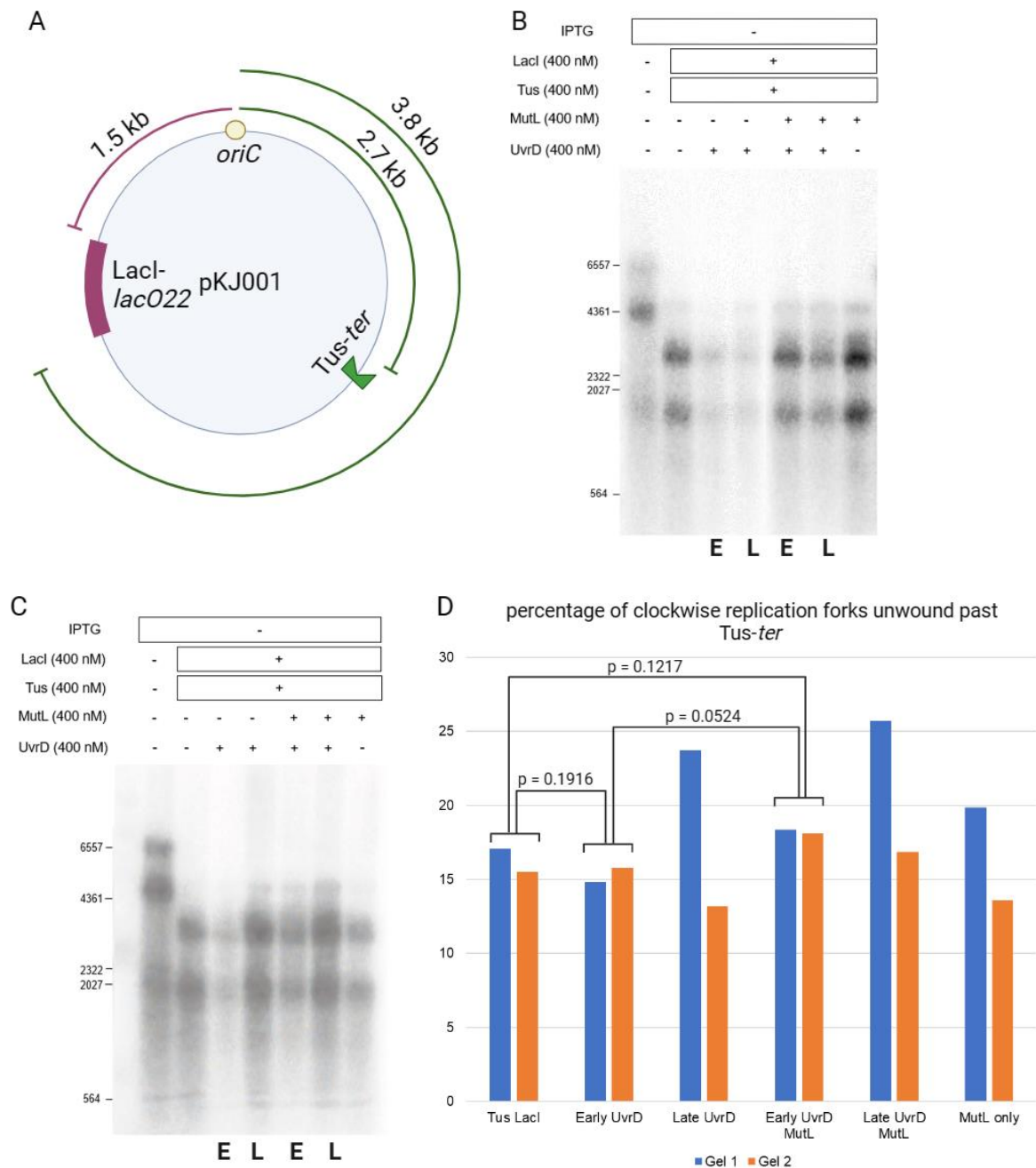


Figure 3.12 The ability of UvrD ± MutL to aid replication fork progression by removing Tus. A. Schematic of the pKJ001 replication assay template, featuring the *oriC* region for DNA replication initiation, the *lacO₂₂* array for LacI binding, and *terB* for Tus binding. The length of expected replication products is indicated. 2 nM of plasmid template added to the assay. B and C. N=2 repeats of a replication assay where two replication forks are blocked. The proteins were added as indicated. 'E' and 'L' labels represent early or late UvrD addition, respectively. D. Quantification of the percentage of replication forks released from *Tus-ter* from the two gel repeats. The p values were calculated using a one-tail t-test. The p values and significance of the mean between the two gels for various reactions have been indicated.

3.3 Discussion

In this chapter UvrD helicase was challenged to unwind dsDNA in assays which included Tus and EcoRI E111G, added with the purpose of forming two blocks, Tus-*ter* and EcoRI E111G on short and long substrates. UvrD unwinding past the permissive and non-permissive orientation of Tus-*ter* was first tested in easy conditions (short dsDNA substrate, 37 °C, 10 min incubation time). UvrD unwinding past the permissive orientation of Tus-*ter* and the EcoRI E111G block were also tested in 'challenging' conditions (long dsDNA substrate, 27 °C, 3 min incubation time). We also tested whether the addition of MutL could enhance the ability of UvrD to unwind dsDNA and if it can help UvrD displace, or unwind past, nucleoprotein blocks.

When analysing our results, it was important consider that the only band shift assay data available was for Tus binding to the short substrate. This meant that we could not be fully confident that our long substrates also contained the blocks, but we do know what proteins were present in the assay and can assume how likely it is that they formed the desired blocks.

The work in this thesis showed that UvrD is capable of unwinding past the Tus-*ter* block in both orientations on the short DNA substrate, and that the addition of Tus to the assay on the long substrate increased the ability of UvrD to unwind the substrate. This work also showed that the addition of MutL did not increase the percentage of unwound long DNA substrate when Tus was added to the assay. The concentrations of UvrD used for the helicase assays using short DNA substrate, otherwise known as "easy conditions", were adapted from Lee and coworkers 1989 (Lee et al., 1989). Lee and coworkers concluded that UvrD was unable to unwind past the non-permissive orientation of Tus-*ter*, despite other literature showing UvrD was capable of unwinding past Tus-*ter* (Khatri et al., 1989; Hiasa and Marians, 1992). This work demonstrates that UvrD can unwind past the Tus block even at the lowest concentrations. When comparing my results and the data from the literature, it is however important to consider that different DNA substrates were used. Lee and coworkers, as well as Khatri and coworkers, used the M13mp18 ssDNA plasmid with a double-stranded *ter* region

for Tus binding, while Hiasa and Marians used the M13YTB53 and M13YTB35 phage DNA as DNA template for their helicase assays where UvrD was able to remove Tus from *terB* (Hiasa and Marians, 1992). Our DNA substrate included two oligos which hybridised into a 25-bp double stranded region including the *ter* site and two single-stranded 25-bp 'arms' to facilitate helicase loading (Lee et al., 1989; Khatri et al., 1989).

When UvrD helicase was tested in a replication assay for Tus removal with the full replisome was present/blocked at Tus-*ter*, UvrD helicase function was limited and we did not see an increase in fork release from Tus-*ter* when UvrD was added early. However, a marginally insignificant increase, from an average of 15.29% to 18.21% with a p value of 0.0524, was visible when both UvrD (early) and MutL were added. If time permitted, we would repeat this assay for both the early and late addition of UvrD, to be able to generate a larger sample size.

It would also be interesting to repeat the termination assay and replication assay with ligase conducted by Jameson and coworkers. In the termination mapping assay, two replication forks were manipulated to terminate replication at Tus-*ter* on pKJ001. Using single strand cutters, the termination region was sequenced using radioactive nucleotides and revealed an unrepligated 15-23 bp gap with the same footprint as the binding of Tus (Jameson et al., 2021). As a response, a replication assay, including RNase HI, DNA Ligase and DNA Polymerase I (RLP) to allow for replication fork fusion, was conducted with an addition of helicases Rep, UvrD and RecG to test for their ability to aid replication fork progression past the Tus-*ter* block. None of the helicases were able to assist (Jameson et al., 2021). It would be interesting to conduct a replication assay of UvrD ± MutL + RLP to see if the addition of MutL would act as the 'missing factor' of termination, especially as UvrD has been shown to remove Tus *in vivo* (Bidnenko et al., 2006).

When UvrD was challenged to unwind a long substrate in an assay with EcoRI E111G present, our data showed that UvrD was inefficient at unwinding the substrate. The addition of MutL however appeared to have a large effect, producing a significant increase in the percentage of dsDNA unwound from the long DNA substrate compared to UvrD alone when EcoRI E111G

was added to the assay. The difference between the ability of UvrD alone to unwind when EcoRI E111G was present and when Tus was present is striking and surprising. Our results suggested that UvrD might have a specific affinity for Tus which could potentially increase its DNA unwinding efficiency.

3.3.1 What can UvrD tell us about how helicases displace DNA-bound proteins?

Though a lot of studies have been done to investigate if various helicases can remove nucleoprotein blocks, not a lot of investigation has been done on the actual mechanism of protein displacement. One of the better investigated protein block removal processes is the removal of stalled RNAP. To remove the block during TCR and replication-transcription conflicts, Mfd is able to push RNAP forward, which allows for DNA damage machinery to reach a DNA lesion (Park et al., 2002; Smith and Savery, 2005; Howan et al., 2012). UvrD is also able to remove a stalled RNAP block, but unlike Mfd, it pulls RNAP backwards using the EC complex (Epshtein et al., 2014). However, we do not know how helicases remove most proteins that they encounter on the DNA – do they apply an active mechanism such as the ‘pulling’ of RNAP by UvrD, or does helicase collision with the protein block cause for its displacement without an active role of the helicase?

The helicase assays in this study shine some light on how the mechanism of protein displacement might vary depending on which protein block the helicase approaches. Based on my results in this work and on the data present in literature, I propose that there are three mechanisms that helicases might use to approach DNA-bound protein blocks (figure 3.13).

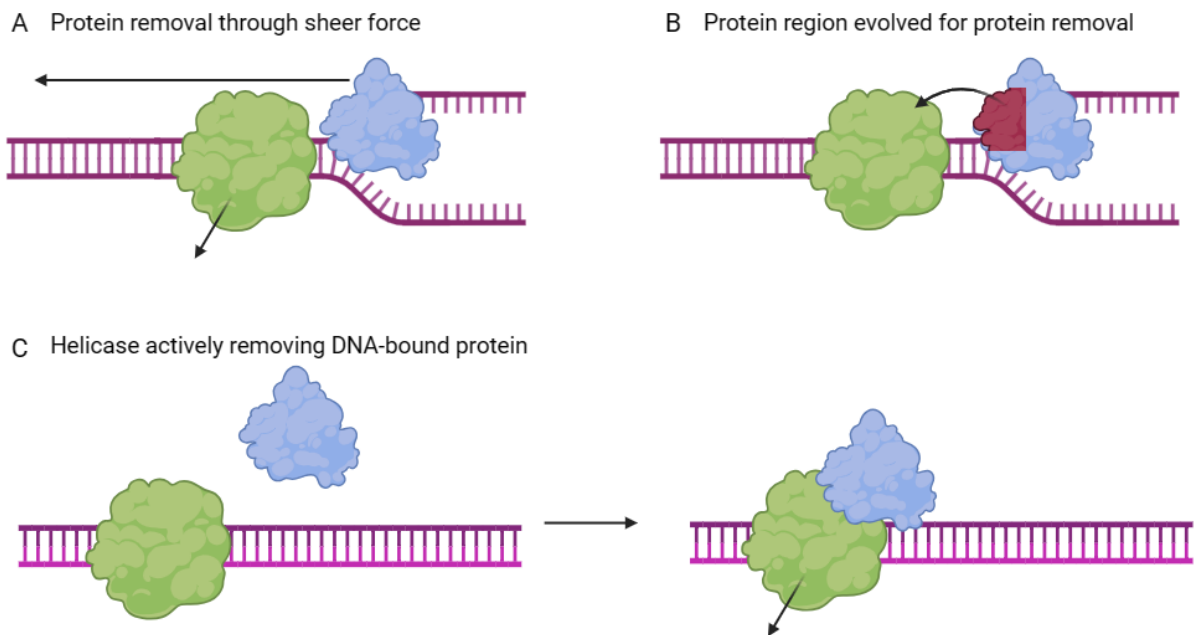


Figure 3.13 Models for the mechanism of protein displacement by helicases. A. The helicase can displace a DNA-bound protein through collision with the block. B. The helicase can displace a DNA-bound protein because it contains a specific region evolved for DNA-bound protein removal. C. The helicase can displace a DNA-bound protein through an active mechanism, which might include binding to the protein or the area surrounding it. Created on biorender.com.

The first mechanism (figure 3.13 A) exploits the presence of helicases on dsDNA, the speed of the helicase, and the movement of the DNA strands away from one another as the duplex breaks. These factors can combine to cause for the action of the helicase moving towards the block to displace the block. Alternatively, the block may be displaced by sheer force of the helicase-block collision. Examples of this mechanism might include the removal of the Tus block by DnaB in the case of a failed mousetrap mechanism (Elshenawy et al., 2015).

In this study, we suggest that the removal of EcoRI E111G by UvrD (with and without MutL) can act as an example of this mechanism. This is supported by the inefficiency of UvrD alone to unwind past the block, whereas the addition of MutL, which has been shown to increase the DNA processivity of UvrD (Mechanic et al., 2000; Ordabayev et al., 2018, 2019), allowed UvrD to potentially 'push' past the block with greater force.

The second mechanism (figure 3.13 B) indicates that some or all helicases can 'change' conformation to increase their ability to remove DNA-bound proteins or have regions which are responsible for protein removal. This might or might not be dependant on how the helicase approaches the block – whether through DNA unwinding or not. An example of this can be seen in the Brüning study where the 2B subdomain of Rep helicase was linked to its ability to remove DNA bound proteins. Rep Δ 2B was unable to remove DNA bound proteins (EcoRI E111G and Streptavidin) compared to WT Rep, suggesting that the 2B subdomain of Rep has a specific function for DNA-bound protein removal (Brüning et al., 2018).

In our study, this mechanism could apply to the 2B subdomain of UvrD helicase, since complex formation between MutL and UvrD causes rotation of the 2B subdomain of UvrD into an 'open' conformation (Ordabayev et al., 2019). It would be interesting to adapt our helicase assay against the EcoRI E111G block by stimulating the rotation of the 2B subdomain without the presence of MutL, potentially through the use of a low salt concentration buffer (Jia et al., 2011). By doing this we could compare whether the addition of MutL had any specific effect on the ability of UvrD to unwind past the block, or if MutL was only helpful through its ability to rotate the 2B subdomain of UvrD.

The third mechanism (figure 3.13 C) suggests that certain helicases can have an active mechanism of nucleoprotein block removal, which does not have to be associated with the helicase unwinding the DNA. An example includes the role of UvrD in the removal of the RNAP by pulling it backwards using the EC (elongation complex of RNAP), where UvrD is bound to RNAP rather than to the DNA (Epshtein et al., 2014). Another example was illustrated by Petrova and coworkers who showed that when UvrD was tested for protein displacement against RecA, an active mechanism which required UvrD-mediated ATP hydrolysis was initiated (Petrova et al., 2015). To make it even more interesting, removal of the C-terminal of the RecA protein disabled the ability of UvrD to remove it from the DNA, suggesting that the helicase was able to specifically recognise RecA to remove it (Petrova et al., 2015).

Our results suggest that UvrD might remove Tus using a specific active mechanism. This is illustrated by the ability of UvrD to unwind the long substrate past the Tus-*ter* block with greater efficiency than unwinding the substrate without the block, but also through the lack of increased efficiency when MutL was added. Our results cannot indicate what the active mechanism might be, but they do show that UvrD 'behaved' differently when Tus was present in the assay than when it was not present.

Future work could include further investigation of these three potential mechanisms of nucleoprotein block removal by helicases. Tests might include helicase assays, stopped-flow DNA unwinding experiments to determine unwinding speed past a block, and single-molecule experiments (such as the time traces conducted by Ordabayev et al., 2019).

For UvrD, future work would include testing whether the speed of UvrD helicase approaching the Tus-*ter*, EcoRI E111G, and other blocks affects its ability to remove it. This could potentially be conducted through stopped-flow DNA unwinding experiments. Further studies of the 2B subdomain of UvrD could also determine whether it has a role in nucleoprotein block removal in a similar way that the 2B subdomain of its homologue Rep. Surface plasmon resonance (SPR) might also be used to investigate the interaction of UvrD (or UvrD regions) with nucleoprotein blocks, such as Tus and RecA. Lastly, determining the degree of UvrD and Tus interaction might shine a light on how Tus might be removed, which could be further investigated through generating a CryoEM structure of UvrD and Tus on DNA.

CHAPTER 4

PROTEIN PURIFICATION OF UVRD HELICASE WITH N-TERMINAL DELETIONS AND 2B SUBDOMAIN DELETION

Chapter 4. Protein Purification of UvrD Helicase with N-Terminal Deletions and 2B Subdomain Deletion

4.1 Introduction

UvrD helicase is the main helicase of the MMR mechanism in *E. coli*. During MMR, MutS detects the mismatched bases and MutH nicks the nascent strand, identified through hemimethylation of d(GATC) sites (Su and Modrich, 1986; Au, Welsh and Modrich, 1992; Hall and Matson, 1999; Sixma, 2001; Tessmer et al., 2008). MutL protein then loads UvrD onto the nicked DNA towards the mismatch to unwind the incorrectly synthesised nascent strand (Dao and Modrich, 1998; Yamaguchi et al., 1998; Mechanic et al., 2000; Hall et al., 1998). A complex between the MutL dimer and UvrD (as a monomer (Ordabayev et al., 2018)) has been well documented (Hall et al., 1998), but the interaction between MutL and UvrD during MMR is still being investigated. Studies have shown that the binding of MutL to UvrD has two effects on the helicase (Ordabayev et al., 2018, 2019). First, the binding of MutL causes a rotation of the 2B subdomain of UvrD from a 'closed' into an 'open' conformation by 130° to 160° (Ordabayev et al., 2019). Second, the binding of MutL to UvrD enhances UvrD processivity of DNA by 2-3 fold (Ordabayev et al., 2018).

The first aim of this study was to increase our understanding of the MutL:UvrD complex formation by investigating which regions of UvrD are required for binding to MutL.

Little research has been conducted on UvrD regions responsible for binding with MutL (Figure 1.4). Hall, Jordan and Matson conducted a yeast two-hybrid test where regions of UvrD and MutL were removed to determine if the proteins can still interact. They found that deletion of the first 100 and the last 40 amino acids of UvrD prevented interaction with MutL (Hall et al.,

1998). The first 100 amino acids of UvrD can be found in the 1A subdomain which is partly responsible for UvrD DNA unwinding (Meir and Greene, 2021). The last 40 amino acids can be found in the uncharacterised C-terminal domain of UvrD, which has been demonstrated to interact with some proteins, such as UvrB (Manelyte et al., 2009). Recent structural studies were able to characterise the C-terminal of PcrA helicase, a *B. subtilis* UvrD homologue, which is likely similar to the C-terminal tail of UvrD (Urrutia-Irazabal et al., 2021). In this study, we decided to narrow down the MutL binding region by removing the first 50 and 100 amino acids to determine which area of the N-terminal of UvrD contains the MutL binding domain (figure 4.1). Once produced, we planned to test for UvrD and MutL interaction through cross-linking analysis and SPR.

The second aim of this study was to gain a better understanding of the link between the MutL:UvrD complex formation and the 2B subdomain of UvrD. We wanted to determine the effect of the 2B subdomain rotation on not only DNA unwinding, which is well documented (Jia et al., 2011; Ordabayev et al., 2018, 2019), but also on DNA-bound protein displacement by UvrD.

The 2B subdomain of Rep, a UvrD homologue, was also investigated for its part in DNA unwinding and protein displacement (Brüning et al., 2018). Rep Δ 2B was found to have increased DNA processivity, but was no longer able to remove DNA-bound proteins (Brüning et al., 2018). Since removal of the 2B subdomain of UvrD also affected DNA processivity (Ordabayev et al., 2018), we wanted to test whether complete removal of the 2B subdomain of UvrD would have a similar effect as in Rep Δ 2B. We decided to purify a UvrD Δ 2B protein (figure 4.1) and to test for the MutL:UvrD Δ 2B interaction through cross-linking and SPR. Additionally, we wanted to test for DNA unwinding of DNA and against nucleoprotein blocks of UvrD Δ 2B compared to WT.

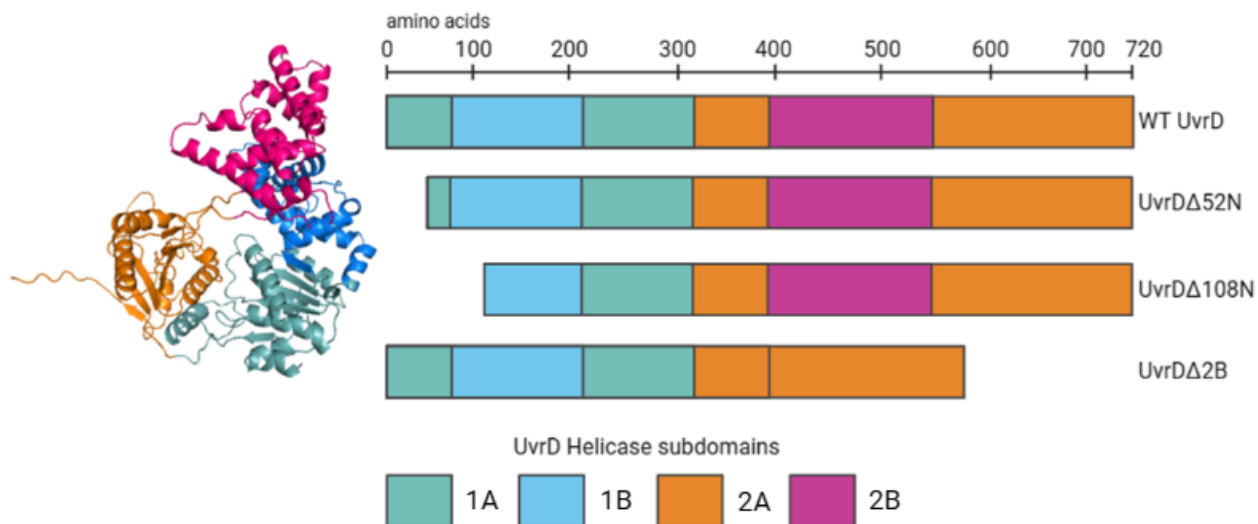


Figure 4.1 UvrD Helicase subdomains and deletion plan. UvrD helicase (PDB 2IS1) consists of four subdomains, 1A, 2A, 1B, and 2B. In this chapter, we attempt to create UvrD helicase mutants with two N-terminal deletions, UvrD Δ 52N and UvrD Δ 108N, and with a deletion of the full 2B subdomain, UvrD Δ 2B.

4.2 Results

4.2.1 Cloning *uvrD* into pET28α-HisSUMO

To generate UvrD helicase mutants, we started by cloning the complete *uvrD* gene into an expression plasmid, generating the pET28α-HisSUMO-*uvrD* plasmid, pDW006 (figure 4.2).

PCR was used to generate a linearised pET28α-HisSUMO vector (Figure 3.1 B), and to isolate the *uvrD* gene (figure 4.2 B) from the *E. coli* genome. As previously described in section 3.2.1.1, the pET28α vector is a 5369-bp over-expression plasmid with a kanamycin resistance gene, a lac operator sequence for inducing protein-of-interest expression and a T7 promoter region for protein transcription (Shilling et al., 2020; Dubendorf and Studier, 1991). The pET28α vector used also contained an N-terminal his-tagged SUMO gene.

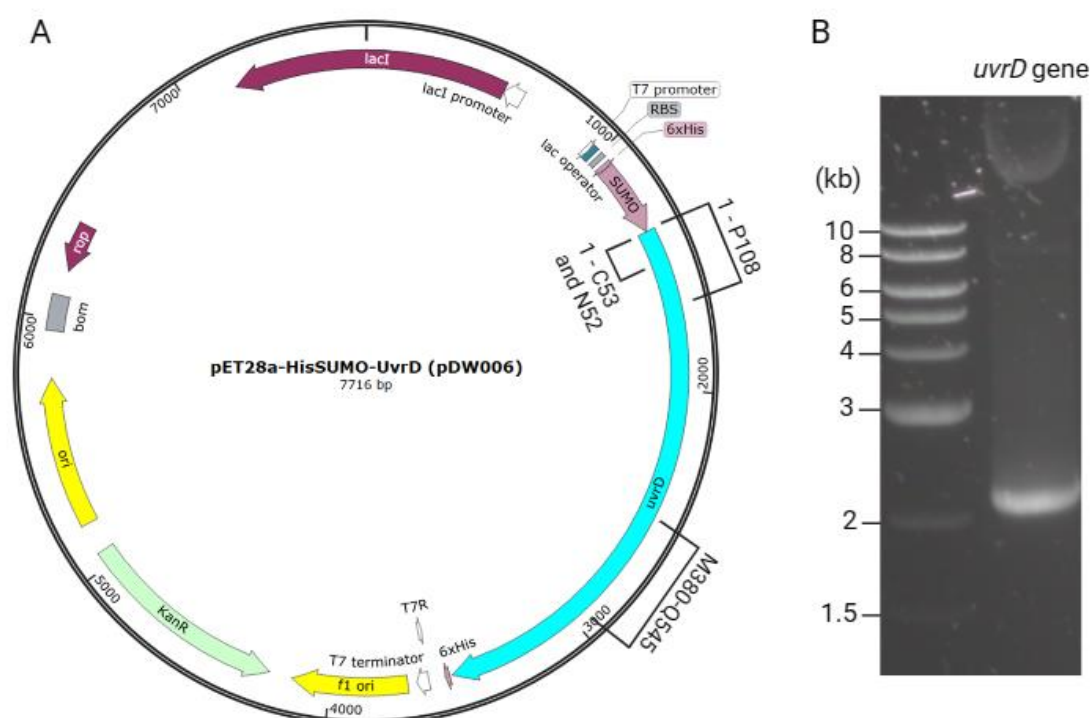


Figure 4.2 Map of UvrD expression plasmid. A. pET28α-HisSUMO-*uvrD* plasmid (pDW006). Regions designed for deletion from *uvrD* to generate *uvrD* Δ 52N *uvrD* Δ 108N, and *uvrD* Δ 2B have been annotated. B. Linearised *uvrD* gene amplified using PCR for InFusion. Expected size 2.16 kb.

InFusion cloning was used to insert the amplified *uvrD* gene into the vector through homologous recombination. The correct insertion of the gene was confirmed using both SourceBioscience Sanger sequencing and Plasmidsaurus nanopore sequencing.

4.2.2 Cloning and protein purification of UvrD Δ 108N

4.2.2.1 Generating the pET28 α -HisSUMO-*uvrD* Δ 108N expression plasmid

Hall and coworkers conducted a yeast two-hybrid test where UvrD Δ 100N was not able to interact with MutL. To purify a mutant UvrD Δ 100N, we decided to remove the first 108 amino acids instead of 100. When deciding on the site, we considered the amino acid properties of the amino acids around A100 of UvrD (99-RAHHMDANLPQD-110) and used PyMol to observe the protein structure of UvrD around A100. It was important to consider amino acids that were not very hydrophobic, so that the Gly-Gly region for SUMO cleavage wouldn't be obstructed, as well as which amino acids were found on the surface of the protein to avoid protein unfolding around the region.

We identified that the first 108 amino acids of UvrD can be found to contain approximately half of the 1A subdomain and part of the 1B (figure 4.3 C, 108 amino acids shown in yellow) (Lee and Yang, 2006, PDB 2IS1). The 1A subdomain is required for DNA translocation (section 1.2) and therefore the deletion of this region might impact the translocation ability of our mutant (Lee and Yang, 2006). Important residues which will be deleted includes R37, which is found within motif I and which weakly binds the 2'-OH of ATP, and T36, which functions with residues D220 and E221 of motif II to acquire a Mg₂₊ for ATP hydrolysis (Lee and Yang, 2006).

AlphaFold was used to generate a model protein structure for UvrD Δ 108N (figure 4.3 D), which was further viewed and annotated using PyMol. The AlphaFold predicted structure showed

similar folding of the remaining amino acids to the WT protein. This indicates that the loss of 108 amino acids from the N-terminal of UvrD should not be crucial to overall protein structure.

pDW006 was used as a template for generating an expression plasmid for the UvrD Δ 108N protein, pET28 α -HisSUMO-*uvrD* Δ 108N (pDW008). The first 324 nucleotides of *uvrD* were removed from pDW006 (full *uvrD* gene) using PCR. The process was similar to site-directed mutagenesis PCR but removed a large gene region instead of individual nucleotides. Plasmidsaurus nanopore sequencing was used to confirm correct deletion of the region (figure 4.3 A).

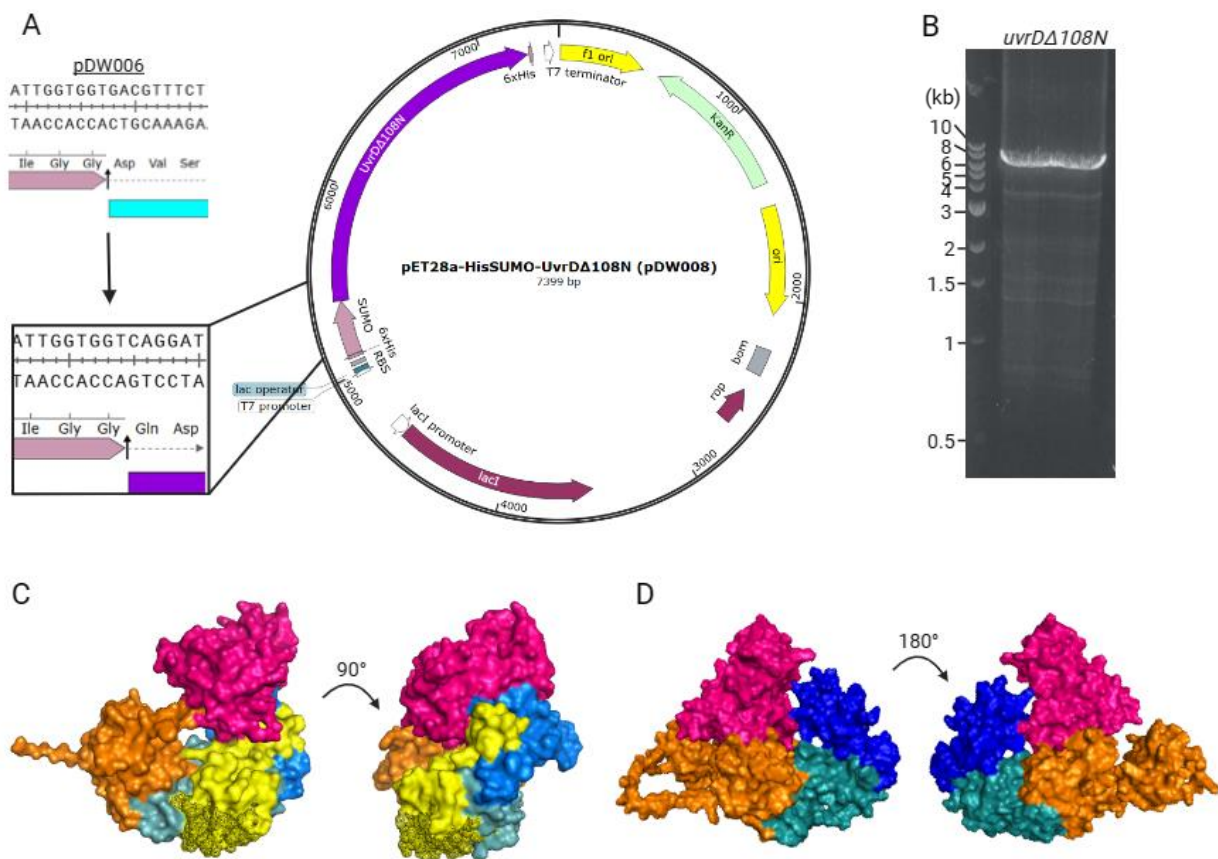


Figure 4.3 UvrD Δ 108N expression plasmid map and predicted protein structure. A. pET28 α -HisSUMO-*uvrD* Δ 108N (pDW008) expression plasmid generated by InFusion cloning. B. Linearised HisSUMO-*uvrD* Δ 108N before gel extraction. Expected size 7.399 kb. C. Protein structure of UvrD helicase (PDB 2IS1) generated using PyMol with the first 52 amino acids shown in yellow-black and the remaining first 108 amino acids in yellow, shown to occupy a large part of the 1A (teal) and 1B (blue) subdomains. D. AlphaFold generated model of truncated UvrD, UvrD Δ 108N.

4.2.2.2 DNA precipitation with poly(ethyleneimine) precipitates HisSUMO-UvrD Δ 108N protein

DNA precipitation is conducted to remove DNA from proteins that interact with nucleic acid. This step ensures that there is no DNA purified alongside the protein which might interfere with protein function during *in vitro* experiments. In our group we have previously used Poly(ethyleneimine) (also known as PolyminP or PEI) to precipitate DNA in protein purification samples after separation of the insoluble and soluble lysate fractions (conducted as per Jameson et al., 2021).

A DNA precipitation step using PolyminP was included in the protein purification of the HisSUMO-UvrD Δ 108N protein. When visualising the first steps of the protein purification protocol on a 10% SDS-PAGE gel, we saw the expected protein band (82.1 kDa) in the total, insoluble and soluble fractions, but did not see any in the fraction after DNA purification and supernatant filtering (figure 4.4 A). The lack of HisSUMO-UvrD Δ 108N protein in both samples indicates that the protein precipitated alongside DNA during the DNA precipitation step.

Optimisation of the PolyminP DNA precipitation step was attempted during HisSUMO-UvrD Δ 108N protein purification (Figure 4.4 B). We tested our standard final concentration of PolyminP (0.075%) and a lower concentration (0.05%) alongside varying concentrations of NaCl (300 mM, 500 mM, 700 mM, and 1 M) in 50 mM Tris-HCl, pH 7 buffer. Both concentrations of PolyminP showed protein precipitation at NaCl concentrations of 300-700 mM. Some protein was visible at 1 M NaCl concentration, which was not surprising since at NaCl concentrations of 1 M or higher, Polymin P should not precipitate protein (Burgess, 1991). We decided not to use PolyminP for DNA precipitation of UvrD mutants.

As an alternative, we added DNase I to a final concentration of 2 $\mu\text{g}/\text{ml}$ to the lysis buffer and included a high salt (3 M NaCl) wash in the first affinity chromatography step (personal communication, Chechik 2023). DNA was shown to precipitate in high salt concentrations (Fang et al., 1992). In retrospect, testing other DNA precipitation techniques, such as sodium deoxycholate, would have been preferred (conducted on UvrD in Atkinson et al., 2009).

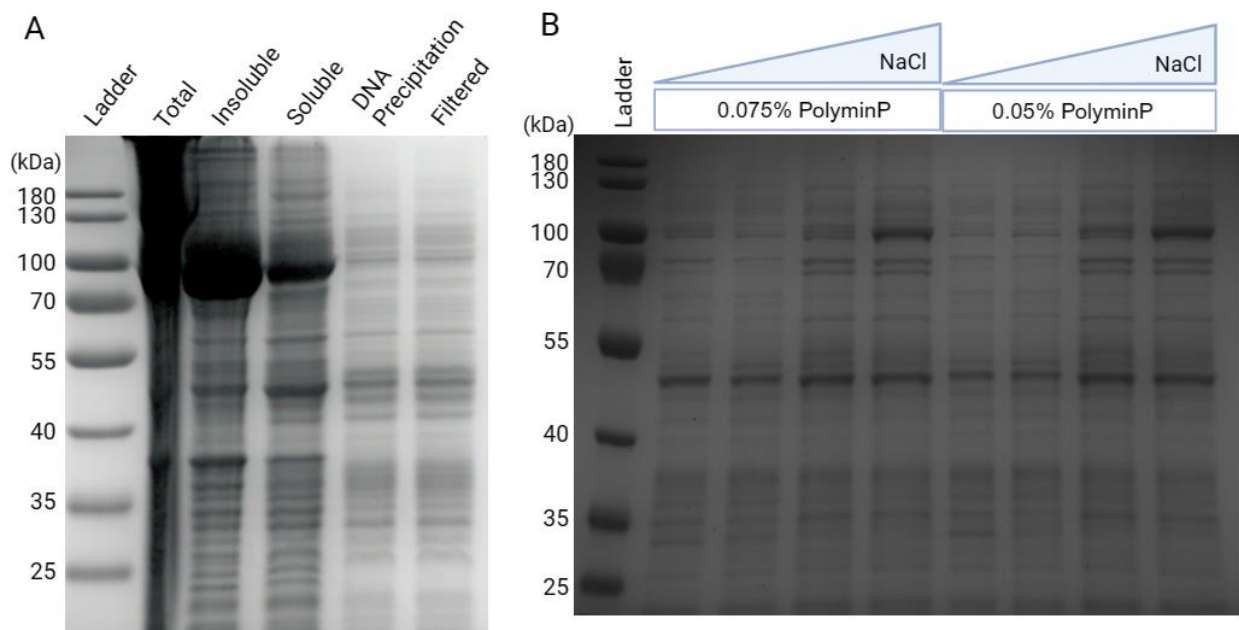


Figure 4.4 HisSUMO-UvrD Δ 108N DNA precipitation step optimisation.. A. 10% SDS-PAGE gel showing the HisSUMO-UvrD Δ 108N protein (band of interest 82.1 kDa) precipitating alongside DNA during the DNA precipitation step using 0.075% PolyminP. B. 10% SDS-PAGE gel showing DNA precipitation test using 0.075% or 0.05% Polymin P in 300 mM, 500 mM, 700 mM or 1 M NaCl.

4.2.2.3 Protein purification of UvrD Δ 108N using affinity chromatography and the SEC pathway

The first attempt at protein purification of UvrD Δ 108N was conducted using two affinity chromatography steps and a SEC chromatography step (hereafter known as the SEC strategy). In this method we expected HisSUMO-UvrD Δ 108N to bind to the nickel column during the first affinity chromatography step before the HisSUMO tag was cleaved away using a SUMO specific protease, Ulp1. In the second affinity chromatography step, the cleaved HisSUMO tag was expected to bind to the column while the untagged protein-of-interest would not. The SEC step was added to remove any additional protein contaminants.

After the first affinity column and overnight cleavage, UvrD Δ 108N was injected into an affinity column for the second affinity step. We observed a high peak during the elution step where we only expected to see the HisSUMO protein (figure 4.5 C). When visualised on a 10% SDS-PAGE gel (figure 4.5 D), the majority of UvrD Δ 108N was found in the elution fraction alongside an incompletely cleaved HisSUMO- UvrD Δ 108N. The cleaved and uncleaved proteins were also found in the flow through fractions, where UvrD Δ 108N was expected. This might have occurred due to dimer and/or tetramer formation which could have obscured some of the Ulp1 cleavage sites and in turn left an exposed His-tag site for binding to the HisTrap column.

When the mixed cleaved and uncleaved protein sample was injected into a SEC column, we were able to isolate a fraction where most of the protein was cleaved. The final purified protein (figure 4.5 E) contained some unidentified protein bands, likely other protein contaminants or protein homodimers and tetramers which did not break during protein boiling before loading onto the denaturing SDS gel (personal communication, Hill 2023). Upon analysis, we decided that the protein of interest was much more concentrated than the contaminants and in the full sample volume the contaminants would be negligible and would likely not affect UvrD Δ 108N function.

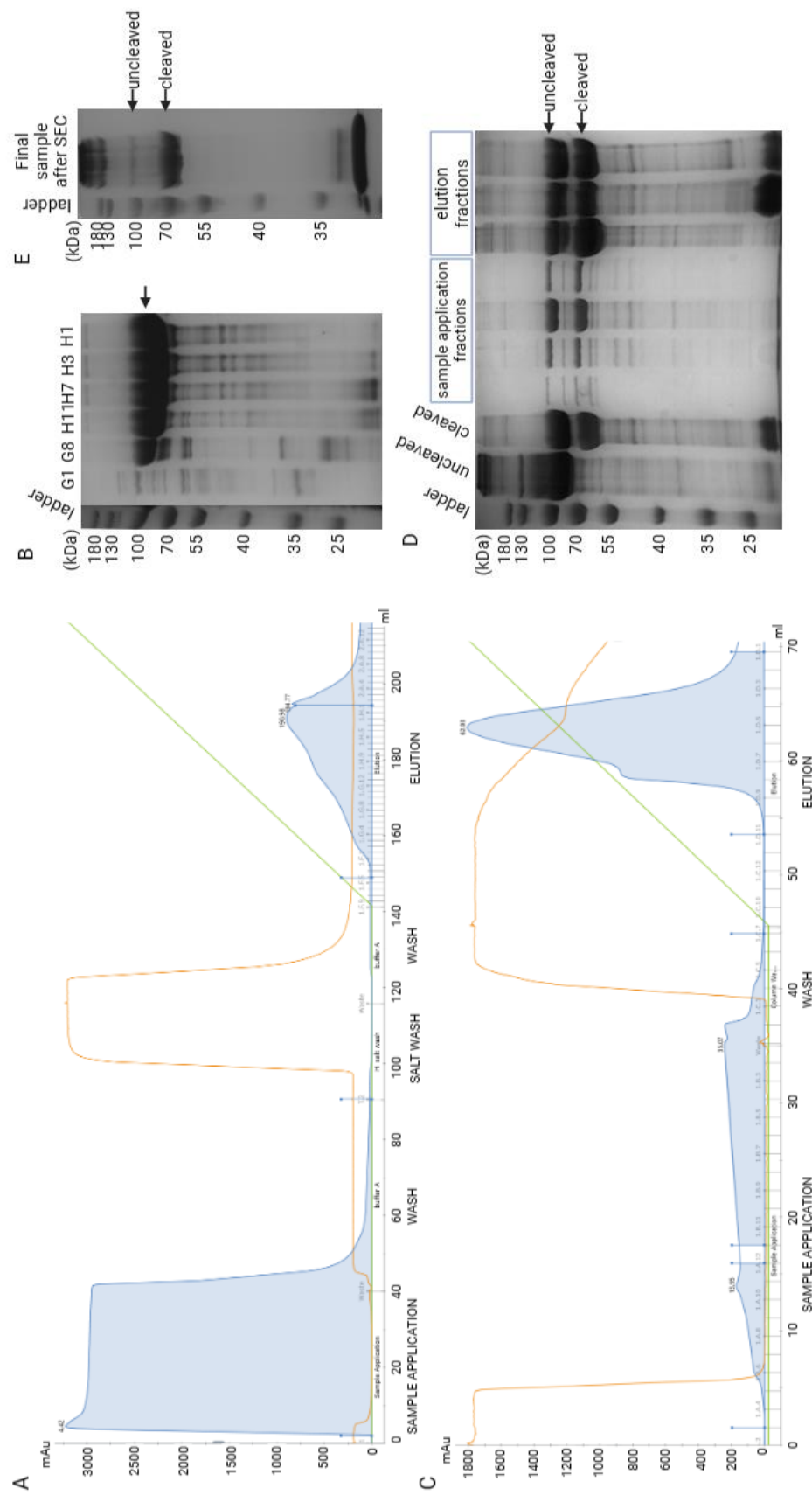


Figure 4.5 Affinity chromatography protein purification step for UvrD Δ 108N protein. A. First affinity chromatography isolating HisSUMO-UvrD Δ 108N. B. 10% SDS-PAGE protein gel showing fractions from the elution peak. Expected band size 82.1 kDa for HisSUMO-UvrD Δ 108N. C. Chromatogram from the second affinity chromatography conducted on HisSUMO-UvrD Δ 108N post HisSUMO-cleavage. D. 10% SDS-PAGE protein gel showing samples A. Fractions A6, A10, B4, C2 from sample application, and fractions D8, D6, D4 from elution. UvrD Δ 108N expected size is 70.1 kDa, while uncleaved HisSUMO-UvrD Δ 108N expected size is 82.1 kDa. E. 10% SDS-PAGE protein gel showing the final purified UvrD Δ 108N protein after the SEC chromatography.

4.2.2.4 Protein purification of UvrD Δ 108N using the ion exchange pathway

We were curious to see whether a different protein purification technique would be able to separate cleaved and uncleaved UvrD Δ 108N better. We conducted a second attempt at protein purification of UvrD Δ 108N using one affinity chromatography step and an ion exchange chromatography step (hereafter known as the ion exchange strategy). In this method, the HisSUMO-UvrD Δ 108N protein was isolated using a nickel column during the affinity step, before HisSUMO tag cleavage from UvrD Δ 108N. The sample was then injected into a MonoQ ion exchange chromatography column where UvrD Δ 108N and HisSUMO-UvrD Δ 108N could be isolated using their negative charge difference.

Buffer optimisation tests were performed to check whether HisSUMO-UvrD Δ 108N was soluble and stable (did not precipitate) in ion exchange chromatography conditions (Figure 4.6 A and B). First, we tested a change of pH, from pH 7.0 to pH 8.0. This was done to achieve a better charge difference between HisSUMO-UvrD Δ 108N (-24.6) and UvrD Δ 108N (-18.7) post cleavage. HisSUMO-UvrD Δ 108N was soluble at both pH 7.0 and 8.0 (figure 4.6 A). Second, we tested a change of NaCl concentration. Ion exchange chromatography requires a low salt buffer for sample loading and a high salt buffer for elution from the column. HisSUMO-UvrD Δ 108N was soluble in salt concentrations from 50 to 500 mM (Figure 4.6 B).

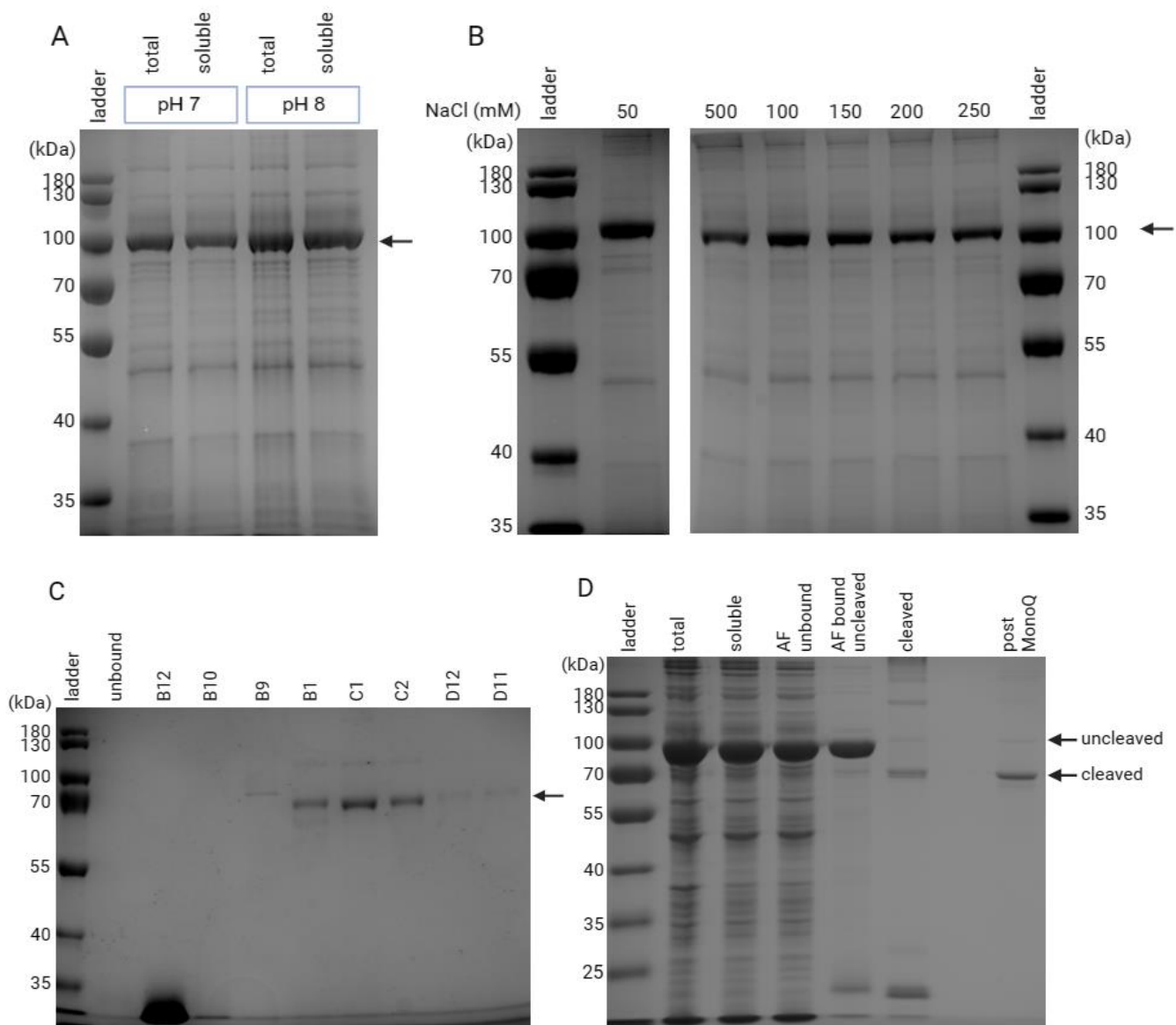


Figure 4.6 Protein purification of UvrD Δ 108N using ion exchange chromatography. A. 10% SDS-PAGE protein gel showing a solubility test of HisSUMO-UvrD Δ 108N in pH 7.0 and 8.0 lysis buffers. B. 10% SDS-PAGE gel showing the solubility of HisSUMO-UvrD Δ 108N at NaCl concentrations of 50 mM, 100 mM, 150 mM, 200 mM, 250 mM, and 500 mM. C. 10% SDS-PAGE protein gel showing fractions from the ion exchange chromatography. HisSUMO-UvrD Δ 108N was expected at 82.1 kDa, while UvrD Δ 108N was expected at 70.1 kDa. D. 10% SDS-PAGE protein gel showing the steps conducted as part of the ion exchange route of UvrD Δ 108N protein purification. 'AF' shows samples from the affinity chromatography while 'post-MonoQ' shows the final protein aliquot.

Ion exchange chromatography eluted the protein in a single peak, which mostly contained the cleaved UvrD Δ 108N protein (figure 4.6 C). The most intense band migrated at the correct size for cleaved UvrD Δ 108 (70.1 kDa), with only a very weak band for uncleaved HisSUMO-UvrD Δ 108N (82.1 kDa). Due to a lack of HisSUMO-UvrD Δ 108N in any other fractions, it is unlikely that it eluted elsewhere. The binding of the protein to the MonoQ column could have somehow exposed the cleavage site and increased the amount of protein cleavage. The chromatograph of the peak is not available due to a mistake in saving it on the system.

UvrD Δ 108N was successfully purified using the Ion exchange route of protein purification (figure 4.6 D).

4.2.2.5 UvrD Δ 108N could not unwind dsDNA

A helicase assay was conducted to test whether UvrD Δ 108N could unwind a short dsDNA substrate (in non-challenging conditions at 37 °C with an incubation time of 10 min) (figure 3.6 A) and whether the addition of MutL improved its unwinding ability (Figure 4.7 A). We previously were able to show that WT UvrD was able to unwind this substrate (Figure 3.7). Our hypothesis was that if MutL can assist WT UvrD activity, but not UvrD Δ 108N, then the binding site for UvrD-MutL complex might be found in the first 100 amino acids of UvrD, as suggested by Hall and coworkers (Hall et al. , 1998). The helicase assay was conducted using UvrD Δ 108N purified through the SEC column strategy (section 4.2.2.3). This is because the assay was conducted before UvrD Δ 108N purification through the ion exchange route (section 4.2.2.4) was achieved.

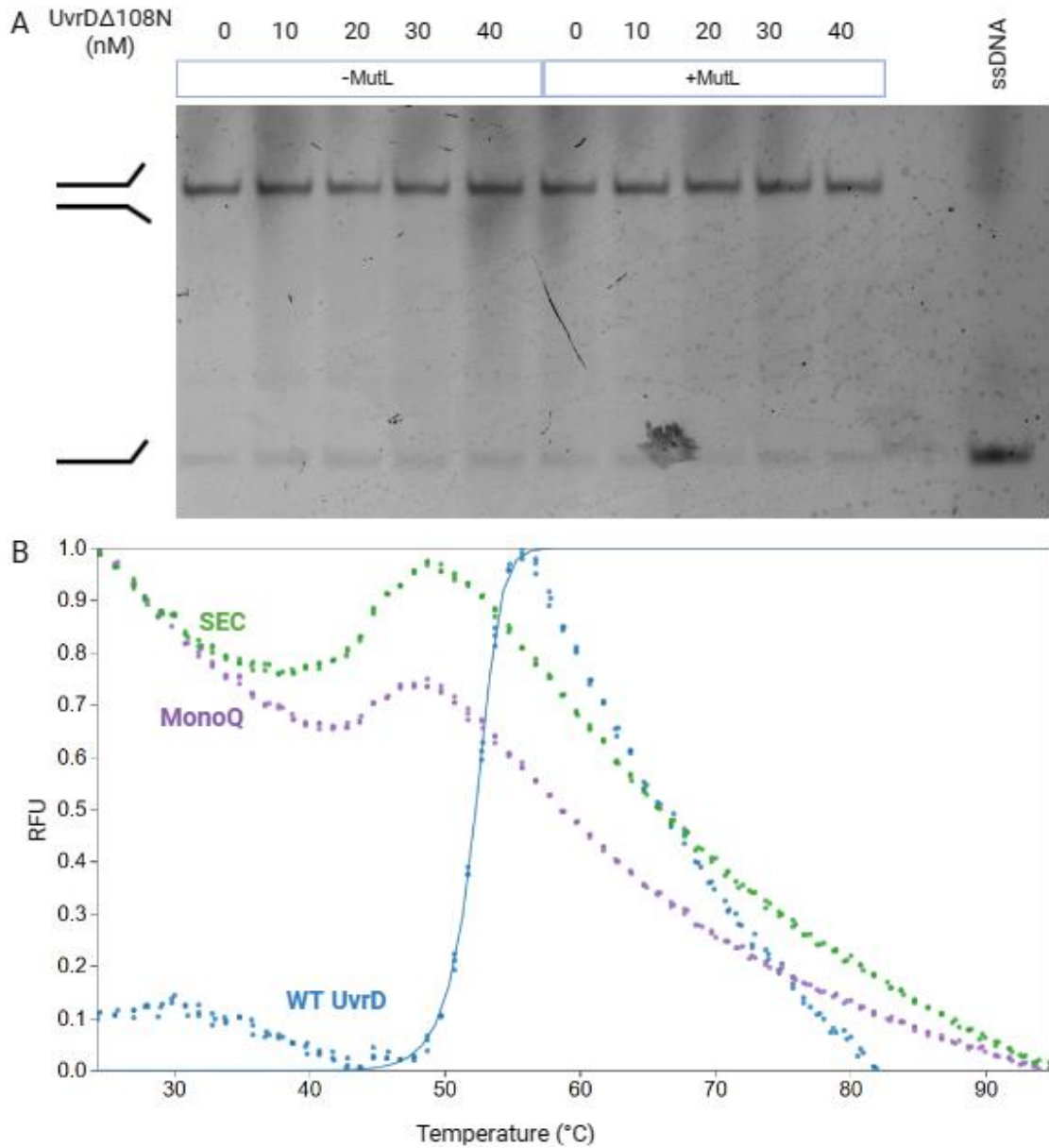


Figure 4.7 UvrD Δ 108N functional assay and TSA. A. Helicase assay testing the ability of UvrD Δ 108N to unwind a short dsDNA replication fork-like substate with and without the addition of 50 nM MutL. B. Thermal shift assay to test the folding of UvrD Δ 108N produced by the SEC strategy (green) route and the ion exchange strategy (MonoQ) route (purple). WT UvrD (blue) has been shown for comparison with a correct TSA peak.

UvrD Δ 108N was not able to unwind the dsDNA substrate alone or with the addition of MutL. As hypothesised in section 4.2.2.1, which is likely due to the removal of important residues (T36 and R37 from motif I) responsible for ATP hydrolysis and binding. The removal of a part of the 1A subdomain, which is essential for DNA translocation (figure 1.1) (Meir and Greene, 2021), likely also prevented UvrD Δ 108N from binding to the DNA. This is likely due to the 1A and 2A subdomains being involved in DNA unwinding, which was not considered when first designing this deletion region. As a comparison, WT UvrD was able to unwind the substrate fully (figure 3.7 A and B, 0 nM Tus 100 nM UvrD lane) as well as against the Tus-*ter* block (figure 3.7 A and B).

Correct folding of UvrD Δ 108N purified through both the SEC and the MonoQ strategies was tested using the thermal shift assay (TSA) (Huynh and Patch, 2015). Both UvrD Δ 108N samples display a similar curve that starts either higher (MonoQ) or as high (SEC) as the highest point of the peak. TSA assesses how much fluorescent signal is released from a the SYPRO dye which binds to the hydrophobic elements of protein (figure 2.5) (Sackett and Wolff, 1987; Steinberg et al., 1996). Therefore, a signal that starts high suggests that the protein is not folded correctly and that its hydrophobic regions are exposed at the start of the test. The signal then dips as the SYPRO dye signal fades, before the rest of the protein unfolds – forming the peak. The TSA results suggest that both purification methods for UvrD Δ 108N produced incorrectly folded protein that could not be used in further experiments. For comparison, the WT UvrD test (figure 4.7 B) shows a curve that shows correct protein folding, with a clear peak, the start of which is lower than the peak itself (figure 2.5, reference to a correct looking peak).

4.2.3 Cloning and protein purification of UvrD Δ 53N

Next, we aimed to generate a deletion of the first 50 amino acids of UvrD to determine if UvrD Δ 50N was able to interact with MutL and therefore where in the first 100 amino acids of UvrD the interacting region with MutL might be found. To purify a mutant UvrD Δ 50N, we decided to remove the first 53 amino acids instead of 50, same as with UvrD Δ 108N. When deciding on the site, we considered the amino acid properties of the amino acids around E50 of UvrD (48-SVENCSPYSIMAV-60) and used PyMol to observe the protein structure of UvrD around E50 to avoid hydrophobic amino acids and ensure Gly-Gly cleavage region would be accessible by Ulp1. When initially designing the construct we did not consider with enough detail that the removal of the first 53 amino acids of UvrD would also remove residues T36 and R37, which are involved in ATP hydrolysis (Lee and Yang, 2006). Similarly to UvrD Δ 108N, this deletion might therefore limit or disable its ATP hydrolysis and DNA translocation function.

We generated a HisSUMO-UvrD Δ 53N (pDW007) expression construct (figure 4.8 A) using PCR with primers designed to omit the synthesis of the first 159 nucleotides of *uvrD* from pDW006 (WT UvrD) expression plasmid (using the same technique as in section 4.2.2.1). pDW007 was sequenced using Plasmidsaurus nanopore sequencing to confirm the correct sequence, (figure 4.8 A).

BL21 DE3 cells were transformed with pDW007 and overexpression of HisSUMO-UvrD Δ 53N was induced with 1 mM IPTG for 3 hrs at 37 °C in LB broth. The correct protein band (88.4 kDa) was only found in the insoluble fraction, (figure 4.8 B), therefore HisSUMO-UvrD Δ 53N was insoluble.

We attempted to optimise expression by altering the NaCl concentration of the lysis buffer (figure 4.8 C), but the protein remained insoluble.

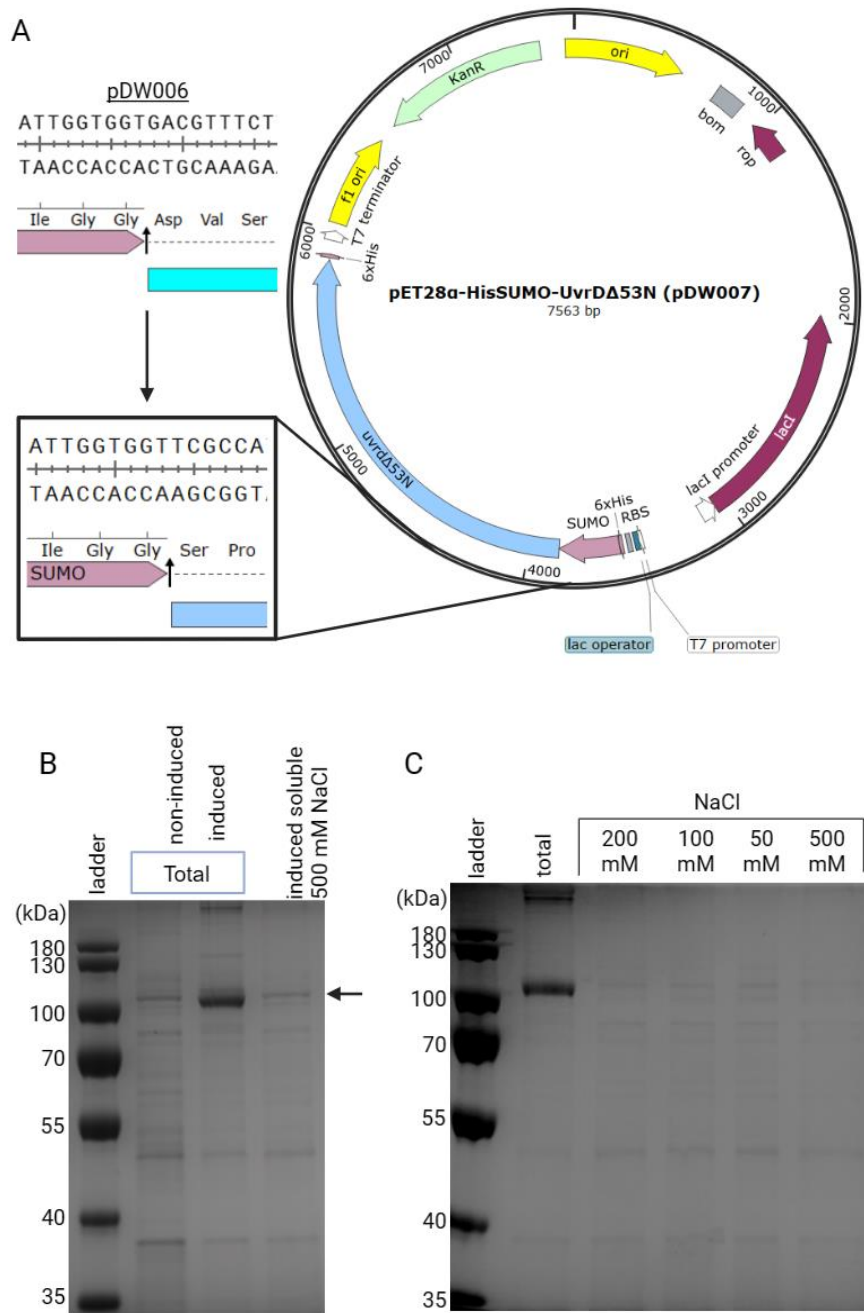


Figure 4.8 Cloning and expression tests for the HisSUMO-UvrD Δ 53N protein. A. HisSUMO-UvrD Δ 53N protein expression plasmid (pDW007) map. B. 10% SDS-PAGE gel showing expression test for HisSUMO-UvrD Δ 53N from pDW007, showing the non-induced and induced total fractions (soluble and insoluble), and the induced soluble fraction. C. 10% SDS-PAGE gel showing a solubility test for HisSUMO-UvrD Δ 53N in 50 mM, 100 mM, 200 mM and 500 mM NaCl.

4.2.4 Cloning and protein purification of UvrD Δ 52N

Rather than attempting to adjust the lysis buffer composition for HisSUMO-UvrD Δ 53N purification or other expression conditions, we decided to redesign our expression plasmid to remove the first 52 amino acids of UvrD instead of 53 amino acids. The decision to alter the construct to remove the first 52 amino acids instead of 53 amino acids was based on trial and error as well as advice from a more experienced colleague (personal communication, Chechik 2023). We have looked at the amino acids found around 53S and chose 52C as it would not leave an exposed hydrophobic site which could conceal the SUMO cleavage region.

pET28 α -HisSUMO-*uvrD* Δ 52N (pDW010) was generated by PCR by removing the first 156 nucleotides from the WT *uvrD* gene in pDW006. The plasmid sequence and correct deletion were confirmed using Plasmidsaurus nanopore sequencing, (figure 4.9 A). WT UvrD protein structure (Lee and Yang, 2006, PDB 2IS1) was viewed using PyMol and the location of the first 52 amino acids were found in the 1A subdomain (figure 4.9 B – the 52 amino acids highlighted in yellow-black). As previously described for UvrD Δ 108N and UvrD Δ 53N, the deletion of the first 52 amino acids would also remove residues T36 and R37, which would limit/disable the ATP hydrolysis function of UvrD (Lee and Yang, 2006).

AlphaFold was used to generate a prediction for the structure of UvrD Δ 52N, (figure 4.9 C). Similarly to UvrD Δ 108N, the AlphaFold structure suggested that the deletion should not critically alter the protein structure.

BL21 DE3 cells were transformed with pDW010 and overexpression of HisSUMO-UvrD Δ 52N was induced using IPTG. The overexpressed protein was purified using the ion exchange strategy of protein purification. Cleavage after affinity chromatography was incomplete (figure 4.9 D) and the yield collected after ion exchange chromatography was very small. The protein precipitated during storage at -70 °C.

Unfortunately, the small yield and protein precipitation did not allow us to use UvrD Δ 52N further in this work.

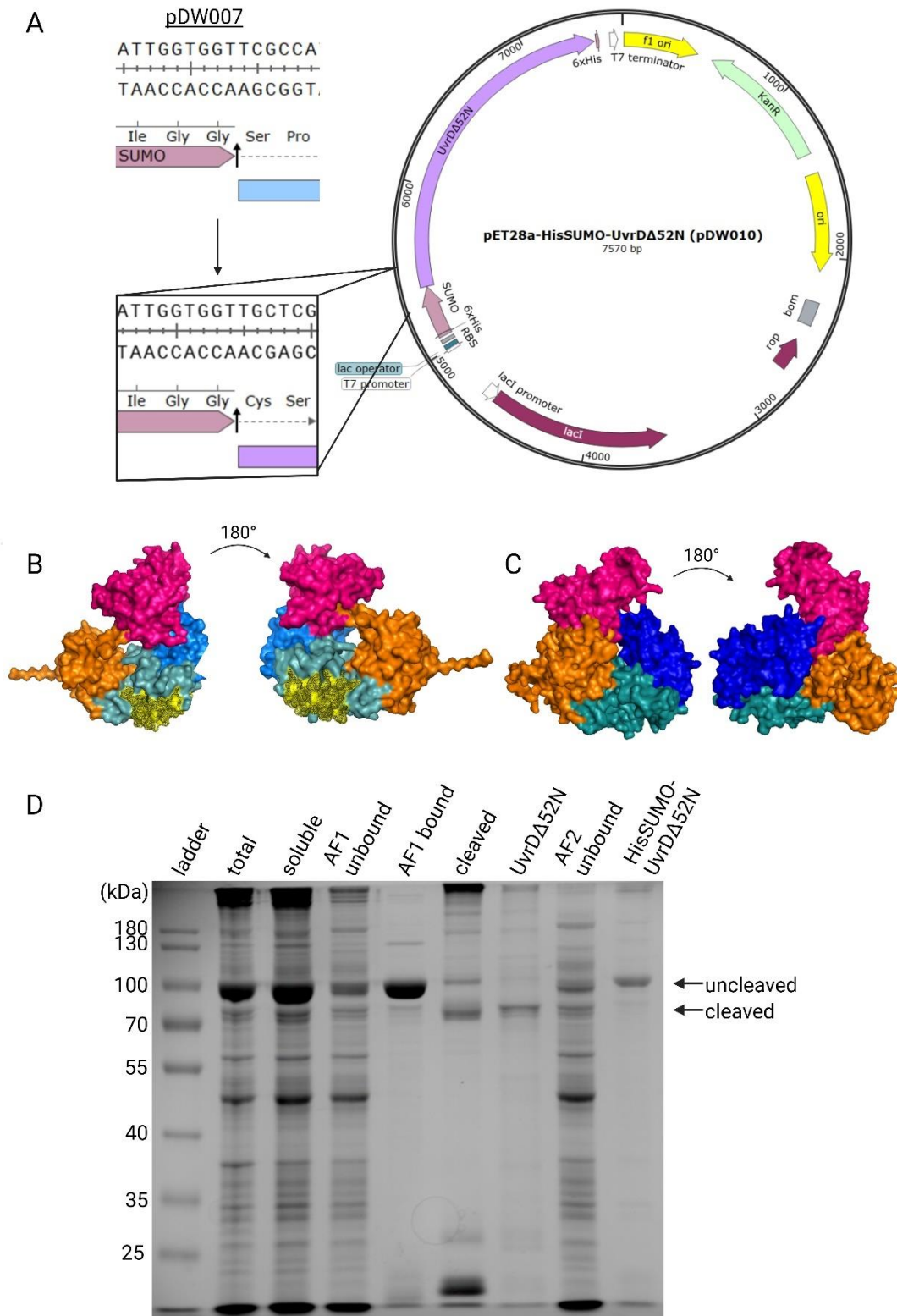


Figure 4.9 UvrD Δ 52N expression plasmid pDW010 and protein purification. A. Plasmid map of oDW010, including the N-terminal comparison between pDW007 and pDW010. B. Protein structure of UvrD (PDB 2IS1) showing the four subdomains, 1A (teal), 1B (blue), 2A (orange), 2B (pink), and the first 52 amino acids highlighted in yellow. C. AlphaFold generated protein structure of UvrD Δ 52N. Domains colour-coded as per B. D. Protein purification of UvrD Δ 52N using the ion exchange strategy.

4.2.5 Cloning and protein purification of UvrD Δ 2B

4.2.5.1 Designing the UvrD Δ 2B expression plasmid

We aimed to produce UvrD Δ 2B protein to test what effect deletion of the 2B subdomain would have on UvrD helicase DNA processivity and protein displacement ability.

The first step in creating the UvrD Δ 2B mutant protein was deciding which amino acids to use as the 'start' and 'end' of the 2B domain deletion. First, we used the published UvrD helicase protein structure (Lee and Yang, 2006, PDB 2IS1) and observed the edges of the 2B subdomain. Using PyMol we found that the 2B subdomain is located between two sections of the 2A subdomain. The 2B subdomain is linked to the 2A subdomain with long linker regions without helices or beta sheets, likely used for 2B rotation (figure 4.10 A). We wanted to make sure that the 2B deletion would not affect the folding and function of the 2A subdomain. We put consideration into which amino acids to choose as the 'edges' of our deletion to ensure that the regions can link without affecting the 2A subdomain. To confirm our choices, we generated an AlphaFold model (figure 4.10 B) for the mutated protein. Based on all these considerations, we decided to remove the 2B subdomain from M380 to Q545 (figure 4.10 C).

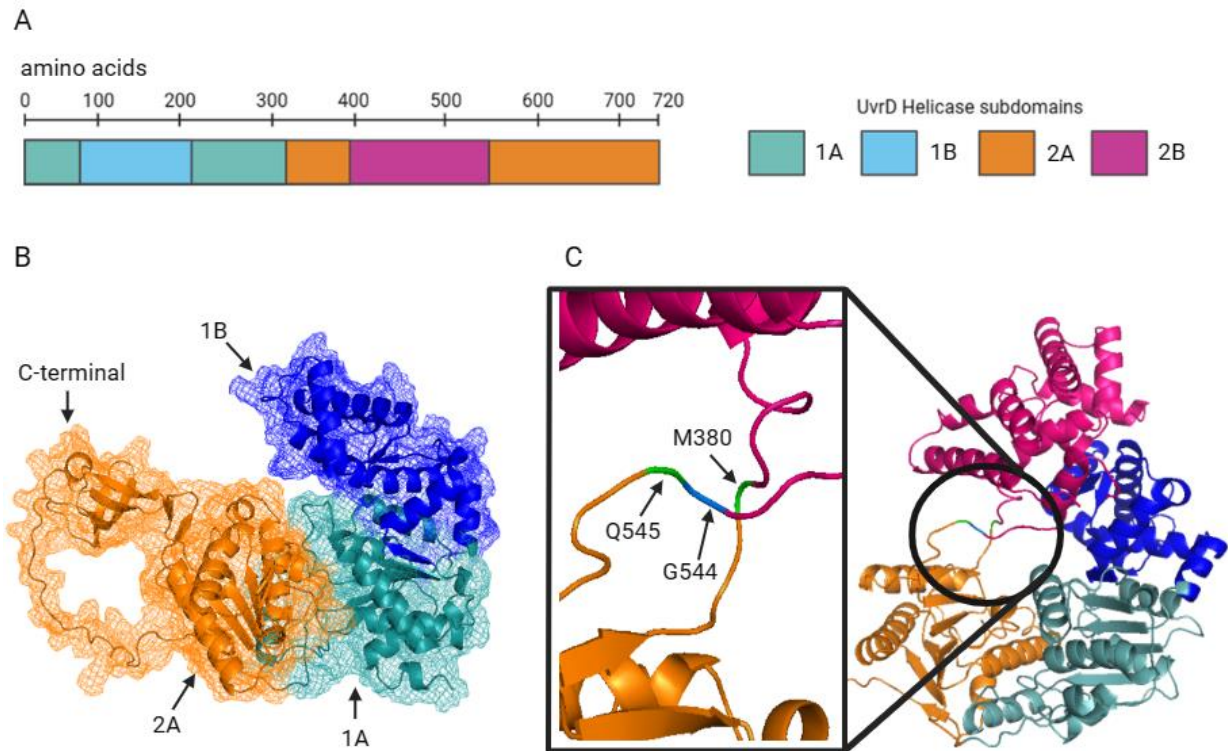


Figure 4.10 Designing UvrD Δ 2B. A. UvrD amino acid chain with the four subdomains as indicated, including the 2B subdomain in pink. B. AlphaFold generated model of UvrD Δ 2B, viewed and colour coded using PyMol. The three remaining UvrD subdomains are labelled, as well as the uncharacterised C-terminal tail. C. UvrD structure (PDB 2IS1) with the linker region between the 2A (orange) and 2B (pink) subdomains of UvrD on closer inspection. The green and blue amino acids represent the amino acids designated as edges used for 2B subdomain removal. The first design spanned M380 and G544, followed by a second design using M380 to Q545. Created on biorender.com.

PCR was used to remove the 2B subdomain of the UvrD protein using pDW006 as a template and generating pET28 α -HisSUMO-*uvrD* Δ 2B plasmid (pDW009). pDW009 was sequenced using SourceBioscience Sanger sequencing (figure 4.11 A), which showed an insertion mutation confirmed by Plasmidsaurus nanopore sequencing (figure 4.11 B). During PCR, the DNA polymerase (Phusion) misread a repeat sequence at the deletion site 'GGGGGG' into 'GGGGGGG'. This insertion changed the *uvrD* reading frame and added a premature stop codon, and therefore the plasmid was not suitable for the expression of UvrD Δ 2B. This insertion was caused by poor primer design. We redesigned the amino acid deletion region to continue from M380 but changing G544 into Q545 (figure 4.11 C) to avoid the long sequence of repeat nucleotides. The new deletion site was designed to read 'GGGCAG' instead.

PCR was conducted to remove the 2B subdomain of UvrD from pDW006 and generate a new pET28 α -HisSUMO-*uvrD* Δ 2B plasmid (pDW011) (figure 4.11 D). Plasmidsaurus nanopore sequencing showed that while the 2B subdomain was removed successfully, DNA polymerase added a base pair upstream from the 2B subdomain during PCR. This changed the reading frame of the protein in line with SUMO (figure 4.11 D). We concluded that the pDW011 plasmid was unable to generate UvrD Δ 2B; however, unlike pDW009, this error was due to the DNA polymerase functioning incorrectly, rather than the PCR primer design. To generate successful expression plasmids, we purchased fresh DNA polymerase (Phusion) and DpnI restriction enzymes. The change to a fresh DNA polymerase helped prevent further mutations in the newly generated DNA, while fresh DpnI ensured that the original template was cleaved (detected through methylation) and was not available to transform into DH5 α cells.

PCR was conducted for the third time using a fresh batch of Phusion DNA polymerase using the same primers used to design pDW011. This generated a new pET28 α -HisSUMO-*uvrD* Δ 2B plasmid (pDW012) (figure 4.11 E). Plasmidsaurus nanopore sequencing showed that the full plasmid and gene sequence were correct.

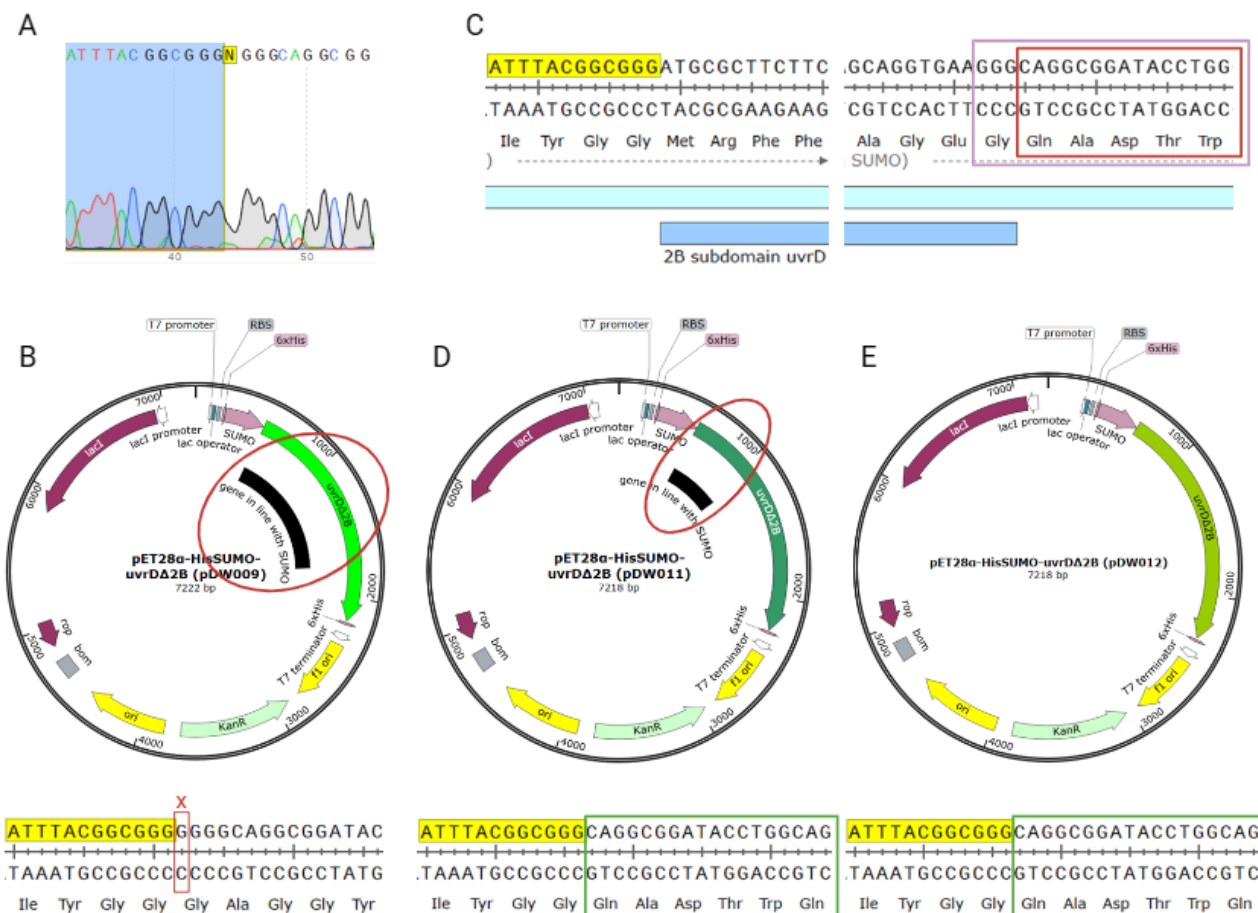


Figure 4.11 Generating the UvrD Δ 2B expression plasmid. A. Sanger sequencing using the T7 reverse primer result showing an unidentified base at the deletion site of pDW009. B. pDW009 plasmid map. Red circle highlights an incorrect reading frame (black) compared to expected (green) and the X on the base pairs shows the incorrect base pair insertion. C. The regions upstream and downstream the 2B region of the *uvrD* gene. The red square represents the region downstream of 2B designed for pDW009, the pink square shows the second region downstream of 2B designed for pDW011 and pDW012. D. pDW011 plasmid map. Correct 2B deletion site is shown in green on the sequence, but the red circle highlights the incorrect reading frame (black) compared to predicted reading frame (green arrow of gene of interest) due to an insertion deletion mid-gene. E. pDW012 plasmid map, with a correct 2B deletion, gene sequence and reading frame.

4.2.5.2 Expression test of UvrDΔ2B from pDW012

BL21 DE3 cells were transformed with pDW012 and overexpression of HisSUMO-UvrDΔ2B was induced with 1 mM IPTG. 10% SDS-PAGE gel was used to show the protein expression results for HisSUMO-UvrDΔ2B using a variety of lysis buffers with either 300, 500, 1000, or 1500 mM of NaCl, and either 0%, 5% or 10% glycerol (Figure 4.12). While a protein of expected size (74.9 kDa) is visible in the total fraction, we did not observe the protein in the soluble fraction in any of the tested buffer conditions.

In conclusion, HisSUMO-UvrDΔ2B produced from pDW012 was insoluble. Due to time constraints, we were unable to vary our expression conditions further or edit the expression plasmid design.

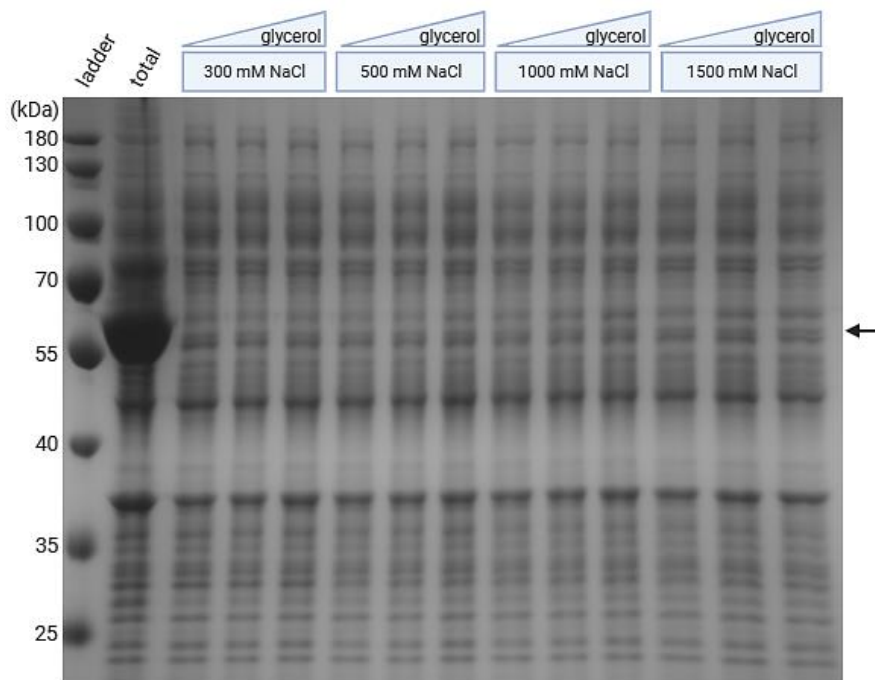


Figure 4.12 Overexpression of HisSUMO-UvrDΔ2B from pDW012. 10% SDS-PAGE gel showing overexpression tests of HisSUMO-UvrDΔ2B using IPTG in BL21 DE3 cells. The total lane includes the soluble and insoluble fractions, in 300 mM NaCl and 0% glycerol. The cell pellet was resuspended in a variety of buffers to check for protein solubility in 300 mM, 500 mM, 1000 mM and 1500 mM NaCl, and in 0%, 5% and 10% glycerol. The arrow shows the location of the expected 74.9 kDa band.

4.3 Discussion

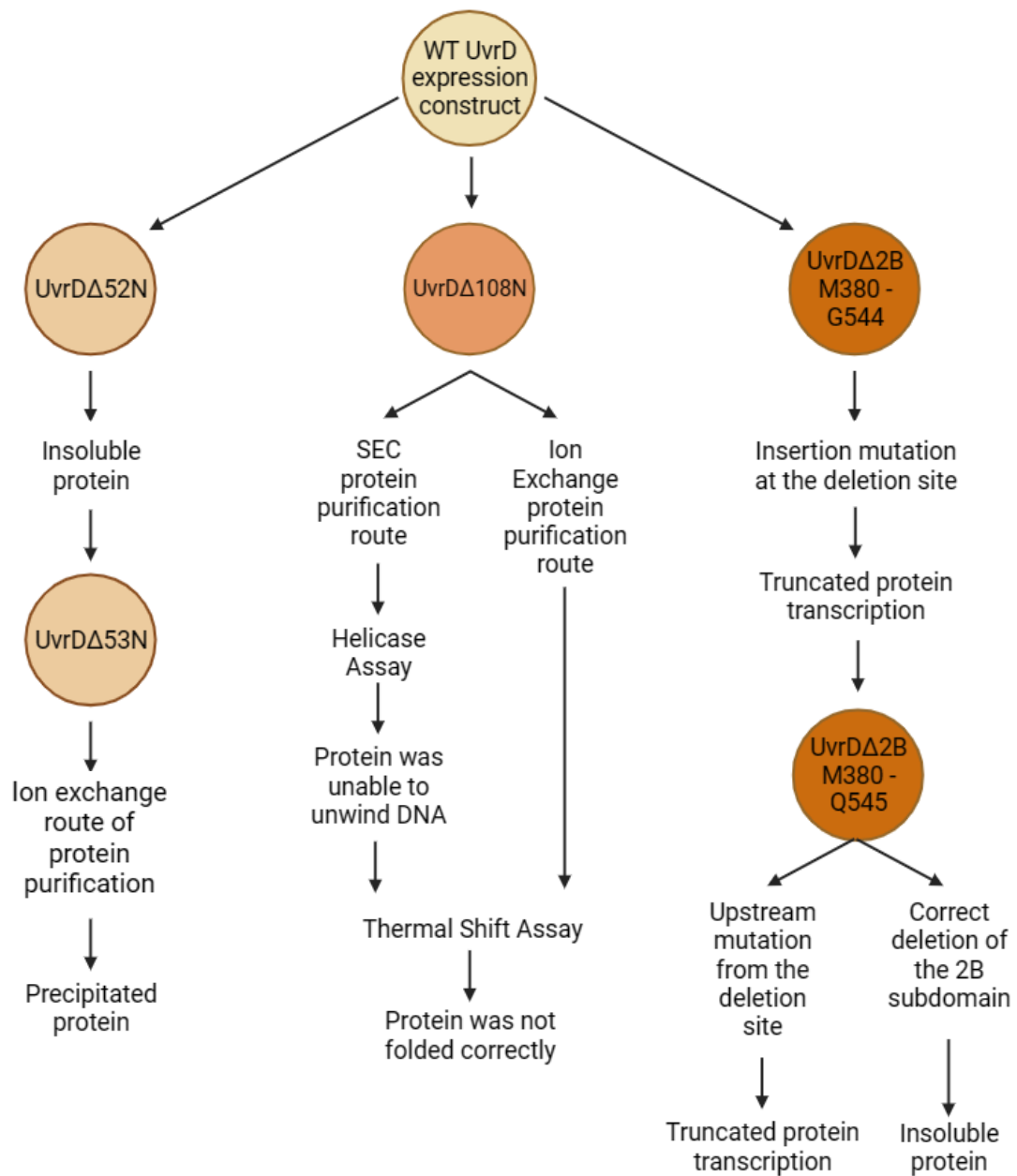


Figure 4.13 Summary of protein purification. Attempts, challenges, and analysis conducted in this results chapter. Created on biorender.com.

In this chapter we attempted to create mutant UvrD helicases, two with N-terminal deletions to test for binding with the MutL protein, UvrD Δ 108N and UvrD Δ 52N, and one with the deletion of the entire 2B subdomain to test for change in DNA unwinding and DNA-bound protein removal abilities, UvrD Δ 2B. Unfortunately, we were unable to purify the intended set of UvrD mutants for further analysis due to a range of technical obstacles at the stage of either expression plasmid design or purification (figure 4.13).

4.3.1 Solubility Problems

One of the problems encountered was the solubility of mutant UvrD constructs. HisSUMO-UvrD Δ 108N and HisSUMO-UvrD Δ 52N were found in the soluble fractions, though HisSUMO-UvrD Δ 52N did not have as strong expression as HisSUMO-UvrD Δ 108N. It was unfortunate that HisSUMO-UvrD Δ 53N and HisSUMO-UvrD Δ 2B were not soluble, especially HisSUMO-UvrD Δ 2B which would have made a very interesting addition to this body of work. As demonstrated in this chapter, the advice we received for expressing insoluble proteins was to redesign the expression plasmid construct. This was successful when altering HisSUMO-UvrD Δ 53N into HisSUMO-UvrD Δ 52N, which was soluble though sadly not stable.

Without time constraints, we would have redesigned the HisSUMO-UvrD Δ 2B expression plasmid and tried a variety of deletion combinations to see which ones could produce a soluble protein. Since Rep helicase was successfully produced with a deletion of its 2B subdomain (Brüning et al., 2018), and since UvrD and Rep share 40% sequence similarity, purification of UvrD without its 2B subdomain seems likely to be possible.

While helping solubility, the change in the deletion site from HisSUMO-UvrD Δ 53N to HisSUMO-UvrD Δ 52N likely increased the difficulty of cleaving the HisSUMO tag, something we were not aware of at the time. After HisSUMO cleavage the UvrD Δ 52N amino acid sequence begins with an exposed cysteine. These residues have been shown to cause

dimer formation in proteins through the formation of cysteine disulfide bonds (Wiedemann et al., 2020; Moghadam et al., 2015). Since we know that WT UvrD helicase can form dimers (Maluf et al., 2003) and even tetramers (Wollman et al., 2023), the addition of free cysteine sites likely encouraged the binding of these proteins, and therefore could have restricted the cleavage site for HisSUMO further. The presence of cysteines in proteins has also been associated with protein aggregation during overexpression (Moghadam et al., 2015), which could explain the precipitation of our final protein.

4.3.2 Chromatography Strategy

4.3.2.1 Columns

When purifying hisSUMO-tagged proteins, the standard protocol in our laboratory was to conduct two affinity chromatography steps, followed by a SEC step (SEC strategy). This was designed to easily separate the his-tag SUMO-protein from untagged proteins and then to separate his-SUMO and the protein-of-interest, before using the SEC column to remove any protein contaminants. This method worked successfully for our MutL protein purification (section 3.2.1.3) and UvrD Δ 108N purification. To troubleshoot the problem of partially cleaved HisSUMO tagged protein, we decided to attempt the ion exchange route – which included a single affinity column, followed by an ion exchange MonoQ column to separate HisSUMO-protein and protein by charge. We used this method to successfully purify UvrD Δ 108N and to purify UvrD Δ 52N but with a very low yield. Due to our sample not being entirely clean of contaminants after the final ion exchange step, we would ideally conduct an additional SEC step to achieve a cleaner product. However, we were unable to do so due to the small protein amounts and decided to use the sample we generated using either the SEC or the ion exchange route only. If time was not a constraint, testing purification with larger volumes of cell culture (2 or 3 L instead of 500 ml) might help get a better yield of protein and allow for extra purification steps.

4.3.2.2 DNA precipitation technique

Another diversion from the MutL protein purification protocol was the removal of the DNA precipitation step and substitution with a 3 M NaCl protein wash. In retrospect, it would have been preferable to test other DNA precipitation techniques, such as the use of sodium deoxycholate (Atkinson et al., 2009) or testing whether UvrD mutants can remain stable after DNA precipitation at 1 M NaCl with PolyminP (though the high salt would prevent us from following the ion exchange strategy). The DNA precipitation method chosen could have affected the ability of UvrD Δ 108N, though likely the protein was incapable of unwinding DNA anyway due to essential DNA-binding regions being deleted.

4.3.3 Expression plasmid design

4.3.3.1 Change of expression plasmid backbone/template

The WT UvrD helicase was previously purified in our laboratory using a pETDuetUvrD expression plasmid (Guy et al., 2009). This WT *uvrD* plasmid was not used as a template due to the solubility and his-affinity advantages of the HisSUMO construct. If time was not a constraint, we could attempt to use the pETDuetUvrD plasmid as a plasmid construct template instead. The advantage of attempting this method would be that this plasmid construct has been shown to produce functional WT UvrD (Atkinson et al., 2009; Jameson et al., 2021), though the lack of an affinity tag makes the purification protocol less straightforward.

4.3.3.2 Deletion site design

Lastly, it is important to discuss the design of the N-terminal deletions. Our strategy was based on the findings of Hall et al. where MutL was not able to interact with UvrD in a yeast two-hybrid test after the removal of the first 100 amino acids of UvrD (Hall et al., 1998). While this

test was a good guide to the UvrD:MutL interaction, the deletion of such a large region in a recombinant protein might be considered quite extreme. The deletion of the first 108, 53, and 52 amino acids of UvrD would unfortunately remove residues T36 and R37, which are involved in ATP hydrolysis where T36 works with D220 and E221 to acquire a magnesium ion while R37 binds weakly to the 2'-OH of ATP (Lee and Yang, 2006). The deletions would also remove a large region of the 1A subdomain, which is required for DNA translocation (Meir and Greene, 2021). The C-terminal of UvrD has also been previously tested for protein-protein interaction, including Hall's yeast two-hybrid test for UvrD and MutL interaction (Hall et al., 1998) and Manelyte and coworkers bacterial two-hybrid test and surface plasmon resonance spectroscopy for UvrD and UvrB interaction (Manelyte et al., 2009). In the future, it would be interesting to further investigate the interaction of the C-terminal domain of UvrD helicase and the MutL protein.

4.3.4 Future work

If more time and funds were available, we would aim to conduct cross-linking mass spectrometry (XL-MS) experiments on WT MutL and WT UvrD to determine the binding site on each protein in the UvrD:MutL complex with higher accuracy. XL-MS combines the tools of mass spectrometry and cross-linking to determine which amino acids are involved in protein-protein complex formation (Piersimoni et al., 2022). The methodology follows addition of a cross-linker to a buffer with both MutL and UvrD proteins, followed by an addition of protease which cleaves the proteins into smaller regions. MS can then define which amino acids of each protein are bound by the cross-linker (Piersimoni et al., 2022). Once these regions are known, further protein mutations can be conducted to determine if the protein-protein interactions are still possible when the correct amino acids are not available.

Other exciting techniques suitable for this work would be a bacterial two-hybrid test and SPR. Bacterial two-hybrid tests are conducted by fusing proteins of interest *in vivo*, one with an RNAP α -subunit and one with λ cl which can activate a *lacZ* promoter. If the proteins interact, LacZ is produced and can be detected using colony screening. This test can be conducted using a reporter strain KS1 (Dove, Joung and Hochschild, 1997; Dove and Hochschild, 1998; Manelyte et al., 2009).

SPR is conducted *in vitro* by immobilising a protein on a streptavidin sensor chip and placing it in a flow cell. The second protein is injected into the flow cell and the association between proteins is detected on a sensogram (Schuck, 1997). This technique can be adapted to using purified protein regions and testing for their interaction, removing the need for purification of a functional mutant protein (Manelyte et al., 2009)

CHAPTER 5

TUS JUMPING ASSAY DEVELOPMENT AND PRELIMINARY RESULTS

Chapter 5. Tus Jumping Assay Development and Preliminary Results

5.1 Introduction

DNA replication is an essential process found in all living organisms and some viruses. In this work we investigate the final stage of DNA replication in *E. coli*, known as replication termination. In *E. coli*, termination can occur in two ways. First is free fusion, where the two replication forks fuse together anywhere on the chromosome, though usually within the region opposite *oriC*. The second occurs at a termination block called Tus-*ter*, which consists of a 23 bp *ter* sequence which the Tus protein binds to, forming an asymmetric block.

The *E. coli* chromosome contains ten *ter* sites, *terA-J* (figure 5.1 A and B) that Tus binds to asymmetrically using a 'mousetrap' mechanism. This mechanism 'locks' the C6 nucleotide of *ter* into a motif of Tus known as the 'cytosine pocket' by flipping the base out of the duplex and into the pocket (figure 5.1 C) (Mulcair et al., 2006). Tus-*ter* is a unidirectional block which permits the replication fork to pass through the permissive orientation of the nucleoprotein complex but stops the replisome approaching in the non-permissive orientation (figure 5.1 D).

Our group conducted an *in vitro* biochemical termination mapping assay in which DNA replication termination was forced to occur at the Tus-*ter* block (Jameson et al., 2021). Results from the assay indicated that replication termination was unable to be completed and that a 15-25 bp unreplicated gap could be found with the same footprint as the binding of Tus (Jameson et al., 2021). This finding raised questions about the location of Tus during termination at Tus-*ter* and whether the protein was stuck between the two replication forks or was previously dislodged by one of the replisomes (figure 5.1 E).

Following the termination mapping result, a replication assay (previously described in 3.2.3.3) was conducted to determine whether addition of helicases UvrD, Rep or RecG could increase the amount of full replication product generated (Jameson et al., 2021). During the assay replication forks were reconstituted on a plasmid to investigate DNA replication on a small scale. Neither the addition of UvrD, Rep, nor RecG appeared to increase the amount of full replication products produced, which suggested that neither of the helicases was able to assist termination by (potentially) removing Tus from the region (Jameson et al., 2021). This result was especially interesting when considering that UvrD has been shown to remove Tus *in vivo* by Bidnenko (Bidnenko et al., 2006); while Rep, which can be found at the replication fork as a secondary motor (Guy et al., 2009), was shown to remove Tus *in vitro* (Hiasa and Marians, 1992; Sahoo et al., 1995).

In this study we developed a novel *in vitro* assay to determine whether Tus remains bound to the replication plasmid or whether it dissociates from *ter* upon replication fork collision.

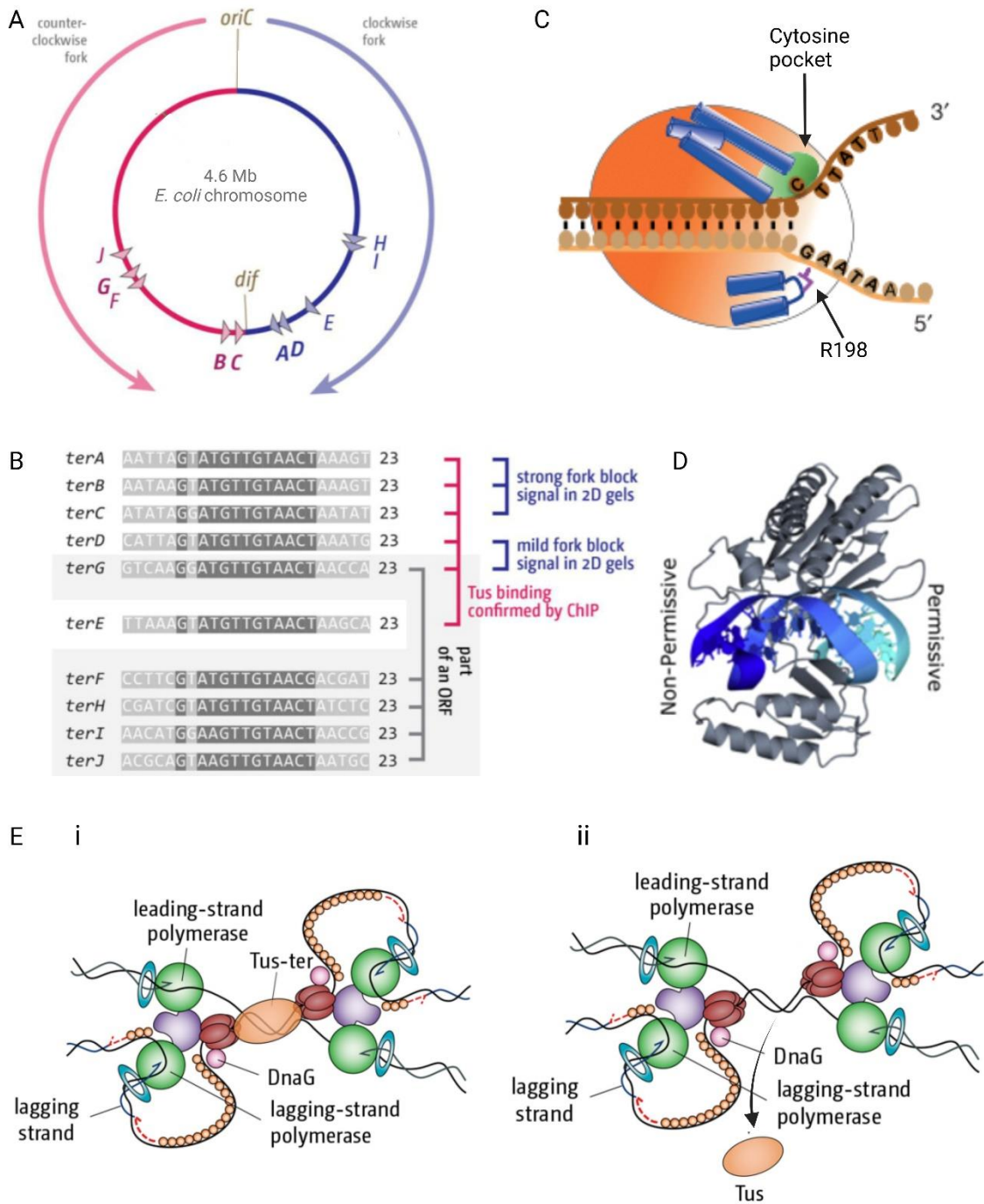


Figure 5.1 The Tus-ter block and its function in termination. A. 4.6 Mb chromosome of *E. coli* with the ten *ter* sites, *terA-J*. B. Sequences of the ten *ter* sites with conserved regions in dark gray. *Ter* sites have been labeled with the strength of the Tus-ter block, Tus binding confirmation, and whether they are a part of an open reading frame (ORF). C. Mousetrap mechanism of the Tus-ter block. D. Protein structure model of the Tus-ter block (PDB 2I06). E. DNA replication termination at Tus-ter. I) Tus-ter sandwiched between the two replisomes. II) Tus dislodged from *ter* by a replication fork. A, B and E have been adapted from Goodall et al., 2023, C has been adapted from Elshenawy et al., 2015, D has been adapted from Jameson et al., 2021 (PDB ID 2I06)

5.2 Results

5.2.1 Assay Development

In this work, replication assays were used as a basis for the development of a new biochemical assay, the Tus Jumping assay. The first step for assay development, was learning how to successfully conduct a replication assay (figure 5.2).

Replication assays in this work were conducted on the pKJ001 plasmid as the DNA template (Jameson et al., 2021). pKJ001 has been designed to include a single origin of replication, *oriC*, which acts as the site of replication fork reconstitution. Replication forks on pKJ001 can be blocked by two existing sites. First, a *lacO₂₂* array forms a reversible block with LacI; blocking the clockwise replication fork after replication of 3.7-4.5 kb and counterclockwise fork after replication of 1.5 kb (figure 5.2 B, lane 3). Addition of IPTG removes LacI from *lacO* and allows for DNA replication to continue (figure 5.2 B, lane 5). Second, addition of Tus to the assay forms the Tus-*terB* block. The clockwise fork encounters the non-permissive face of the Tus-*terB* block and stops replication after synthesising 2.7 kb. The counterclockwise block encounters the permissive orientation of the Tus-*terB* block and should proceed past the block. In a reaction where only the Tus block is added (figure 5.2 B, lane 2) both the clockwise and anticlockwise forks can reach the Tus-*terB* block first. If both Tus and LacI are added to the reaction with IPTG (figure 5.2 B, lane 4) both forks become blocked. DNA replication termination at Tus-*ter* can be simulated by adding both Tus and LacI to the reaction, as well as IPTG (figure 5.2 B, lane 6). This ensures that the counterclockwise fork arrives at Tus-*terB* second and that the two forks meet at the Tus-*terB* site.

Addition of LacI and/or Tus can be used to investigate what happens if/when the forks are stopped by these blocks, what can rescue them, and how their stalling can affect further replication. With addition of radioactive dCTP nucleotide we label nascent DNA, which allows us to visualise the length of DNA replicated and therefore fork progression on the plasmid.

Replication assays require an addition of 13 proteins to form the replication forks and initiate replication. These include DNA polymerase III components α , ϵ , θ , and τ (McHenry, 1985), the replicative helicase DnaB (LeBowitz and McMacken, 1986) and its loader protein DnaC (Martin et al., 1998), β clamp (Stukenberg et al., 1991; Kong et al., 1992; López De Saro et al., 2006; Koleva et al., 2019), primase DnaG (Kitani et al., 1985; Tougu and Marians, 1996), SSB (Cerrón et al., 2019), HU (Rouvière-Yaniv et al., 1979; Bramhill and Kornberg, 1988), and topoisomerase Gyrase A₂B₂ (Morrison and Cozzarelli, 1979; Smelkova and Marians, 2001; Marians, 1987) . Lastly, addition of DnaA at the start of each reaction triggers DNA replication initiation at *oriC* (Bonney and Rouvière-Yaniv, 1992; reviewed in Lewis et al., 2016).

The restriction enzyme SmaI was added to replication assay reactions to linearise the plasmid. The location of the cleavage site allows for both replication forks to be released from *oriC* and continue DNA synthesis before the plasmid is cut. SmaI can be substituted with SacI and NcoI. While two forks are released from *oriC*, cleavage with these enzymes only allows one fork to proceed towards Tus-*terB* (non-permissive and permissive respectively) while the other fork runs off the strand cut by the enzyme. This mechanism can be used to ensure that a replication fork reaches either the permissive or non-permissive orientation of Tus-*ter* only.

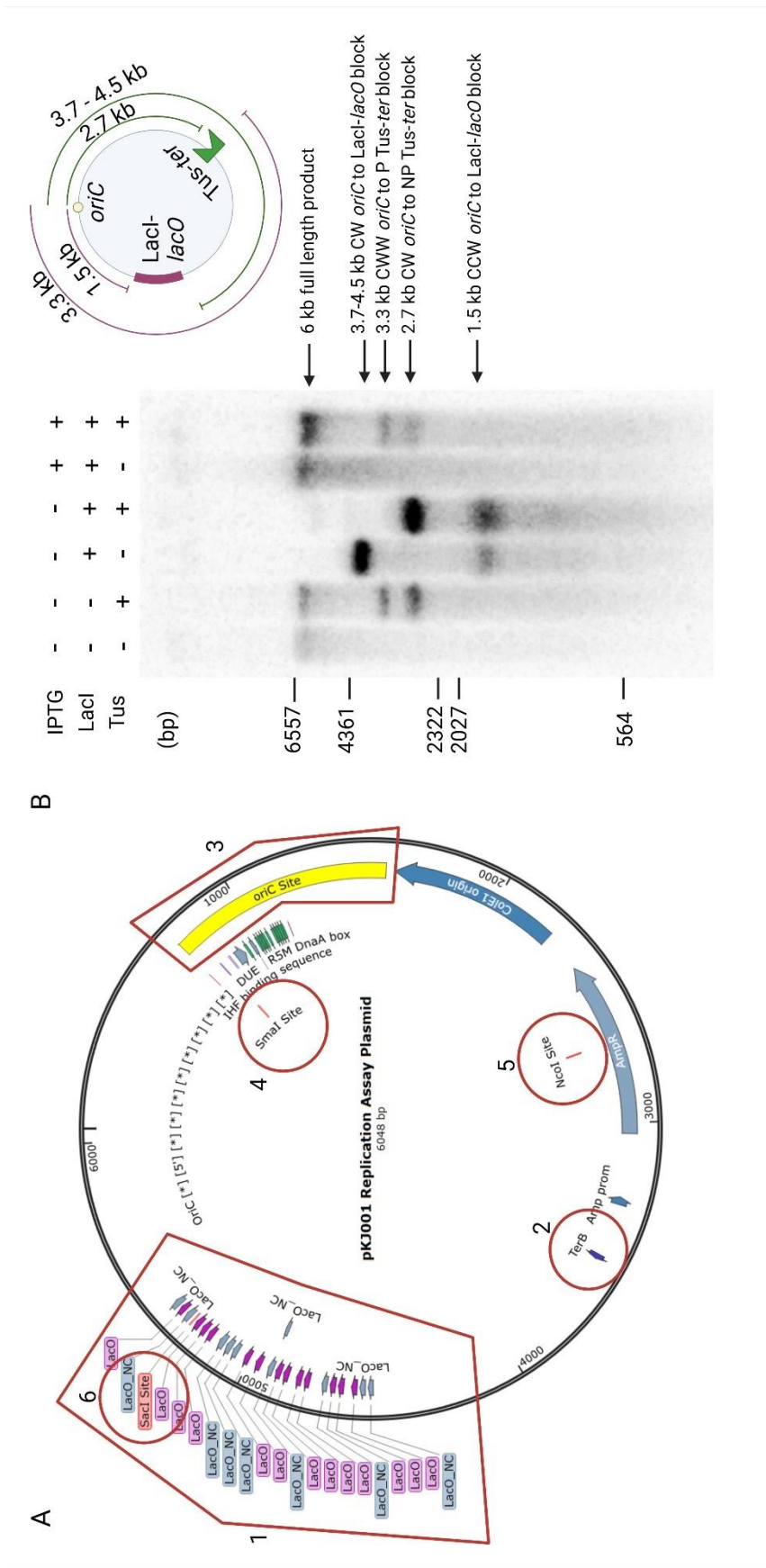


Figure 5.2 Replication assay plasmid and example assay. A. pKJ001 replication assay plasmid. 1. *lacO*₂₂ array for LacI binding. 2. *terB* site for Tus binding. 3. *oriC* origin of DNA replication initiation site. 4. *SmaI* restriction digest site. 5. *NcoI* restriction digest site. 6. *SacI* restriction digest site. B. Example gel of replication assay using Tus and LacI blocks as indicated in the figure. Arrows indicate band size and region replicated. P refers to the permissive orientation of *Tus-ter*, NP refers to the non-permissive orientation of *Tus-ter*. The expected band size has also been labeled on the plasmid diagram in panel B.

5.2.2 Tus Jumping Assay

In this work we developed the Tus jumping assay to investigate whether Tus remains bound to *ter* after a collision with a replication fork and during termination at Tus-*ter*.

The Tus jumping assay (figure 2.7) was developed using the replication assay technique as its foundation. Replication forks were reconstituted on *oriC* and DNA replication was initiated after addition of DnaA. The clockwise and counterclockwise replication forks progress towards Tus-*terB* and LacI-*lacO* blocks respectively. The addition of Smal after two minutes linearised pKJ001, while the addition of IPTG removed LacI and allowed the counterclockwise fork to progress towards Tus-*terB* and the stalled clockwise fork. No dCTP ³²P was included in the Tus jumping assay to label the nascent DNA, instead 5 nM of 'Tus capture substrate' was added alongside Smal. The Tus capture substrate was designed as a short dsDNA substrate featuring the *terB* sequence for Tus binding and was labelled through PNK end-labelling with a radioactive ³²P tag.

The Tus jumping assay was designed on the basis that if Tus was displaced from *ter* when replications forks collide with or terminate at Tus-*terB* on pKJ001, free Tus would proceed to bind to another available *terB* site, such as the one found on the Tus capture substrate. By running the sample on a native gel, we expected to see a size difference between Tus-bound and unbound Tus capture substrate.

5.2.2.1 Tus capture substrate

Tus capture substrate design was based on the oJH117-118 helicase assay substrate known to bind Tus (figure 3.6). We redesigned the substrate by binding oJH117 to its complete complement (oDW035) and used end-labelling to add a radioactive ^{32}P tag to the 5' end of oJH117 using PNK end-labelling. 2 nM of the dsDNA substrate was incubated in helicase assay conditions (method section 2.2.5.6) for 6 min at 37°C with varying concentrations of Tus (0 nM, 1 nM, 2 nM, 4 nM, 8 nM). The samples were run on a 10% TBE-PAGE native gel to test if Tus binds to the substrate and whether separation of Tus-bound and unbound substrate is visible (figure 5.3). This separation was previously seen to be possible using oJH117-118 and oJH123-124 (figure 3.6).

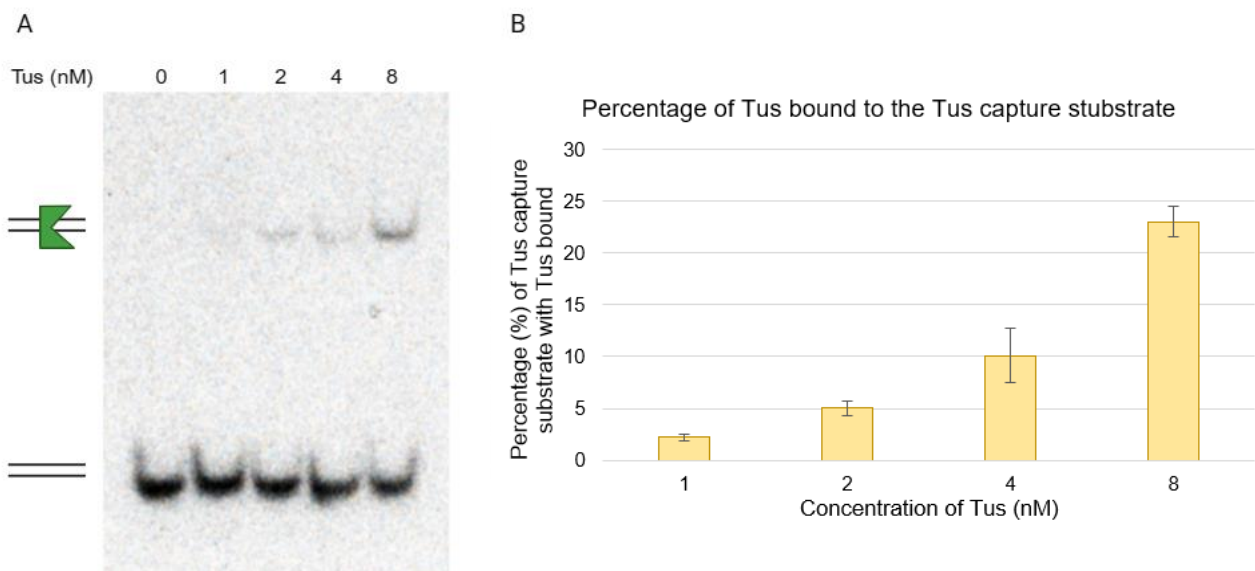


Figure 5.3 Tus-bound Tus capture substrate runs higher on a native gel than unbound substrate.

A. 10% TBE-PAGE native gel showing 2 nM of Tus capture substrate and various concentrations of Tus after incubation for 6 min at 37°C. B. Quantification of n=3 gels as per A. The error bars show standard deviation of each result.

We were able to show separation of the Tus-bound and unbound Tus capture substrate on a 10% TBE-PAGE native gel (figure 5.3). This result gave us two conclusions. First, Tus can

successfully bind to our 'free-floating *ter* site'. Second, that Tus-bound and unbound substrate can be separated on a 10% TBE-PAGE native gel as a higher and lower DNA band with good resolution. While the resolution of the image isn't ideal due to low activity ³²P used to label the substrate, this result showed that it was feasible to use the Tus capture substrate to calculate the percentage increase of Tus-bound, compared to unbound, substrate.

It is important to consider how much of Tus actually bound to the DNA substrate. When 2 nM of Tus was added to the assay, only 5% of the substrate was bound with Tus in the EMSA. This can be analysed as only 0.1 nM of Tus having bound to the template. A further experiment testing 2.5 nM of Tus and 5 nM of substrate would be beneficial to help us determine the percentage of Tus we would expect to see bound to the substrate in perfect conditions.

5.2.3 Tus jumping Assay

Tus jumping assays were conducted to test whether Tus is displaced from *ter* when the two replication forks met at Tus-*ter* (figure 5.4).

We designed three reactions to test how much Tus might be displaced by replication termination at Tus-*ter* (table 5.1 and figure 5.4 A). To determine how much Tus is found free-floating in the buffer, we also designed a reaction where DNA replication would not occur due to lack of DnaA in the reaction.

One-tail t-test was conducted to test for an increase in the percentage of Tus-bound substrate when comparing the control (+Tus +Lacl +IPTG -DnaA) and test samples (+Tus +Lacl +IPTG +DnaA and +Tus +DnaA).

Table 5.1 Conditions tested in the Tus capture assay when termination occurs at Tus-*ter*.

| Reaction Name | Proteins | Purpose |
|-----------------------------------|---|--|
| +Tus +LacI +IPTG +DnaA | Tus and LacI block, plus IPTG to remove LacI during the assay | To simulate DNA replication fork fusion and termination at Tus- <i>ter</i> |
| +Tus +LacI +IPTG -DnaA | Tus and LacI block – no DnaA | To determine how much free-floating Tus can be found in the assay – essential as Tus is added in excess compared to pKJ001. |
| + Tus +DnaA | Tus block only | To determine how much Tus is dislodged by DNA replication when the replication forks can reach the block from both the permissive and non-permissive orientation. |

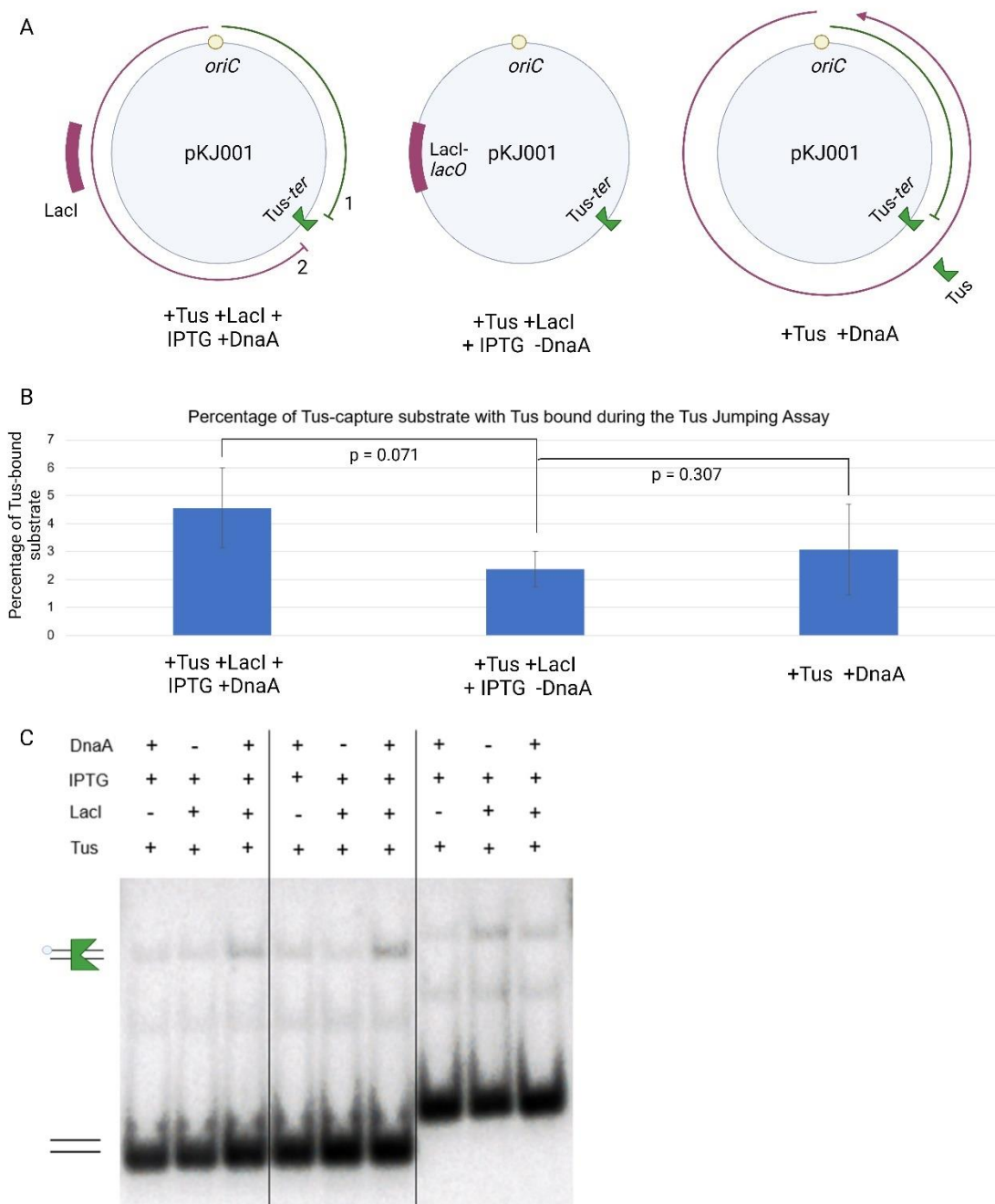


Figure 5.4 Preliminary results of the Tus jumping Assay. A. Visual guide to Tus jumping reactions and the expected replication products. For +Tus +LacI +IPTG +DnaA. The counterclockwise block will be first blocked at the LacI-*lacO* block, which should allow the clockwise fork to reach the non-permissive orientation of Tus-*terB* first (labelled '1'). The counterclockwise fork is released through the addition of IPTG, which allows it to continue towards the permissive orientation of Tus-*terB*. We expect it to arrive second (labelled '2') at the block. B. Percentage of Tus-bound Tus capture substrate (5 nM in the assay) compared to unbound substrate, n=3. Error bars represent standard deviation, and the p value was calculated using a one-tail t-test. Significant result must have a p value of 0.05 or less. C. 10% TBE-PAGE native gel with 3 repeats of the Tus jumping assay, bands used to generate percentage values in B.

We saw an insignificant increase ($p=0.071$) when comparing forks that terminated at Tus-*terB* (+Tus +LacI +IPTG +DnaA) and the reaction where no replication forks were released, and only free-floating Tus was bound to the Tus capture substrate (+Tus +LacI +IPTG -DnaA). While the increase is insignificant, some Tus appears to be displaced by the replication forks.

Another insignificant increase was seen when comparing forks that terminated at Tus-*terB* (+Tus +LacI +IPTG +DnaA) and reactions where the counterclockwise fork was not stopped by LacI and either fork could reach Tus-*ter* first (+Tus +DnaA). This result was surprising as we expected (+Tus +DnaA) to displace more Tus since the reaction includes not only forks which might meet at Tus-*ter*, but also forks which would reach the permissive orientation of Tus-*ter* first and hypothetically displace Tus.

To further understand these results, it is important to consider that in a band shift assay only 0.1 nM (5%) of Tus bound to 2 nM of substrate when 2 nM of Tus was added to the assay. Considering this, results showing ~4.5% of substrate bound with Tus (+Tus +LacI +IPTG +DnaA) can be therefore quite promising and might be interpreted as the majority of Tus being available to bind with the substrate and no longer bound to pKJ001.

If more time was available, we would conduct more repeats of this experiment to increase the sample size and generate independent results not conducted on the same day. Our current results have a high standard deviation and increasing the sample size would allow us to generate a more accurate mean value for each Tus-bound and unbound band.

5.2.4 One Fork Tus jumping Assay

As a response to the Tus Jumping Assay results, we wanted to understand whether individual forks reaching the permissive or the non-permissive orientation of Tus-*terB* were able to displace Tus.

To test this, we cleaved pKJ001 with either NcoI or SacI, instead of SmaI. This enabled only one replication fork to proceed towards Tus-*terB* while the other fork was forced to run off the template. This allowed us to perform a Tus jumping assay testing for an increase in Tus-bound substrate when the replication fork met Tus-*terB* from either the permissive (NcoI) or the non-permissive orientation (SacI) only.

5.2.4.1 Permissive orientation of Tus-*ter*

We first cleaved pKJ001 with NcoI and only elongated the counterclockwise replication fork, traveling towards the permissive orientation of Tus-*terB* (figure 5.5). Table 5.2 displays the four different conditions tested and their purpose.

As for the Tus jumping assay with both replication forks, we conducted a one-tail t-test to determine if we see a significant increase between the control sample (+Tus +LacI) with the test samples (+Tus and +Tus +LacI +IPTG).

Table 5.2 Conditions tested in the Tus capture assay when the replication fork only reached Tus-*ter* in the permissive orientation.

| Name | Proteins | Engineered Scenario |
|---------------------|---|--|
| - Tus – LacI | No blocks | Control, no Tus should bind to the substrate |
| + Tus + LacI | Tus and LacI block | No forks reach Tus- <i>ter</i> . To determine how much free-floating Tus binds to the substrate |
| + Tus | Tus block only | Tus is dislodged by the fork meeting Tus- <i>ter</i> in the permissive orientation |
| + Tus + LacI + IPTG | Tus and LacI block, plus IPTG to remove the LacI block during the assay | Tus is dislodged by the fork meeting Tus- <i>ter</i> in the permissive orientation, after a delay at LacI- <i>lacO</i> |

We expected to see a large increase in Tus-bound substrate when comparing both samples where the counterclockwise fork reached the permissive orientation of the Tus-*terB* block quickly and after a pause at LacI (+Tus and +Tus +LacI +IPTG) with the +Tus +LacI reaction, where the replication fork would stop at the LacI-*lacO* block and not reach Tus-*terB* and therefore the only Tus bound to the substrate we would expect to see in this reaction is free-floating Tus. Both +Tus and +Tus +LacI +IPTG reactions allow the fork to reach Tus-*ter*, but at different times. The fork in the +Tus reaction can reach Tus-*ter* quickly, while +Tus +LacI +IPTG is first stopped at LacI-*lacO*. Allowing Tus to bind to *ter* for longer might ensure that the mousetrap mechanism is securely locked in place (Elshenawy et al., 2015).

However, while we saw an increase of Tus-bound substrate in both reactions, neither of them was significant (figure 5.5). This result suggested that when a replication fork passed through the permissive orientation of Tus-*terB*, Tus remained close by and immediately rebound to the same *ter* site. This finding partly matches Bidnenko's model, which also shows Tus rebinding to *ter* once the replication fork passes (Bidnenko et al., 2006), though their study concentrated on Tus removal after fork stalling at the non-permissive orientation of Tus-*ter*. It is however important to consider the percentage of Tus bound to the substrate during the EMSA (figure 5.3), which would suggest that the presence of 4.5-5% of Tus-bound substrate would indicate that a larger proportion of Tus might have been available to bind to the substrate than the results initially reveal.

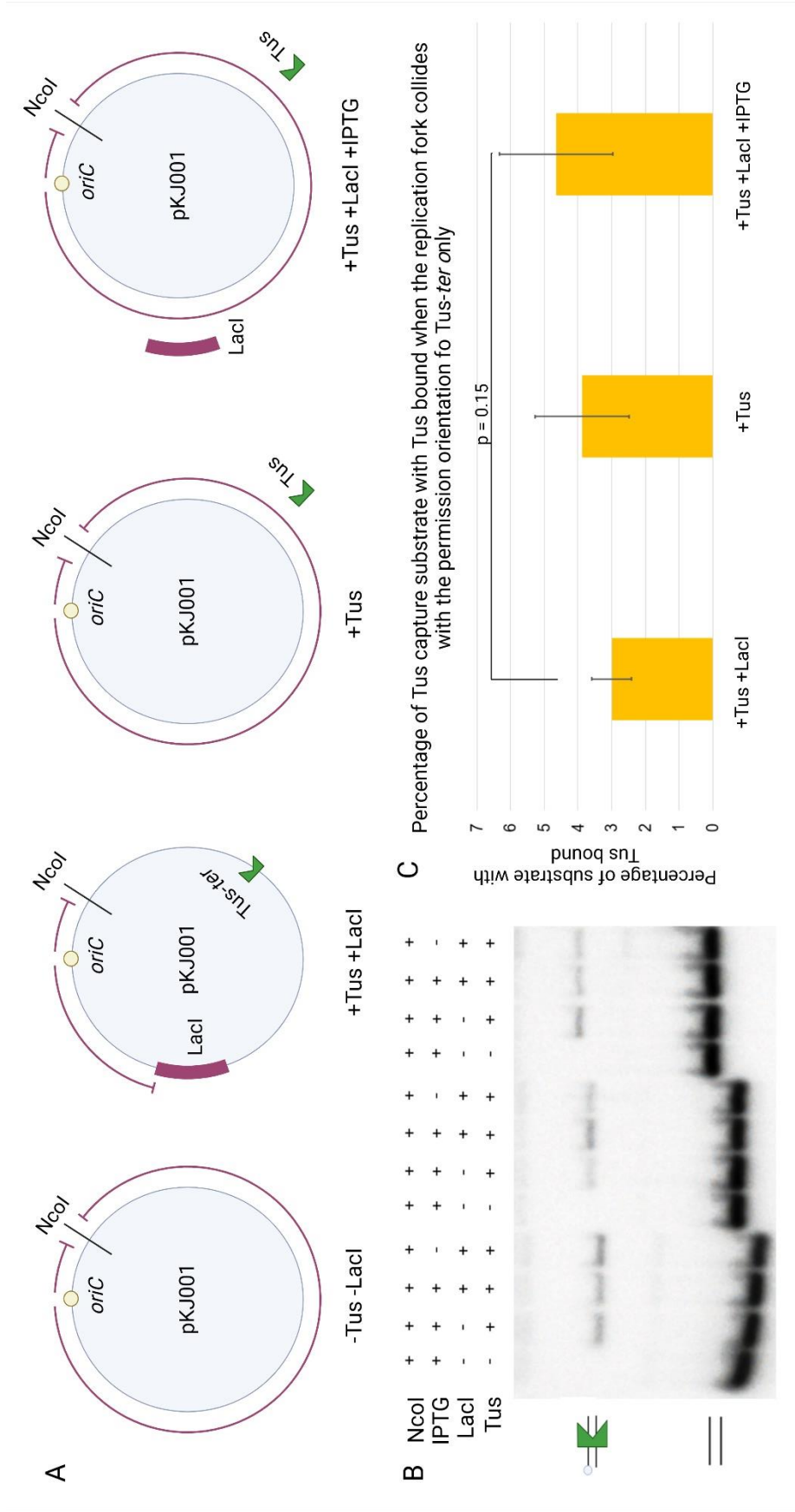


Figure 5.5 Tus jumping assay where the replication fork only meets the permissive orientation of *Tus-ter*. A. Visual guide to the permissive orientation reactions. B. Tus jumping assay with pKJ001 cleaved with NcoI, allowing the replication fork to reach the permissive orientation of *Tus-ter/B* only. Samples run on a 10% TBE-PAGE native gel. Image showing three sample repeats. C. Band quantification using ImageJ to establish the percentage of Tus-bound Tus capture substrate from B. Most samples are $n = 3$, besides the +Tus +LacI sample which

5.2.4.2 Non-permissive orientation of Tus-ter

For the fork travelling towards the non-permissive face of Tus-*terB* (figure 5.6), we controlled replication fork reconstitution at *oriC* through the addition, or lack of, DnaA in the assay – similarly to the reactions in the initial Tus jumping assay (section 5.2.3). By not adding DnaA, we were able to test how much Tus bound to the substrate without the presence of an active replication fork. The conditions tested when pKJ001 was cut with *SacI* only allowed the replication fork to proceed towards the non-permissive orientation of Tus-*terB* and are shown in table 5.3.

As for the Tus jumping assay with both replication forks, we conducted a one-tail t-test to determine if we see a significant increase between the control sample (+Tus -DnaA) with the test sample (+Tus +DnaA).

Table 5.3 Conditions tested in the Tus capture assay when the replication fork only reached Tus-*ter* in the non-permissive orientation.

| Name | Proteins Added/Omitted | Purpose |
|-------------|------------------------|---|
| -Tus -LacI | No blocks | Control, no Tus should bind to the substrate |
| +Tus -DnaA | Tus only, no DnaA | No replication fork should be released from <i>oriC</i> due to lack of DnaA. Used to determine how much free-floating Tus in the assay binds to the substrate |
| + Tus +DnaA | Tus only | To determine the amount of Tus displaced from <i>terB</i> by the replication fork reaching the non-permissive orientation of Tus- <i>ter</i> . |

We saw a significant increase ($p=0.0497$) in the percentage of Tus-bound substrate when DNA replication forks were blocked at the non-permissive orientation of Tus-*ter* (+Tus +DnaA) compared to free-floating Tus only (+Tus -DnaA). This result showed that stalling of the replication fork at the non-permissive orientation of Tus-*terB* caused the displacement of Tus from pKJ001. While previous literature suggested that the stalling of the fork might cause replisome dissociation from the replication fork while keeping the Tus-*ter* block intact (Kaplan, 2006) our results suggest that the collision of the replisome with the block might be enough to remove Tus from *ter*.

Last but not least, when using SmaI in the Tus Jumping Assay we saw an unexpected band above the Tus-bound band. The SmaI cleavage sequence (5' - GAGCTC - 3') is not present on the substrate – though this would likely generate a lower band, unless SmaI used is faulty and does not cleave the DNA well. We do also see a lower band, but this again cannot be explained as SmaI cleaving since no cleavage site is present on the substrate. We are therefore unable to explain exactly what this higher band is, but we hypothesise that it could represent non-specific binding of SmaI to the substrate (Pingoud and Jeltsch, 2001). SmaI is a 39 kDa protein, which is slightly larger than the 35.8 kDa Tus, which could explain the slightly higher band. An EMSA looking at the substrate and SmaI might help determine if the band represents non-specific SmaI binding.

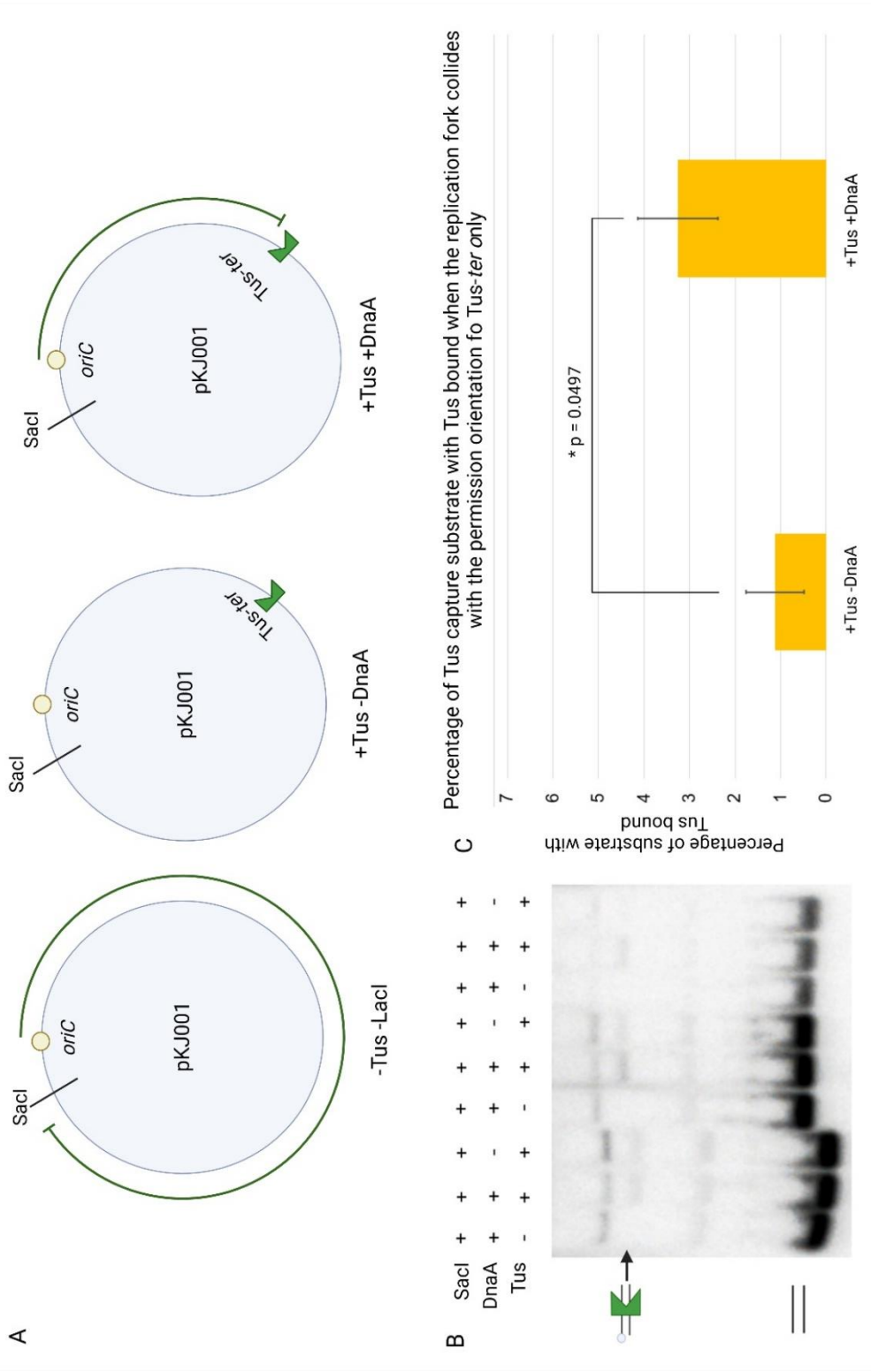


Figure 5.6 Tus jumping assay where the replication fork only meets the non-permissive orientation of *Tus-ter*. A. Visual guide to the non-permissive orientation reactions. B. Tus jumping assay with pKJ001 cleaved with SacI, allowing the replication fork to reach the non-permissive orientation of the *Tus-ter*B block. Samples run on a 10% TBE-PAGE native gel. Image showing three sample repeats. C. Band quantification using ImageJ to establish the percentage of Tus-bound tus capture substrate from B. Average generated from n=3 with p values from one-tail t-test.

5.2.5 Creating Tus-bound template

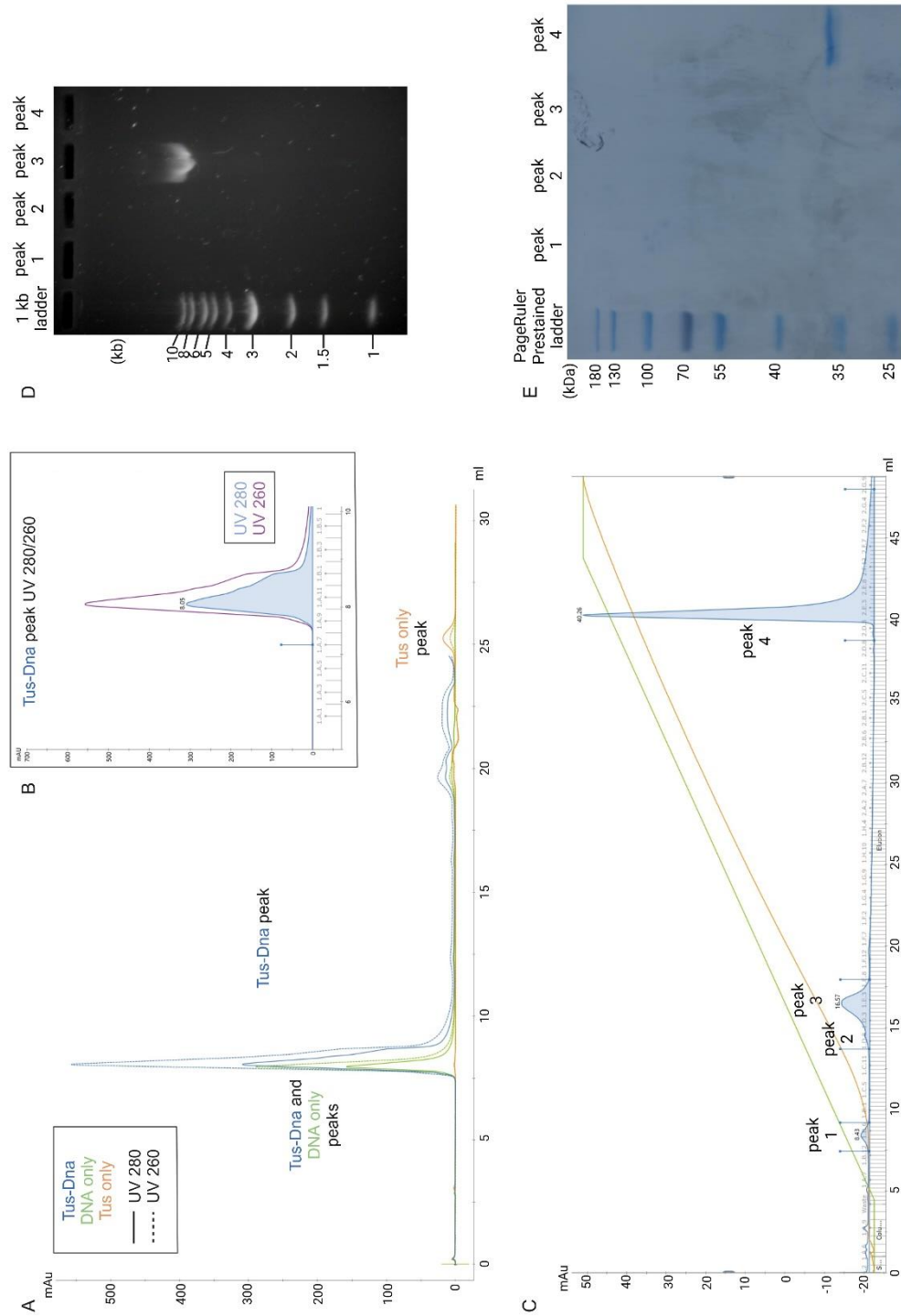
In ideal conditions, we would not have any free-floating Tus in the Tus jumping assay reactions. This would ensure that all Tus bound to the Tus capture substrate was dissociated from pKJ001. We could achieve this by generating a Tus jumping assay DNA template with Tus already bound to it.

There were a few limitations to creating the Tus-bound pKJ001. The first consideration was the need to ensure that Tus-bound pKJ001 complex was purified and that no free-floating Tus or unbound pKJ001 was present in the sample. The second consideration was the unknown stability of the pKJ001-Tus complex, which might mean that long (or even short) term storage and freezing of the complex would not be possible. Though it is important to note that the *Tus-ter* complex has been reported to be very stable, with a K_d of 3.4×10^{-13} (Gottlieb et al., 1992). The third consideration was the low concentration of Tus which would be added to the assay. Normally, 2 nM of pKJ001 was used as standard in replication assays and the Tus jumping assay. This would mean that only 2 nM of Tus would be present in the assay, compared to 50 nM tested in this chapter. We have shown that 2 nM of Tus could be seen bound to the substrate, though the band was very faint (figure 5.3). Using high activity, 'fresh', ^{32}P to label the Tus capture substrate would allow generate an image with a better saturation, but we cannot assume that all Tus would dissociate from pKJ001. Using 2 nM of Tus-bound pKJ001 could make the Tus-bound substrate band too weak to detect and/or quantify. If we would be able to successfully create Tus-bound pKJ001, we could try to test higher pKJ001 concentrations in our replication assays.

We attempted to isolate the Tus-bound pKJ001 plasmid, as well as Tus unbound pKJ001 and Tus protein alone using size exclusion chromatography (figure 5.7).

Figure 5.7 Attempts at purifying Tus-bound pKJ001 using size exclusion and ion exchange chromatography.

A. Chromatograph comparing analytical SEC tests of Tus-pKJ001, Tus only and pKJ001 only on a Superdex 10/300 GL column with 260 and 280 UV absorbance readings. B. Chromatograph of the size exclusion chromatography of Tus-pKJ001 from A. showing the 280 and 260 UV absorbance readings of the largest peak. C. Ion exchange chromatography using a MonoQ column. Chromatograph showing four peaks. D. 1% agarose gel testing for pKJ001 presence in peaks 1-4 from E. 10% SDS-PAGE gel testing for Tus presence in peaks 1-4 from C.



When comparing samples which included Tus and pKJ001, pKJ001 only, and Tus only, we observed that the Tus:pKJ001 peak had a slight 'hump' which was not visible in the pKJ001 only sample (figure 5.7 A and B). This 'hump' however was too close to the main peak to isolate it successfully. We compared the UV 280 and 260 readings of protein and DNA content respectively (figure 5.7 B). Ideally, we would hope to see a higher 260 reading in the peak that contains Tus-bound pKJ001 rather than just pKJ001 alone, with similar 280 readings for both samples. We did not see any significant changes in the 260 readings. This suggests that size exclusion chromatography is not the best method of isolating Tus-bound pKJ001.

Since size separation was not possible with the equipment available, we attempted to separate the Tus-bound pKJ001, Tus unbound pKJ001, and Tus protein alone using ion exchange chromatography with a Mono Q™ 5/50 GL column. This experiment was a late addition to this thesis, and we were therefore unable to purchase a cation column. We were however hopeful that the binding of positive Tus (+14 at pH 7) would alter the binding of the negatively charged DNA to the anion MonoQ column. This should allow us to see two peaks, one for Tus-bound pKJ001 and one for unbound pKJ001 samples. Four peaks were visible on the ion exchange chromatograph (figure 5.7 C). We ran fraction samples on a 1% agarose gel to visualise DNA content (figure 5.7 D) and on a 10% SDS-PAGE gel to view to protein content (figure 5.7 E).

We were unable to isolate a peak that contained both pKJ001 and Tus. 1% agarose DNA (figure 5.7 D) and 10% SDS-PAGE (figure 5.7 E) gels and nanodrop were used to confirm the presence of DNA, protein, or both in the peaks. Peak 3 (figure 5.7 C) was confirmed to contain pKJ001 plasmid only, while peak 4 (figure 5.7 C) contained a protein which matched the expected size of Tus, 35.8 kDa (figure 5.7 E). Neither peak 3 nor 4 contained both protein and DNA. The nanodrop readings disagreed with the gels, with peak 3 showing 19.1 ng/μl nucleic acid concentration, and A280 reading of 0.215 – which suggested that peak 3 should contain both DNA and protein. For comparison, peak 4 contained 0.2 ng/μl nucleic acid and a A280 reading of 0.02. Peak 3 also had the highest 260/280 ratio from all peaks of 0.18, compared to 0.075 of peak 4.

5.3 Discussion

5.3.1 Method Development

5.3.1.1 Stopping the replication reaction

When conducting a standard replication assay, we finish the reaction by adding a STOP buffer to a 1x final concentration. Proteinase K and EDTA in the STOP buffer ensure that the replisome proteins are denatured and can no longer continue the replication reaction. We were unable to use the standard STOP buffer in our Tus jumping assay because its protein denaturing ability would prevent us from visualising Tus bound to the Tus capture substrate.

Instead of using the STOP buffer, we decided to add 80% glycerol to a final concentration of 15% at the end of our reaction, followed by loading the reactions immediately onto the 10% TBE-PAGE native gel and running samples at 150V. The reactions were conducted in sets of four or six, with each set being loaded and run on a gel while the next one was being set up. This created a 'step-ladder' pattern on the gel (figure 5.4, 5.5, 5.6).

The addition of glycerol enabled DNA loading onto the gel and was used as an alternative to a loading dye due to the small amounts of SDS present in the NEB DNA loading dye. The addition of glycerol and immediately running reactions on the gel was done with the intention of slowing the function of the proteins in the assay when the STOP buffer could not be added.

5.3.1.2 Concentration of Tus vs substrate vs pKJ001

A problem with our assay was the high concentration of the substrate and the relatively low concentration of Tus. We set these concentrations so that there was an excess of substrate for Tus to bind, but the work presented is preliminary and meant to be adapted and improved. Adding an excess of substrate was done to reduce the likelihood of including too much Tus in

the buffer which would remain unbound from pKJ001 and occupy the majority of *ter* sites on the Tus capture substrate.

Because our results included an excess of substrate, on gels we see a very strong band of unbound substrate. The Tus-bound substrate band when compared is very low, which means that any percentage difference we quantify is also very small and therefore can vary a lot. If we included less substrate, the ratio between the bound and unbound substrate lanes on the gel would decrease, likely generating clearer results after quantification.

Another interesting aspect to consider is the result of the EMSA (figure 5.3), where we show that not all Tus binds to the Tus-capture substrate in non-challenging conditions. Due to this, it would be beneficial to conduct an EMSA with the same concentrations of Tus (2.5 nM) and the Tus-capture substrate (5 nM) as used in the Tus Jumping Assays to determine what percentage of Tus we could expect to bind to the substrate. This should allow us to better analyse our data based on the 'expected' Tus binding rather than 'actual' Tus binding.

5.3.1.3 Affinity of Tus to pKJ001 and substrate

If more time was available, we would determine whether Tus has the same or similar affinity to both pKJ001 and the Tus capture substrate. An imbalance in K_d would mean that Tus would be biased towards one *ter* site over the other and would not provide accurate results. For example, if Tus had a higher affinity for the *ter* site on pKJ001, then if Tus dissociated from pKJ001, it would be more likely to rebind the *ter* site on pKJ001 rather than the *ter* site on the Tus capture substrate, preventing us from seeing dissociation. Similarly, if Tus has a higher affinity for the substrate, it might not bind to pKJ001.

An electrophoretic mobility shift assay (EMSA), SPR, calorimetric assay and filter binding assay could be used to measure the affinity of protein-DNA interactions (reviewed in Yang et

al., 2005) and therefore to determine the kD of Tus to both pKJ001 *terB* site and Tus capture substrate *terB* site.

5.3.1.4 Development of Tus-bound pKJ001 isolation/purification

We have conducted both size exclusion and ion exchange chromatography to test if Tus-bound pKJ001, Tus unbound pKJ001, and Tus alone can be separated using chromatography.

We were unable to separate the Tus-bound and unbound plasmid using size exclusion chromatography. When comparing a sample with pKJ001 only and with both pKJ001 and Tus we saw both produce a peak in the same elution, but the pKJ001-Tus peak contained a 'hump'. The 'hump' could indicate Tus presence – potentially due to a change in supercoiling when the protein is bound and therefore running through the column differently from DNA alone. The 'hump' however was not differentiated enough to separate it in a different fraction.

When using ion exchange chromatography we were unable to isolate Tus-bound pKJ001; instead, we saw distinct peaks which were shown on a 10% SDS-PAGE protein gel and 1% agarose DNA gel to contain pKJ001 only and Tus only. The presence of distinct peaks suggests that ion exchange chromatography might be a good method of isolation of Tus-bound pKJ001, though it requires further optimisation to determine how to create a stable Tus-pKJ001 complex.

Another solution for isolating Tus-bound pKJ001 complex would be to use Tus with an affinity tag. During affinity chromatography Tus only and Tus-bound pKJ001 would bind to the affinity column and would be eluted in different fractions due to their big size difference. There are two limitations to this solution. First, we would need to clone and purify Tus with an affinity tag, which can be time consuming. Second, we do not know how the tag might affect the function of Tus and would therefore have to test its activity in helicase and replication assays.

Once we can isolate a Tus-bound pKJ001 plasmid, we would need to test for the stability of the complex and to determine acceptable storage conditions and storage length. Stability of DNA:protein complexes can be tested using an EMSA, SPR, calorimetric assay and filter binding assay (reviewed in Yang et al., 2005). An affinity test would need to be conducted over time in assay conditions, as well as after storage at various temperatures (4°C, -20°C, and -70°C), after thawing.

5.3.2 Future Work

The Tus jumping assay is a technique which can be used to determine what happens to DNA-bound proteins when a replication fork reaches them. It was developed from a well-established replication assay and here we describe how we adapted it and took the first steps in making it a new biochemical tool. In our assay this method was used to test for dissociation of Tus from DNA, however in theory the Tus jumping assay could be used to test for displacement of any DNA-bound protein, by a replication fork, helicase or even RNAP, as long as the capture substrate was designed with a specific binding site for the protein. Our assay could become a beneficial *in vitro* tool for investigating the interplay between proteins and molecular machines.

Even though the Tus jumping assay needs further development; the preliminary findings are promising. Our results showed a significant increase in Tus-bound substrate concentration when a replication fork is stopped at the non-permissive orientation of the Tus-*ter* block. This result was surprising as the accepted consensus in literature states that Tus remains bound to *ter* when a replication fork is stalled by the non-permissive orientation of the complex (Kaplan, 2006), and has been modelled as bound to *ter* even after the stalled replisome dissociates from the replication fork (Kaplan, 2006; Bidnenko et al., 2006). It was also unexpected to not see a significant increase in the percentage of Tus-bound substrate when the fork reached the permissive orientation of Tus-*ter*, which suggested that Tus might quickly rebind to the same *ter* site.

It is especially interesting to compare the percentage of Tus-bound substrate in the samples cleaved with SmaI with the fork released in the non-permissive orientation only (+Tus +DnaA) at 3.25% (n=3, SD=0.88) (figure 5.7) and cleaved with SmaI where the non-permissive replication fork was blocked at Tus-*ter* only to be joined by the permissive orientation fork once it was released from LacI-*lacO*₂₂ (+Tus +LacI +IPTG +DnaA) at 4.56% (n=3, SD=1.43) (figure 5.5). In our hypothesis, we would expect to see a significant increase when both forks reach Tus-*terB* since the non-permissive orientation fork should not displace Tus, while the permissive orientation fork should. It was therefore surprising to see non-significant increase ($p = 0.2$) when comparing +Tus +LacI +IPTG +DnaA (SmaI) and +Tus +DnaA (SmaI).

When looking at the interaction between the non-permissive orientation of Tus-*terB* and the replisome, we were able to show a significant increase of Tus-bound substrate ($p = 0.0497$) from the control with no replication forks (+Tus -DnaA) to a single fork reaching the non-permissive orientation of Tus-*terB* (+Tus +DnaA). These results were surprising as it is generally assumed that Tus does not dissociate from *ter* after a replisome collision with the non-permissive face of the block. This result suggests that when the replication forks met at Tus-*terB* in the SmaI sample, that the majority of Tus would have already been displaced by the fork which reached the non-permissive face of Tus first. The non-significant increase seen when the second fork is also included (+Tus +LacI +IPTG +DnaA), suggests that some Tus might remain bound or might rebind to the same *terB* after being first displaced.

This finding should be viewed alongside the termination mapping assay result presented by Jameson and coworkers, where *in vitro* termination at Tus-*terB*, conducted in the same way as the Tus jumping assay showed an unreplicated 15-23 bp region with the same footprint as the binding of Tus (Jameson et al., 2021). If our results show that Tus is displaced by the first fork which reaches the non-permissive face of Tus-*terB*, then why were the forks not able to replicate the *terB* site?

Since our results suggest that Tus is likely not present during replication termination at *Tuster*, why was an unreplicated gap present and if the same occurs *in vivo* what mechanism is responsible for the under-replication and for finishing DNA synthesis? Jamesons termination mapping results could occur either if Tus is sandwiched between the replisomes, which is unlikely based on our results, or if something else is preventing the region from being reached. Our results point towards the second possibility. One 'blockade' to full termination could be the replisomes themselves. Replisomes are very large molecular machineries, and it is not unlikely that two replisomes pressed against one another might block the replication of a small DNA region between them.

CHAPTER 6
CONCLUDING
REMARKS

Chapter 6. Concluding Remarks

In this thesis, two distinct *E. coli* topics were explored: the function and structure of the SF1 helicase UvrD, and DNA replication termination at the Tus-*ter* block.

First, I was able to show that UvrD was able to unwind dsDNA past the permissive and non-permissive orientation of the Tus-*ter* block during *in vitro* helicase assays. While this topic has previously been explored in literature for UvrD *E. coli* helicase (Lee et al., 1989; Khatri et al., 1989; Hiasa and Marians, 1992; Bidnenko et al., 2006), it also showed varied conclusions and methods of analysis. I believe that my results provide strong evidence that UvrD can unwind past the Tus-*ter* block in both orientations in helicase assay conditions.

While I was able to conclude that UvrD could unwind past the Tus-*ter* block in a helicase assay, I was unable to show that UvrD could aid a replisome stuck at the non-permissive orientation of the Tus-*ter* block in a replication assay. This result agrees with Jameson and coworkers, but also with Bidnenko and coworkers that concluded that while UvrD could remove Tus in their *in vivo* experiments, it was unable to do so when DnaB was present at the site (Jameson et al., 2021; Bidnenko et al., 2006). Unfortunately, my replication assay results for UvrD are limited due to time constraints.

I also investigated the ability of UvrD to unwind a challenging dsDNA substrate against an EcoRI E111G block in a helicase assay. My results showed that UvrD alone could not efficiently unwind past this block. While EcoRI restriction enzyme might be encountered by UvrD, it is not a protein UvrD might encounter physiologically as a nucleoprotein block. Due to this, EcoRI E111G was used to represent a small block that was not physiologically familiar to UvrD. Interestingly, when UvrD was unwinding past both Tus and EcoRI E111G blocks bound to the same substrate, its efficiency increased from the ability to EcoRI E111G block

alone. This suggests that the presence of Tus influenced UvrD unwinding in a currently unknown mechanism.

I was also interested in finding out whether an addition of the MMR MutL protein might affect the ability of UvrD to unwind DNA, as previously shown by Ordabayev and coworkers (Ordabayev et al., 2018, 2019), and to unwind DNA past/displacing nucleoprotein blocks. My results confirmed that the addition of MutL increased the ability of UvrD to unwind a long dsDNA substrate. When testing against nucleoprotein blocks, MutL had a limited effect in assisting UvrD past the Tus-*ter* block, but showed a significant increase in DNA unwinding past the EcoRI E111G block. Since the binding of MutL to UvrD has been shown to increase its processivity (Ordabayev et al., 2018), my hypothesis is that UvrD employs a specific mechanism to remove Tus, but removes EcoRI E111G by displacing it through collision during DNA unwinding. UvrD without MutL might not have been processive, and potentially fast, enough for the collision with EcoRI E111G to displace the nucleoprotein block.

In this thesis, I attempted to purify three UvrD mutant proteins: UvrD Δ 52N, UvrD Δ 108N, and UvrD Δ 2B. The purification of UvrD Δ 52N (later altered to UvrD Δ 53N) and UvrD Δ 2B was unsuccessful due to solubility problems. UvrD Δ 108N was successfully purified using two chromatography strategies, using two affinity columns and a SEC column, and using one affinity column and an ion exchange column. Further tests showed that UvrD Δ 108N was not folded correctly and was unable to unwind DNA.

The N-terminal UvrD mutants required deletion of large regions of the protein and in retrospect the limited solubility and function of these proteins is not surprising. The deletions also removed a large section of the 1A subdomain which is required for DNA translocation – a function that likely would have been limited in these proteins if their purification was successful. For future work it would be interesting to conduct MS-XL experiments instead to determine which amino acids of UvrD and MutL form bonds. This method is however expensive and therefore was unable to be conducted as part of this thesis.

If more time was available, I would have made further attempts at purifying UvrD Δ 2B. The rotation of the 2B subdomain on both UvrD and its homologue Rep has been shown to have an effect on the helicases ability to unwind DNA (Ordabayev et al., 2019; Brüning et al., 2018), as well as for protein displacement in Rep (Brüning et al., 2018). It would be interesting to test whether the 2B subdomain of UvrD also affects protein displacement. This was however attempted through the addition of MutL to UvrD helicase assays due to the ability of MutL to rotate the 2B subdomain of UvrD (Ordabayev et al., 2019). Another method of testing the rotation of the 2B subdomain of UvrD might be through conducting an assay in high salt conditions (Jia et al., 2011). In our assay we used 25 mM and 10 mM of MgAc for helicase and replication assays respectively. Jia and coworkers suggested that the 2B subdomain of UvrD was open at 600 mM NaCl and closed at 20 mM NaCl (Jia et al., 2011).

Lastly, in this thesis I began developing a new biochemical tool called the 'Tus jumping assay'. This assay is an adaptation of the *in vitro* replication assay but designed to identify protein displacement rather than the length of DNA replicated. The development of this assay was a direct follow up from the termination mapping results from a recent paper published by our group (Jameson et al., 2021). Jameson showed that when the two replication forks met at the Tus-*ter* block an unreplicated gap with the same footprint as the binding of Tus was found. This led to two conclusions: either Tus is 'sandwiched' between the two replication forks, or it is dislodged and something else is preventing the two replication forks from replicating the final gap.

My preliminary results showed a significant increase in Tus displacement (indicated by an increase in Tus-bound Tus capture substrate) when a single replication fork approached the Tus-*ter* block from the non-permissive orientation. This was a surprising result as the current literature consensus states that when the replisome is stalled at Tus-*ter*, the replisome dissociates but Tus remains bound to *ter*. My results suggest that Tus did dissociate from *ter* during the replisome collision. Surprisingly, no significant increase was seen in Tus displacement when the replication fork approached the permissive face of the Tus-*ter* block.

My hypothesis is that the dislodged Tus by the permissive fork remained close to the *ter* site and rebound to it immediately after the fork went by. This hypothesis matches the quick rebinding of Tus suggested by Bidnenko and coworkers.

A slight increase from Tus displacement by the non-permissive orientation fork was seen when both replication forks met at Tus-*ter*. The reaction was designed to first block the clockwise fork by the non-permissive face of the Tus-*ter* block, followed by the counterclockwise fork reaching the site. Considering the single-fork data from this thesis and the termination mapping assay results (Jameson et al., 2021), my hypothesis suggests that most Tus is dislodged by the collision of Tus-*ter* with the replisome approaching it from the non-permissive orientation. Unlike the current literature consensus, I suggest that the replisome remains bound to the DNA, or at least remains bound for longer than Tus or quickly reassembles. When the second replication fork approaches the site, it encounters the first stalled replisome without Tus present. The meeting of the two large molecular machineries prevents the final DNA region, the *ter* site that Tus was bound to, from being replicated. The problem is likely resolved by a single replisome dissociation from the DNA, followed by reactivation of the remaining replisome and therefore the replication of the final DNA region.

The Tus jumping assay results are preliminary and require further repetitions and assay development. They are however promising and suggest that the assay might be able to provide us with useful insight into the mechanism of DNA replication termination at Tus-*ter* in *E. coli*.

All in all, this work demonstrates the ability of UvrD helicase to remove Tus, even in challenging conditions. UvrD was however unable to remove a physiologically irrelevant block EcoRI E111G unless it received aid from the MMR protein MutL. This led us understand more about the different ways helicases might remove nucleoprotein blocks. This work also developed a new biochemical tool and shined light on DNA replication termination. We showed

that Tus was displaced *in vitro* by the replication fork approaching the non-permissive orientation of Tus-*ter* and should not be present at *ter* during termination at Tus-*ter*.

References

- Abbate, E. A., Berger, J. M. and Botchan, M. R. (2004). The X-ray structure of the papillomavirus helicase in complex with its molecular matchmaker E2. *Genes & Development*, 18 (16), pp.1981–1996. [Online]. Available at: doi:10.1101/gad.1220104.
- Abbondanzieri, E. A. et al. (2005). Direct observation of base-pair stepping by RNA polymerase. *Nature*, 438 (7067), pp.460–465. [Online]. Available at: doi:10.1038/nature04268.
- Abdel-Monem, M., Durwald, H. and Hoffmann-Barling, H. (1976). Enzymic Unwinding of DNA. *European Journal of Biochemistry*, 65 (2), pp.441–449. [Online]. Available at: doi:10.1111/j.1432-1033.1976.tb10359.x.
- Abdelhaleem, M. (2019). *Helicases: Methods and Protocols*. [Online]. Available at: http://www.afes-press-books.de/html/APESS_18.htm.
- Acharya, S. et al. (1996). hMSH2 forms specific mispair-binding complexes with hMSH3 and hMSH6. *Proceedings of the National Academy of Sciences*, 93 (24), pp.13629–13634. [Online]. Available at: doi:10.1073/pnas.93.24.13629.
- Ali, J. A. et al. (1997). *Kinetic Measurement of the Step Size of DNA Unwinding by Escherichia coli UvrD Helicase Published by : American Association for the Advancement of Science Stable URL : <https://www.jstor.org/stable/2891002> American Association for the Advancement of Scienc.* 275 (5298), pp.377–380.
- Ali, J. A., Maluf, N. K. and Lohman, T. M. (1999). An oligomeric form of E. coli UvrD is required for optimal helicase activity 1 Edited by D. E. Draper. *Journal of Molecular Biology*, 293 (4), pp.815–834. [Online]. Available at: doi:10.1006/jmbi.1999.3185.
- AlphaFold. (2021). *AlphaFold2 ColabFold*. [Online]. Available at: <https://colab.research.google.com/github/sokrypton/ColabFold/blob/main/AlphaFold2.ipynb#scrollTo=kObIAo-xetgx>.
- Amarh, V. and Arthur, P. K. (2019). DNA double-strand break formation and repair as targets for novel antibiotic combination chemotherapy. *Future Science OA*, 5 (8). [Online]. Available at: doi:10.2144/fsoa-2019-0034.
- Arthur, H. M. and Eastlake, P. B. (1983). Transcriptional control of the UvrD gene of Escherichia coli. *Gene*, 25, pp.309–316.

Atkinson, J. et al. (2009). Stimulation of UvrD Helicase by UvrAB. *Journal of Biological Chemistry*, 284 (14), pp.9612–9623. [Online]. Available at: doi:10.1074/jbc.M808030200.

Atkinson, J. et al. (2011). Localization of an accessory helicase at the replisome is critical in sustaining efficient genome duplication. *Nucleic Acids Research*, 39 (3), pp.949–957. [Online]. Available at: doi:10.1093/nar/gkq889.

Atkinson, J. and McGlynn, P. (2009). Replication fork reversal and the maintenance of genome stability. *Nucleic Acids Research*, 37 (11), pp.3475–3492. [Online]. Available at: doi:10.1093/nar/gkp244.

Au, K. G., Welsh, K. and Modrich, P. (1992). Initiation of methyl-directed mismatch repair. *Journal of Biological Chemistry*, 267 (17), pp.12142–12148. [Online]. Available at: doi:10.1016/s0021-9258(19)49816-5.

Azeroglu, B. et al. (2016). RecG Directs DNA Synthesis during Double-Strand Break Repair. Courcelle, J. (Ed). *PLOS Genetics*, 12 (2), p.e1005799. [Online]. Available at: doi:10.1371/journal.pgen.1005799.

Azeroglu, B. and Leach, D. R. F. (2017). RecG controls DNA amplification at double-strand breaks and arrested replication forks. *FEBS Letters*, 591 (8), pp.1101–1113. [Online]. Available at: doi:10.1002/1873-3468.12583.

Ban, C., Junop, M. and Yang, W. (1999). Transformation of MutL by ATP Binding and Hydrolysis. *Cell*, 97 (1), pp.85–97. [Online]. Available at: doi:10.1016/S0092-8674(00)80717-5.

Ban, C. and Yang, W. (1998). Crystal Structure and ATPase Activity of MutL. *Cell*, 95 (4), pp.541–552. [Online]. Available at: doi:10.1016/S0092-8674(00)81621-9.

Bateman, A. et al. (2023). UniProt: the Universal Protein Knowledgebase in 2023. *Nucleic Acids Research*, 51 (D1), pp.D523–D531. [Online]. Available at: doi:10.1093/nar/gkac1052.

Bell, C. E. (2005). Structure and mechanism of Escherichia coli RecA ATPase. *Molecular Microbiology*, 58 (2), pp.358–366. [Online]. Available at: doi:10.1111/j.1365-2958.2005.04876.x.

Belotserkovskii, B. P. et al. (2018). R-loop generation during transcription: Formation, processing and cellular outcomes. *DNA repair*, 71, pp.69–81. [Online]. Available at: doi:10.1016/j.dnarep.2018.08.009.

- Berman, H. M. et al. (2000). The Protein Data Bank. *Nucleic Acids Research*, 28 (1), pp.235–242. [Online]. Available at: doi:10.1093/nar/28.1.235.
- Bhowmick, R., Hickson, I. D. and Liu, Y. (2023). Completing genome replication outside of S phase. *Molecular Cell*, 83 (20), pp.3596–3607. [Online]. Available at: doi:10.1016/j.molcel.2023.08.023.
- Bianco, P. R. and Lyubchenko, Y. L. (2017). SSB and the RecG DNA helicase: an intimate association to rescue a stalled replication fork. *Protein Science*, 26 (4), pp.638–649. [Online]. Available at: doi:10.1002/pro.3114.
- Bidnenko, V., Ehrlich, S. D. and Michel, Å. (2002). *Replication fork collapse at replication terminator sequences*. 21 (14).
- Bidnenko, V., Lestini, R. and Michel, B. (2006). The Escherichia coli UvrD helicase is essential for Tus removal during recombination-dependent replication restart from Ter sites. *Molecular Microbiology*, 62 (2), pp.382–396. [Online]. Available at: doi:10.1111/j.1365-2958.2006.05382.x.
- Bird, L. E., Subramanya, H. S. and Wigley, D. B. (1998). Helicases: a unifying structural theme? *Current Opinion in Structural Biology*, 8 (1), pp.14–18. [Online]. Available at: doi:10.1016/S0959-440X(98)80004-3.
- Bird, R. E. et al. (1972). Origin and sequence of chromosome replication in Escherichia coli. *Journal of Molecular Biology*, 70 (3), pp.549–566. [Online]. Available at: doi:10.1016/0022-2836(72)90559-1.
- Blattner, F. R. et al. (1997). The Complete Genome Sequence of Escherichia coli K-12. *Science*, 277 (5331), pp.1453–1462. [Online]. Available at: doi:10.1126/science.277.5331.1453.
- Bonnefoy, E. and Rouvière-Yaniv, J. (1992). HU, the major histone-like protein of E. coli, modulates the binding of IHF to oriC. *The EMBO Journal*, 11 (12), pp.4489–4496. [Online]. Available at: doi:10.1002/j.1460-2075.1992.tb05550.x.
- Boué, J. B. and Zakian, V. A. (2007). The yeast Pif1p DNA helicase preferentially unwinds RNA-DNA substrates. *Nucleic Acids Research*, 35 (17), pp.5809–5818. [Online]. Available at: doi:10.1093/nar/gkm613.
- Bourgeois, C. F., Mortreux, F. and Auboeuf, D. (2016). The multiple functions of RNA

helicases as drivers and regulators of gene expression. *Nature Reviews Molecular Cell Biology*, 17 (7), pp.426–438. [Online]. Available at: doi:10.1038/nrm.2016.50.

Bramhill, D. and Kornberg, A. (1988). Duplex opening by dnaA protein at novel sequences in initiation of replication at the origin of the E. coli chromosome. *Cell*, 52 (5), pp.743–755. [Online]. Available at: doi:10.1016/0092-8674(88)90412-6.

Brosh, Jr., R. M. (2014). UvrD helicase: The little engine that could. *Cell Cycle*, 13 (8), pp.1213–1215. [Online]. Available at: doi:10.4161/cc.28382.

Brüning, J.-G., Myka, K. K. and McGlynn, P. (2016). Overexpression of the Replicative Helicase in Escherichia coli Inhibits Replication Initiation and Replication Fork Reloading. *Journal of Molecular Biology*, 428 (6), pp.1068–1079. [Online]. Available at: doi:10.1016/j.jmb.2016.01.018.

Brüning, J. G. et al. (2018). The 2B subdomain of Rep helicase links translocation along DNA with protein displacement. *Nucleic Acids Research*, 46 (17), pp.8917–8925. [Online]. Available at: doi:10.1093/nar/gky673.

Brüning, J. G. and Marians, K. J. (2021). Bypass of complex co-directional replication-transcription collisions by replisome skipping. *Nucleic Acids Research*, 49 (17), pp.9870–9885. [Online]. Available at: doi:10.1093/nar/gkab760.

Burdett, V. et al. (2001). In vivo requirement for RecJ, ExoVII, ExoI, and ExoX in methyl-directed mismatch repair. *Proceedings of the National Academy of Sciences of the United States of America*, 98 (12), pp.6765–6770. [Online]. Available at: doi:10.1073/pnas.121183298.

Burgess, R. R. (1991). Use of Polyethyleneimine in Purification of DNA-Binding Proteins. *Methods in Enzymology*, 208 (C), pp.3–10. [Online]. Available at: doi:10.1016/0076-6879(91)08003-Z.

Busch, C. R. and DiRuggiero, J. (2010). MutS and MutL Are Dispensable for Maintenance of the Genomic Mutation Rate in the Halophilic Archaeon Halobacterium salinarum NRC-1. Aramayo, R. (Ed). *PLoS ONE*, 5 (2), p.e9045. [Online]. Available at: doi:10.1371/journal.pone.0009045.

Byrd, D. R. et al. (2002). Structure-Function Analysis of Escherichia coli DNA Helicase I Reveals Non-overlapping Transesterase and Helicase Domains. *Journal of Biological Chemistry*, 277 (45), pp.42645–42653. [Online]. Available at: doi:10.1074/jbc.M205984200.

Camara, J. E. et al. (2005). Hda inactivation of DnaA is the predominant mechanism preventing hyperinitiation of Escherichia coli DNA replication. *EMBO reports*, 6 (8), pp.736–741. [Online]. Available at: doi:10.1038/sj.embor.7400467.

Campbell, J. L. and Kleckner, N. (1990). E. coli oriC and the dnaA gene promoter are sequestered from dam methyltransferase following the passage of the chromosomal replication fork. *Cell*, 62 (5), pp.967–979. [Online]. Available at: doi:10.1016/0092-8674(90)90271-F.

Carter, A. S. et al. (2012). Resolving Holliday Junctions with Escherichia coli UvrD Helicase. *Journal of Biological Chemistry*, 287 (11), pp.8126–8134. [Online]. Available at: doi:10.1074/jbc.M111.314047.

Cerrón, F. et al. (2019). Replicative DNA polymerases promote active displacement of SSB proteins during lagging strand synthesis. *Nucleic Acids Research*, 47 (11), pp.5723–5734. [Online]. Available at: doi:10.1093/nar/gkz249.

Chayot, R. et al. (2010). An end-joining repair mechanism in Escherichia coli. *Proceedings of the National Academy of Sciences*, 107 (5), pp.2141–2146. [Online]. Available at: doi:10.1073/pnas.0906355107.

Chen, Z., Yang, H. and Pavletich, N. P. (2008). Mechanism of homologous recombination from the RecA–ssDNA/dsDNA structures. *Nature*, 453 (7194), pp.489–494. [Online]. Available at: doi:10.1038/nature06971.

Chmielewska-Jeznach, M. et al. (2022). An Adenosine Triphosphate- Dependent 5'-3' DNA Helicase From sk1-Like Lactococcus lactis F13 Phage. *Frontiers in Microbiology*, 13. [Online]. Available at: doi:10.3389/fmicb.2022.840219.

Comstock, M. J. et al. (2015). Direct observation of structure-function relationship in a nucleic acid -processing enzyme. *Science*, 348 (6232), pp.352–354. [Online]. Available at: doi:10.1126/science.aaa0130.

Connolly, B. et al. (1991). Resolution of Holliday junctions in vitro requires the Escherichia coli ruvC gene product. *Proceedings of the National Academy of Sciences*, 88 (14), pp.6063–6067. [Online]. Available at: doi:10.1073/pnas.88.14.6063.

Cooper, S. and Helmstetter, C. E. (1968). Chromosome replication and the division cycle of Escherichia coli. *Journal of Molecular Biology*, 31 (3), pp.519–540. [Online]. Available at: doi:10.1016/0022-2836(68)90425-7.

CorelCorp. (2019). *PaintShop Pro*. [Online]. Available at: <https://www.paintshoppro.com/en/>.

Coskun-Ari, F. F. and Hill, T. M. (1997). Sequence-specific Interactions in the Tus-Ter Complex and the Effect of Base Pair Substitutions on Arrest of DNA Replication in *Escherichia coli*. *Journal of Biological Chemistry*, 272 (42), pp.26448–26456. [Online]. Available at: doi:10.1074/jbc.272.42.26448.

Courcelle, J. et al. (2015). RecBCD is required to complete chromosomal replication: Implications for double-strand break frequencies and repair mechanisms. *DNA Repair*, 32, pp.86–95. [Online]. Available at: doi:10.1016/j.dnarep.2015.04.018.

Creze, C. et al. (2012). Modulation of the *Pyrococcus abyssi* NucS Endonuclease Activity by Replication Clamp at Functional and Structural Levels. *Journal of Biological Chemistry*, 287 (19), pp.15648–15660. [Online]. Available at: doi:10.1074/jbc.M112.346361.

Cvetic, C. and Walter, J. (2005). Eukaryotic origins of DNA replication: could you please be more specific? *Seminars in Cell & Developmental Biology*, 16 (3), pp.343–353. [Online]. Available at: doi:10.1016/j.semcdb.2005.02.009.

Dalhoff, A. (2012). Global Fluoroquinolone Resistance Epidemiology and Implications for Clinical Use. *Interdisciplinary Perspectives on Infectious Diseases*, 2012, pp.1–37. [Online]. Available at: doi:10.1155/2012/976273.

Dao, V. and Modrich, P. (1998). Mismatch-, MutS-, MutL-, and helicase II-dependent unwinding from the single-strand break of an incised heteroduplex. *Journal of Biological Chemistry*, 273 (15), pp.9202–9207. [Online]. Available at: doi:10.1074/jbc.273.15.9202.

Datta, A. and Brosh, R. M. (2018). New Insights Into DNA Helicases as Druggable Targets for Cancer Therapy. *Frontiers in Molecular Biosciences*, 5. [Online]. Available at: doi:10.3389/fmolb.2018.00059.

Deaconescu, A. M. et al. (2006). Structural Basis for Bacterial Transcription-Coupled DNA Repair. *Cell*, 124 (3), pp.507–520. [Online]. Available at: doi:10.1016/j.cell.2005.11.045.

Dewar, J. M., Budzowska, M. and Walter, J. C. (2015). The mechanism of DNA replication termination in vertebrates. *Nature*, 525 (7569), pp.345–350. [Online]. Available at: doi:10.1038/nature14887.

Dewar, J. M. and Walter, J. C. (2017). Mechanisms of DNA replication termination. *Nature Reviews Molecular Cell Biology*, 18 (8), pp.507–516. [Online]. Available at:

doi:10.1038/nrm.2017.42.

Dhar, S., Datta, A. and Brosh, R. M. (2020). DNA helicases and their roles in cancer. *DNA Repair*, 96, p.102994. [Online]. Available at: doi:10.1016/j.dnarep.2020.102994.

Dixon, D. A. and Kowalczykowski, S. C. (1993). The recombination hotspot χ is a regulatory sequence that acts by attenuating the nuclease activity of the E. coli RecBCD enzyme. *Cell*, 73 (1), pp.87–96. [Online]. Available at: doi:10.1016/0092-8674(93)90162-J.

Dorn, A. and Puchta, H. (2019). DNA Helicases as Safekeepers of Genome Stability in Plants. *Genes*, 10 (12), p.1028. [Online]. Available at: doi:10.3390/genes10121028.

Dove, S. L. and Hochschild, A. (1998). Conversion of the omega subunit of Escherichia coli RNA polymerase into a transcriptional activator or an activation target. *Genes & Development*, 12 (5), pp.745–754. [Online]. Available at: doi:10.1101/gad.12.5.745.

Dove, S. L., Joung, J. K. and Hochschild, A. (1997). Activation of prokaryotic transcription through arbitrary protein–protein contacts. *Nature*, 386 (6625), pp.627–630. [Online]. Available at: doi:10.1038/386627a0.

Downen, J. M., Putnam, C. D. and Kolodner, R. D. (2010). Functional Studies and Homology Modeling of Msh2-Msh3 Predict that Mismatch Recognition Involves DNA Bending and Strand Separation. *Molecular and Cellular Biology*, 30 (13), pp.3321–3328. [Online]. Available at: doi:10.1128/MCB.01558-09.

Drake, J. W. et al. (1998). Rates of Spontaneous Mutation. *Genetics*, 148 (4), pp.1667–1686. [Online]. Available at: doi:10.1093/genetics/148.4.1667.

Drotschmann, K. (1998). The Escherichia coli MutL protein stimulates binding of Vsr and MutS to heteroduplex DNA. *Nucleic Acids Research*, 26 (4), pp.948–953. [Online]. Available at: doi:10.1093/nar/26.4.948.

Drummond, J. T. et al. (1995). Isolation of an hMSH2-p160 Heterodimer That Restores DNA Mismatch Repair to Tumor Cells. *Science*, 268 (5219), pp.1909–1912. [Online]. Available at: doi:10.1126/science.7604264.

Dubaele, S., Lourdel, C. and Chène, P. (2006). Study of the ATP-binding site of helicase IV from Escherichia coli. *Biochemical and Biophysical Research Communications*, 341 (3), pp.828–836. [Online]. Available at: doi:10.1016/j.bbrc.2006.01.040.

Dubendorf, J. W. and Studier, F. W. (1991). Controlling basal expression in an inducible T7

expression system by blocking the target T7 promoter with lac repressor. *Journal of Molecular Biology*, 219 (1), pp.45–59. [Online]. Available at: doi:10.1016/0022-2836(91)90856-2.

Duggin, I. G. and Bell, S. D. (2009). Termination Structures in the Escherichia coli Chromosome Replication Fork Trap. *Journal of Molecular Biology*, 387 (3), pp.532–539. [Online]. Available at: doi:10.1016/j.jmb.2009.02.027.

Dunderdale, H. J. et al. (1991). Formation and resolution of recombination intermediates by E. coli RecA and RuvC proteins. *Nature*, 354 (6354), pp.506–510. [Online]. Available at: doi:10.1038/354506a0.

Dutta, D. et al. (2011). Linking RNA Polymerase Backtracking to Genome Instability in E. coli. *Cell*, 146 (4), pp.533–543. [Online]. Available at: doi:10.1016/j.cell.2011.07.034.

Easton, A. M. and Kushner, S. R. (1983). Transcription of the uvrD gene of Escherichia coli is controlled by the lexA repressor and by attenuation. *Nucleic Acids Research*, 11 (24), pp.8625–8640. [Online]. Available at: doi:10.1093/nar/11.24.8625.

Elshenawy, M. M. et al. (2015). *Replisome speed determines the efficiency of the Tus 2 Ter replication termination barrier*. [Online]. Available at: doi:10.1038/nature14866.

EMBL-EBI. (2022). *Clustal Omega*. [Online]. Available at: www.ebi.ac.uk/Tools/msa/clustalo/.

Epshtein, V. et al. (2014). UvrD facilitates DNA repair by pulling RNA polymerase backwards. *Nature*, 505 (7483), pp.372–377. [Online]. Available at: doi:10.1038/nature12928.UvrD.

Epshtein, V. (2015). UvrD helicase: An old dog with a new trick. *BioEssays*, 37 (1), pp.12–19. [Online]. Available at: doi:10.1002/bies.201400106.

Expasy. (2020). *DNA to Amino Acid Translate Tool*. [Online]. Available at: <https://web.expasy.org/translate/>.

Fairman-Williams, M. E., Guenther, U. P. and Jankowsky, E. (2010). SF1 and SF2 helicases: Family matters. *Current Opinion in Structural Biology*, 20 (3), pp.313–324. [Online]. Available at: doi:10.1016/j.sbi.2010.03.011.

Fang, G., Hammar, S. and Grumet, R. (1992). A quick and inexpensive method for removing polysaccharides from plant genomic DNA. *BioTechniques*, 13 (1), pp.52–54, 56. [Online].

Available at: <http://www.ncbi.nlm.nih.gov/pubmed/1503775>.

Felczak, M. M., Chodavarapu, S. and Kaguni, J. M. (2017). DnaC, the indispensable companion of DnaB helicase, controls the accessibility of DnaB helicase by primase. *Journal of Biological Chemistry*, 292 (51), pp.20871–20882. [Online]. Available at: doi:10.1074/jbc.M117.807644.

Feligioni, M. and Nisticò, R. (2013). SUMO: a (Oxidative) Stressed Protein. *NeuroMolecular Medicine*, 15 (4), pp.707–719. [Online]. Available at: doi:10.1007/s12017-013-8266-6.

Fijalkowska, I. J., Schaaper, R. M. and Jonczyk, P. (2012). DNA replication fidelity in *Escherichia coli*: a multi-DNA polymerase affair. *FEMS Microbiology Reviews*, 36 (6), pp.1105–1121. [Online]. Available at: doi:10.1111/j.1574-6976.2012.00338.x.

Finch, P. and Emmerson, P. T. (1983). Nucleotide sequence of the regulatory region of the *uvrD* gene of *Escherichia coli*. *Gene*, 25 (2–3), pp.317–323. [Online]. Available at: doi:10.1016/0378-1119(83)90236-6.

Fishel, R. et al. (1993). The human mutator gene homolog MSH2 and its association with hereditary nonpolyposis colon cancer. *Cell*, 75 (5), pp.1027–1038. [Online]. Available at: doi:10.1016/0092-8674(93)90546-3.

Flores-Rozas, H. and Kolodner, R. D. (1998). The *Saccharomyces cerevisiae* MLH 3 gene functions in MSH3-dependent suppression of frameshift mutations. *Proceedings of the National Academy of Sciences*, 95 (21), pp.12404–12409. [Online]. Available at: doi:10.1073/pnas.95.21.12404.

Fotadar, U., Zaveloff, P. and Terracio, L. (2005). Growth of *Escherichia coli* at elevated temperatures. *Journal of Basic Microbiology*, 45 (5), pp.403–404. [Online]. Available at: doi:10.1002/jobm.200410542.

Frick, D. and Lam, A. (2006). Understanding Helicases as a Means of Virus Control. *Current Pharmaceutical Design*, 12 (11), pp.1315–1338. [Online]. Available at: doi:10.2174/138161206776361147.

Fujimitsu, K., Senriuchi, T. and Katayama, T. (2009). Specific genomic sequences of *E. coli* promote replicational initiation by directly reactivating ADP-DnaA. *Genes & Development*, 23 (10), pp.1221–1233. [Online]. Available at: doi:10.1101/gad.1775809.

Fukui, K. et al. (2017). Crystal structure and DNA-binding property of the ATPase domain of

bacterial mismatch repair endonuclease MutL from *Aquifex aeolicus*. *Biochimica et Biophysica Acta (BBA) - Proteins and Proteomics*, 1865 (9), pp.1178–1187. [Online]. Available at: doi:10.1016/j.bbapap.2017.06.024.

Fuller, R. S., Funnell, B. E. and Kornberg, A. (1984). The dnaA protein complex with the *E. coli* chromosomal replication origin (oriC) and other DNA sites. *Cell*, 38 (3), pp.889–900. [Online]. Available at: doi:10.1016/0092-8674(84)90284-8.

Fuller, R. S. and Kornberg, A. (1983). Purified dnaA protein in initiation of replication at the *Escherichia coli* chromosomal origin of replication. *Proceedings of the National Academy of Sciences*, 80 (19), pp.5817–5821. [Online]. Available at: doi:10.1073/pnas.80.19.5817.

Gabbai, C. B. and Marians, K. J. (2010). Recruitment to stalled replication forks of the PriA DNA helicase and replisome-loading activities is essential for survival. *DNA Repair*, 9 (3), pp.202–209. [Online]. Available at: doi:10.1016/j.dnarep.2009.12.009.

Galli, E. et al. (2019). Replication termination without a replication fork trap. *Scientific Reports*, 9 (1), p.8315. [Online]. Available at: doi:10.1038/s41598-019-43795-2.

Gilhooly, N. S., Gwynn, E. J. and Dillingham, M. S. (2013). Superfamily 1 helicases. *Frontiers in Bioscience*, S5 (1), p.S367. [Online]. Available at: doi:10.2741/S367.

Goodall, D. J. et al. (2021). A Fork Trap in the Chromosomal Termination Area Is Highly Conserved across All *Escherichia coli* Phylogenetic Groups. *International Journal of Molecular Sciences*, 22 (15), p.7928. [Online]. Available at: doi:10.3390/ijms22157928.

Goodall, D. J. et al. (2023). Interplay between chromosomal architecture and termination of DNA replication in bacteria. *Frontiers in Microbiology*, 14 (June). [Online]. Available at: doi:10.3389/fmicb.2023.1180848.

Gottlieb, P. A. et al. (1992). Equilibrium, kinetic, and footprinting studies of the Tus-Ter protein-DNA interaction. *The Journal of biological chemistry*, 267 (11), pp.7434–7443. [Online]. Available at: <http://www.ncbi.nlm.nih.gov/pubmed/1313800>.

Gradia, S. et al. (1999). hMSH2-hMSH6 forms a hydrolysis-independent sliding clamp on mismatched DNA. *Molecular Cell*, 3 (2), pp.255–261. [Online]. Available at: doi:10.1016/S1097-2765(00)80316-0.

Guarné, A. et al. (2004). Structure of the MutL C-terminal domain: a model of intact MutL and its roles in mismatch repair. *The EMBO journal*, 23 (21), pp.4134–4145. [Online].

Available at: doi:10.1038/sj.emboj.7600412.

Gueneau, E. et al. (2013). Structure of the MutL α C-terminal domain reveals how Mlh1 contributes to Pms1 endonuclease site. *Nature Structural & Molecular Biology*, 20 (4), pp.461–468. [Online]. Available at: doi:10.1038/nsmb.2511.

Guy, C. P. et al. (2009). Rep Provides a Second Motor at the Replisome to Promote Duplication of Protein-Bound DNA. *Molecular Cell*, 36 (4), pp.654–666. [Online]. Available at: doi:10.1016/j.molcel.2009.11.009.

Gwynn, E. J. et al. (2013). The Conserved C-Terminus of the PcrA/UvrD Helicase Interacts Directly with RNA Polymerase. Spies, M. (Ed). *PLoS ONE*, 8 (10), p.e78141. [Online]. Available at: doi:10.1371/journal.pone.0078141.

Hall, M. C., Jordan, J. R. and Matson, S. W. (1998). Evidence for a physical interaction between the Escherichia coli methyl-directed mismatch repair proteins MutL and UvrD. *EMBO Journal*, 17 (5), pp.1535–1541. [Online]. Available at: doi:10.1093/emboj/17.5.1535.

Hall, M. C. and Matson, S. W. (1999). The Escherichia coli MutL protein physically interacts with MutH and stimulates the MutH-associated endonuclease activity. *Journal of Biological Chemistry*, 274 (3), pp.1306–1312. [Online]. Available at: doi:10.1074/jbc.274.3.1306.

Hamilton, N. A. et al. (2019). RecBCD, SbcCD and ExoI process a substrate created by convergent replisomes to complete DNA replication. *Molecular Microbiology*, 111 (6), pp.1638–1651. [Online]. Available at: doi:10.1111/mmi.14242.

Hamilton, N. A. et al. (2023). chi sequences switch the RecBCD helicase–nuclease complex from degradative to replicative modes during the completion of DNA replication. *Journal of Biological Chemistry*, 299 (3), p.103013. [Online]. Available at: doi:10.1016/j.jbc.2023.103013.

Hamperl, S. et al. (2017). Transcription-Replication Conflict Orientation Modulates R-Loop Levels and Activates Distinct DNA Damage Responses. *Cell*, 170 (4), pp.774–786.e19. [Online]. Available at: doi:10.1016/j.cell.2017.07.043.

Hansen, F. G. and Atlung, T. (1995). Initiation of chromosome replication after induction of DnaA protein synthesis in a dnaA(null) rhn mutant of Escherichia coli. *Molecular Microbiology*, 15 (1), pp.149–154. [Online]. Available at: doi:10.1111/j.1365-2958.1995.tb02229.x.

Hattman, S., Brooks, J. E. and Masurekar, M. (1978). Sequence specificity of the P1 modification methylase (M·Eco P1) and the DNA methylase (M·Eco dam) controlled by the Escherichia coli dam gene. *Journal of Molecular Biology*, 126 (3), pp.367–380. [Online]. Available at: doi:10.1016/0022-2836(78)90046-3.

Hawkins, M. et al. (2019). Direct removal of RNA polymerase barriers to replication by accessory replicative helicases. *Nucleic Acids Research*. [Online]. Available at: <https://doi.org/10.1093/nar/gkz170> [Accessed 28 October 2020].

Heller, R. C. and Marians, K. J. (2005). Unwinding of the Nascent Lagging Strand by Rep and PriA Enables the Direct Restart of Stalled Replication Forks. *Journal of Biological Chemistry*, 280 (40), pp.34143–34151. [Online]. Available at: doi:10.1074/jbc.M507224200.

Herman, G. E. and Modrich, P. (1981). Escherichia coli K-12 clones that overproduce dam methylase are hypermutable. *Journal of Bacteriology*, 145 (1), pp.644–646. [Online]. Available at: doi:10.1128/jb.145.1.644-646.1981.

Hiasa, H. and Marians, K. J. (1992). Differential inhibition of the DNA translocation and DNA unwinding activities of DNA helicases by the Escherichia coli Tus protein. *Journal of Biological Chemistry*, 267 (16), pp.11379–11385. [Online]. Available at: doi:10.1016/s0021-9258(19)49921-3.

Hofstatter, P. G. and Lahr, D. J. G. (2021). Complex Evolution of the Mismatch Repair System in Eukaryotes is Illuminated by Novel Archaeal Genomes. *Journal of Molecular Evolution*, 89 (1–2), pp.12–18. [Online]. Available at: doi:10.1007/s00239-020-09979-5.

Howan, K. et al. (2012). Initiation of transcription-coupled repair characterized at single-molecule resolution. *Nature*, 490 (7420), pp.431–434. [Online]. Available at: doi:10.1038/nature11430.

Howan, K. et al. (2014). Stopped in its tracks: The RNA polymerase molecular motor as a robust sensor of DNA damage. *DNA Repair*, 20, pp.49–57. [Online]. Available at: doi:10.1016/j.dnarep.2014.02.018.

Hu, X., Machius, M. and Yang, W. (2003). Monovalent cation dependence and preference of GHKL ATPases and kinases 1. *FEBS Letters*, 544 (1–3), pp.268–273. [Online]. Available at: doi:10.1016/S0014-5793(03)00519-2.

Huynh, K. and Partch, C. L. (2015). Analysis of Protein Stability and Ligand Interactions by Thermal Shift Assay. *Current Protocols in Protein Science*, 79 (1). [Online]. Available at:

doi:10.1002/0471140864.ps2809s79.

Hwang, D. S. and Kornberg, A. (1992). Opening of the replication origin of *Escherichia coli* by DnaA protein with protein HU or IHF. *Journal of Biological Chemistry*, 267 (32), pp.23083–23086. [Online]. Available at: doi:10.1016/S0021-9258(18)50059-4.

Ivanova, D. et al. (2015). Shaping the landscape of the *Escherichia coli* chromosome: replication-transcription encounters in cells with an ectopic replication origin. *Nucleic Acids Research*, 43 (16), pp.7865–7877. [Online]. Available at: doi:10.1093/nar/gkv704.

Iwasaki, H. et al. (1991). *Escherichia coli* RuvC protein is an endonuclease that resolves the Holliday structure. *The EMBO Journal*, 10 (13), pp.4381–4389. [Online]. Available at: doi:10.1002/j.1460-2075.1991.tb05016.x.

Iwasaki, H. et al. (1992). *Escherichia coli* RuvA and RuvB proteins specifically interact with Holliday junctions and promote branch migration. *Genes & Development*, 6 (11), pp.2214–2220. [Online]. Available at: doi:10.1101/gad.6.11.2214.

James, J. A. et al. (2003). Crystal Structure of the SF3 Helicase from Adeno-Associated Virus Type 2. *Structure*, 11 (8), pp.1025–1035. [Online]. Available at: doi:10.1016/S0969-2126(03)00152-7.

Jameson, K. H., Rudolph, C. J. and Hawkins, M. (2021). Termination of DNA replication at Tus-ter barriers results in under-replication of template DNA. *Journal of Biological Chemistry*, 297 (6), p.101409. [Online]. Available at: doi:10.1016/j.jbc.2021.101409.

Jeong, C. et al. (2011). MutS Switches Between Two Fundamentally Distinct Clamps during Mismatch Repair. *Nat Struct Mol Biol*, 18 (3), pp.379–385. [Online]. Available at: doi:10.1038/nsmb.2009.MutS.

Jia, H. et al. (2011). Rotations of the 2B sub-domain of *E. coli* UvrD helicase/translocase coupled to nucleotide and DNA binding. *Journal of Molecular Biology*, 411 (3), pp.633–648. [Online]. Available at: doi:10.1016/j.jmb.2011.06.019.

Jumper, J. et al. (2021). Highly accurate protein structure prediction with AlphaFold. *Nature*, 596 (7873), pp.583–589. [Online]. Available at: doi:10.1038/s41586-021-03819-2.

Kadyrov, F. A. et al. (2006). Endonucleolytic Function of MutL α in Human Mismatch Repair. *Cell*, 126 (2), pp.297–308. [Online]. Available at: doi:10.1016/j.cell.2006.05.039.

Kadyrov, F. A. et al. (2007). *Saccharomyces cerevisiae* MutL α Is a Mismatch Repair

- Endonuclease. *Journal of Biological Chemistry*, 282 (51), pp.37181–37190. [Online]. Available at: doi:10.1074/jbc.M707617200.
- Kaguni, J. M. (2011). Replication initiation at the Escherichia coli chromosomal origin. *Current Opinion in Chemical Biology*, 15 (5), pp.606–613. [Online]. Available at: doi:10.1016/j.cbpa.2011.07.016.
- Kamarthapu, V. and Nudler, E. (2015). Rethinking transcription coupled DNA repair. *Current Opinion in Microbiology*, 24, pp.15–20. [Online]. Available at: doi:10.1016/j.mib.2014.12.005.
- Kang, S. et al. (1999). Interaction of SeqA and Dam Methylase on the Hemimethylated Origin of Escherichia coli Chromosomal DNA Replication. *Journal of Biological Chemistry*, 274 (17), pp.11463–11468. [Online]. Available at: doi:10.1074/jbc.274.17.11463.
- Kaplan, D. L. (2006). Replication Termination: Mechanism of Polar Arrest Revealed. *Current Biology*, 16 (17), pp.684–686. [Online]. Available at: doi:10.1016/j.cub.2006.08.007.
- Katayama, T., Kasho, K. and Kawakami, H. (2017). The DnaA Cycle in Escherichia coli: Activation, Function and Inactivation of the Initiator Protein. *Frontiers in Microbiology*, 8. [Online]. Available at: doi:10.3389/fmicb.2017.02496.
- Kato, J. -i. and Katayama, T. (2001). Hda, a novel DnaA-related protein, regulates the replication cycle in Escherichia coli. *The EMBO Journal*, 20 (15), pp.4253–4262. [Online]. Available at: doi:10.1093/emboj/20.15.4253.
- Kawale, A. A. and Burmann, B. M. (2020). UvrD helicase–RNA polymerase interactions are governed by UvrD’s carboxy-terminal Tudor domain. *Communications Biology*, 3 (1), pp.1–13. [Online]. Available at: doi:10.1038/s42003-020-01332-2.
- Khatri, G. S. et al. (1989). The replication terminator protein of E. coli is a DNA sequence-specific contra-helicase. *Cell*, 59 (4), pp.667–674. [Online]. Available at: doi:10.1016/0092-8674(89)90012-3.
- Kimple, M. E., Brill, A. L. and Pasker, R. L. (2013). Overview of Affinity Tags for Protein Purification. *Current Protocols in Protein Science*, 73 (1). [Online]. Available at: doi:10.1002/0471140864.ps0909s73.
- King, K., Benkovic, S. J. and Modrich, P. (1989). Glu-111 is required for activation of the DNA cleavage center of EcoRI endonuclease. *Journal of Biological Chemistry*, 264 (20), pp.11807–11815. [Online]. Available at: doi:10.1016/S0021-9258(18)80137-5.

Kitagawa, R. et al. (1998). Negative control of replication initiation by a novel chromosomal locus exhibiting exceptional affinity for Escherichia coli DnaA protein. *Genes & Development*, 12 (19), pp.3032–3043. [Online]. Available at: doi:10.1101/gad.12.19.3032.

Kitani, T. et al. (1985). Evidence that discontinuous DNA replication in Escherichia coli is primed by approximately 10 to 12 residues of RNA starting with a purine. *Journal of Molecular Biology*, 184 (1), pp.45–52. [Online]. Available at: doi:10.1016/0022-2836(85)90042-7.

Klinkert, M. Q., Klein, A. and Abdel-Monem, M. (1980). Studies on the functions of DNA helicase I and DNA helicase II of Escherichia coli. *The Journal of biological chemistry*, 255 (20), pp.9746–9752. [Online]. Available at: <http://www.ncbi.nlm.nih.gov/pubmed/6107294>.

Kobori, J. A. and Kornberg, A. (1982). The Escherichia coli dnaC gene product. III. Properties of the dnaB-dnaC protein complex. *Journal of Biological Chemistry*, 257 (22), pp.13770–13775. [Online]. Available at: doi:10.1016/S0021-9258(18)33515-4.

Kohiyama, M., Herrick, J. and Norris, V. (2023). Open Questions about the Roles of DnaA, Related Proteins, and Hyperstructure Dynamics in the Cell Cycle. *Life*, 13 (9), p.1890. [Online]. Available at: doi:10.3390/life13091890.

Koleva, B. N. et al. (2019). Dynamics of the E. coli β -Clamp Dimer Interface and Its Influence on DNA Loading. *Biophysical Journal*, 117 (3), pp.587–601. [Online]. Available at: doi:10.1016/j.bpj.2019.06.035.

Kong, X. P. et al. (1992). Three-dimensional structure of the β subunit of E. coli DNA polymerase III holoenzyme: A sliding DNA clamp. *Cell*, 69 (3), pp.425–437. [Online]. Available at: doi:10.1016/0092-8674(92)90445-l.

Korolev, S. et al. (1998). Comparisons between the structures of HCV and Rep helicases reveal structural similarities between SF1 and SF2 super-families of helicases. *Protein Science*, 7 (3), pp.605–610. [Online]. Available at: doi:10.1002/pro.5560070309.

Korzheva, N. et al. (2000). A Structural Model of Transcription Elongation. *Science*, 289 (5479), pp.619–625. [Online]. Available at: doi:10.1126/science.289.5479.619.

Kosinski, J. et al. (2005). Analysis of the quaternary structure of the MutL C-terminal domain. *Journal of Molecular Biology*, 351 (4), pp.895–909. [Online]. Available at: doi:10.1016/j.jmb.2005.06.044.

- Kowalczykowski, S. C. et al. (1994). Biochemistry of homologous recombination in *Escherichia coli*. *Microbiological Reviews*, 58 (3), pp.401–465. [Online]. Available at: doi:10.1128/mr.58.3.401-465.1994.
- Kuempel, P. L., Duerr, S. A. and Seeley, N. R. (1977). Terminus region of the chromosome in *Escherichia coli* inhibits replication forks. *Proceedings of the National Academy of Sciences*, 74 (9), pp.3927–3931. [Online]. Available at: doi:10.1073/pnas.74.9.3927.
- Kunst, F. et al. (1997). The complete genome sequence of the Gram-positive bacterium *Bacillus subtilis*. *Nature*, 390 (6657), pp.249–256. [Online]. Available at: doi:10.1038/36786.
- Labib, K. and Hodgson, B. (2007). Replication fork barriers: pausing for a break or stalling for time? *EMBO reports*, 8 (4), pp.346–353. [Online]. Available at: doi:10.1038/sj.embor.7400940.
- Lahue, R. S., Au, K. G. and Modrich, P. (1989). DNA Mismatch Correction in a Defined System. *Science*, 245 (4914), pp.160–164. [Online]. Available at: doi:10.1126/science.2665076.
- Lam, S. T. et al. (1974). Rec-mediated recombinational hot spot activity in bacteriophage lambda II. A mutation which causes hot spot activity. *Genetics*, 77 (3), pp.425–433. [Online]. Available at: doi:10.1093/genetics/77.3.425.
- Lang, K. S. et al. (2017). Replication-Transcription Conflicts Generate R-Loops that Orchestrate Bacterial Stress Survival and Pathogenesis. *Cell*, 170 (4), pp.787–799.e18. [Online]. Available at: doi:10.1016/j.cell.2017.07.044.
- Laptenko, O. et al. (2003). Transcript cleavage factors GreA and GreB act as transient catalytic components of RNA polymerase. *The EMBO Journal*, 22 (23), pp.6322–6334. [Online]. Available at: doi:10.1093/emboj/cdg610.
- Larsen, N. B. et al. (2017). Stalled replication forks generate a distinct mutational signature in yeast. *Proceedings of the National Academy of Sciences*, 114 (36), pp.9665–9670. [Online]. Available at: doi:10.1073/pnas.1706640114.
- Larsen, N. B., Hickson, I. D. and Mankouri, H. W. (2014). Tus-Ter as a tool to study site-specific DNA replication perturbation in eukaryotes. *Cell Cycle*, 13 (19), pp.2994–2998. [Online]. Available at: doi:10.4161/15384101.2014.958912.
- LeBowitz, J. H. and McMacken, R. (1986). The *Escherichia coli* dnaB replication protein is a

DNA helicase. *Journal of Biological Chemistry*, 261 (10), pp.4738–4748. [Online]. Available at: doi:10.1016/S0021-9258(17)38564-2.

Lee, E. H. et al. (1989). Escherichia coli replication termination protein impedes the action of helicases. *Proceedings of the National Academy of Sciences*, 86 (23), pp.9104–9108. [Online]. Available at: doi:10.1073/pnas.86.23.9104.

Lee, J. Y. and Yang, W. (2006). UvrD Helicase Unwinds DNA One Base Pair At A Time By A Two- Part Power Stroke. *Cell*, 127 (7), pp.1349–1360. [Online]. Available at: <https://www.ncbi.nlm.nih.gov/pmc/articles/PMC3624763/pdf/nihms412728.pdf>.

Lee, K. S. et al. (2013). Direct imaging of single UvrD helicase dynamics on long single-stranded DNA. *Nature Communications*, 4 (May), pp.1–9. [Online]. Available at: doi:10.1038/ncomms2882.

Lee, M. S. and Marians, K. J. (1990). Differential ATP requirements distinguish the DNA translocation and DNA unwinding activities of the Escherichia coli PRI A protein. *Journal of Biological Chemistry*, 265 (28), pp.17078–17083. [Online]. Available at: doi:10.1016/S0021-9258(17)44871-X.

Levine, C., Hiasa, H. and Marians, K. J. (1998). DNA gyrase and topoisomerase IV: biochemical activities, physiological roles during chromosome replication, and drug sensitivities. *Biochimica et Biophysica Acta (BBA) - Gene Structure and Expression*, 1400 (1–3), pp.29–43. [Online]. Available at: doi:10.1016/S0167-4781(98)00126-2.

Lewis, J. S., Jergic, S. and Dixon, N. E. (2016). The E. coli DNA Replication Fork. In: *The Enzymes*. pp.31–88. [Online]. Available at: doi:10.1016/bs.enz.2016.04.001.

Li, D. et al. (2003). Structure of the replicative helicase of the oncoprotein SV40 large tumour antigen. *Nature*, 423 (6939), pp.512–518. [Online]. Available at: doi:10.1038/nature01691.

Li, H. and O'Donnell, M. E. (2018). The Eukaryotic CMG Helicase at the Replication Fork: Emerging Architecture Reveals an Unexpected Mechanism. *BioEssays*, 40 (3). [Online]. Available at: doi:10.1002/bies.201700208.

Liskay, R. M. et al. (1999). Mammalian DNA mismatch repair genes MLH1 and PMS1. *United States Patent*, (19).

Løbner-Olesen, A., Skovgaard, O. and Marinus, M. G. (2005). Dam methylation: coordinating cellular processes. *Current Opinion in Microbiology*, 8 (2), pp.154–160. [Online].

Available at: doi:10.1016/j.mib.2005.02.009.

van Loenhout, M. T. J. et al. (2009). Dynamics of RecA filaments on single-stranded DNA. *Nucleic Acids Research*, 37 (12), pp.4089–4099. [Online]. Available at: doi:10.1093/nar/gkp326.

Longley, M. J., Pierce, A. J. and Modrich, P. (1997). DNA Polymerase δ Is Required for Human Mismatch Repair in Vitro. *Journal of Biological Chemistry*, 272 (16), pp.10917–10921. [Online]. Available at: doi:10.1074/jbc.272.16.10917.

López De Saro, F. J. et al. (2006). The β sliding clamp binds to multiple sites within MutL and MutS. *Journal of Biological Chemistry*, 281 (20), pp.14340–14349. [Online]. Available at: doi:10.1074/jbc.M601264200.

Louarn, J., Patte, J. and Louarn, J.-M. (1977). Evidence for a fixed termination site of chromosome replication in *Escherichia coli* K12. *Journal of Molecular Biology*, 115 (3), pp.295–314. [Online]. Available at: doi:10.1016/0022-2836(77)90156-5.

Madeira, F. et al. (2022). Search and sequence analysis tools services from EMBL-EBI in 2022. *Nucleic Acids Research*, 50 (W1), pp.W276–W279. [Online]. Available at: doi:10.1093/nar/gkac240.

Maejima, Y. and Sadoshima, J. (2014). SUMOylation. *Circulation Research*, 115 (8), pp.686–689. [Online]. Available at: doi:10.1161/CIRCRESAHA.114.304989.

Malakhov, M. P. et al. (2004). SUMO fusions and SUMO-specific protease for efficient expression and purification of proteins. *Journal of Structural and Functional Genomics*, 5 (1/2), pp.75–86. [Online]. Available at: doi:10.1023/B:JSFG.0000029237.70316.52.

Malta, E. et al. (2008). Functions of base flipping in *E. coli* nucleotide excision repair. *DNA Repair*, 7 (10), pp.1647–1658. [Online]. Available at: doi:10.1016/j.dnarep.2008.06.011.

Maluf, N. K., Ali, J. A. and Lohman, T. M. (2003). Kinetic Mechanism for Formation of the Active, Dimeric UvrD Helicase-DNA Complex. *Journal of Biological Chemistry*, 278 (34), pp.31930–31940. [Online]. Available at: doi:10.1074/jbc.M304223200.

Maluf, N. K., Fischer, C. J. and Lohman, T. M. (2003). A dimer of *Escherichia coli* UvrD is the active form of the helicase in vitro. *Journal of Molecular Biology*, 325 (5), pp.913–935. [Online]. Available at: doi:10.1016/S0022-2836(02)01277-9.

Maluf, N. K. and Lohman, T. M. (2003). Self-association Equilibria of *Escherichia coli* UvrD

Helicase Studied by Analytical Ultracentrifugation. *Journal of Molecular Biology*, 325 (5), pp.889–912. [Online]. Available at: doi:10.1016/S0022-2836(02)01276-7.

Manelyte, L. et al. (2009). The unstructured C-terminal extension of UvrD interacts with UvrB, but is dispensable for nucleotide excision repair. *DNA Repair*, 8 (11), pp.1300–1310. [Online]. Available at: doi:10.1016/j.dnarep.2009.08.005.

Marians, K. J. (1987). DNA gyrase-catalyzed decatenation of multiply linked DNA dimers. *Journal of Biological Chemistry*, 262 (21), pp.10362–10368. [Online]. Available at: doi:10.1016/s0021-9258(18)61121-4.

Marians, K. J. (2000). PriA-directed replication fork restart in Escherichia coli. *Trends in Biochemical Sciences*, 25 (4), pp.185–189. [Online]. Available at: doi:10.1016/S0968-0004(00)01565-6.

Marinus, M. G. (1976). Adenine methylation of Okazaki fragments in Escherichia coli. *Journal of Bacteriology*, 128 (3), pp.853–854. [Online]. Available at: doi:10.1128/jb.128.3.853-854.1976.

Marinus, M. G., Poteete, A. and Arraj, J. A. (1984). Correlation of DNA adenine methylase activity with spontaneous mutability in Escherichia coli K-12. *Gene*, 28 (1), pp.123–125. [Online]. Available at: doi:10.1016/0378-1119(84)90095-7.

Marshall, C. J. and Santangelo, T. J. (2020). Archaeal DNA repair mechanisms. *Biomolecules*, 10 (11), pp.1–23. [Online]. Available at: doi:10.3390/biom10111472.

Marszalek, J. and Kaguni, J. M. (1994). DnaA protein directs the binding of DnaB protein in initiation of DNA replication in Escherichia coli. *Journal of Biological Chemistry*, 269 (7), pp.4883–4890. [Online]. Available at: doi:10.1016/S0021-9258(17)37627-5.

Marti, T. M., Kunz, C. and Fleck, O. (2002). DNA mismatch repair and mutation avoidance pathways. *Journal of Cellular Physiology*, 191 (1), pp.28–41. [Online]. Available at: doi:10.1002/jcp.10077.

Martin, C. S. et al. (1998). Three-dimensional reconstructions from cryoelectron microscopy images reveal an intimate complex between helicase DnaB and its loading partner DnaC. *Structure*, 6 (4), pp.501–509. [Online]. Available at: doi:10.1016/S0969-2126(98)00051-3.

Matson, S. W. (1986). Escherichia coli helicase II (uvrD gene product) translocates unidirectionally in a 3' to 5' direction. *Journal of Biological Chemistry*, 261 (22), pp.10169–

10175. [Online]. Available at: doi:10.1016/s0021-9258(18)67506-4.

Matson, S. W. (1991). *DNA Helicases of Escherichia coli*. In: pp.289–326. [Online]. Available at: doi:10.1016/S0079-6603(08)60845-4.

Matson, S. W. and Kaiser-Rogers, K. A. (1990). DNA helicases. *Annual Review of Biochemistry*, 59 (1), pp.289–329. [Online]. Available at: doi:10.1146/annurev.bi.59.070190.001445.

Matson, S. W. and Robertson, A. B. (2006). The UvrD helicase and its modulation by the mismatch repair protein MutL. *Nucleic Acids Research*, 34 (15), pp.4089–4097. [Online]. Available at: doi:10.1093/nar/gkl450.

Matson, S. W. and Wood, E. R. (1985). Production of antibodies directed against *Escherichia coli* helicase III and the molecular cloning of the helicase III gene. *Journal of Biological Chemistry*, 260 (21), pp.11811–11816. [Online]. Available at: doi:10.1016/S0021-9258(17)39103-2.

McCool, J. D., Ford, C. C. and Sandler, S. J. (2004). A dnaT Mutant With Phenotypes Similar to Those of a priA2::kan Mutant in *Escherichia coli* K-12. *Genetics*, 167 (2), pp.569–578. [Online]. Available at: doi:10.1534/genetics.103.025296.

McCool, J. D. and Sandler, S. J. (2001). Effects of mutations involving cell division, recombination, and chromosome dimer resolution on a priA2 :: kan mutant. *Proceedings of the National Academy of Sciences*, 98 (15), pp.8203–8210. [Online]. Available at: doi:10.1073/pnas.121007698.

McGlynn, P. et al. (1997). The DNA replication protein PriA and the recombination protein RecG bind D-loops. *Journal of Molecular Biology*, 270 (2), pp.212–221. [Online]. Available at: doi:10.1006/jmbi.1997.1120.

McGlynn, P. and Lloyd, R. G. (2002). Recombinational repair and restart of damaged replication forks. *Nature Reviews Molecular Cell Biology*, 3 (11), pp.859–870. [Online]. Available at: doi:10.1038/nrm951.

McHenry, C. (1985). DNA polymerase III holoenzyme of *Escherichia coli*: Components and function of a true replicative complex. *Molecular and Cellular Biochemistry*, 66 (1). [Online]. Available at: doi:10.1007/BF00231826.

Mechanic, L. E., Frankel, B. A. and Matson, S. W. (2000). *Escherichia coli* MutL loads DNA

helicase II onto DNA. *Journal of Biological Chemistry*, 275 (49), pp.38337–38346. [Online]. Available at: doi:10.1074/jbc.M006268200.

Mechanic, L. E., Hall, M. C. and Matson, S. W. (1999). Escherichia coli DNA Helicase II Is Active as a Monomer. *Journal of Biological Chemistry*, 274 (18), pp.12488–12498. [Online]. Available at: doi:10.1074/jbc.274.18.12488.

Mechanic, L. E., Latta, M. E. and Matson, S. W. (1999). A Region Near the C-Terminal End of Escherichia coli DNA Helicase II Is Required for Single-Stranded DNA Binding. *Journal of Bacteriology*, 181 (8), pp.2519–2526. [Online]. Available at: doi:10.1128/JB.181.8.2519-2526.1999.

Meir, A. and Greene, E. C. (2021). Srs2 and Pif1 as Model Systems for Understanding Sf1a and Sf1b Helicase Structure and Function. *Genes*, 12 (9), p.1319. [Online]. Available at: doi:10.3390/genes12091319.

Mellon, I. and Hanawalt, P. C. (1989). Induction of the Escherichia coli lactose operon selectively increases repair of its transcribed DNA strand. *Nature*, 342 (6245), pp.95–98. [Online]. Available at: doi:10.1038/342095a0.

Mendillo, M. L. et al. (2009). A conserved MutS homolog connector domain interface interacts with MutL homologs. *Proceedings of the National Academy of Sciences of the United States of America*, 106 (52), pp.22223–22228. [Online]. Available at: doi:10.1073/pnas.0912250106.

Mendillo, M. L., Mazur, D. J. and Kolodner, R. D. (2005). Analysis of the Interaction between the Saccharomyces cerevisiae MSH2-MSH6 and MLH1-PMS1 Complexes with DNA Using a Reversible DNA End-blocking System. *Journal of Biological Chemistry*, 280 (23), pp.22245–22257. [Online]. Available at: doi:10.1074/jbc.M407545200.

Merrikh, C. N., Brewer, B. J. and Merrikh, H. (2015). The B. subtilis Accessory Helicase PcrA Facilitates DNA Replication through Transcription Units. Viollier, P. H. (Ed). *PLOS Genetics*, 11 (6), p.e1005289. [Online]. Available at: doi:10.1371/journal.pgen.1005289.

Merrikh, H. et al. (2012). Replication–transcription conflicts in bacteria. *Nature Reviews Microbiology*, 10 (7), pp.449–458. [Online]. Available at: doi:10.1038/nrmicro2800.

Michel, B., Sinha, A. K. and Leach, D. R. F. (2018). Replication Fork Breakage and Restart in Escherichia coli. *Microbiology and Molecular Biology Reviews*, 82 (3). [Online]. Available at: doi:10.1128/MMBR.00013-18.

- Minobe, A. et al. (2019). Biochemical characterization of mismatch-binding protein MutS1 and nicking endonuclease MutL from a euryarchaeon *Methanosaeta thermophila*. *DNA Repair*, 75, pp.29–38. [Online]. Available at: doi:10.1016/j.dnarep.2019.01.005.
- Mirkin, E. V. and Mirkin, S. M. (2005). Mechanisms of Transcription-Replication Collisions in Bacteria. *Molecular and Cellular Biology*, 25 (3), pp.888–895. [Online]. Available at: doi:10.1128/MCB.25.3.888-895.2005.
- Moghadam, M. et al. (2015). Refolding process of cysteine-rich proteins: Chitinase as a model. *Reports of biochemistry & molecular biology*, 4 (1), pp.19–24. [Online]. Available at: <http://www.ncbi.nlm.nih.gov/pubmed/26989746>.
- Monakhova, M. et al. (2020). Probing the DNA-binding center of the MutL protein from the *Escherichia coli* mismatch repair system via crosslinking and Förster resonance energy transfer. *Biochimie*, 171–172, pp.43–54. [Online]. Available at: doi:10.1016/j.biochi.2020.02.004.
- Moolenaar, G. F., Höglund, L. and Goosen, N. (2001). Clue to damage recognition by UvrB: residues in the beta-hairpin structure prevent binding to non-damaged DNA. *The EMBO Journal*, 20 (21), pp.6140–6149. [Online]. Available at: doi:10.1093/emboj/20.21.6140.
- Morrison, A. and Cozzarelli, N. R. (1979). Site-specific cleavage of DNA by *E. coli* DNA gyrase. *Cell*, 17 (1), pp.175–184. [Online]. Available at: doi:10.1016/0092-8674(79)90305-2.
- Mulcair, M. D. et al. (2006). *A Molecular Mousetrap Determines Polarity of Termination of DNA Replication in E. coli*. pp.1309–1319. [Online]. Available at: doi:10.1016/j.cell.2006.04.040.
- Nagata, T. and Meselson, M. (1968). Periodic Replication of DNA in Steadily Growing *Escherichia coli*: The Localized Origin of Replication. *Cold Spring Harbor Symposia on Quantitative Biology*, 33, pp.553–557. [Online]. Available at: doi:10.1101/SQB.1968.033.01.062.
- Neylon, C. et al. (2005). Replication Termination in *Escherichia coli*: Structure and Antihelicase Activity of the Tus-Ter Complex. *Microbiology and Molecular Biology Reviews*, 69 (3), pp.501–526. [Online]. Available at: doi:10.1128/MMBR.69.3.501-526.2005.
- Nguyen, B. et al. (2017). Large domain movements upon UvrD dimerization and helicase activation. *Proceedings of the National Academy of Sciences*, 114 (46), pp.12178–12183. [Online]. Available at: doi:10.1073/pnas.1712882114.

Nievera, C. et al. (2006). SeqA Blocking of DnaA-oriC Interactions Ensures Staged Assembly of the E. coli Pre-RC. *Molecular Cell*, 24 (4), pp.581–592. [Online]. Available at: doi:10.1016/j.molcel.2006.09.016.

NIH. (2018). *ImageJ*. [Online]. Available at: www.imagej.org/.

Nudler, E. (2009). RNA Polymerase Active Center: The Molecular Engine of Transcription. *Annual Review of Biochemistry*, 78 (1), pp.335–361. [Online]. Available at: doi:10.1146/annurev.biochem.76.052705.164655.

O'Donnell, M. E. and Li, H. (2018). The ring-shaped hexameric helicases that function at DNA replication forks. *Nature Structural & Molecular Biology*, 25 (2), pp.122–130. [Online]. Available at: doi:10.1038/s41594-018-0024-x.

Ogawa, T. and Okazaki, T. (1980). Discontinuous DNA Replication. *Annual Review of Biochemistry*, 49 (1), pp.421–457. [Online]. Available at: doi:10.1146/annurev.bi.49.070180.002225.

Oh, E. Y. and Grossman, L. (1989). Characterization of the Helicase Activity of the Escherichia coli UvrAB Protein Complex. *Journal of Biological Chemistry*, 264 (2), pp.1336–1343. [Online]. Available at: doi:10.1016/S0021-9258(19)85091-3.

Okazaki, R. et al. (1968). Mechanism of DNA chain growth. I. Possible discontinuity and unusual secondary structure of newly synthesized chains. *Proceedings of the National Academy of Sciences*, 59 (2), pp.598–605. [Online]. Available at: doi:10.1073/pnas.59.2.598.

Olavarrieta, L. et al. (2002). DNA Knotting Caused by Head-on Collision of Transcription and Replication. *Journal of Molecular Biology*, 322 (1), pp.1–6. [Online]. Available at: doi:10.1016/S0022-2836(02)00740-4.

Ordabayev, Y. A. et al. (2018). Regulation of UvrD Helicase Activity by MutL. *Journal of Molecular Biology*, 430 (21), pp.4260–4274. [Online]. Available at: doi:10.1016/j.jmb.2018.08.022.

Ordabayev, Y. A. et al. (2019). UvrD helicase activation by MutL involves rotation of its 2B subdomain. *Proceedings of the National Academy of Sciences of the United States of America*, 116 (33), pp.16320–16325. [Online]. Available at: doi:10.1073/pnas.1905513116.

Owerbach, D. et al. (2005). A proline-90 residue unique to SUMO-4 prevents maturation and

sumoylation. *Biochemical and Biophysical Research Communications*, 337 (2), pp.517–520. [Online]. Available at: doi:10.1016/j.bbrc.2005.09.090.

Palombo, F. et al. (1995). GTBP, a 160-Kilodalton Protein Essential for Mismatch-binding Activity in Human Cells. *Science*, 268 (5219), pp.1912–1914. [Online]. Available at: doi:10.1126/science.7604265.

Park, J.-S., Marr, M. T. and Roberts, J. W. (2002). E. coli Transcription Repair Coupling Factor (Mfd Protein) Rescues Arrested Complexes by Promoting Forward Translocation. *Cell*, 109 (6), pp.757–767. [Online]. Available at: doi:10.1016/S0092-8674(02)00769-9.

PeakProteins. *Protein Tags and Leader Sequences*. [Online]. Available at: Microsoft Word - PPP_Protein Tag Info.docx (peakproteins.com) [Accessed 24 March 2022].

Peter, B. J. et al. (1998). The Structure of Supercoiled Intermediates in DNA Replication. *Cell*, 94 (6), pp.819–827. [Online]. Available at: doi:10.1016/S0092-8674(00)81740-7.

Petit, M. et al. (1998). PcrA is an essential DNA helicase of *Bacillus subtilis* fulfilling functions both in repair and rolling-circle replication. *Molecular Microbiology*, 29 (1), pp.261–273. [Online]. Available at: doi:10.1046/j.1365-2958.1998.00927.x.

Petrova, V. et al. (2015). Active displacement of RecA filaments by UvrD translocase activity. *Nucleic Acids Research*, 43 (8), pp.4133–4149. [Online]. Available at: doi:10.1093/nar/gkv186.

Pham, T. M. et al. (2013). A single-molecule approach to DNA replication in *Escherichia coli* cells demonstrated that ϵ -DNA polymerase III is a major determinant of fork speed. *Molecular Microbiology*, 90 (3), pp.584–596. [Online]. Available at: doi:10.1111/mmi.12386.

Piersimoni, L. et al. (2022). Cross-Linking Mass Spectrometry for Investigating Protein Conformations and Protein–Protein Interactions—A Method for All Seasons. *Chemical Reviews*, 122 (8), pp.7500–7531. [Online]. Available at: doi:10.1021/acs.chemrev.1c00786.

Pillon, M. C. et al. (2010). Structure of the Endonuclease Domain of MutL: Unlicensed to Cut. *Molecular Cell*, 39 (1), pp.145–151. [Online]. Available at: doi:10.1016/j.molcel.2010.06.027.

Pingoud, A. and Jeltsch, A. (2001). Structure and function of type II restriction endonucleases. *Nucleic Acids Research*, 29 (18), pp.3705–3727. [Online]. Available at: doi:10.1093/nar/29.18.3705.

Pinz, S., Duskocil, E. and Seufert, W. Thermofluor-Based Analysis of Protein Integrity and Ligand Interactions. In: *Ribosome Biogenesis: Methods and Protocols*. New York. pp.247–257. [Online]. Available at: doi:10.1007/978-1-0716-2501-9_15.

Pitcher, R. S. et al. (2007). NHEJ protects mycobacteria in stationary phase against the harmful effects of desiccation. *DNA Repair*, 6 (9), pp.1271–1276. [Online]. Available at: doi:10.1016/j.dnarep.2007.02.009.

Pizzul, P. et al. (2022). The DNA damage checkpoint: A tale from budding yeast. *Frontiers in Genetics*, 13. [Online]. Available at: doi:10.3389/fgene.2022.995163.

Pomerantz, R. T. and O'Donnell, M. (2008). The replisome uses mRNA as a primer after colliding with RNA polymerase. *Nature*, 456 (7223), pp.762–766. [Online]. Available at: doi:10.1038/nature07527.

Pomerantz, R. T. and O'Donnell, M. (2010). Direct Restart of a Replication Fork Stalled by a Head-On RNA Polymerase. *Science*, 327 (5965), pp.590–592. [Online]. Available at: doi:10.1126/science.1179595.

Postow, L. et al. (2004). Topological domain structure of the Escherichia coli chromosome. *Genes and Development*, 18 (14), pp.1766–1779. [Online]. Available at: doi:10.1101/gad.1207504.

Prolla, T. A. et al. (1994). MLH1, PMS1, and MSH2 Interactions During the Initiation of DNA Mismatch Repair in Yeast. *Science*, 265 (5175), pp.1091–1093. [Online]. Available at: doi:10.1126/science.8066446.

Ramilo, C. et al. (2002). Partial Reconstitution of Human DNA Mismatch Repair In Vitro: Characterization of the Role of Human Replication Protein A. *Molecular and Cellular Biology*, 22 (7), pp.2037–2046. [Online]. Available at: doi:10.1128/MCB.22.7.2037-2046.2002.

Raney, K. D., Byrd, A. K. and Aarattuthodiyil, S. (2013). *Structure and Mechanisms of SF1 DNA Helicases*. In: pp.17–46. [Online]. Available at: doi:10.1007/978-1-4614-5037-5_2.

ReactionBiology. *No Title*. [Online]. Available at: <https://www.reactionbiology.com/services/biophysical-assays/thermal-shift-assay-tsa#:~:text=Thermal shift assay uses the,in the compound-target interaction.>

Reardon, J. T. and Sancar, A. (2005). *Nucleotide Excision Repair*. In: pp.183–235. [Online]. Available at: doi:10.1016/S0079-6603(04)79004-2.

- Reenan, R. A. and Kolodner, R. D. (1992). Isolation and characterization of two *Saccharomyces cerevisiae* genes encoding homologs of the bacterial HexA and MutS mismatch repair proteins. *Genetics*, 132 (4), pp.963–973. [Online]. Available at: doi:10.1093/genetics/132.4.963.
- Roman, L. J. and Kowalczykowski, S. C. (1992). Processivity of the DNA helicase activity of *Escherichia coli* recBCD enzyme. *Journal of Biological Chemistry*, 267 (6), pp.4207–4214. [Online]. Available at: doi:10.1016/s0021-9258(19)50649-4.
- Rouvière-Yaniv, J., Yaniv, M. and Germond, J. E. (1979). *E. coli* DNA binding protein HU forms nucleosome-like structure with circular double-stranded DNA. *Cell*, 17 (2), pp.265–274. [Online]. Available at: doi:10.1016/0092-8674(79)90152-1.
- Rudolph, C. J. et al. (2013). Avoiding chromosome pathology when replication forks collide. *Nature*, 500 (7464), pp.608–611. [Online]. Available at: doi:10.1038/nature12312.
- Runyon, G. T., Bear, D. G. and Lohman, T. M. (1990). *Escherichia coli* helicase II (UvrD) protein initiates DNA unwinding at nicks and blunt ends. *Proceedings of the National Academy of Sciences*, 87 (16), pp.6383–6387. [Online]. Available at: doi:10.1073/pnas.87.16.6383.
- Sackett, D. L. and Wolff, J. (1987). Nile red as a polarity-sensitive fluorescent probe of hydrophobic protein surfaces. *Analytical Biochemistry*, 167 (2), pp.228–234. [Online]. Available at: doi:10.1016/0003-2697(87)90157-6.
- Sahoo, T. et al. (1995). The Contrahelicase Activities of the Replication Terminator Proteins of *Escherichia coli* and *Bacillus subtilis* Are Helicase-specific and Impede both Helicase Translocation and Authentic DNA Unwinding* Downloaded from. *The Journal of Biological Chemistry*, 270 (49). [Online]. Available at: doi:10.1074/jbc.270.49.29138.
- Saikrishnan, K. et al. (2009). Mechanistic Basis of 5'-3' Translocation in SF1B Helicases. *Cell*, 137 (5), pp.849–859. [Online]. Available at: doi:10.1016/j.cell.2009.03.036.
- Sanders, K. et al. (2017). The structure and function of an RNA polymerase interaction domain in the PcrA/UvrD helicase. *Nucleic Acids Research*, 45 (7), pp.3875–3887. [Online]. Available at: doi:10.1093/nar/gkx074.
- Sandler, S. J. (2000). Multiple Genetic Pathways for Restarting DNA Replication Forks in *Escherichia coli* K-12. *Genetics*, 155 (2), pp.487–497. [Online]. Available at: doi:10.1093/genetics/155.2.487.

- Schaaper, R. M. (1993). Base selection, proofreading, and mismatch repair during DNA replication in *Escherichia coli*. *Journal of Biological Chemistry*, 268 (32), pp.23762–23765. [Online]. Available at: doi:10.1016/S0021-9258(20)80446-3.
- Schofield, M. J. et al. (2001). Interaction of *Escherichia coli* MutS and MutL at a DNA Mismatch. *Journal of Biological Chemistry*, 276 (30), pp.28291–28299. [Online]. Available at: doi:10.1074/jbc.M103148200.
- Schuck, P. (1997). Use of the surface plasmon resonance to probe the equilibrium and dynamic aspects of interactions between biological macromolecules. *Annual Review of Biophysics and Biomolecular Structure*, 26 (1), pp.541–566. [Online]. Available at: doi:10.1146/annurev.biophys.26.1.541.
- Schwartzman, J. B. et al. (2019). Closing the DNA replication cycle: from simple circular molecules to supercoiled and knotted DNA catenanes. *Nucleic Acids Research*, 47 (14), pp.7182–7198. [Online]. Available at: doi:10.1093/nar/gkz586.
- Selby, C. P. and Sancar, A. (1990). Transcription preferentially inhibits nucleotide excision repair of the template DNA strand in vitro. *Journal of Biological Chemistry*, 265 (34), pp.21330–21336. [Online]. Available at: doi:10.1016/s0021-9258(17)45364-6.
- Selby, C. P. and Sancar, A. (1993a). Molecular Mechanism of Transcription-Repair Coupling. *Science*, 260 (5104), pp.53–58.
- Selby, C. P. and Sancar, A. (1993b). Molecular Mechanism of Transcription-Repair Coupling. *Science*, 260 (5104), pp.53–58. [Online]. Available at: doi:10.1126/science.8465200.
- Selby, C. P. and Sancar, A. (1995). Structure and Function of Transcription-Repair Coupling Factor. *Journal of Biological Chemistry*, 270 (9), pp.4890–4895. [Online]. Available at: doi:10.1074/jbc.270.9.4890.
- Selby, C. P., Witkin, E. M. and Sancar, A. (1991). *Escherichia coli* mfd mutant deficient in 'mutation frequency decline' lacks strand-specific repair: in vitro complementation with purified coupling factor. *Proceedings of the National Academy of Sciences*, 88 (24), pp.11574–11578. [Online]. Available at: doi:10.1073/pnas.88.24.11574.
- De Septenville, A. L. et al. (2012). *Replication Fork Reversal after Replication – Transcription Collision*. 8 (4). [Online]. Available at: doi:10.1371/journal.pgen.1002622.

Sergeeva, O. and Zatsepin, T. (2021). RNA Helicases as Shadow Modulators of Cell Cycle Progression. *International Journal of Molecular Sciences*, 22 (6), p.2984. [Online]. Available at: doi:10.3390/ijms22062984.

Setlow, R. B. and Carrier, W. L. (1964). THE DISAPPEARANCE OF THYMINE DIMERS FROM DNA: AN ERROR-CORRECTING MECHANISM. *Proceedings of the National Academy of Sciences*, 51 (2), pp.226–231. [Online]. Available at: doi:10.1073/pnas.51.2.226.

Sharples, G. J. and Leach, D. R. F. (1995). Structural and functional similarities between the SbcCD proteins of Escherichia coli and the RAD50 and MRE11 (RAD32) recombination and repair proteins of yeast. *Molecular Microbiology*, 17 (6), pp.1215–1217. [Online]. Available at: doi:10.1111/j.1365-2958.1995.mmi_17061215_1.x.

Shepherd, N. S., Churchward, G. and Bremer, H. (1980). Synthesis and activity of ribonucleic acid polymerase in Escherichia coli. *Journal of Bacteriology*, 141 (3), pp.1098–1108. [Online]. Available at: doi:10.1128/jb.141.3.1098-1108.1980.

Shilling, P. J. et al. (2020). Improved designs for pET expression plasmids increase protein production yield in Escherichia coli. *Communications Biology*, 3 (1), p.214. [Online]. Available at: doi:10.1038/s42003-020-0939-8.

Singleton, M. R., Dillingham, M. S. and Wigley, D. B. (2007). Structure and mechanism of helicases and nucleic acid translocases. *Annual Review of Biochemistry*, 76, pp.23–50. [Online]. Available at: doi:10.1146/annurev.biochem.76.052305.115300.

Sixma, T. K. (2001). DNA mismatch repair: MutS structures bound to mismatches. *Current Opinion in Structural Biology*, 11 (1), pp.47–52. [Online]. Available at: doi:10.1016/S0959-440X(00)00169-X.

Slater, S. et al. (1995). E. coli SeqA protein binds oriC in two different methyl-modulated reactions appropriate to its roles in DNA replication initiation and origin sequestration. *Cell*, 82 (6), pp.927–936. [Online]. Available at: doi:10.1016/0092-8674(95)90272-4.

van Sluis, C. A., Moolenaar, G. F. and Backendorf, C. (1983). Regulation of the uvrC gene of Escherichia coli K12: localization and characterization of a damage-inducible promoter. *The EMBO Journal*, 2 (12), pp.2313–2318. [Online]. Available at: doi:10.1002/j.1460-2075.1983.tb01739.x.

Smelkova, N. and Marians, K. J. (2001). Timely Release of Both Replication Forks from

oriC Requires Modulation of Origin Topology. *Journal of Biological Chemistry*, 276 (42), pp.39186–39191. [Online]. Available at: doi:10.1074/jbc.M104411200.

Smith, A. J., Pernstich, C. and Savery, N. J. (2012). Multipartite control of the DNA translocase, Mfd. *Nucleic Acids Research*, 40 (20), pp.10408–10416. [Online]. Available at: doi:10.1093/nar/gks775.

Smith, A. J. and Savery, N. J. (2005). RNA polymerase mutants defective in the initiation of transcription-coupled DNA repair. *Nucleic Acids Research*, 33 (2), pp.755–764. [Online]. Available at: doi:10.1093/nar/gki225.

Smith, G. R. et al. (1981). Structure of chi hotspots of generalized recombination. *Cell*, 24 (2), pp.429–436. [Online]. Available at: doi:10.1016/0092-8674(81)90333-0.

Smith, G. R. (2012). How RecBCD Enzyme and Chi Promote DNA Break Repair and Recombination: a Molecular Biologist's View. *Microbiology and Molecular Biology Reviews*, 76 (2), pp.217–228. [Online]. Available at: doi:10.1128/MMBR.05026-11.

Soultanas, P. and Wigley, D. B. (2000). DNA helicases: 'inching forward'. *Current Opinion in Structural Biology*, 10 (1), pp.124–128. [Online]. Available at: doi:10.1016/S0959-440X(99)00059-7.

Steinberg, T. H., Haugland, R. P. and Singer, V. L. (1996). Applications of SYPRO Orange and SYPRO Red Protein Gel Stains. *Analytical Biochemistry*, 239 (2), pp.238–245. [Online]. Available at: doi:10.1006/abio.1996.0320.

Steinmetz, E. J., Brennan, C. A. and Platt, T. (1990). A short intervening structure can block rho factor helicase action at a distance. *The Journal of biological chemistry*, 265 (30), pp.18408–18413. [Online]. Available at: <http://www.ncbi.nlm.nih.gov/pubmed/2145282>.

Stothard, P. (2000). *DNA Reverse Complement Tool*. [Online]. Available at: www.bioinformatics.org/sms/rev_comp.html.

Stoy, H. et al. (2023). Direct visualization of transcription-replication conflicts reveals post-replicative DNA:RNA hybrids. *Nature Structural & Molecular Biology*, 30 (3), pp.348–359. [Online]. Available at: doi:10.1038/s41594-023-00928-6.

Stukenberg, P. T., Studwell-Vaughan, P. S. and O'Donnell, M. (1991). Mechanism of the sliding beta-clamp of DNA polymerase III holoenzyme. *Journal of Biological Chemistry*, 266 (17), pp.11328–11334. [Online]. Available at: doi:10.1016/S0021-9258(18)99166-0.

Su'etsugu, M. et al. (2005). Protein Associations in DnaA-ATP Hydrolysis Mediated by the Hda-Replicase Clamp Complex. *Journal of Biological Chemistry*, 280 (8), pp.6528–6536. [Online]. Available at: doi:10.1074/jbc.M412060200.

Su, S. S. and Modrich, P. (1986). Escherichia coli mutS-encoded protein binds to mismatched DNA base pairs. *Proceedings of the National Academy of Sciences of the United States of America*, 83 (14), pp.5057–5061. [Online]. Available at: doi:10.1073/pnas.83.14.5057.

Sun, B. et al. (2008). Impediment of E. coli UvrD by DNA-destabilizing force reveals a strained-inchworm mechanism of DNA unwinding. *The EMBO Journal*, 27 (24), pp.3279–3287. [Online]. Available at: doi:10.1038/emboj.2008.240.

Sutton, M. D. et al. (1998). Escherichia coli DnaA Protein. *Journal of Biological Chemistry*, 273 (51), pp.34255–34262. [Online]. Available at: doi:10.1074/jbc.273.51.34255.

Syeda, A. H. et al. (2019). Single-molecule live cell imaging of Rep reveals the dynamic interplay between an accessory replicative helicase and the replisome. *Nucleic acids research*, 47 (12), pp.6287–6298. [Online]. Available at: doi:10.1093/nar/gkz298.

Tabata, S. et al. (1983). The 245 base-pair oriC sequence of the E. coli chromosome directs bidirectional replication at an adjacent region. *Nucleic Acids Research*, 11 (9), pp.2617–2626. [Online]. Available at: doi:10.1093/nar/11.9.2617.

TakaraBio. (2018). *InFusion Cloning Manual*. [Online]. Available at: https://www.takarabio.com/documents/User Manual/In/In-Fusion HD Cloning Kit User Manual_102518.pdf.

Tan, H. Y. and Bianco, P. R. (2021). SSB Facilitates Fork-Substrate Discrimination by the PriA DNA Helicase. *ACS Omega*, 6 (25), pp.16324–16335. [Online]. Available at: doi:10.1021/acsomega.1c00722.

Tanner, N. K. et al. (2003). The Q motif: A newly identified motif in DEAD box helicases may regulate ATP binding and hydrolysis. *Molecular Cell*, 11 (1), pp.127–138. [Online]. Available at: doi:10.1016/S1097-2765(03)00006-6.

Taucher-Scholzt, G. and Hoffmann-Berling, H. (1983). Identification of the gene for DNA helicase II of Escherichia coli. *European Journal of Biochemistry*, 137 (3), pp.573–580. [Online]. Available at: doi:10.1111/j.1432-1033.1983.tb07864.x.

Taylor, A. F. and Smith, G. R. (1985). Substrate specificity of the DNA unwinding activity of the RecBC enzyme of *Escherichia coli*. *Journal of Molecular Biology*, 185 (2), pp.431–443. [Online]. Available at: doi:10.1016/0022-2836(85)90414-0.

Tessmer, I. et al. (2008). Mechanism of MutS searching for DNA mismatches and signaling repair. *Journal of Biological Chemistry*, 283 (52), pp.36646–36654. [Online]. Available at: doi:10.1074/jbc.M805712200.

ThermoFisher. (2023). *Tm Calculator*. [Online]. Available at: www.thermofisher.com/uk/en/home/brands/thermo-scientific/molecular-biology/molecular-biology-learning-center/molecular-biology-resource-library/thermo-scientific-web-tools/tm-calculator.html.

Thomas, M., White, R. L. and Davis, R. W. (1976). Hybridization of RNA to double-stranded DNA: formation of R-loops. *Proceedings of the National Academy of Sciences*, 73 (7), pp.2294–2298. [Online]. Available at: doi:10.1073/pnas.73.7.2294.

Thomsen, N. D. and Berger, J. M. (2009). Running in Reverse: The Structural Basis for Translocation Polarity in Hexameric Helicases. *Cell*, 139 (3), pp.523–534. [Online]. Available at: doi:10.1016/j.cell.2009.08.043.

Tishkoff, D. X. et al. (1997). Identification and characterization of *Saccharomyces cerevisiae* EXO1, a gene encoding an exonuclease that interacts with MSH2. *Proceedings of the National Academy of Sciences*, 94 (14), pp.7487–7492. [Online]. Available at: doi:10.1073/pnas.94.14.7487.

Tishkoff, D. X. et al. (1998). Identification of a human gene encoding a homologue of *Saccharomyces cerevisiae* EXO1, an exonuclease implicated in mismatch repair and recombination. *Cancer Research*, 58 (22), pp.5027–5031.

Toft, C. J. et al. (2021). Delineation of the ancestral tus-dependent replication fork trap. *International Journal of Molecular Sciences*, 22 (24). [Online]. Available at: doi:10.3390/ijms222413533.

Toft, C. J., Sorenson, A. E. and Schaeffer, P. M. (2022). A soft Tus-Ter interaction is hiding a fail-safe lock in the replication fork trap of *Dickeya paradisiaca*. *Microbiological Research*, 263, p.127147. [Online]. Available at: doi:10.1016/j.micres.2022.127147.

Torres, K. A. et al. (2022). The unstructured linker of Mlh1 contains a motif required for endonuclease function which is mutated in cancers. *Proceedings of the National Academy of*

Sciences, 119 (42). [Online]. Available at: doi:10.1073/pnas.2212870119.

Tougu, K. and Marians, K. J. (1996). The Interaction between Helicase and Primase Sets the Replication Fork Clock. *Journal of Biological Chemistry*, 271 (35), pp.21398–21405. [Online]. Available at: doi:10.1074/jbc.271.35.21398.

Trakselis, M. A. (2016). Structural Mechanisms of Hexameric Helicase Loading, Assembly, and Unwinding. *F1000Research*, 5, p.111. [Online]. Available at: doi:10.12688/f1000research.7509.1.

Triman, K. L., Chattoraj, D. K. and Smith, G. R. (1982). Identity of a Chi site of *Escherichia coli* and Chi recombinational hotspots of bacteriophage λ . *Journal of Molecular Biology*, 154 (2), pp.393–398. [Online]. Available at: doi:10.1016/0022-2836(82)90072-9.

Tsaneva, I. R., Müller, B. and West, S. C. (1993). RuvA and RuvB proteins of *Escherichia coli* exhibit DNA helicase activity in vitro. *Proceedings of the National Academy of Sciences*, 90 (4), pp.1315–1319. [Online]. Available at: doi:10.1073/pnas.90.4.1315.

Tuteja, N. and Tuteja, R. (2004). Prokaryotic and eukaryotic DNA helicases. Essential molecular motor proteins for cellular machinery. *European Journal of Biochemistry*, 271 (10), pp.1835–1848. [Online]. Available at: doi:10.1111/j.1432-1033.2004.04093.x.

Tuttle, A. R., Trahan, N. D. and Son, M. S. (2021). Growth and Maintenance of *Escherichia coli* Laboratory Strains. *Current Protocols*, 1 (1). [Online]. Available at: doi:10.1002/cpz1.20.

Umezu, K., Nakayama, K. and Nakayama, H. (1990). *Escherichia coli* RecQ protein is a DNA helicase. *Proceedings of the National Academy of Sciences*, 87 (14), pp.5363–5367. [Online]. Available at: doi:10.1073/pnas.87.14.5363.

Urrutia-Irazabal, I. et al. (2021). Analysis of the PcrA-RNA polymerase complex reveals a helicase interaction motif and a role for PcrA/UvrD helicase in the suppression of R-loops. *eLife*, 10. [Online]. Available at: doi:10.7554/eLife.68829.

Veaute, X. et al. (2005). UvrD helicase, unlike Rep helicase, dismantles RecA nucleoprotein filaments in *Escherichia coli*. *The EMBO Journal*, 24 (1), pp.180–189. [Online]. Available at: doi:10.1038/sj.emboj.7600485.

Velankar, S. S. et al. (1999). Crystal Structures of Complexes of PcrA DNA Helicase with a DNA Substrate Indicate an Inchworm Mechanism. *Cell*, 97 (1), pp.75–84. [Online]. Available at: doi:10.1016/S0092-8674(00)80716-3.

Viguera, E. et al. (1996). The ColE1 Unidirectional Origin Acts as a Polar Replication Fork Pausing Site. *Journal of Biological Chemistry*, 271 (37), pp.22414–22421. [Online]. Available at: doi:10.1074/jbc.271.37.22414.

Vilette, D., Ehrlich, S. D. and Michel, B. (1996). Transcription-induced deletions in plasmid vectors: M13 DNA replication as a source of instability. *Molecular and General Genetics MGG*, 252 (4), pp.398–403. [Online]. Available at: doi:10.1007/BF02173004.

Voloshin, O. N. et al. (2003). Characterization of the DNA damage-inducible helicase DinG from Escherichia coli. *Journal of Biological Chemistry*, 278 (30), pp.28284–28293. [Online]. Available at: doi:10.1074/jbc.M301188200.

Wahle, E., Lasken, R. S. and Kornberg, A. (1989). The dnaB-dnaC replication protein complex of Escherichia coli. II. Role of the complex in mobilizing dnaB functions. *The Journal of biological chemistry*, 264 (5), pp.2469–2475. [Online]. Available at: <http://www.ncbi.nlm.nih.gov/pubmed/2536713>.

Wang, J. C. (1984). DNA supercoiling and its effects on the structure of DNA. *Journal of Cell Science*, 1984 (Supplement_1), pp.21–29. [Online]. Available at: doi:10.1242/jcs.1984.Supplement_1.2.

Wang, L. et al. (2023). Head-on and co-directional RNA polymerase collisions orchestrate bidirectional transcription termination. *Molecular Cell*, 83 (7), pp.1153-1164.e4. [Online]. Available at: doi:10.1016/j.molcel.2023.02.017.

Wang, M. D. et al. (1998). Force and Velocity Measured for Single Molecules of RNA Polymerase. *Science*, 282 (5390), pp.902–907. [Online]. Available at: doi:10.1126/science.282.5390.902.

Weigel, C. et al. (1997). DnaA protein binding to individual DnaA boxes in the Escherichia coli replication origin, oriC. *The EMBO Journal*, 16 (21), pp.6574–6583. [Online]. Available at: doi:10.1093/emboj/16.21.6574.

Weiss, A. S., Hariharan, I. K. and Wake, R. G. (1981). Analysis of the terminus region of the Bacillus subtilis chromosome. *Nature*, 293 (5834), pp.673–675. [Online]. Available at: doi:10.1038/293673a0.

Wendel, B. M. et al. (2018). SbcC-SbcD and ExoI process convergent forks to complete chromosome replication. *Proceedings of the National Academy of Sciences*, 115 (2), pp.349–354. [Online]. Available at: doi:10.1073/pnas.1715960114.

Whitby, M. C. and Lloyd, R. G. (1995). Branch migration of three-strand recombination intermediates by RecG, a possible pathway for securing exchanges initiated by 3'-tailed duplex DNA. *The EMBO Journal*, 14 (14), pp.3302–3310. [Online]. Available at: doi:10.1002/j.1460-2075.1995.tb07337.x.

Wickner, S. (1976). Mechanism of DNA elongation catalyzed by Escherichia coli DNA polymerase III, dnaZ protein, and DNA elongation factors I and III. *Proceedings of the National Academy of Sciences*, 73 (10), pp.3511–3515. [Online]. Available at: doi:10.1073/pnas.73.10.3511.

Wickner, S. and Hurwitz, J. (1975). Interaction of Escherichia coli dnaB and dnaC(D) gene products in vitro. *Proceedings of the National Academy of Sciences*, 72 (3), pp.921–925. [Online]. Available at: doi:10.1073/pnas.72.3.921.

Wiedemann, C. et al. (2020). Cysteines and Disulfide Bonds as Structure-Forming Units: Insights From Different Domains of Life and the Potential for Characterization by NMR. *Frontiers in Chemistry*, 8. [Online]. Available at: doi:10.3389/fchem.2020.00280.

Wilson, T. E., Topper, L. M. and Palmbos, P. L. (2003). Non-homologous end-joining: bacteria join the chromosome breakdance. *Trends in Biochemical Sciences*, 28 (2), pp.62–66. [Online]. Available at: doi:10.1016/S0968-0004(03)00005-7.

Witkin, E. M. (1956). Time, Temperature, and Protein Synthesis: A Study of Ultraviolet-Induced Mutation in Bacteria. *Cold Spring Harbor Symposia on Quantitative Biology*, 21, pp.123–140. [Online]. Available at: doi:10.1101/SQB.1956.021.01.011.

Wohlkonig, A. et al. (2010). Structural basis of quinolone inhibition of type IIA topoisomerases and target-mediated resistance. *Nature Structural & Molecular Biology*, 17 (9), pp.1152–1153. [Online]. Available at: doi:10.1038/nsmb.1892.

Wolanski, M. et al. (2015). oriC-encoded instructions for the initiation of bacterial chromosome replication. *Frontiers in Microbiology*, 5. [Online]. Available at: doi:10.3389/fmicb.2014.00735.

Wollman, A. J. M. et al. (2023). Tetrameric UvrD helicase is located at the E. coli replisome due to frequent replication blocks. *Journal of Molecular Biology*, 436 (2), pp. 1-51. [Online]. Available at: doi:10.1016/j.jmb.2023.168369.

Wood, E. R. and Matson, S. W. (1987). Purification and characterization of a new DNA-dependent ATPase with helicase activity from Escherichia coli. *Journal of Biological*

Chemistry, 262 (31), pp.15269–15276. [Online]. Available at: doi:10.1016/S0021-9258(18)48170-7.

Xu, Z. and Au, S. W. N. (2005). Mapping residues of SUMO precursors essential in differential maturation by SUMO-specific protease, SENP1. *Biochemical Journal*, 386 (2), pp.325–330. [Online]. Available at: doi:10.1042/BJ20041210.

Yamaguchi, M., Dao, V. and Modrich, P. (1998). MutS and MutL activate DNA helicase II in a mismatch-dependent manner. *Journal of Biological Chemistry*, 273 (15), pp.9197–9201. [Online]. Available at: doi:10.1074/jbc.273.15.9197.

Yang, Y. et al. (2005). Determination of protein-DNA binding constants and specificities from statistical analyses of single molecules: MutS-DNA interactions. *Nucleic Acids Research*, 33 (13), pp.4322–4334. [Online]. Available at: doi:10.1093/nar/gki708.

Yarranton, G. T., Das, R. H. and Gefter, M. L. (1979). Enzyme-catalyzed DNA unwinding. A DNA-dependent ATPase from *E. coli*. *The Journal of biological chemistry*, 254 (23), pp.11997–12001. [Online]. Available at: <http://www.ncbi.nlm.nih.gov/pubmed/227886>.

Yarranton, G. T. and Gefter, M. L. (1979). Enzyme-catalyzed DNA unwinding: Studies on *Escherichia coli* rep protein. *Proceedings of the National Academy of Sciences*, 76 (4), pp.1658–1662. [Online]. Available at: doi:10.1073/pnas.76.4.1658.

Yokota, H. (2020). DNA-Unwinding Dynamics of *Escherichia coli* UvrD Lacking the C-Terminal 40 Amino Acids. *Biophysical Journal*, 118 (7), pp.1634–1648. [Online]. Available at: doi:10.1016/j.bpj.2020.02.014.

Yokota, H. (2022). Quantitative and kinetic single-molecule analysis of DNA unwinding by *Escherichia coli* UvrD helicase. *Biophysics and Physicobiology*, 19, p.e190006. [Online]. Available at: doi:10.2142/biophysico.bppb-v19.0006.

Yokota, H., Chujo, Y. A. and Harada, Y. (2013). Single-Molecule Imaging of the Oligomer Formation of the Nonhexameric *Escherichia coli* UvrD Helicase. *Biophysical Journal*, 104 (4), pp.924–933. [Online]. Available at: doi:10.1016/j.bpj.2013.01.014.

Yu, C. et al. (2016). SSB binds to the RecG and PriA helicases *in vivo* in the absence of DNA. *Genes to Cells*, 21 (2), pp.163–184. [Online]. Available at: doi:10.1111/gtc.12334.

Zhang, S. and Grosse, F. (1994). Nuclear DNA Helicase II Unwinds both DNA and RNA. *Biochemistry*, 33 (13), pp.3906–3912. [Online]. Available at: doi:10.1021/bi00179a016.

Zhang, Y. et al. (2005). Reconstitution of 5'-Directed Human Mismatch Repair in a Purified System. *Cell*, 122 (5), pp.693–705. [Online]. Available at: doi:10.1016/j.cell.2005.06.027.

Zou, Y. et al. (1997). Formation of DNA Repair Intermediates and Incision by the ATP-dependent UvrB-UvrC Endonuclease. *Journal of Biological Chemistry*, 272 (8), pp.4820–4827. [Online]. Available at: doi:10.1074/jbc.272.8.4820.

List of Abbreviations

| | |
|---------------|---|
| Δ | Deletion |
| μl | Microliter |
| μM | Micromolar |
| Amp | Ampicillin |
| ATP | AdenosineTtriphosphate |
| bp | Base Pair(s) |
| BSA | Bovine Serum Albumin |
| chi | Crossover Hot Spot Investigator |
| CryoEM | Cryogenic Electron Microscopy |
| dif | Deletion-Induced Filamentation |
| DSB | Double-Stranded Break |
| DSBR | Double-Stranded Break Repair |
| dCTP | Deoxycytidine Triphosphate |
| DUE | Duplex-Unwinding Element |
| DNA | Deoxyribonucleic Acid |
| DTT | Dithiothreitol |
| ds | Double Stranded |
| et al. | et alia (and others) |
| FRET | Fluorescence Resonance Energy Transfer |
| g | Grams |
| G | Relative Centrifugal Force, also known as RCF |
| h | Hour(s) |
| HEPES | 2-[4-(2-hydroxyethyl)piperazin-1-yl]ethanesulfonic acid |

| | |
|-----------------|--|
| HR | Homologous Recombination |
| IHF | Integration Host Gactor |
| IPTG | Isopropyl β -D-1-thiogalactopyranoside |
| Kan | Kanamycin |
| kb | Kilobase(s) |
| Kd | Dissociation Constant |
| LB | Lysogeny Broth |
| mg | Miligram |
| min | Minute(s) |
| Mm | Millimolar |
| MMR | Methyl Directed Mismatch Repair |
| ml | Milliliter |
| NER | Nucleotide Excision Repair |
| nM | Nanomolar |
| NMR | Nuclear Magnetic Resonance Spectroscopy |
| nt | Nucleotide(s) |
| ORF | Open Reading Frame |
| ^{32}P | Phosphorus-32 (^{32}P) |
| PAGE | Polyacrylamide gel electrophoresis |
| PCR | Polymerase Chain Reaction |
| PNK | Polynucleotide Kinase |
| RNA | Ribonucleic Acid |
| RNAP | Ribonucleic Acid Polymerase |
| rpm | Rounds Per Minute |
| s | Second(s) |

| | |
|-------|---|
| ss | Single Stranded |
| SDS | Sodium Dodecyl Sulphate |
| SF | Superfamily (classification of helicases) |
| SPR | Surface Plasmon Resonance |
| SSC | Saline sodium citrate |
| TBE | Tris-borate-EDTA |
| TCR | Transcription Coupled Repair |
| TEMED | Tetramethylethylenediamine |
| Tris | Tris(hydroxymethyl)methylamine |
| UV | Ultraviolet |
| WT | Wild Type |

PGR COVID-19 IMPACT STATEMENT

Purpose of the impact statement

The impact statement is designed to capture contextual information about the **effect of the Covid-19 pandemic restrictions on your research project and/or thesis**. The information you provide will enable your examiners to understand, if applicable, how your research project and/or thesis has been altered by the Covid-19 restrictions.

Adapting research projects in the light of unforeseen circumstances is a normal part of research and you will not be penalised for this if you are able to meet the criteria for the relevant award ([section 2 of the Policy on Research Degrees](#)) which are set at a threshold level. Indeed, the criteria for a PhD specifically highlight that successful candidates are expected to demonstrate: *'the general ability to conceptualise, design and implement a project for the generation of new knowledge, applications or understanding at the forefront of the discipline, and to **adjust the project design in the light of unforeseen problems;**'* and will have *'the qualities and transferable skills necessary for employment requiring the exercise of personal responsibility and largely autonomous initiative in **complex and unpredictable situations, in professional or equivalent environments**'*.

The impact statement is not designed to:

- replace a request for a leave of absence (LoA)/extension if you believe that you have grounds for a LoA/extension due to the effect of the Covid-19 restrictions on your research project/thesis;
- capture information about your personal circumstances; if the Covid-19 pandemic is having/has had a significant negative impact on your personal circumstances (e.g. led to physical or mental ill-health or created a challenging domestic situation), then you should request a LoA/extension.

Completing the impact statement

- You may submit an impact statement (it is optional) if you are a PGR whose research has been impacted by the Covid-19 restrictions.
- Please complete parts A, B and D, and if applicable part C.
- You should complete the impact statement just before you submit your thesis for examination, to ensure that it provides the most accurate and up to date information.
- Please [upload](#) the completed impact statement (saved as a .pdf file) with your thesis.
- RSA will forward the impact statement to your examiners together with your thesis.
- If you decide not to submit an impact statement you cannot use that decision as grounds for an appeal at a later stage.

Part A: Student details

| | |
|---|------------|
| First name | Dominika |
| Surname | Warecka |
| Student number | 206066864 |
| Department | Biology |
| Intended award | PhD |
| Programme of study e.g. Biology, History | Biology |
| Date your studies began | 01/10/2020 |
| Mode of attendance | Full-time |
| Current submission date | 07/01/2024 |

Part B: Summary of the effect of the Covid-19 restrictions on your research project

How has your research project/thesis been affected by the Covid-19 pandemic restrictions:
Significant/substantial changes to research project/thesis

Part C: Details (if applicable) of how the Covid-19 restrictions have affected your research project

| | |
|--|--|
| Title/brief description of original research project | Obstacles to DNA replication in Escherichia coli and the role of UvrD helicase in their resolution |
| Title/brief description of your revised research project (if applicable) | n/a |
| How the Covid-19 restrictions have altered your research project/thesis (max 800 words). | |
| <p>I began my PhD, funded by the University of York Biology Department, in October 2020 in the middle of the Covid-19 pandemic. During this time, the Biology Department instated laboratory capacity restrictions. In my corridor, L0, the capacity was regulated by distributing slots to each group based on their size. This meant that with 50% capacity, we were able to have two people from the Hawkins group in the building (1 st of October 2020 until the 5 th of January 2021; 1 st of March 2021 until 19 th of July 2021), while at 25% capacity, we were only allowed a single person (5 th of January 2021 until the 1 st of March 2021).</p> <p>These Covid-19 laboratory capacity restrictions had a severe impact on the first year of my PhD, impacting the basic laboratory training, access to colleagues for help with troubleshooting and experimental design, but importantly by affecting essential training using radioactive isotopes. As part of my project, I conduct biochemical assays using radioactive isotopes; a high-risk work requiring intensive 1:1 training and the use of a dedicated room with single-person capacity during the Covid-19 lockdowns. Due to the restrictions, I was unable to begin crucial training in the safe use of radioactive material until the 29 th of March 2021. This caused a severe delay to my initial experimental work, which set the foundation for the rest of my PhD.</p> | |

You may comment on (see the [guidance](#) for further detail):

- the challenges that the Covid-19 restrictions presented for your research project/thesis
- what steps you took to address those challenges.

As a reminder, you must not use the impact statement to comment on your personal circumstances (e.g. ill health, domestic situation etc.).

It is recommended that you discuss Part C with your supervisor(s).

Please state if you discussed Part C with your supervisor(s): yes no

Part D: Signature of student

| | |
|------------------|------------|
| Dominika Warecka | 07/01/2024 |
|------------------|------------|

Note for examiners

As an examiner, you are required to read this impact statement and may choose to explore the contents with the PGR during the oral examination. Examiners should note that there is **no** change to the criteria that a PGR needs to meet to obtain a particular award ([section 2 of the Policy on Research Degrees](#)) in order to protect the integrity of our awards.

END